

UNCLASSIFIED

AD NUMBER: AD0817503

LIMITATION CHANGES

TO:

Approved for public release; distribution is unlimited.

FROM:

Distribution authorized to US Government Agencies only;  
Export Controlled; 1 Jun 1967. Other requests shall be referred to Air Force  
Flight Dynamics Laboratory, Wright-Patterson AFB, OH 45433.

AUTHORITY

AFFDL ltr 8 Jun 1972

**APPLICATION OF MAGNETIC TORQUING FOR  
DESATURATION OF CONTROL MOMENT  
GYROS IN SPACE VEHICLE CONTROL**

*L. R. HART, ET AL*

*WESTINGHOUSE DEFENSE AND SPACE CENTER*

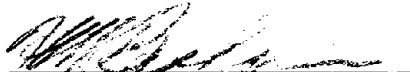
This document is subject to special export controls and each transmittal to foreign government or foreign nationals may be made only with prior approval of AFFDL (FDCL), Wright-Patterson AFB, Ohio.

## FOREWORD

This report was prepared by the Aerospace Division of the Defense and Space Center Westinghouse Electric Corporation, Baltimore, Maryland for the Flight Dynamics Laboratory of the US Air Force under Contract number AF33(615)-3602. The contract was initiated under Project 8225, Flight Control Equipment Techniques; Task Number 822509, Space Vehicle Attitude Control and Stabilization.

The study program was begun 1 April 1966 and was completed on 15 December 1966. The work was performed under the direction of Lt. David Anderton, the Project Engineer for the US Air Force Flight Dynamics Laboratory. Principal contributors to this study were Messrs. Leonard R. Hart, Harold W. Alatalo, Jack Braumiller, Edgar J. Bowers, and Charles E. Williams.

The manuscript was released by the authors on 23 February 1967 as an RTD Technical Report. This Technical Report has been reviewed and is approved.



H. W. Basham  
Chief, Control Elements Branch  
Flight Controls Division  
AF Flight Dynamics Laboratory

## ABSTRACT

A group of control moment gyros can be used to control the attitude of a space vehicle by exchanging momentum with the rest of the spacecraft. However, externally caused disturbance torques acting on the vehicle would saturate the momentum capability of the gyros if no auxiliary torquing methods were provided to unload the stored momentum. This function can be performed by a set of three current-carrying coils which interact with the earth's magnetic field in a process of continually resetting the control moment gyro gimbal angles to "zero" positions.

The performance and weight of a magnetic system to momentum desaturate control moment gyros have been determined as functions of spacecraft size, altitude, and orbit inclination over the ranges of interest for a large, earth-orbiting manned space vehicle. In a digital computer simulation of the combined control moment gyro and magnetic systems, the torques exerted by the latter had a negligible effect on the pointing accuracy of the former. Designs have been completed for the elements of the magnetic system, and the interface with the control gyros has been defined.

This abstract is subject to special export controls and each transmittal to foreign governments or foreign nationals may be made only with prior approval of the AF Flight Dynamics Laboratory (FDCL), Wright-Patterson AFB, Ohio.

1. The first part of the document discusses the importance of maintaining accurate records of all transactions and activities. It emphasizes that proper record-keeping is essential for ensuring transparency and accountability in financial reporting. This section also highlights the role of internal controls in preventing errors and fraud, and the need for regular audits to verify the accuracy of the data.

2. The second part of the document focuses on the importance of clear communication and collaboration between all stakeholders involved in the process. It stresses that effective communication is key to ensuring that everyone is on the same page and that all necessary information is shared in a timely and accurate manner. This section also discusses the importance of documenting all decisions and actions taken, and the need for regular updates and reports to keep all parties informed of the current status of the project.

3. The third part of the document addresses the importance of maintaining a high level of integrity and ethical standards throughout the entire process. It emphasizes that honesty and transparency are essential for building trust and credibility with all stakeholders. This section also discusses the importance of adhering to all applicable laws and regulations, and the need for a strong code of ethics to guide all actions and decisions.

4. The fourth part of the document discusses the importance of maintaining a high level of confidentiality and security for all sensitive information. It emphasizes that protecting this information is essential for ensuring the privacy and integrity of the data. This section also discusses the importance of implementing strong security measures, such as encryption and access controls, to prevent unauthorized access and data breaches.

5. The fifth part of the document discusses the importance of maintaining a high level of accuracy and precision in all calculations and data analysis. It emphasizes that even small errors can have significant consequences, and that it is essential to double-check all work and use appropriate statistical methods to ensure the reliability of the results. This section also discusses the importance of using high-quality data sources and ensuring that all data is properly validated and verified.

6. The sixth part of the document discusses the importance of maintaining a high level of flexibility and adaptability in the face of changing circumstances. It emphasizes that the ability to respond quickly and effectively to unexpected challenges is essential for ensuring the success of the project. This section also discusses the importance of having a contingency plan in place and the need for regular communication and collaboration to ensure that all parties are aware of the current status of the project and any potential risks.

7. The seventh part of the document discusses the importance of maintaining a high level of professionalism and courtesy in all interactions. It emphasizes that a positive and professional attitude is essential for building strong relationships and ensuring that all stakeholders feel respected and valued. This section also discusses the importance of using clear and concise language and avoiding any unnecessary jargon or technical terms.

8. The eighth part of the document discusses the importance of maintaining a high level of transparency and openness in all communications. It emphasizes that being open and honest about all activities and decisions is essential for building trust and credibility. This section also discusses the importance of providing regular updates and reports to all stakeholders and the need for a strong communication plan to ensure that all necessary information is shared in a timely and accurate manner.

9. The ninth part of the document discusses the importance of maintaining a high level of accountability and responsibility for all actions and decisions. It emphasizes that each individual has a role to play in the success of the project, and that it is essential to take ownership of one's actions and decisions. This section also discusses the importance of holding all parties accountable for their actions and the need for a strong system of checks and balances to ensure that all actions are properly documented and reviewed.

10. The tenth part of the document discusses the importance of maintaining a high level of consistency and uniformity in all processes and procedures. It emphasizes that having a clear and consistent set of rules and guidelines is essential for ensuring that all activities are performed in a standardized and efficient manner. This section also discusses the importance of regularly reviewing and updating these procedures to ensure that they remain relevant and effective.

## TABLE OF CONTENTS

	<u>Page</u>
I. INTRODUCTION AND SUMMARY . . . . .	1
1.1 Introduction . . . . .	1
II. CONCLUSIONS . . . . .	5
III. SCOPE OF THE STUDY PROGRAM . . . . .	7
IV. SUMMARY OF RESULTS . . . . .	13
4.1 Magnetic Desaturation System Performance . . . . .	13
4.2 Magnetic Torquer Specification and Weights . . . . .	19
4.3 Effect on CMG System Stabilization . . . . .	22
4.4 The Mechanization of the Magnetic Torquer System . . . . .	23
V. GENERAL FEASIBILITY STUDY . . . . .	25
5.1 Analytical Approach . . . . .	25
5.2 Analog Computer Program . . . . .	26
5.3 Hand Solution . . . . .	28
5.4 Digital Computer Program . . . . .	73
5.5 CAIN 48-Coefficient Field Subroutine . . . . .	75
VI. DETAILED STUDY OF A SPECIAL CASE . . . . .	77
6.1 Specific Orbits . . . . .	77
6.2 CMG System Design . . . . .	78
6.3 Complete System Simulation . . . . .	82
6.4 Variation of Altitude and Inclination . . . . .	88
VII. MAGNETIC SYSTEM MECHANIZATION. . . . .	91
7.1 Coil Size, Weight, and Power Requirements . . . . .	91
7.2 Weight Comparison of Magnetic Torquing System with Gas- Jet Systems . . . . .	105
7.3 Interface of CMG and Magnetic Torquers . . . . .	107

	<u>Page</u>
7.3.1 Circuit Mechanization. . . . .	109
7.3.2 Consideration of Time-Sharing. . . . .	118
7.3.3 Mechanical Design of the Magnetic Torquers . . . . .	118
7.3.4 Electronics Packaging Plan. . . . .	120
7.4 Magnetometer . . . . .	123
7.5 Reliability Estimate . . . . .	126
Appendix 1. Momentum Unloading Simulation Digital Program. . .	131
Appendix 2. Complete System Simulation Digital Program. . . . .	141
Appendix 3. CMG System Design. . . . .	155
Appendix 4. Electromagnetic Actuator Design. . . . .	181
Appendix 5. References. . . . .	203

#### LIST OF ILLUSTRATIONS

<u>Figure</u>		<u>Page</u>
1	Magnetic System Torque vs. Loop Gain . . . . .	8
2	Diagram of Gyroscope Configuration in Vehicle Coordinates . . . . .	11
3	Normalized Y-Axis Unloading Torque vs. Normalized Loop Gain--Analytical Method. . . . .	14
4	Lowest Feasible Altitude to Limit Stored Momentum to 10 Percent of CMG Rating. . . . .	17
5	Normalized Decay Time vs. Orbit Inclination. . . . .	18
6	Sample of Magnetic Torquer Ratings. . . . .	20
7	Sample of Magnetic Torquer Ratings. . . . .	21
8	Simplified Block Diagram. . . . .	23
9	Dipole Model of the Earth's Field. . . . .	27
10	Orbit Coordinates . . . . .	28
11	Dipole Coordinates . . . . .	30
12	Transformation Angles. . . . .	31
13	Block Diagram of Analog Computer Simulation. . . . .	33

<u>Figure</u>		<u>Page</u>
14	Field Components . . . . .	34
15	Y-Axis Disturbance Response at $\alpha = 0.50$ , $\phi = 30^\circ$ . . . . .	37
16	Y-Axis Disturbance Response at $\alpha = 1.20$ , $\phi = 30^\circ$ . . . . .	38
17	Y-Axis Disturbance Response at $\alpha = 3.00$ , $\phi = 30^\circ$ . . . . .	39
18	X-Axis Disturbance Response at $\alpha = 0.7$ , $\phi = 30^\circ$ . . . . .	40
19	Y-Axis Disturbance Response at $\alpha = 0.7$ , $\phi = 30^\circ$ . . . . .	41
20	Z-Axis Disturbance Response at $\alpha = 0.7$ , $\phi = 30^\circ$ . . . . .	42
21	Unloading Response at $\alpha = 0.50$ , $\phi = 30^\circ$ . . . . .	43
22	Unloading Response at $\alpha = 1.20$ , $\phi = 30^\circ$ . . . . .	44
23	Unloading Response at $\alpha = 3.00$ , $\phi = 30^\circ$ . . . . .	45
24	Unloading Response at $\alpha = 0.60$ and $\xi = 0$ , $\phi = 30^\circ$ . . . . .	46
25	Unloading Response at $\alpha = 0.60$ and $\xi = 170$ , $\phi = 30^\circ$ . . . . .	47
26	Peak Unloading Cross-Coupling Factor vs. Orbit Inclination Relative to Magnetic Equator . . . . .	74
27	Vehicle Axis Nomenclature . . . . .	79
28	Two-D.O.F. Gyro Gimbal Torquer Control . . . . .	82
29	Step Response of CMG Control System for a Small Angle Error . . . . .	84
30	CMG Initial Response to A Large Pitch Error . . . . .	85
31	Large Pitch Error Response Prior to Torque Reversal . . . . .	87
32	Spacecraft Mounting of Iron-Core and Air-Core Windings . . . . .	92
33	Weight of Air-Core Roll Axis Coil (Including Power Supply) . . . . .	93
34	Weight of Air-Core Pitch or Yaw Coils (Including Power Supply) . . . . .	95
35	$l/M$ Ratio vs. $T/B_t$ for Various Length Coils . . . . .	99
36	$Z^2$ vs. $T/B_t$ for Various Coil Lengths . . . . .	100
37	$\psi$ vs. $F(\psi)$ . . . . .	101
38	$\psi$ vs. $T/B_t$ for Various Coil Lengths . . . . .	102



<u>Figure</u>		<u>Page</u>
39	Iron-Core Torquer System Weight as Function of Required Torque/Field Ratio for Coil Lengths of 10 - 15 ft. . . . .	103
40	System Block Diagram . . . . .	108
41	Operational Amplifier . . . . .	110
42	Coil Driver Stage . . . . .	112
43	Multiplier Block Diagram . . . . .	114
44	Straight Line Approximations . . . . .	116
45	Approximation Errors. . . . .	117
46	Mechanical Design of Torquer Bars. . . . .	119
47	Magnetic Electronics Assembly . . . . .	121
48	Details of Spacer Block. . . . .	124
49	Variable Definitions, First View. . . . .	132
50	Variable Definitions, Second View. . . . .	133
51	Variable Definitions, Third View . . . . .	134
52	Variable Definitions, Fourth View. . . . .	135
53	Variable Definitions, Fifth View. . . . .	136
54	Variable Definitions, Sixth View. . . . .	137
55	Momentum Unloading of Control Moment Gyros, Digital Flow . . . . .	143
56	Variable Definitions, Seventh View . . . . .	144
57	Variable Definitions, Eighth View. . . . .	144
58	Vehicle Attitude and Rate Maneuver Profile (Pitch Axis) . . . .	162
59	Disturbance Torque History During Maneuver (Pitch Axis). . . . .	163
60	Acquisition and Tracking Torque Requirements (Pitch Axis). . . . .	165
61	Gyro Orientation Relative to Vehicle Axes . . . . .	168
62	General Control Loop Block Diagram . . . . .	169

<u>Figure</u>		<u>Page</u>
63	Bode Plot of System Crossover Region . . . . .	173
64	Bode Plot of System Operating Region (Tracking Mode) . . . . .	174
65	Pitch Axis Block Diagram . . . . .	175
66	Uncompensated One-D. O. F. Control System Block Diagram . . . . .	177
67	Bode Plots of Roll Axis IDOF System . . . . .	179
68	Dimensions of Core-Coil Combination . . . . .	187
69	Cross-Section of Winding . . . . .	190
70	$\psi$ Versus $f$ ( $\psi$ ) . . . . .	194
71	Flux Distribution in Bar as a Function of Distance from End . . . . .	195
72	Average Flux Density in Bar Versus Core Length Diameter Ratio . . . . .	196
73	Demagnetizing Factor as a Function of $l/m$ . . . . .	200

#### LIST OF TABLES

<u>Table</u>		<u>Page</u>
1	Stored y-Axis Momentum = $M_{Y0}$ . . . . .	54
2	Required Values of $T_{av}/(\omega_o M_{Y0})$ . . . . .	55
3	Values of Minimum $\alpha$ that Counteract Momentum Buildup of Assumed Disturbances . . . . .	56
4	Table of Dimensionless Decay Time ( $\alpha \omega_o t = T_o$ ) . . . . .	60
5	Peak Values of Ft-Lb/Gauss, Using Minimum $\alpha$ Vehicle A1 (Currents in $10^{-2}$ Ft-Lb/Gauss) X-Axis Current . . . . .	64
6	Digital Check of Decay Time . . . . .	73
7	Digital Data Used to Check Minimum Loop Gain . . . . .	75
8	Control Moment Gyro Actuator Physical Characteristics . . . . .	83
9	Pointing Errors for the Two Isolated Cases, Vehicle A2 . . . . .	86
10	Effect of Altitude and Inclination Variation for the Particular Vehicle (Vehicle A2) . . . . .	89

LIST OF TABLES (Continued)

<u>Table</u>		<u>Page</u>
11	Summary of Core and Coil Characteristics . . . . .	104
12	Summary of System Weights and Operations . . . . .	106
13	Reliability Tabulation . . . . .	130
14	Peak Torque Generated by Movement of Various Body Appendages . . . . .	160

SECTION I  
INTRODUCTION AND SUMMARY

1.1 INTRODUCTION

Where a system of control moment gyros (CMG's) is used to stabilize and control the attitude of a space vehicle, an auxiliary control torquing system must also be included. The control moment gyros function by exchanging momentum with the remainder of the spacecraft, with the total momentum of the CMG-spacecraft system remaining constant. When the CMG's stabilize the spacecraft in the presence of externally caused disturbance torques, they act as momentum storage units. They are subject to momentum saturation unless a control torque outside of the momentum conservative CMG-spacecraft system is applied to counter the stored momentum.

The auxiliary control torque could conceivably be generated by mass-ejecting thrusters, by employing the gravity gradient through the use of movable booms which determine moments of inertia, by shifting the center of mass or the center of pressure to use the sun's radiation pressure, or by interaction between a set of current-carrying coils and the earth's magnetic field. This last item, the magnetic torquer method, has important advantages with regard to convenience, reliability and weight, and has been the subject of this investigation.

Magnetic torquers, a set of three or more coils, can be used to produce a momentum unloading control torque by generating a field vector  $\bar{I}$  according to the control law:

$$\bar{I} = \bar{M} \times \bar{B}$$

where  $\bar{M}$  is the stored momentum and  $\bar{B}$  is a vector representing the earth's magnetic field. The control torque thus produced is

$$\bar{T} = \bar{I} \times \bar{B}$$

The currents in three orthogonal coils are continuously controlled to produce a field vector  $\bar{I}$  perpendicular to both the instantaneous direction of the earth's field and the vector representation of the momentum stored in the CMG's, with the result that a torque is produced which opposes the CMG stored momentum. The CMG system stored momentum is the difference between the actual momentum and the momentum the system has when all of the gyro gimbals are at the nominal "zero" positions.

When the directions of the stored momentum and the earth's field momentarily coincide, the magnetic torquers can produce no useful control torque. However,  $\bar{B}$  is continuously changing relative to  $\bar{M}$  for a vehicle orbiting the earth. The magnetic torquers are not required to perform the highly accurate and responsive stabilization functions of the CMG's, but only to perform a relatively slow momentum desaturation function. A momentary inability to produce a useful torque is not important.

$\bar{B}$  is determined by three mutually perpendicular magnetometer probes, and  $\bar{M}$  is defined by the positions of the CMG gimbals. Thus the elements of the magnetic torquer momentum desaturation system are three coils, a three-axis magnetometer, and a signal processing unit which computes  $\bar{M}$  from gimbal position transducer inputs and mechanizes the equation

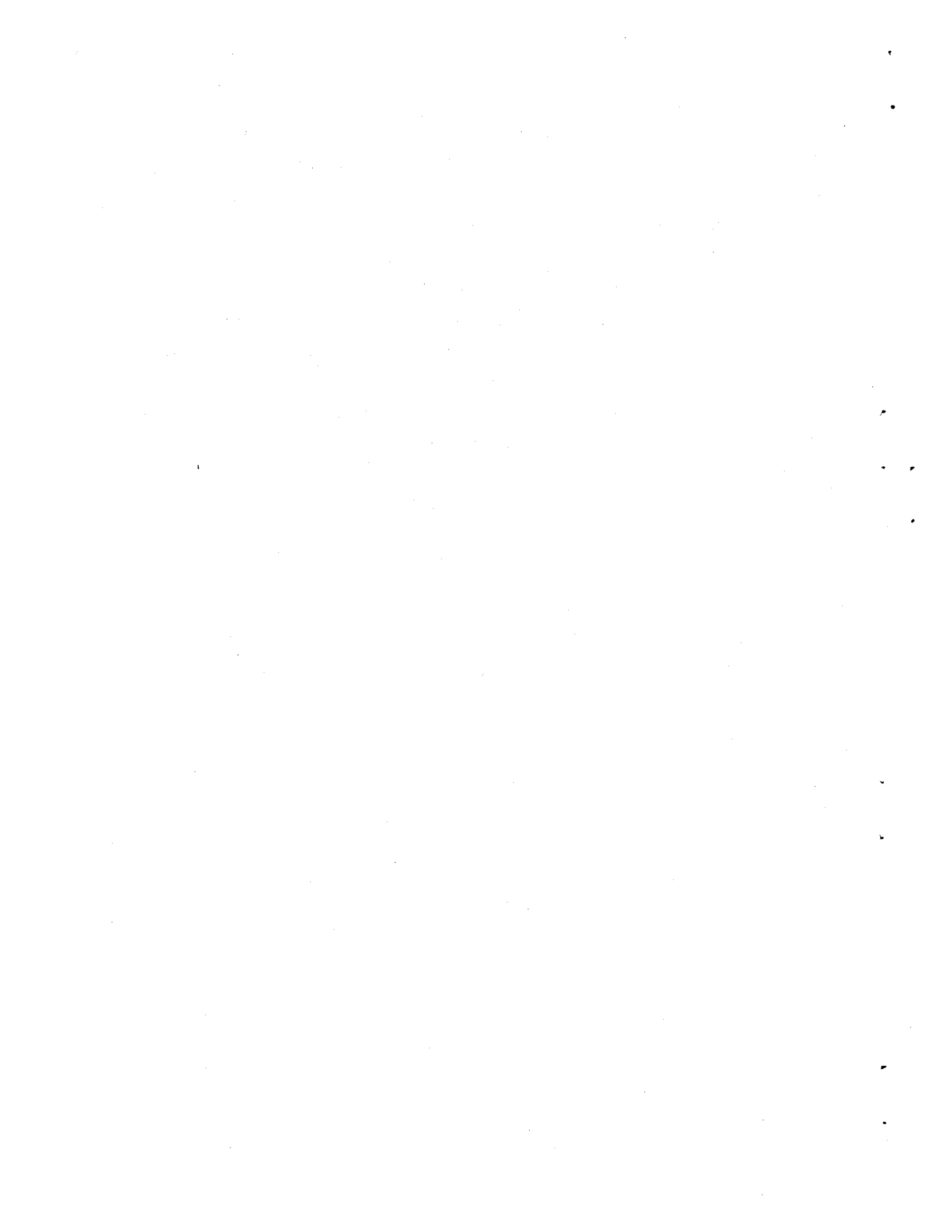
$$\bar{I} = \bar{M} \times \bar{B}$$

This report describes an investigation of the use of magnetic torquers to momentum desaturate CMG systems in large manned earth orbiting vehicles. Data have been generated on the weight and size of the magnetic torquer system as a function of the required momentum reset response, the spacecraft size and the altitude and orbit inclination over wide ranges of these independent variables. The power for the magnetic torquers is taken into account by including the power supply weight (at one pound per watt) in the total magnetic torquer weight. To facilitate this study, certain reasonable assumptions are made regarding the dependence of disturbance torques (solar pressure, gravity gradient and aerodynamic effects) on vehicle size.

The effect of the magnetic torquer system on the attitude control performance of the CMG's is also important, and these data were also determined. The method used for all these tasks was to develop and run a digital computer program which simulated the attitude controlled orbiting vehicle, the disturbances, the earth's magnetic field, and all the elements of both the CMG and magnetic torquer control systems.

In addition, outline drawings and packaging plans for the magnetic torquers and signal processor are given in this report, as well as a reliability analysis.

References 1, 2, and 3 were helpful in preparing the computer program and in the optimum magnetic torquer design.



## SECTION II

### CONCLUSIONS

It has been determined that a magnetic torquing system is feasible for the task of momentum desaturating a control moment gyro (CMG) attitude control system in a large space vehicle. Implementing the magnetic system requires no new hardware developments.

The magnetic torquing method is a better choice than a system of thrusters, which is the only other approach to momentum desaturation that can be seriously considered at this time. This choice rests largely on the higher reliability of the magnetic system, which includes only simple static devices (a magnetometer, a signal processor and three coils). Thruster systems typically include a number of solenoid valves, nozzles, high pressure tanks and lines and pressure reducers, or fuel heaters and pressure transducers. In addition, the magnetic system does not depend on a fixed fuel supply or a convenient fuel resupply rate and is more adaptable to the environment of disturbance torques which store momentum and to the mission life or resupply schedule. The magnetic approach is much less heavy than the simplest thruster systems with low specific impulse and weighs approximately the same as more sophisticated techniques with higher specific impulses. A power supply weighing one pound per watt has been included in the magnetic torquer weight.

Thrusters for desaturating momentum would have to be rated at a few millipounds thrust in order to avoid significant disturbances to the CMG system. Therefore, it is not likely that a reaction jet system which may or may not be on board for coarse attitude maneuvers could be used satisfactorily as a CMG momentum desaturating device.



The effect of the magnetic torquers on the stability and pointing accuracy of the CMG system is completely negligible. Also, the application of magnetic torquers does not affect any of the required specifications for the CMG's. Finally, the magnetic system requires only CMG gimbal resolver signals which the CMG's already have available.

For the space vehicle size considered in this program (diameters of 10 to 15 feet and lengths in the range 12 to 60 feet), the weights for iron-core and air-core magnetic torquers are approximately equal. However, iron-core torquers are slim cylinders that can be made as short as three feet with only a minor increase in weight; the three torquers can be separated and mounted in any convenient location. For reasonable weight efficiency, the air-core torquers would be thin coils wrapped around the outside of the spacecraft.

As an example, the weight of a magnetic system for a 40,000 pound vehicle (12 feet in diameter and 36 feet long) in a 200 nmi circular orbit inclined at 30 degrees to the equator is 200 pounds, including a one pound per watt power supply. This figure results from a pessimistic assumption regarding the size of the aerodynamic disturbance torque, which would otherwise saturate the CMG system and which is the dominant influence on the magnetic system at low altitudes. At 300 nmi the magnetic system weight is down by a factor of four.

### SECTION III

#### SCOPE OF THE STUDY PROGRAM

The three basic aims of this study of the application of magnetic torquers for momentum desaturation of control moment gyros (CMG's) were: (1) to generate parametric performance and weight information, (2) to arrive at a design plan which includes the interface with the CMG's, and (3) to find the effects of the magnetic torquers on the CMG system performance. The increments specified for the parametric part of the study led to many permutations, and it was especially necessary to have a carefully designed approach to solving that part of the problem. As a consequence, some new and useful analytical tools for designing magnetic torquer momentum desaturation systems have been developed.

Since an understanding of the whole approach for the study program adds insight for examining the results, the steps used are summarized below:

1. An analysis of the external disturbance torques which would lead to momentum saturation of the CMG's was made, including some necessary assumptions about the characteristics of the spacecraft. The important effects are the aerodynamic and solar radiation torques and the gravity gradient. The results of this analysis included zero frequency disturbance torque components about the spacecraft y-axis (nominally normal to the orbit plane), which is a "worst-case" condition because of the shape of the earth's field. This is true because the y-axis is the only one which is nearly in continuous alignment with the earth's field for some orbit inclinations.

2. The normalized y-axis unloading (momentum desaturation) torque was derived as a function of the normalized magnetic torquing loop gain and the

angle  $\beta$  between the orbit plane and the magnetic equator. It was observed that this torque reaches a maximum when plotted versus loop gain for a given value of  $\beta$ . The general shape of the curves is shown in figure 1.

3. An analog computer simulation of the magnetic torquing system indicated the approach for the derivation of step 2 and also verified the results. In both steps 2 and 3, a dipole model of the earth's field was used.

4. Steps 2 and 3 were further checked by a digital computer simulation of the magnetic torquing system which incorporated the Cain 48-coefficient spherical harmonic earth's field representation.

5. From the curves produced in step 2 and the disturbance torque information, a determination was made of the combinations of low altitude and low inclination which will not allow the magnetic momentum unloading system to keep the momentum down to an arbitrary low level of 10 percent of the CMG capacities. For a given  $\beta$  and normalized average disturbance torque

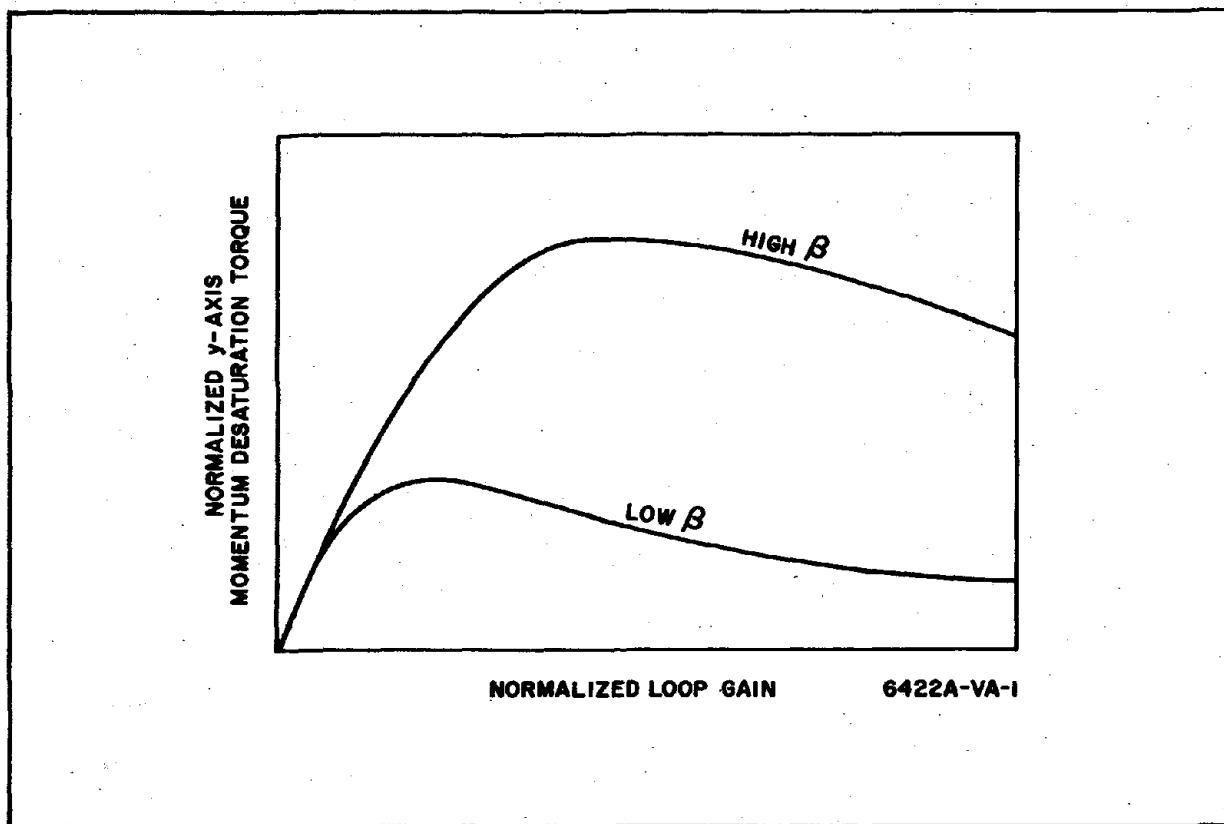


Figure 1. Magnetic System Torque vs. Loop Gain

(which is equated to the normalized y-axis momentum desaturation torque), the curves also show the normalized loop gain needed in order to just balance the disturbance torque. This same loop gain was arbitrarily applied to the x axis and z axis, as well as the y axis. The next step was to solve for each of the three magnetic torquer ratings in peak foot-pounds per gauss of the normal component of the earth's field, which ratings were needed to produce the required y-axis momentum desaturation torque at the needed normalized loop gain.

6. Expressions for the momentum components as functions of time, initial momentum and loop gain were derived. The decay time of the momentum stored in the CMG's was shown as a function of orbit inclination for each vehicle size. The decay time was normalized with respect to altitude and loop gain.

7. Using the design procedures developed in a previous study of magnetic torquers<sup>1</sup>, the torquer weight, including power supply, was computed as a function of the rating in peak foot-pounds per gauss of the normal earth's field component and for the various vehicle sizes. The magnetic torquer system weight was compared to the weights of several types of thruster systems for momentum desaturation.

8. A digital computer program was developed to simulate the complete CMG attitude control-magnetic torquer desaturation system for a particular vehicle and orbit case. This program was used to determine the effect on the CMG system pointing accuracy of applying the maximum magnetic desaturation torque. The particular case was a 40,000-pound, 12-foot-diameter, 35.4-foot long vehicle in a 200-nmi circular orbit inclined at 30 degrees to the equator.

9. A block diagram of the magnetic torquer system was prepared, showing the interface with the CMG system.

10. Schematics for the magnetic torquer signal processor were designed in order to estimate the magnetic torquer system reliability and to develop a packaging plan for the electronics as well as the magnetic torquers.

The parametric performance and weight study covered ranges of 100 to 1000 nmi for altitude, 0 degree to 90 degrees for orbit inclination to the equator and spacecraft characteristics as follows:

Weight (lb)	Diameter (ft)	Length (ft)	$J_{\text{Roll}}$ (slug-ft <sup>2</sup> )	$J_{\text{Pitch/Yaw}}$ (slug-ft <sup>2</sup> )	C.M. Offset (ft)
10000	10	12.7	3890	6110	1.3
40000	12	35.4	22400	141500	3.5
70000	14	45.4	53300	392000	4.5
70000	12	61.9	39200	497000	6.2
100000	14	64.8	76200	1127000	6.5
100000	15	56.6	87400	875000	5.7

For the purposes of determining disturbance torques and simulating the CMG system, it was assumed that the vehicle was oriented with its longitudinal axis generally vertical and another axis normal to the orbit plane. However, operation of the magnetic momentum desaturation system is not limited to this orientation.

The center of mass offsets tabulated above are along the longitudinal axis of the cylindrical vehicle and were assumed to develop aerodynamic and solar radiation torques. It was further assumed that the longitudinal or z axis was actually oriented one degree from the vertical, producing a steady gravity gradient torque in addition to the constant aerodynamic torque.

It was assumed that the CMG system must be accurate within 10 arc seconds while the vehicle is tracking a ground station offset from the orbit plane. The configuration of CMG's is shown in figure 2. The rotor momenta are 1000 foot-pound-seconds for each of the two double-gimballed gyros and 500 foot-pound-seconds for each of the two single gimballed units for the particular case of the 40,000 pound spacecraft. For other spacecraft sizes in the parametric study, the CMG rotor momenta were assumed to be scaled up or down from this base level in proportion to the vehicle moments of

inertia. This assumption is essentially valid because the CMG rotor momenta are mainly dictated by the anticipated vehicle slewing maneuvers.

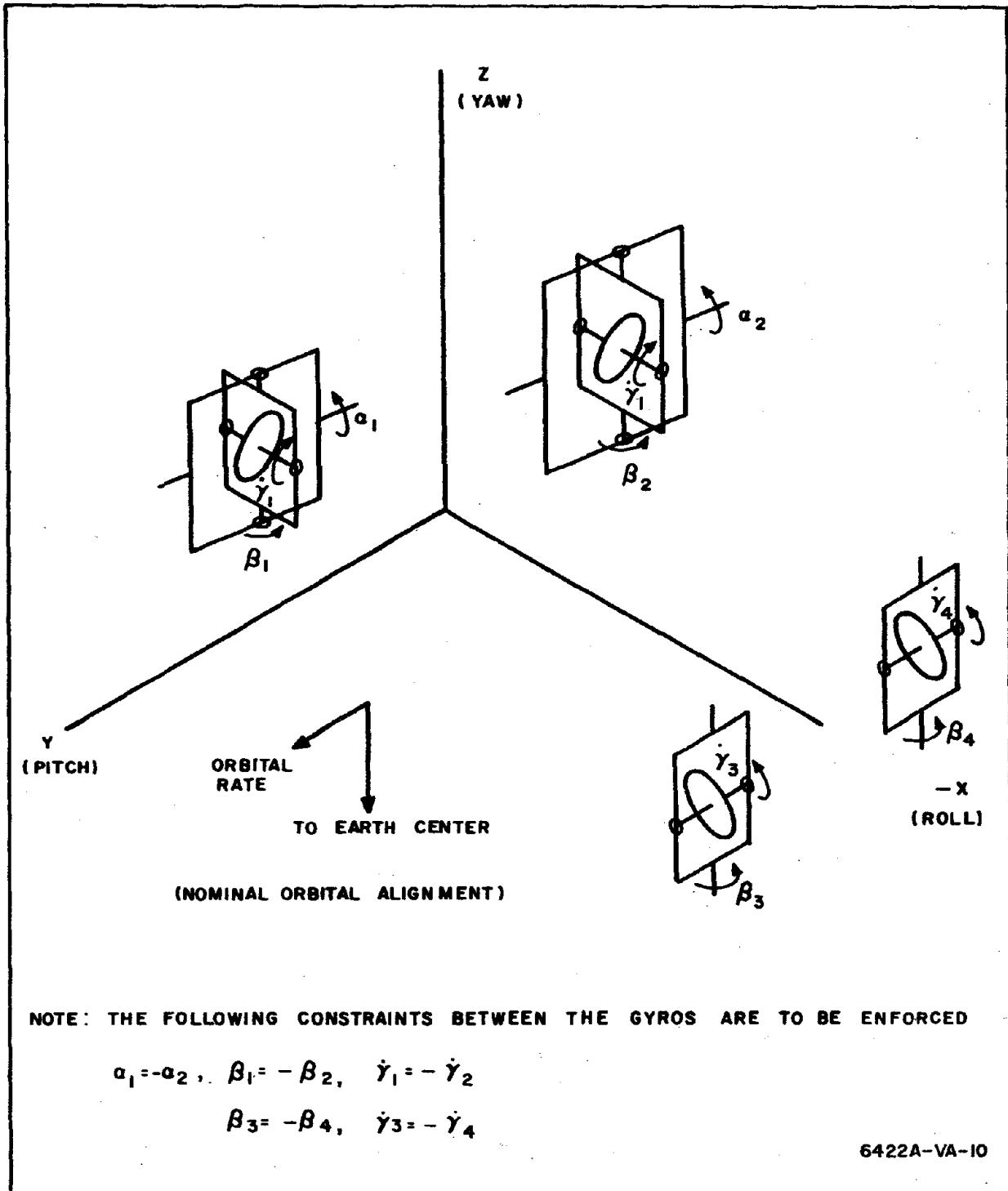
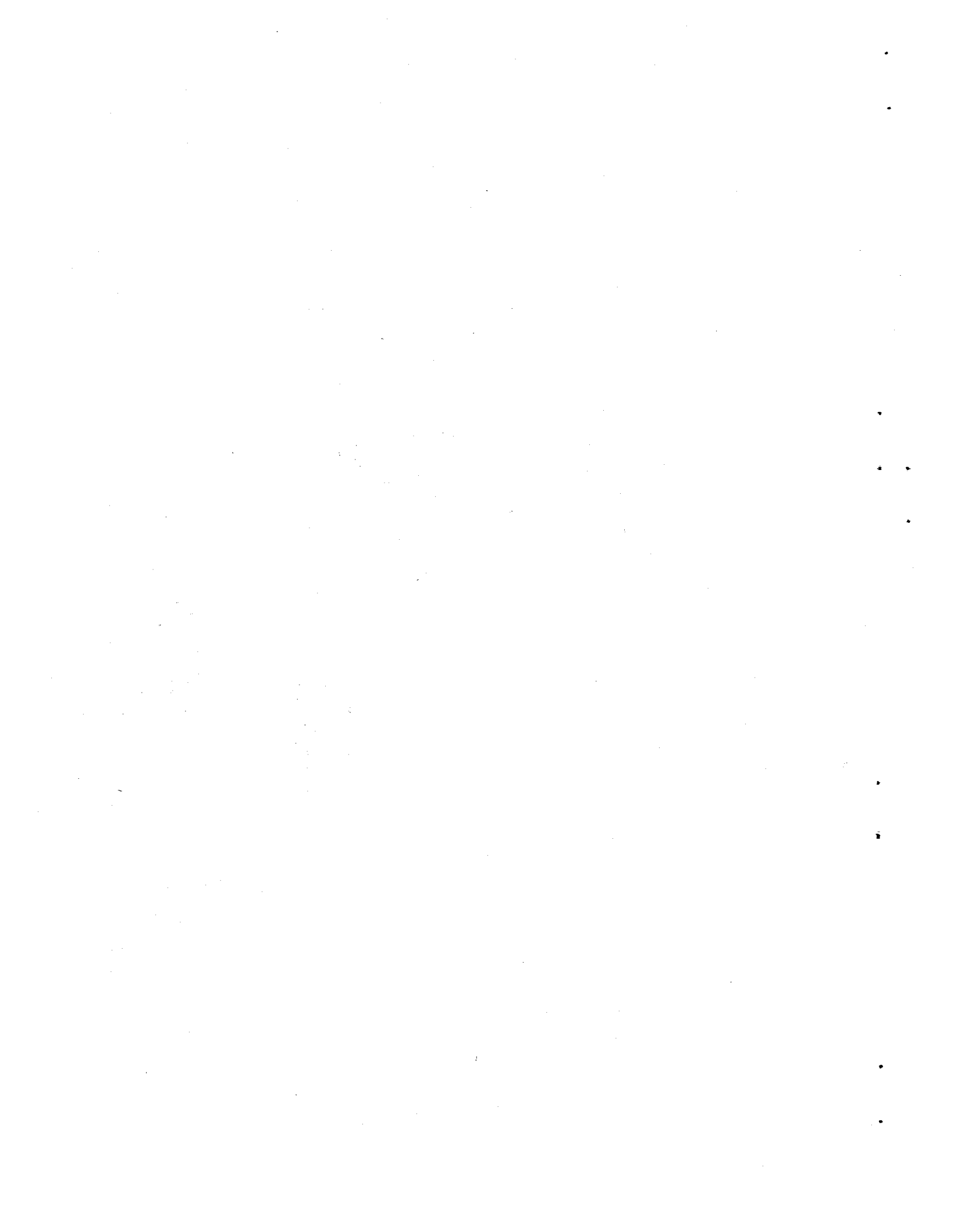


Figure 2. Diagram of Gyroscope Configuration in Vehicle Coordinates



SECTION IV  
SUMMARY OF RESULTS

4.1 MAGNETIC DESATURATION SYSTEM PERFORMANCE

The most basic and important relationships for defining a magnetic system to desaturate momentum has proven to be those which exist among the average desaturation torque, the loop gain  $\alpha$  and the angle  $\beta$  between the orbit plane and the magnetic equator. The typical relationships among the normalized versions of these parameters are shown in figure 3.

The desaturation capability of the system is a function of  $\sin^2 \beta$ . This can be explained as follows. First,

$$\bar{T} = (\bar{M} \times \bar{B}) \times \bar{B}$$

and

$$|T| \propto B^2$$

Considering the y-axis torque, the earth's field components of interest are  $B_x$  and  $B_z$ , those along the vehicle x and z axes.  $B_x$  and  $B_z$  are functions of  $\sin \beta$ . Hence  $|T|$  is proportional to  $\sin^2 \beta$ .

The relationships typified by figure 3:

- Show the normalized loop gain which maximizes the average normalized y-axis desaturation torque for a given orbit.
- Show the maximum average normalized disturbance torque (due to aerodynamic and gravity gradient effects) which can be tolerated for a given orbit. This is seen by merely equating the average normalized disturbance torque to the average normalized desaturation torque.



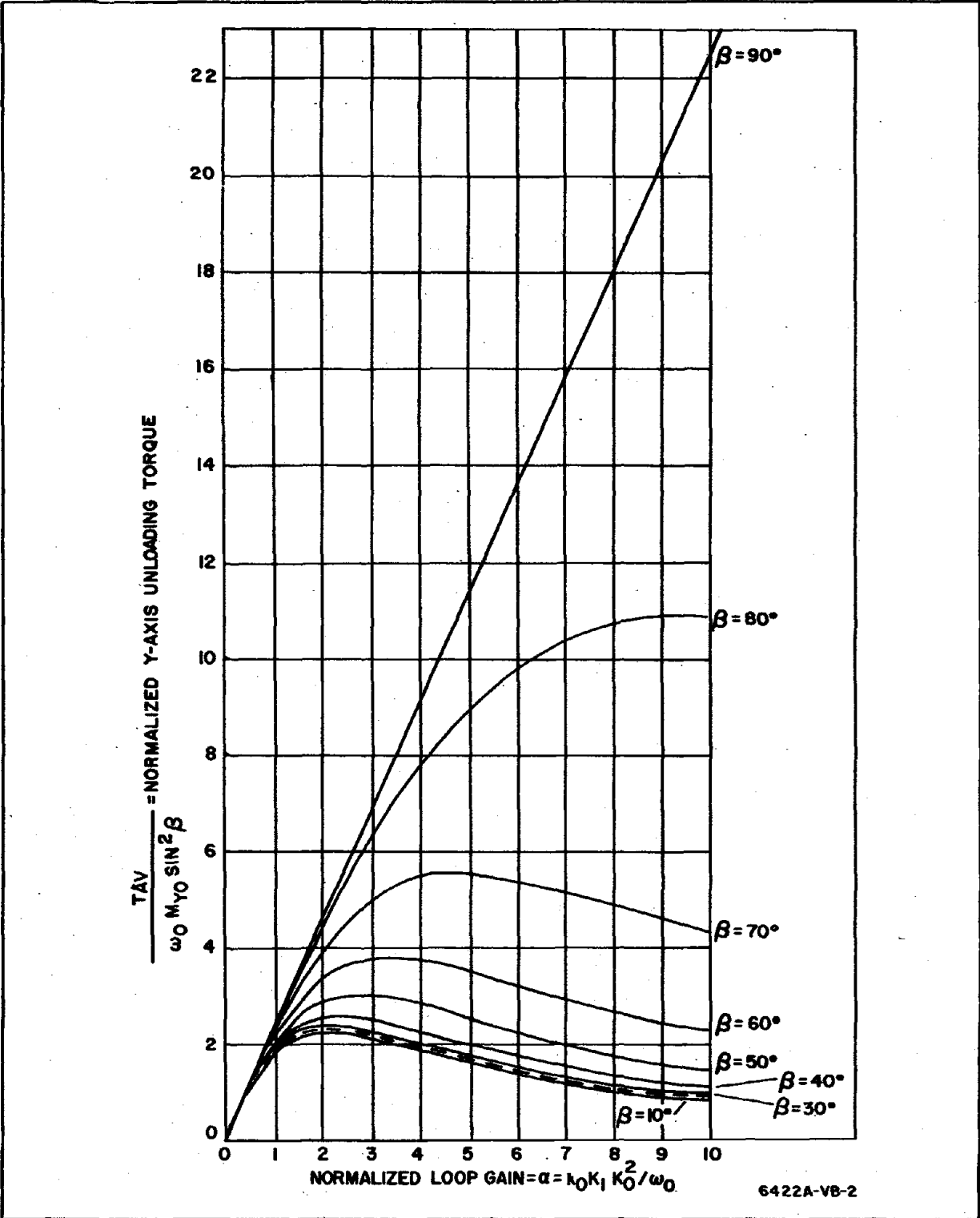


Figure 3. Normalized Y-Axis Unloading Torque vs. Normalized Loop Gain—Analytical Method

- Show the loop gain necessary to provide a given average normalized desaturation torque. Use of a higher loop gain would entail larger magnetic torquers.

The family of torque-loop gain -  $\beta$  relationships is shown in figure 3, where

$T_{AV}$  = average y-axis desaturation torque

$\omega_o$  = orbital rate

$M_{Y_o}$  = initial y-axis stored momentum

$k_o$  = torque gain from  $\bar{T} = k_o (\bar{I} \times \bar{B})$

$K_1$  = current gain from  $\bar{I} = K_1 (\bar{M} \times \bar{B})$

$K_o$  = magnitude of the earth's field at the equator for the altitude being considered.

The rms value of  $\beta$  can be used in applying the curves.  $\beta$  is a function of time, and it can be shown that

$$[\sin^2 \beta]_{AV} = \sin^2 \lambda + \sin^2 \phi \left[ 1 - \frac{3 \sin^2 \lambda}{2} \right]$$

where

$\lambda = 11.1^\circ$ , the angle between the magnetic and spin axes of the earth,

$\phi$  = inclination of the orbit to the geographic equator

Also,

$$\beta_{rms} = \arcsin \left[ \sqrt{(\sin^2 \beta)_{AV}} \right]$$

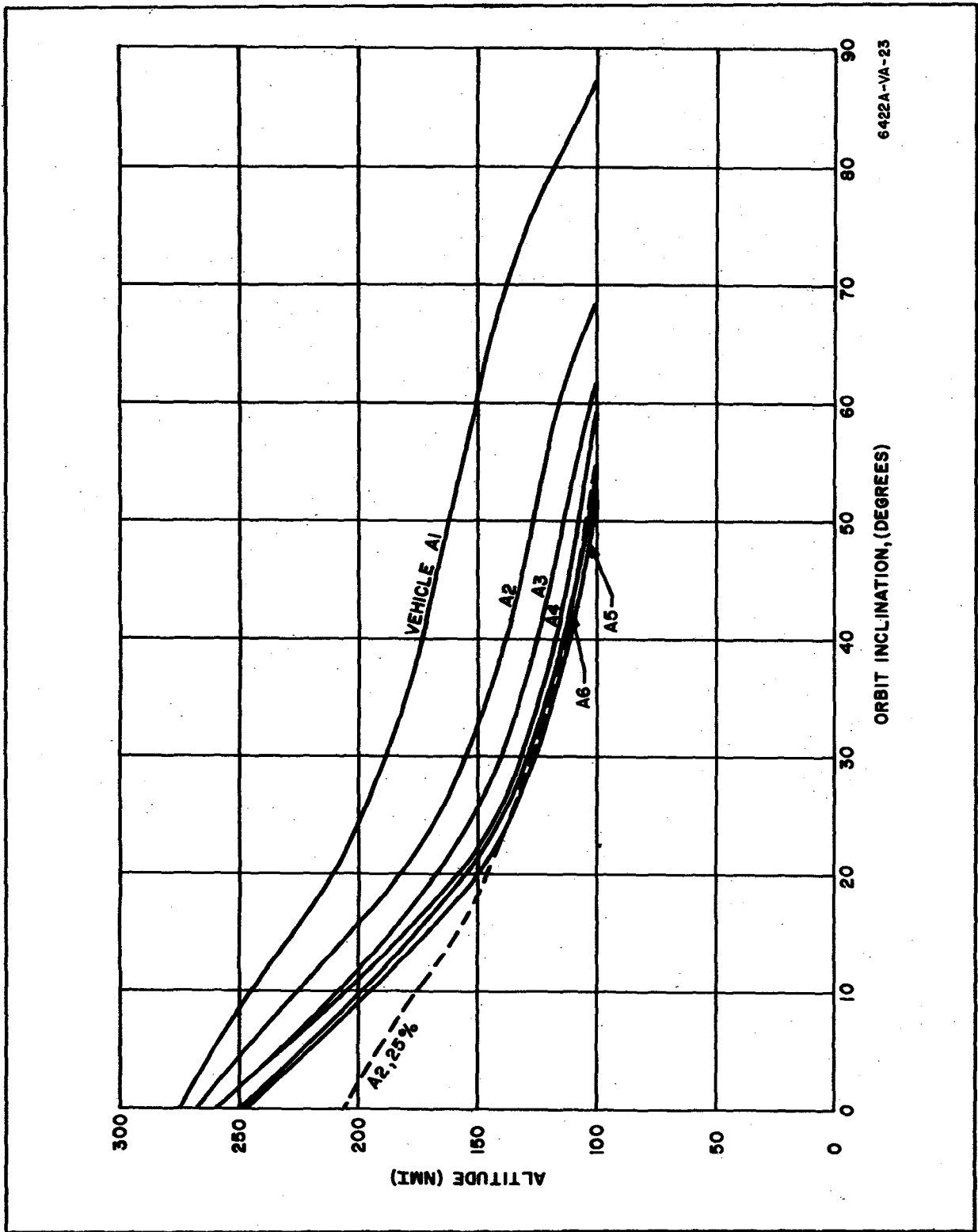
A final summary statement that can be made regarding figure 3 is that for normalized loop gains  $\alpha$  below 1.0

$$\frac{T_{AV}}{\omega_o M_{Y_o}} = 2.25 \alpha \sin^2 \beta$$

In most cases the chosen  $\alpha$  is below 1.0.

The most stringent requirements for the magnetic torquing system are found in the low altitude, low orbit inclination cases. The term "orbit inclination" is used synonymously with the  $\phi$  defined above. The effect of low inclination has already been explained. Low altitudes are more stringent because the constant disturbance torque effects (aerodynamic torque and the gravity gradient) both increase rapidly with a decrease in altitude. Figure 4 shows the altitude-inclination combinations which produce peaks in the momentum stored in the CMG's which are 10 percent of the total momentum which the CMG's are capable of storing. The six vehicles A1 through A6 are those listed in the table of Section III. For any altitude inclination above the curve, the CMG stored momentum never reaches 10 percent of rating. If a stored momentum of more than 10 percent of CMG rating is allowed, the curves move downward and to the left. A 25-percent stored momentum curve is drawn for vehicle A2 (the 40,000-pound case) as a dashed line. Ordinarily, the lowest of the six "10 percent" curves would be that for vehicle A1 (the smallest). This order is inverted, however, as a result of the previously stated assumption that the CMG rotor momenta are proportional to the vehicle moments of inertia.

A magnetic torquing system to momentum-desaturate or reset a CMG system might be specified by stating a required reset response. The curves of figure 5 provide the basic information for such a specification and show the time required to reduce a stored momentum to 10% of its initial value. These curves further illustrate that the system is least capable of unloading a y-axis momentum (normal to the orbit plane) and that the assumption of constant y-axis disturbance torques was a conservative basis for the study. They also further illustrate the effect of orbit inclination.



6422A-VA-23

Figure 4. Lowest Feasible Altitude to Limit Stored Momentum to 10 Percent of CMG Rating

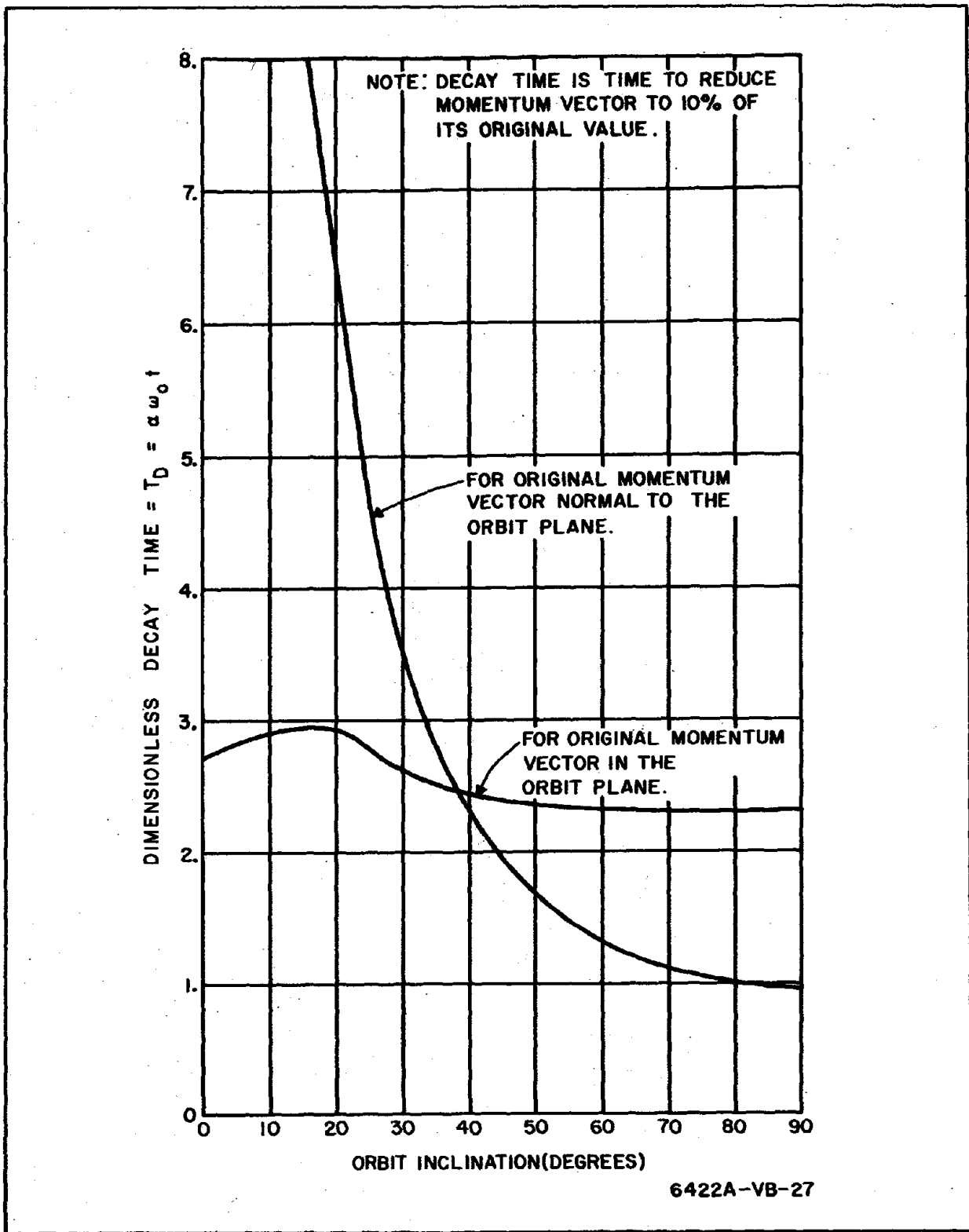


Figure 5. Normalized Decay Time vs. Orbit Inclination

## 4.2 MAGNETIC TORQUER SPECIFICATION AND WEIGHTS

Ratings of the x, y, and z magnetic torquers have been computed as functions of altitude, orbit inclination and spacecraft size. The magnetic torquers may be long cylindrical nickel-iron cores wound with many turns of wire, in which case the x, y, and z torquers are arranged with longitudinal axes along the vehicle x, y and z axes, respectively. Or they may be large diameter air-core torquers designated in a functionally similar manner. The ratings are expressed in foot-pounds per gauss of the normal earth's field component.

Because of the assumption of constant y-axis disturbance torques, the necessary ratings for x and z torquers is larger than that for the y torquer in every case. The ratings can be summarized, however, by stating only the sum of x, y and z torquer ratings. This is meaningful because the ratio of torquer weight to torquer rating is essentially constant for a large range of ratings.

Figure 6 shows how the total rating depends on altitude for the 40,000-pound vehicle with an orbit inclination of 30 degrees. Below 300 nmi, the aerodynamic torque is a very important influence. Above 300 nmi, two effects oppose each other and produce a rating nearly invariant with altitude. One is the diminishing earth's field, leading to higher torquer ratings. The other is the diminishing gravity gradient disturbance.

Figure 7 shows the expected variation of total torquer rating with orbit inclination.

It should be remembered that the data below 300 nmi are based largely on a pessimistic assumption that the center of mass and center of pressure are constantly separated by one-tenth of the spacecraft length.

A family of torquer designs has been calculated, optimizing the total weight of the torquer and its part of a power supply which is assumed to weigh one pound per watt. Each of the nickel-iron core torquers were assigned lengths equal to the diameter of the spacecraft (six spacecraft sizes

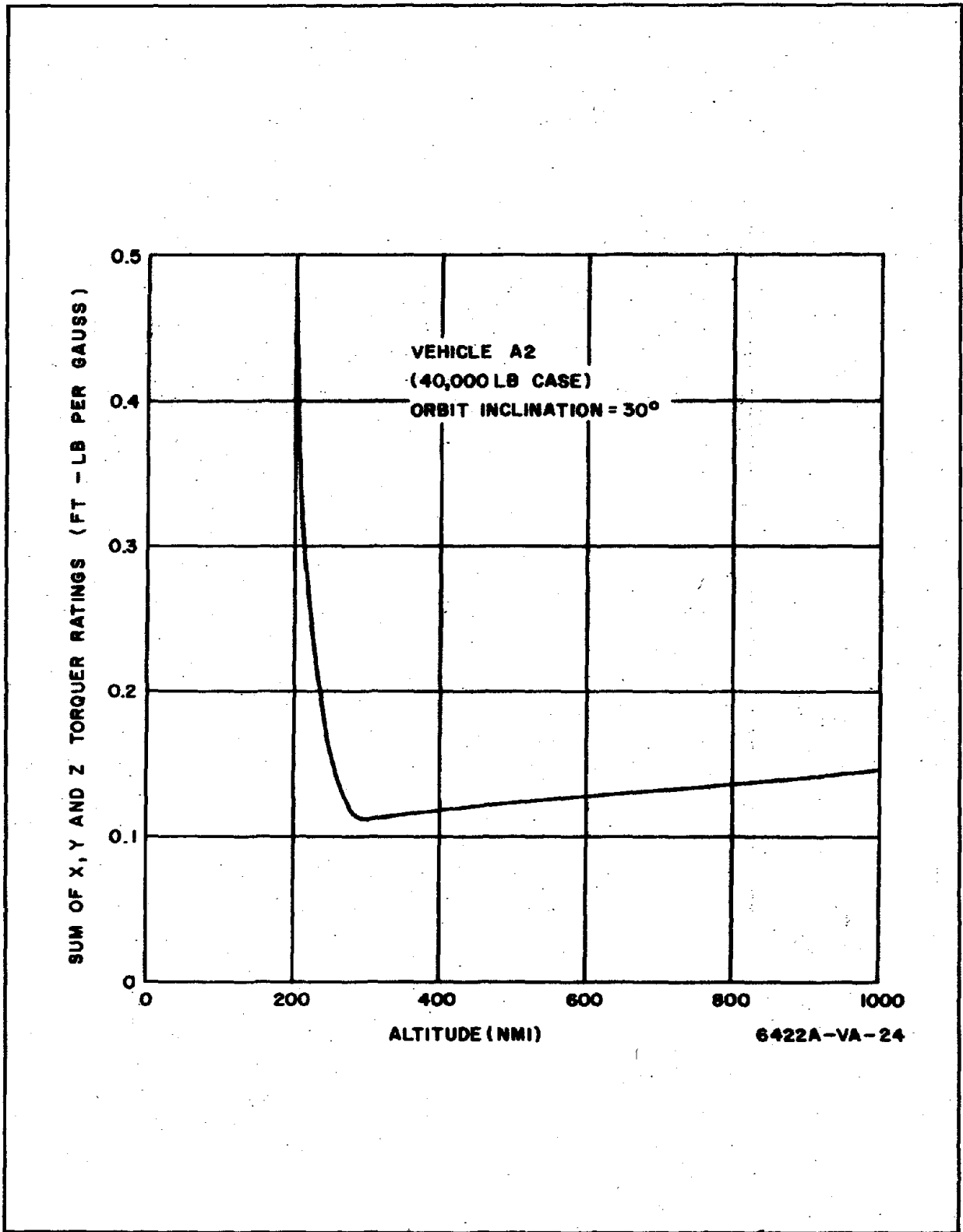


Figure 6. Sample of Magnetic Torquer Ratings

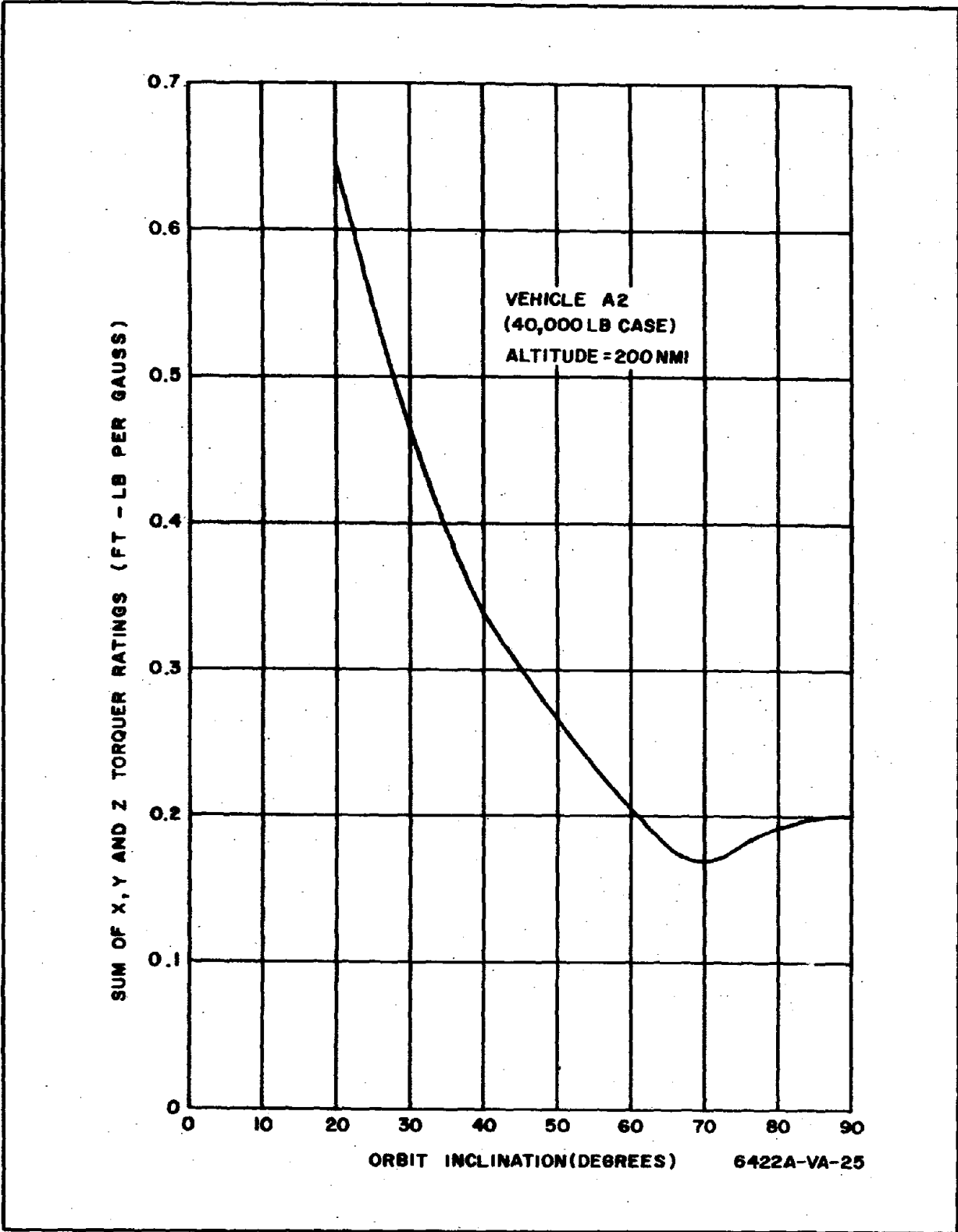


Figure 7. Sample of Magnetic Torquer Ratings



were considered). Using the 40,000-pound vehicle as an example, the total iron-cored torquer-power supply weight to rating ratio is 430 pounds per foot-pound per gauss.

For the same vehicle case, the air core torquers are slightly less heavy, having ratios of 390 for the z unit (a circle with diameter equal to that of the vehicle) and 260 for the x and y units (rectangles having sides equal to the length and diameter of the vehicle). While the orientation of the torquers is specified, reasonable mounting arrangements allow some latitude in the choice of locations for either type of torquer. There is much more freedom in locating the iron-core torquers on the spacecraft, however, because they can be made much shorter with only a slight increase in weight-to-rating ratio. If the full-size iron-core torquers were used, two could form an X across one end of the spacecraft and one would lie somewhere along the side.

Typically, magnetic torquers have a large weight advantage over thruster systems to momentum desaturate CMG or reaction wheel systems. Part of this advantage is lost, however, for very long spacecraft. In a system of 12 nozzles the 4 or 8 which perform most of the momentum desaturation function will benefit by having moment arms equal to half the length of the vehicle. For the 35-foot-long, 40,000-pound case in a 200 nmi circular orbit inclined at 30 degrees, the magnetic torquer system is one-third to one-fourth as heavy as a cold gas thruster system but somewhat heavier than a resistojet or monopropellant hydrazine system with higher specific impulse. However, the magnetic torquer system, which has no moving parts, has a very obvious reliability advantage over the thruster systems with their valves, pressure reducers, high pressure tanks and lines, nozzles and heaters.

#### 4.3 EFFECT ON CMG SYSTEM STABILIZATION

The momentum desaturation system acts like any other external disturbance in causing CMG system attitude errors. The errors caused by the occasional maximum torques exerted by the magnetic system were found in a computer simulation which included the 40,000-pound satellite at an altitude

of 200 nmi and the CMG system grossly specified at the end of Section II. The worst pointing errors were less than 2 arc seconds.

#### 4.4 THE MECHANIZATION OF THE MAGNETIC TORQUER SYSTEM

The combined CMG-magnetic torquer system is shown in figure 8. The magnetic torquer system consists of a three-axis magnetometer, the three torquer units and the torquer current computer and is enclosed by the dashed line. The inputs to the magnetic torquer system are trigonometric functions of  $\alpha_1$ ,  $\beta_1$ , and  $\beta_3$  (see figure 2) from the CMG system and  $B_x$ ,  $B_y$  and  $B_z$  as measured by the magnetometer. The coil current computer consists of signal amplifiers, multipliers, and power amplifiers. The function of these circuits is to mechanize  $\bar{I} = K_1 (\bar{M} \times \bar{B})$  and to derive the momentum components

$$M_x = -H \sin \beta_3$$

$$M_y = 2H \sin \beta_1$$

$$M_z = -2H \sin \alpha_1 \cos \beta_1$$

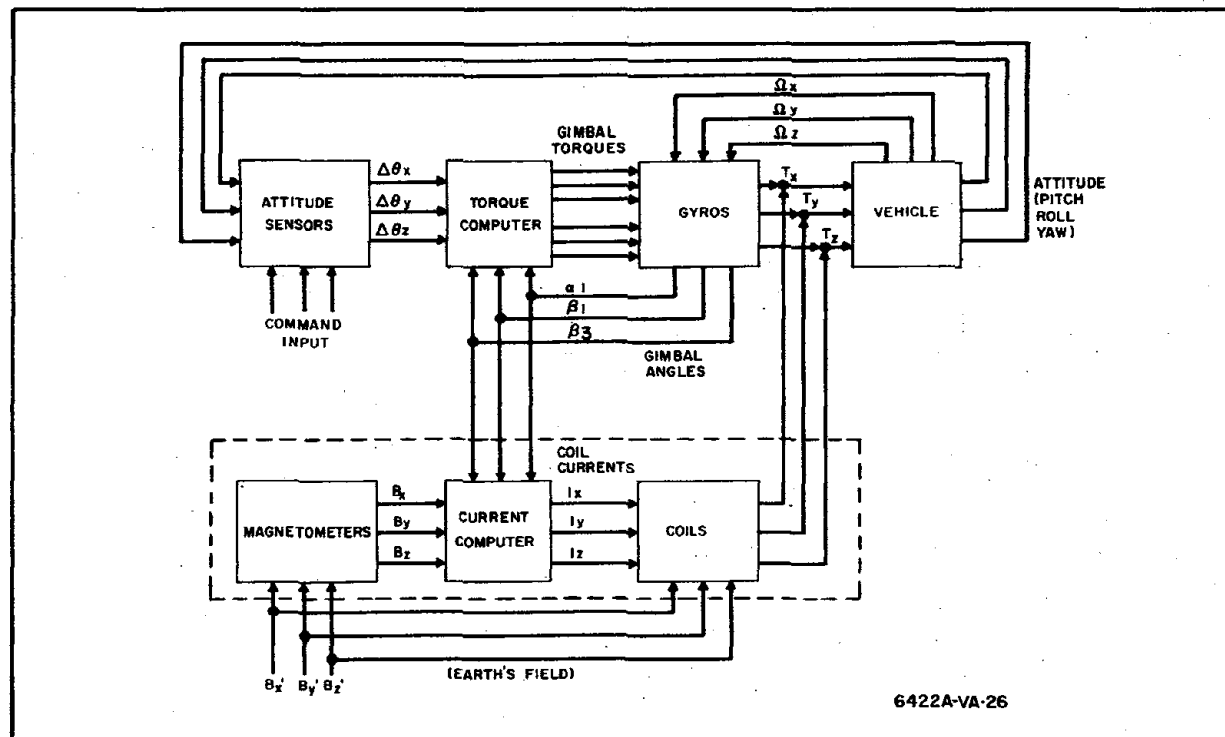


Figure 8. Simplified Block Diagram

where  $H$  is the rotor momentum of a double-gimballed gyro, and the rotor momentum of a single gimballed gyro is  $\frac{1}{2}H$ .

Circuit and packaging plans are also given in this report.

The probability of success of the magnetic momentum desaturation system, including torquers, magnetometer and signal processor, is calculated to be 0.915.

## SECTION V

### GENERAL FEASIBILITY STUDY

#### 5.1 ANALYTICAL APPROACH

As has been explained, the spacecraft was assumed to be oriented vertically. This orientation resulted in the vehicle experiencing constant pitch axis disturbance torques due to aerodynamic and gravity gradient effects.

Using the analog computer to simulate the orbiting craft and its disturbances, it was found that the average y-axis magnetic momentum unloading torque had a peak value that varied with orbit inclination, orbit altitude and average stored y-axis momentum. The analog program and results obtained are explained further in paragraph 5.2.

From the analog computer results it was possible to obtain analytical expressions that were expanded to get more general results than those obtained from the analog computer. From these results it was possible to define certain less desirable orbits, and the minimum gains that could be used in the other cases, without momentum buildup. The orbits which are "less desirable" from the standpoint of the magnetic torquer system are those which led to CMG-stored momentum buildups of greater than an arbitrarily chosen 10 percent of the CMG momentum rating.

The digital computer was used to verify the results of the hand solution, and to determine the amount of error that was introduced into the solution when a dipole field model was used.

It became necessary to find a measure of system performance that could be used to compare various gains. For this purpose the variable hereafter referred to as decay time was developed. Decay time is the number of orbits required for the system to reduce a momentum vector to 10 percent

of its initial value. The decay time was derived approximately analytically and verified with selected digital computer runs.

The size of the magnetic systems depends on the peak torque per unit field (foot-pounds/gauss) that is required from the coils in counteracting the momentum buildup that occurs as a result of the zero frequency pitch torques and on the torque required to reset an initial momentum vector in a pre-determined amount of time. The torque per unit field is found, for each of the three axes, for all six vehicles at all except the less desirable altitude and inclination cases.

## 5.2 ANALOG COMPUTER PROGRAM

An analog computer simulation was made to demonstrate the capability of the magnetic momentum unloading system to operate in the presence of steady disturbance torques and to desaturate the CMG system after a large angular impulse. This analysis used the dipole model of the earth's field.

The dipole model is illustrated in figure 9 where  $B_v$  represents the vertical component of the field and  $B_t$  represents the tangential component. The relationship of the two components to the orbit altitude  $h$  and the angle  $\gamma$  (magnetic latitude) is given by the equations:

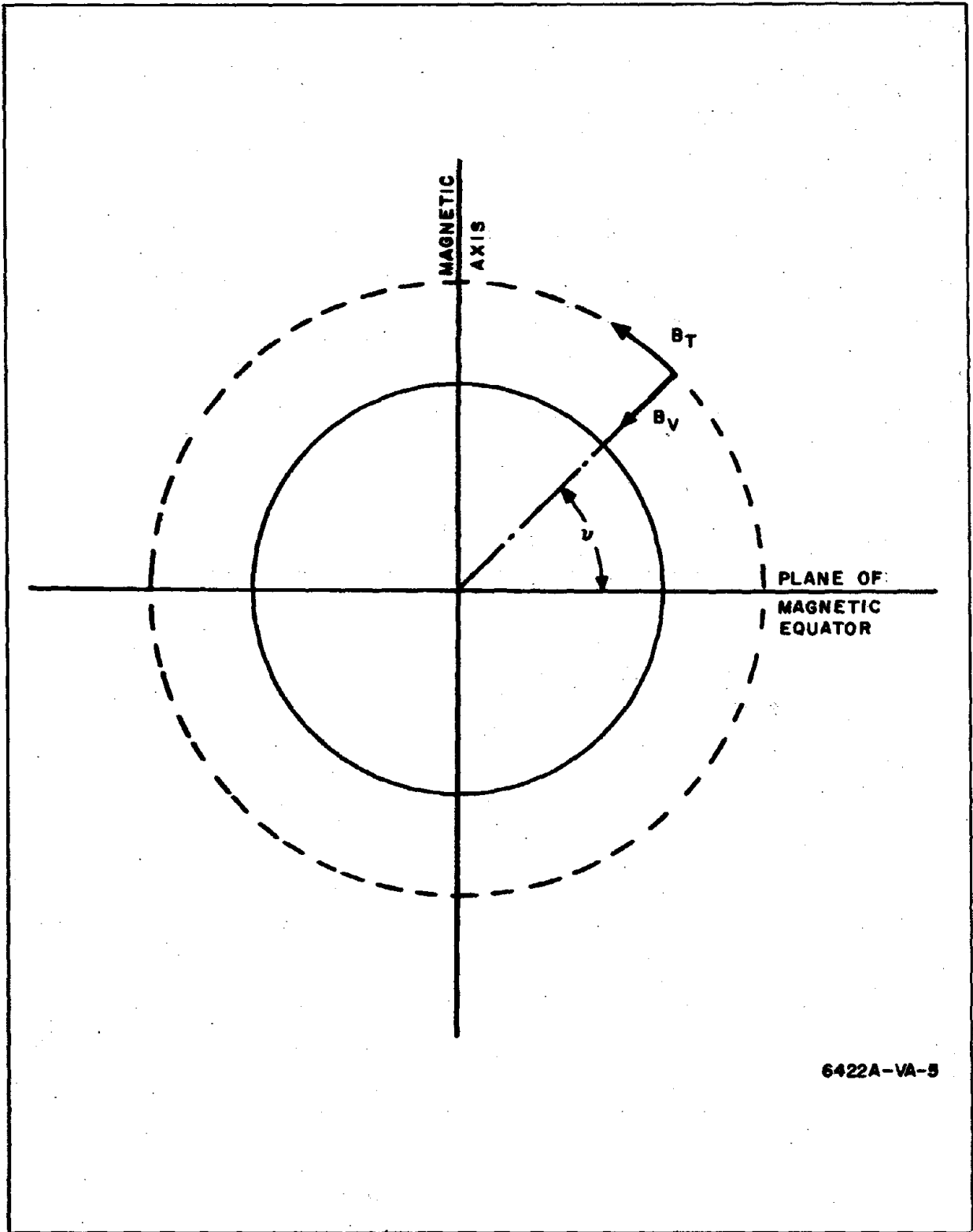
$$B_v = \frac{2 B_o r_e^3}{(r_e + h)^3} \sin \gamma = 2 K_o \sin \gamma$$

$$B_t = \frac{B_o r_e^3}{(r_e + h)^3} \cos \gamma = K_o \cos \gamma$$

where  $B_o$  = the field strength in gauss for a point on the earth's surface at the magnetic equator.

$r_e$  = earth radius (mean)

$K_o$  = the field strength at the orbit altitude along the magnetic equator.



6422A-VA-5

Figure 9. Dipole Model of the Earth's Field

Although the field represented by this model is free from the anomalies actually present in the earth's field, the lower harmonics will be well represented and it has been favorably compared with the Jensen-Whitaker program and Cain data. The Cain data are explained further in References 4, 5, 6, and 7. It is therefore felt to be a good basis for preliminary analysis.

The major portion of the analog computer mechanization was taken up with the dipole model. The equations listed below were mechanized to produce the components of the earth's field in orbit coordinates: (See figure 10.)

$$\xi = A_0 + 160.1^\circ - \omega_e t ; \theta = \omega_o t$$

$$Q_{11} = \cos \theta \cos \phi \cos \xi \cos \lambda - \cos \theta \sin \phi \sin \lambda - \sin \theta \sin \xi \cos \lambda$$

$$Q_{12} = \cos \theta \cos \phi \cos \xi \sin \lambda + \cos \theta \sin \phi \cos \lambda - \sin \theta \sin \xi \sin \lambda$$

$$Q_{13} = -\cos \theta \cos \phi \sin \xi - \sin \theta \cos \xi$$

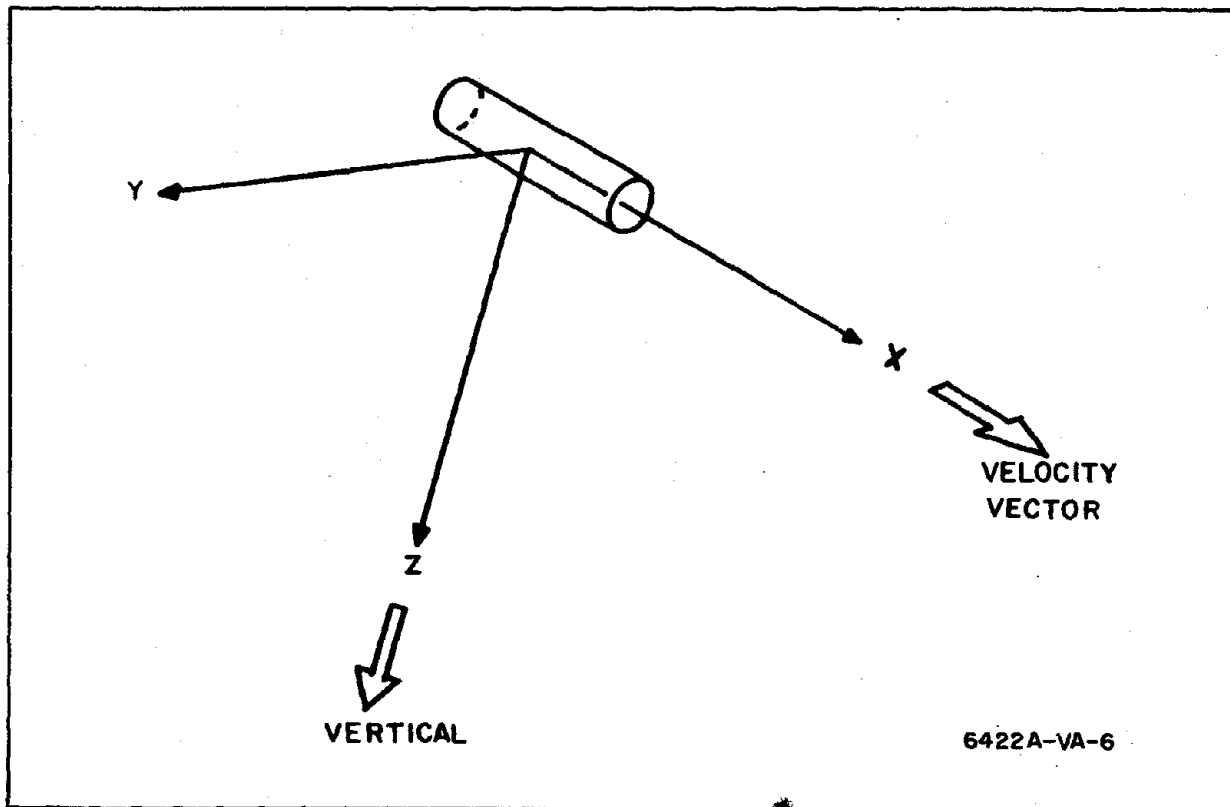


Figure 10. Orbit Coordinates

$$\begin{aligned}
Q_{21} &= -\sin \phi \cos \xi \cos \lambda - \cos \phi \sin \lambda \\
Q_{22} &= -\sin \phi \cos \xi \sin \lambda + \cos \phi \cos \lambda \\
Q_{23} &= \sin \phi \sin \xi \\
Q_{31} &= \sin \theta \cos \phi \cos \xi \cos \lambda - \sin \theta \sin \phi \sin \lambda + \cos \theta \sin \xi \cos \lambda \\
Q_{32} &= \sin \theta \cos \phi \cos \xi \sin \lambda + \sin \theta \sin \phi \cos \lambda + \cos \theta \sin \xi \sin \lambda \\
Q_{33} &= -\sin \theta \cos \phi \sin \xi + \cos \theta \cos \xi \\
B_v &= 2 Q_{32} K_o \\
B_A &= -3 Q_{31} Q_{32} K_o \\
B_B &= -3 Q_{32} Q_{33} K_o \\
B_C &= [ 1 - 3 Q_{32}^2 ] K_o \\
B_X &= Q_{11} B_A + Q_{12} B_B + Q_{13} B_C \\
B_Y &= -Q_{21} B_A - Q_{22} B_B - Q_{23} B_C \\
B_Z &= B_v
\end{aligned}$$

where  $Q_{11} \dots Q_{33}$  = matrix elements relating the dipole coordinate frame to the orbit reference frame. (See figure 11.)

$B_A, B_B, B_C$  = field components in dipole coordinates

$B_X, B_Y, B_Z$  = field components in orbit coordinates

$\xi$  = angle between longitude of the intersection of the geographic and magnetic equators and the longitude of the ascending node.

$A_o$  = longitude (+ measured east) of the ascending node

$\omega_e$  = earth rotation rate

$t$  = elapsed time

$\theta$  = orbit angle

$\omega_o$  = orbit rate

$\phi$  = orbit inclination



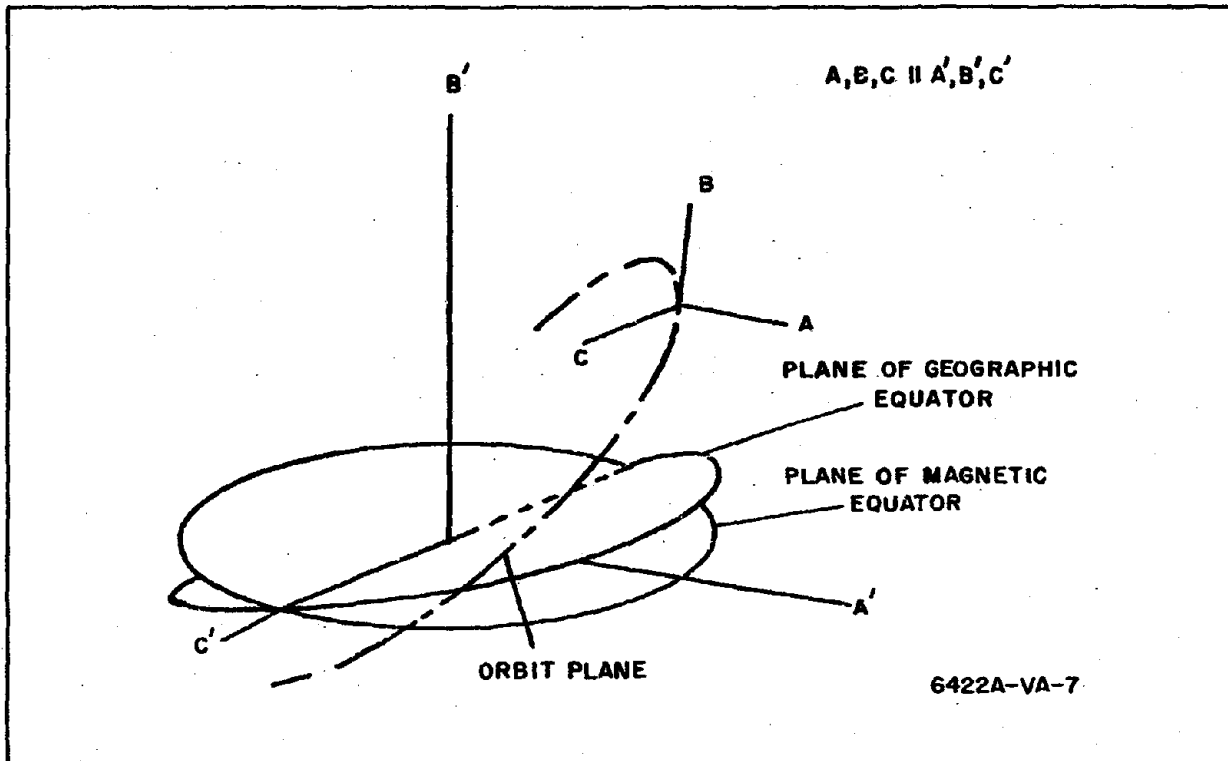


Figure 11. Dipole Coordinates

$\lambda$  = tilt angle between the earth's magnetic and geographic axes =  
 $11.1^\circ$

$K_o$  and  $B_v$  were defined previously

Figures 11 and 12 demonstrate the dipole coordinates and the angles which were defined above.

In addition to the dipole model equations, the following equations were programmed on the analog computer:

$$I_x = k_1 (M_y B_z - M_z B_y)$$

$$I_y = k_1 (M_z B_x - M_x B_z)$$

$$I_z = k_1 (M_x B_y - M_y B_x)$$

$$T_x = (I_y B_z - I_z B_y) = \dot{M}_x - T_{Dx} + \omega_o M_z$$

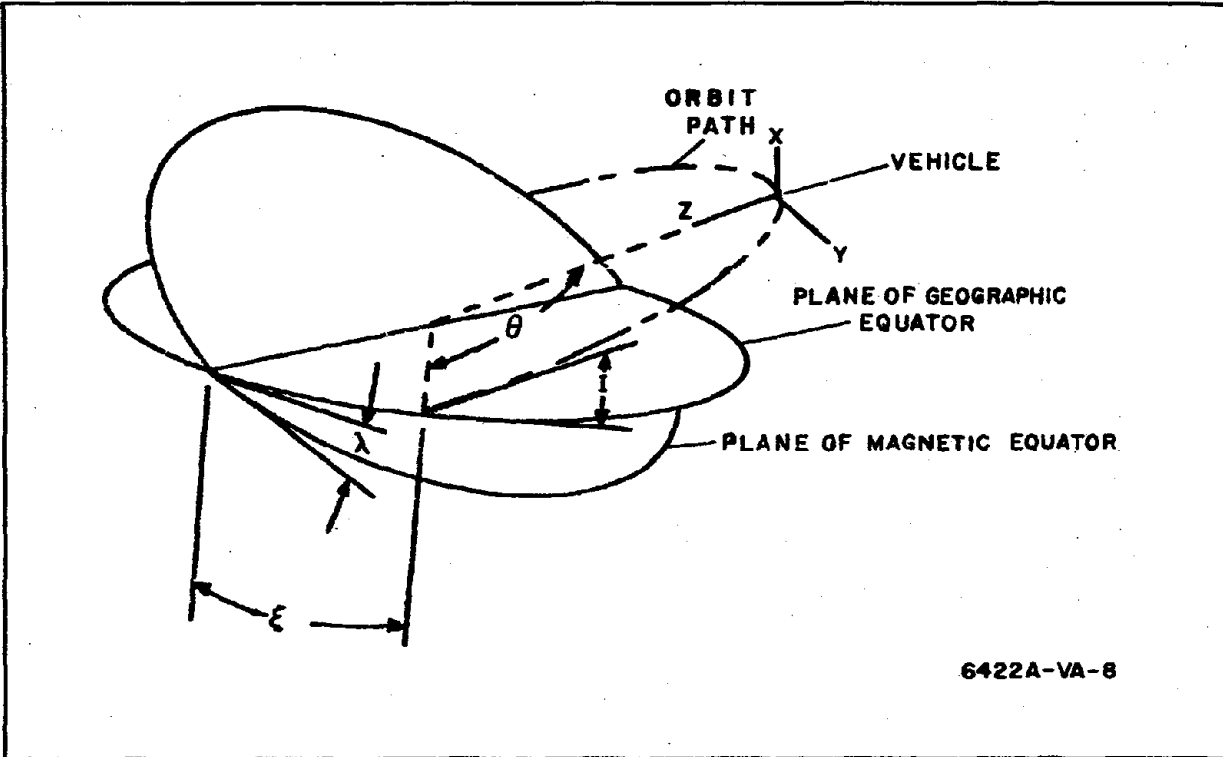


Figure 12. Transformation Angles

$$T_y = (I_z B_x - I_x B_z) = \dot{M}_y - T_{Dy}$$

$$T_z = (I_x B_y - I_y B_x) = \dot{M}_z - T_{Dz} - \omega_o M_x$$

where:  $k_1$  = Loop gain

$M_{x, y, z}$  = momentum about the x, y, z axis

$I_{x, y, z}$  = current ( $\frac{\text{ft-lb}}{\text{gauss}}$ ) about the x, y, z axis

$T_{x, y, z}$  = magnetic system torque about the x, y, z axis

$T_{Dx, Dy, Dz}$  = Disturbance torque about the x, y, z axis

$B_{x, y, z}$  = magnetic field along the x, y, z axis

$$\dot{M} = \frac{d}{dt} M$$

$\omega_o$  = orbital rate in radians/second

Figure 13 illustrates the simplified block diagram of the analog computer simulation\* (The mechanization of the dipole model equations is shown as a single block). The scaling was left unspecified so that both large and small amplitude effects could be studied without the problem of scale changes. Altitude changes would be reflected only in the velocity input to the  $\theta$  velocity servo. The time scaling was limited to 360/1 by velocity limitations of the multiplying servos. The basic control loop was concerned only with the momentum in orbit coordinates. It was not necessary to simulate the CMG loops in this first approximation, since the CMG system is conservative and merely serves to transfer the total vehicle momentum vector to achieve vehicle motion. Consequently, CMG system performance will have no effect on the total momentum vector.

Figure 14 shows a computer run of the earth's field components as a function of time for approximately one full day. In the simulation, the components were generated as a percent of  $K_0$  in order to simplify the resulting comparison with the derived equations, but  $\theta$  was set equivalent to a 200-mile orbit altitude, so that  $K_0$  is approximately 0.30 gauss.

From the problem definition in paragraph 5.1 it can be seen that the net unloading torque will be proportional to the function  $(1 - \cos \angle \frac{B}{M})$  where  $\angle \frac{B}{M}$  is the angle between the earth's magnetic field vector and the vehicle momentum vector. This means that the system will be least effective during orbits when the field tends to be pointed in the same direction and stored momentum exists along the time centroid of the field. Figure 14 illustrates that as the angle  $\xi$  approaches  $180^\circ$ , the field vector will tend to form a more narrow cone in rotating about the Y (orbit plane normal) axis. This occurs because the orbit plane most nearby approaches the magnetic equator when  $\xi = 180^\circ$ , and, consequently, the variations in  $B_x$  and  $B_z$  are minimal while  $B_y$  is at a maximum. The system design was thus based on optimizing the

---

\* (The complete simulation diagrams have been sent under item 5 of the contract.)

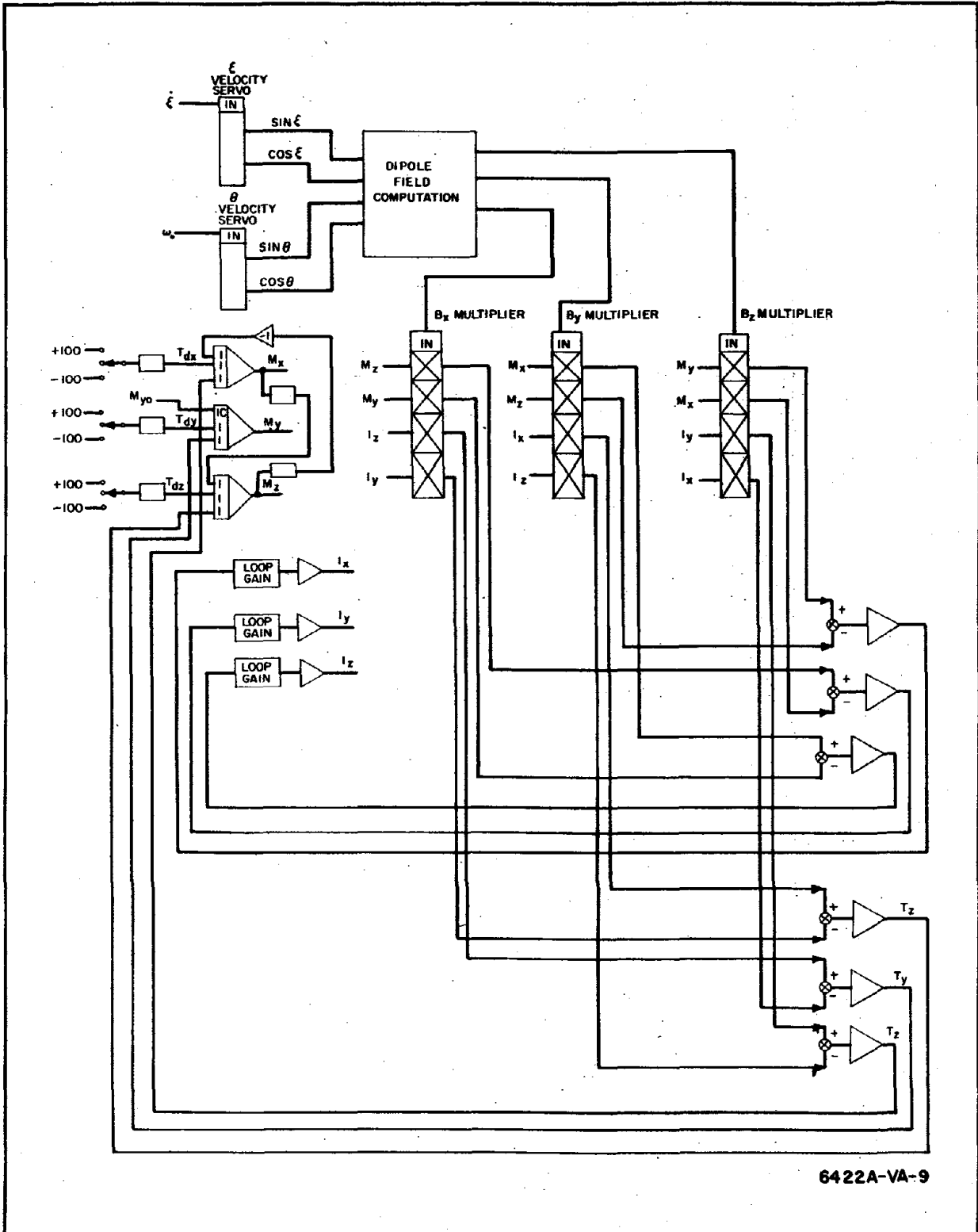


Figure 13. Block Diagram of Analog Computer Simulation

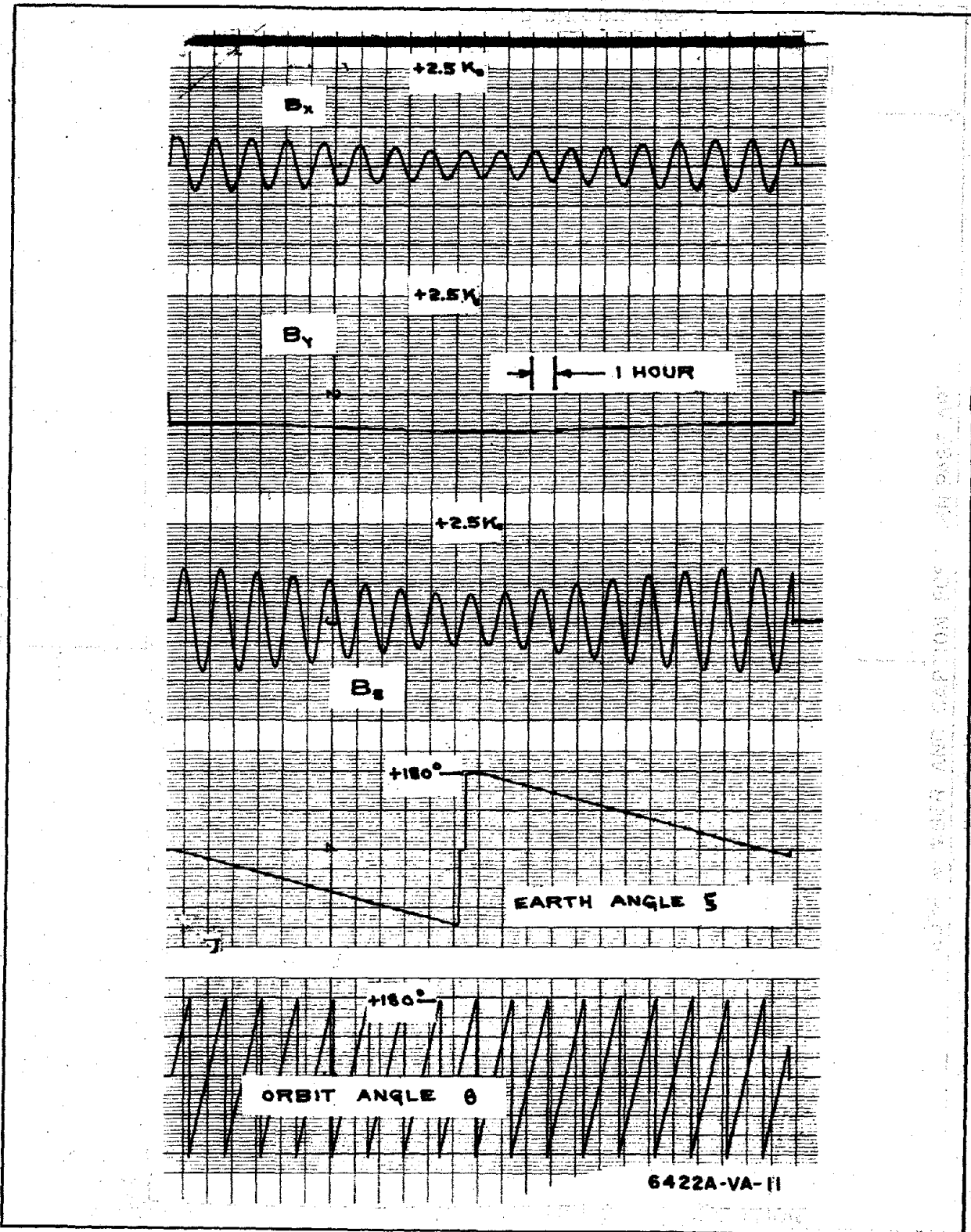


Figure 14. Field Components

unloading capability of the system during the period when  $\xi = 180$  degrees and a large momentum buildup is present about the Y axis. This could correspond to optimizing the unloading of an angular impulse generated by an orbit-correction linear impulse directed off the center of mass.

Analog runs were made for various orbit altitudes, inclinations, and various values of magnetic system gain. From these runs the curves similar to those of figure 3 for normalized y-axis torque as a function of system gain were derived. The normalized torque and the loop gain are both dimensionless quantities that are functions of altitude. The use of these quantities makes the curves of figure 3 applicable to all altitudes.

For every orbit inclination there is a value of  $\beta_{\text{rms}}$ , the rms value of the angle between the orbit plane and the magnetic equator plane as the earth rotates under the orbiting vehicle. Hereafter any reference to  $\beta$  will be a reference to  $\beta_{\text{rms}}$ .

Since the orbit inclination with respect to the magnetic equator is a function of time, and the desaturation capability of the system is a function of the square of the sine of the magnetic inclination angle ( $\beta$ ), the average effective (or rms) angle  $\beta$  was computed from the equation for the magnetic inclination angle:

$$\beta = \text{arc cos} \left[ -\sin \phi \cos \xi \sin \lambda + \cos \phi \cos \lambda \right]$$

which yields, for the average  $\sin^2 \beta$ :

$$\left[ \sin^2 \beta \right]_{\text{ave}} = \sin^2 \lambda + \sin^2 \phi \left[ 1 - \frac{3 \sin^2 \lambda}{2} \right]$$

where:  $\lambda$  = angle between the magnetic and geographic axes of the earth  
( $11.1^\circ$ )

$\phi$  = orbit inclination to the earth's equator.

$\xi$  = angle of ascending node measured with respect to the line of nodes made by the magnetic and geographic equators  
=  $160.1^\circ - \omega_e t$

$\omega_e$  = earth's rotation rate.

The rms value of  $\beta$  then becomes:

$$\beta_{\text{rms}} = \text{arc sin} \left[ \sqrt{(\sin^2 \beta)_{\text{ave}}} \right]$$

From these analog runs (figures 15, 16, and 17) it is seen that for one orbit the momentum can be expressed as shown below. The x and z axis have no zero frequency components and the y-axis can be approximated by a zero frequency component and a second harmonic of orbital frequency component.

$$M_x = -M_{x1} \sin(\theta + \mu)$$

$$M_y = M_{y0} + M_{y2} \sin[2(\theta + \xi)]$$

$$M_z = M_{z1} \cos(\theta + \psi)$$

where: M = Momentum

$\theta$  = orbit angle

$\mu, \xi, \psi$  = phase angles

In figures 15, 16, and 17 a peak value of  $M_y$  occurs at  $\xi = 180^\circ$ , and this is the region where system design was optimized.

In figures 18 through 20 the system momentum unloading capability is shown for x, y and z axis zero frequency disturbance torques. It is evident from these figures that the momentum buildup is maximum for y-axis disturbances, and that concentrating on the system y-axis performance at  $\xi = 180$  degrees is justified.

The normalized y-axis unloading torque (figure 3) is found to have a peak value for various orbit inclinations. Setting the loop gain higher than the value that yields the peak torque serves no useful purpose. At these higher gains ( $\alpha$ ) the system performance is degraded, and higher coil currents are required. The recordings of figures 21, 22, and 23 illustrate that the system performance is optimum for that gain that produces the peak unloading torque ( $\alpha = 1.2$  for the case illustrated). Figures 24 and 25 verify that the momentum unloading is slowest at  $\xi = 180$  degrees.

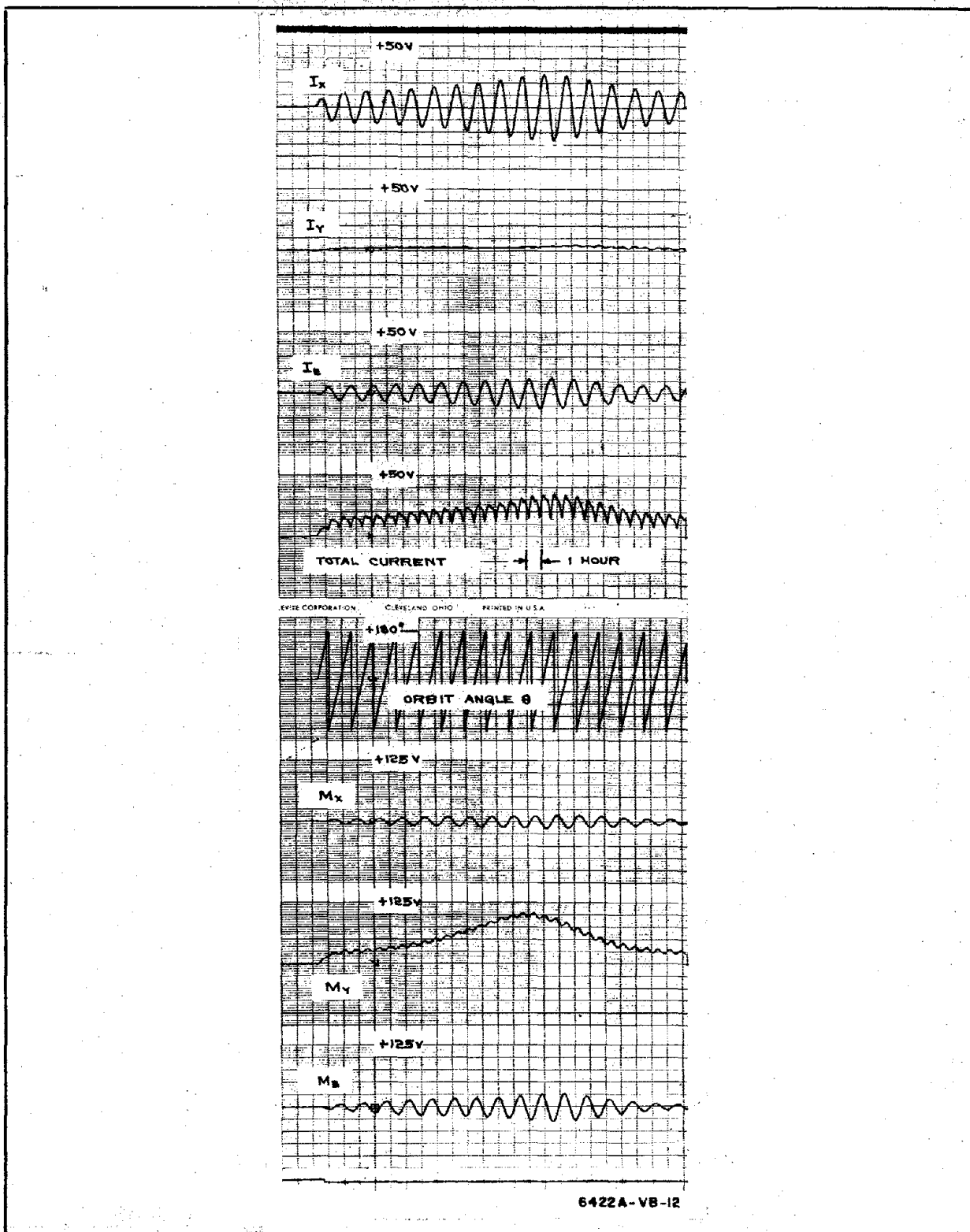


Figure 15. Y-Axis Disturbance Response at  $\alpha = 0.50$ ,  $\phi = 30^\circ$



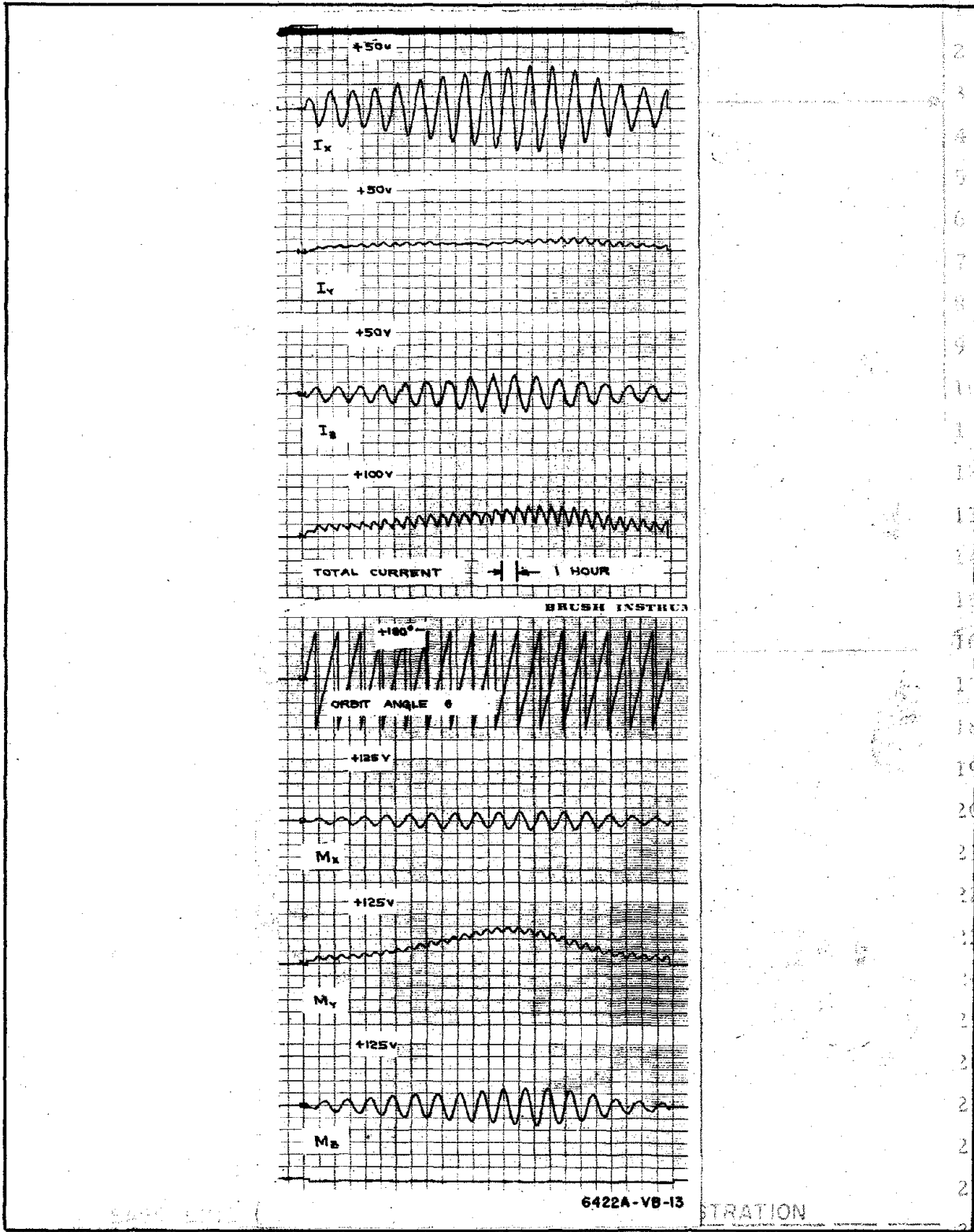


Figure 16. Y-Axis Disturbance Response at  $\alpha = 1.20$ ,  $\phi = 30^\circ$

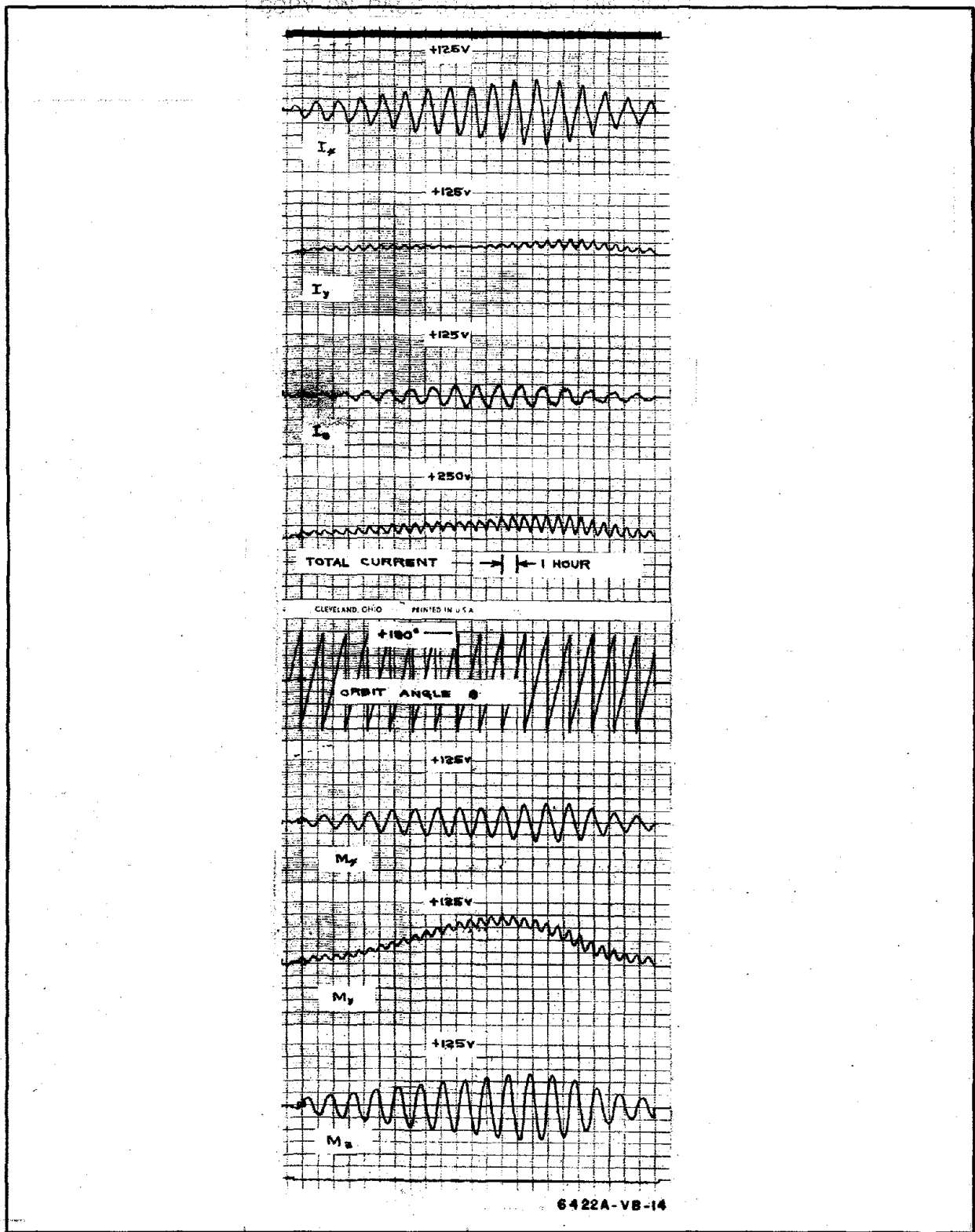


Figure 17. Y-Axis Disturbance Response at  $\alpha = 3.00$ ,  $\phi = 30^\circ$

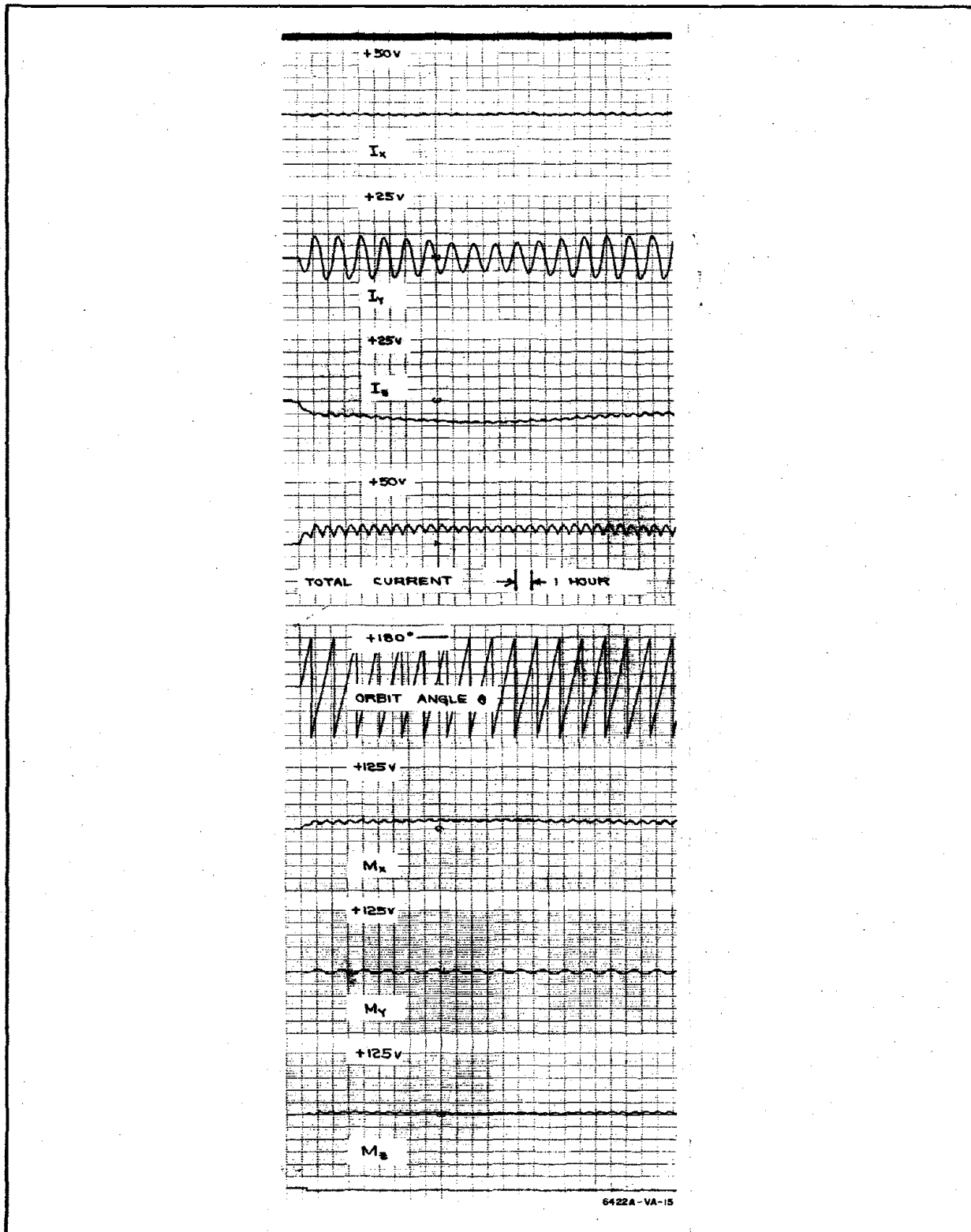


Figure 18. X-Axis Disturbance Response at  $\alpha = 0.7$ ,  $\phi = 30^\circ$

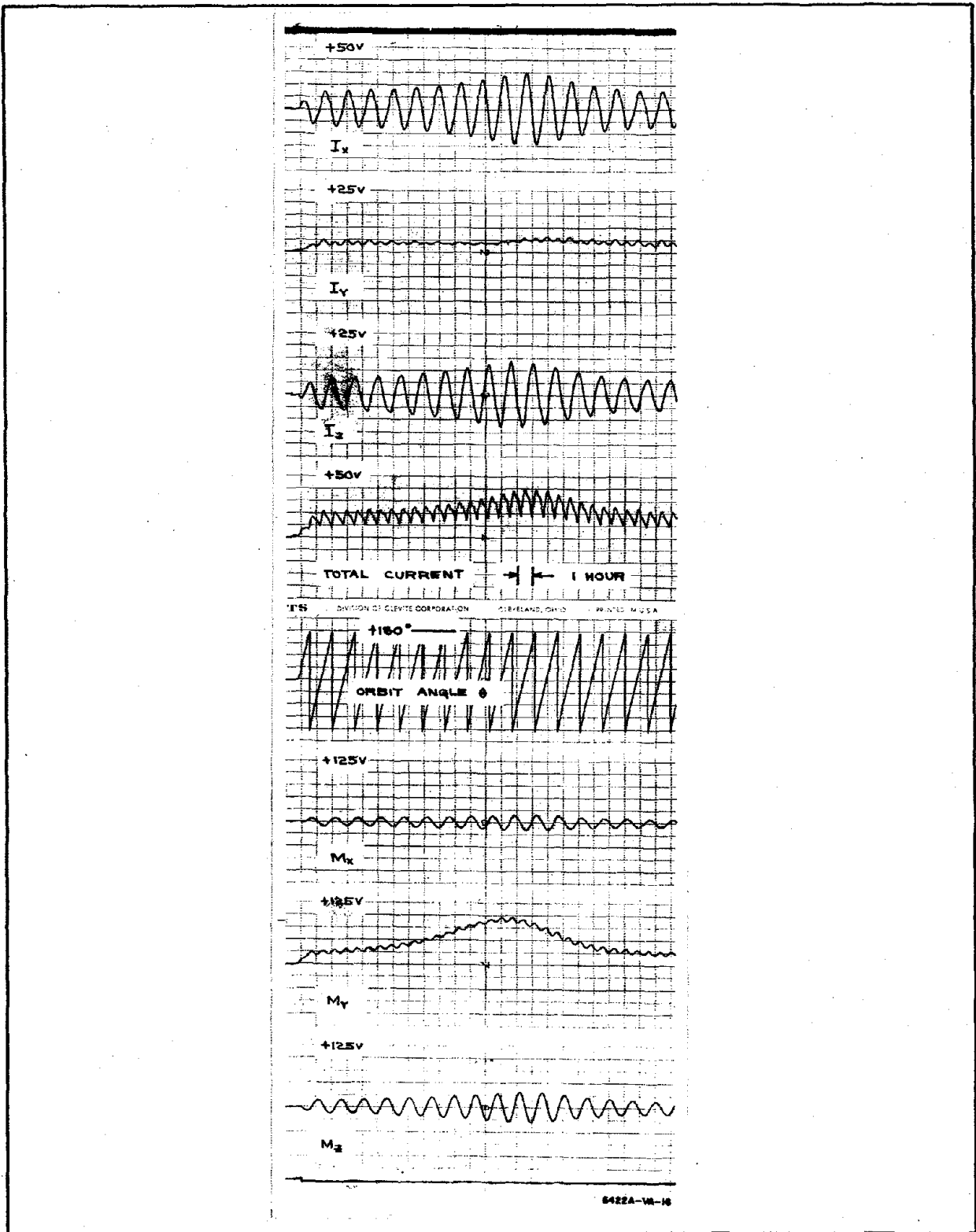


Figure 19. Y-Axis Disturbance Response at  $\alpha = 0.7$ ,  $\phi = 30^\circ$

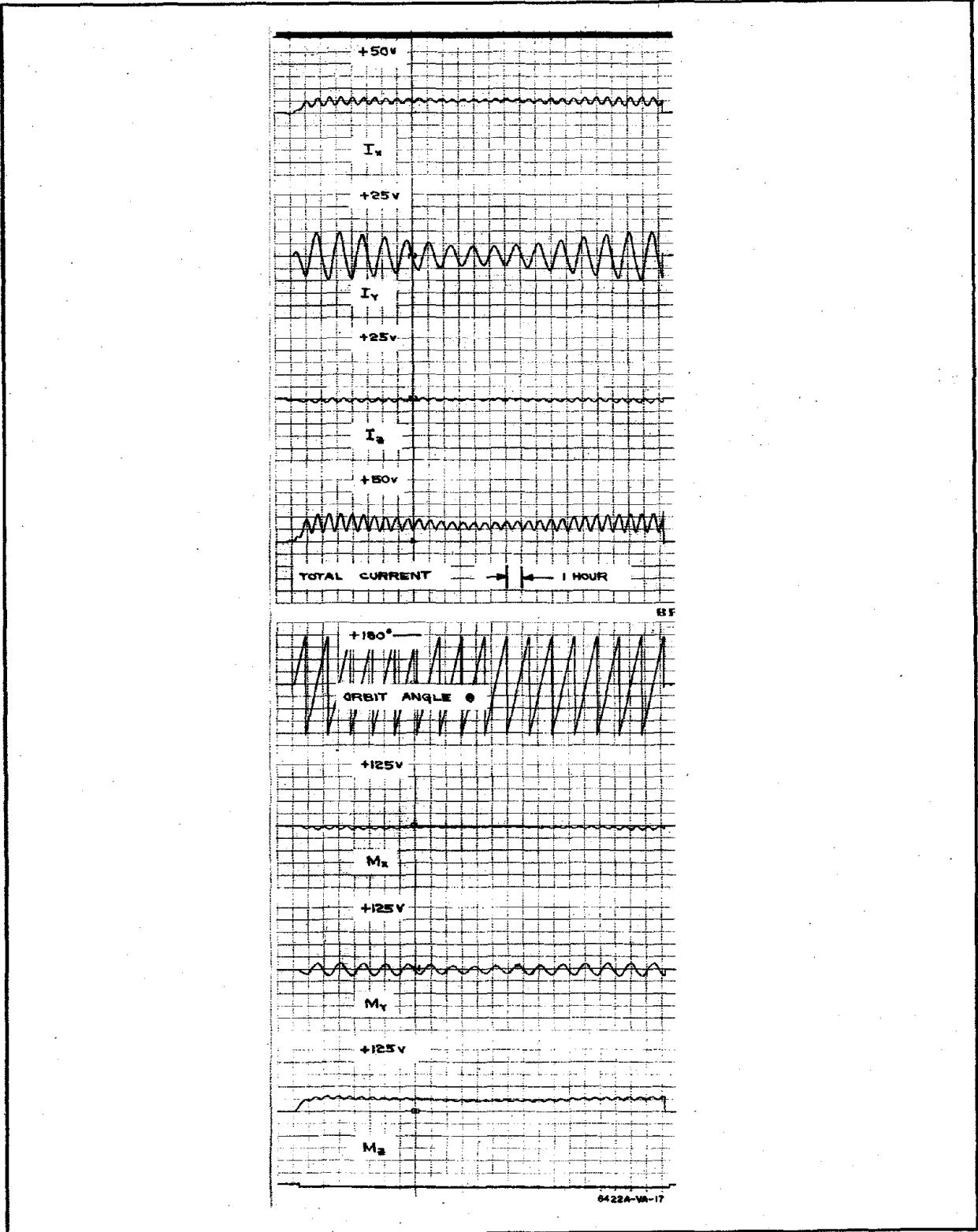


Figure 20. Z-Axis Disturbance Response at  $\alpha = 0.7$ ,  $\phi = 30^\circ$

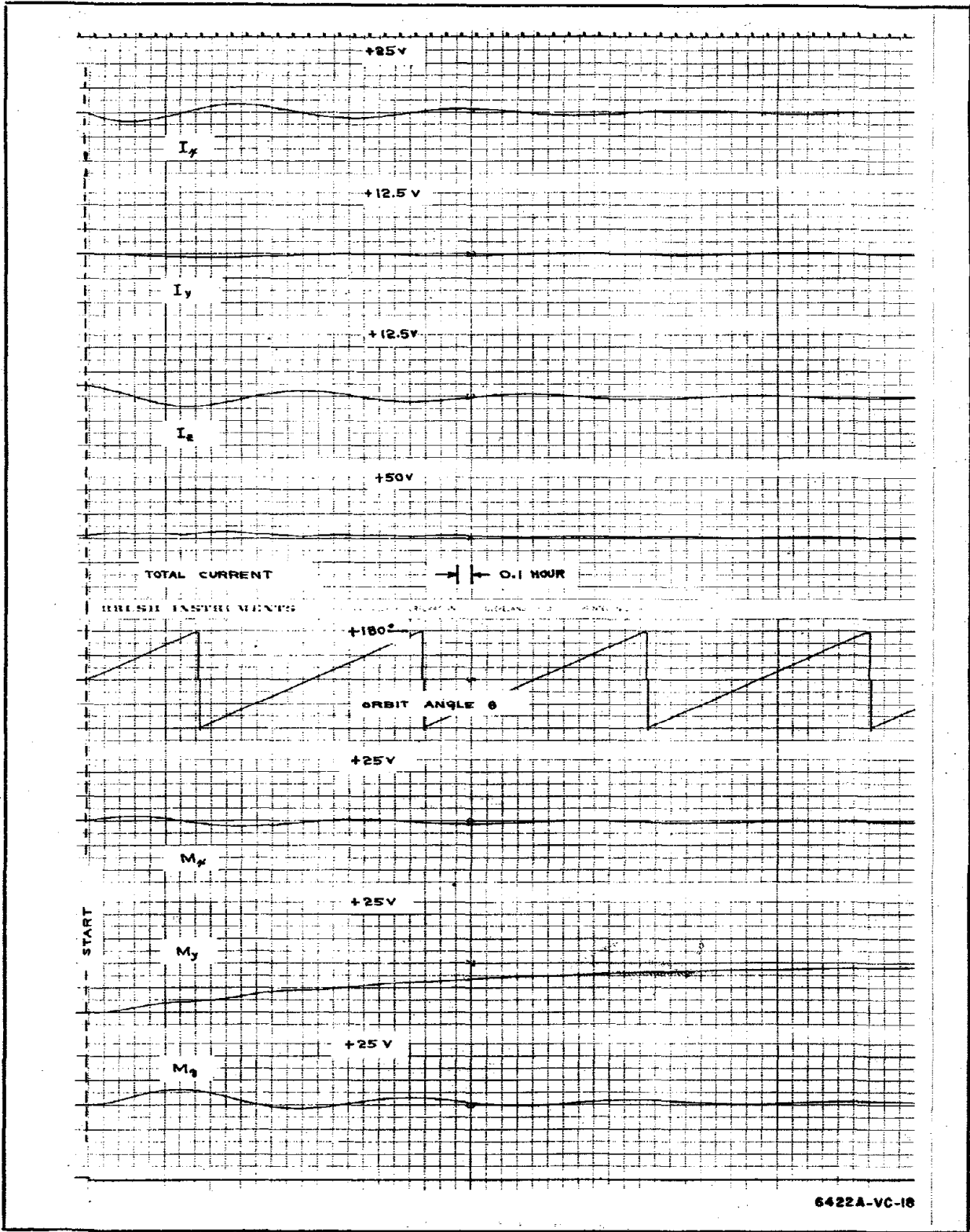


Figure 21. Unloading Response at  $\alpha = 0.50$ ,  $\phi = 30^\circ$

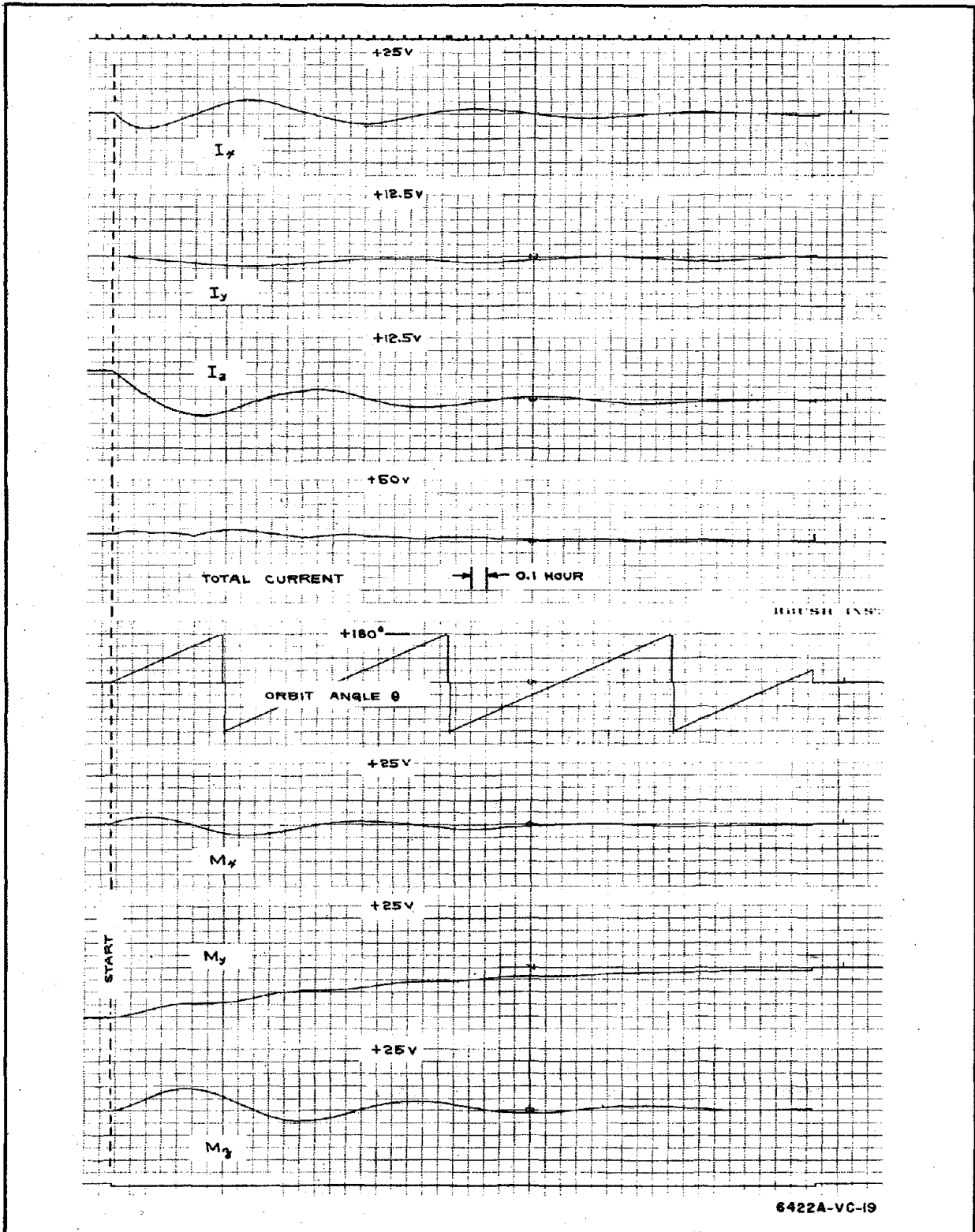


Figure 22. Unloading Response at  $\alpha = 1.20$ ,  $\phi = 30^\circ$

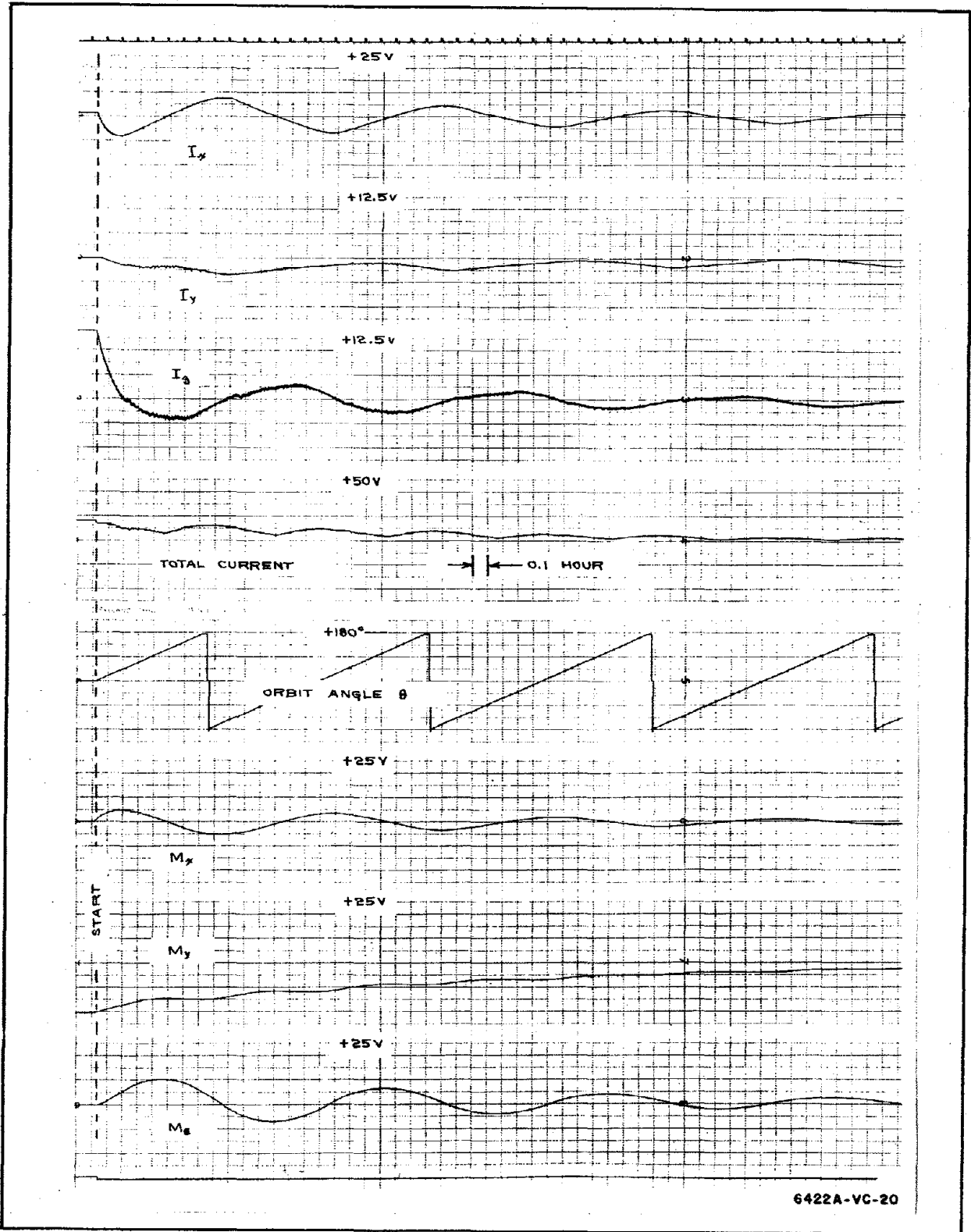


Figure 23. Unloading Response at  $\alpha = 3.00$ ,  $\phi = 30^\circ$



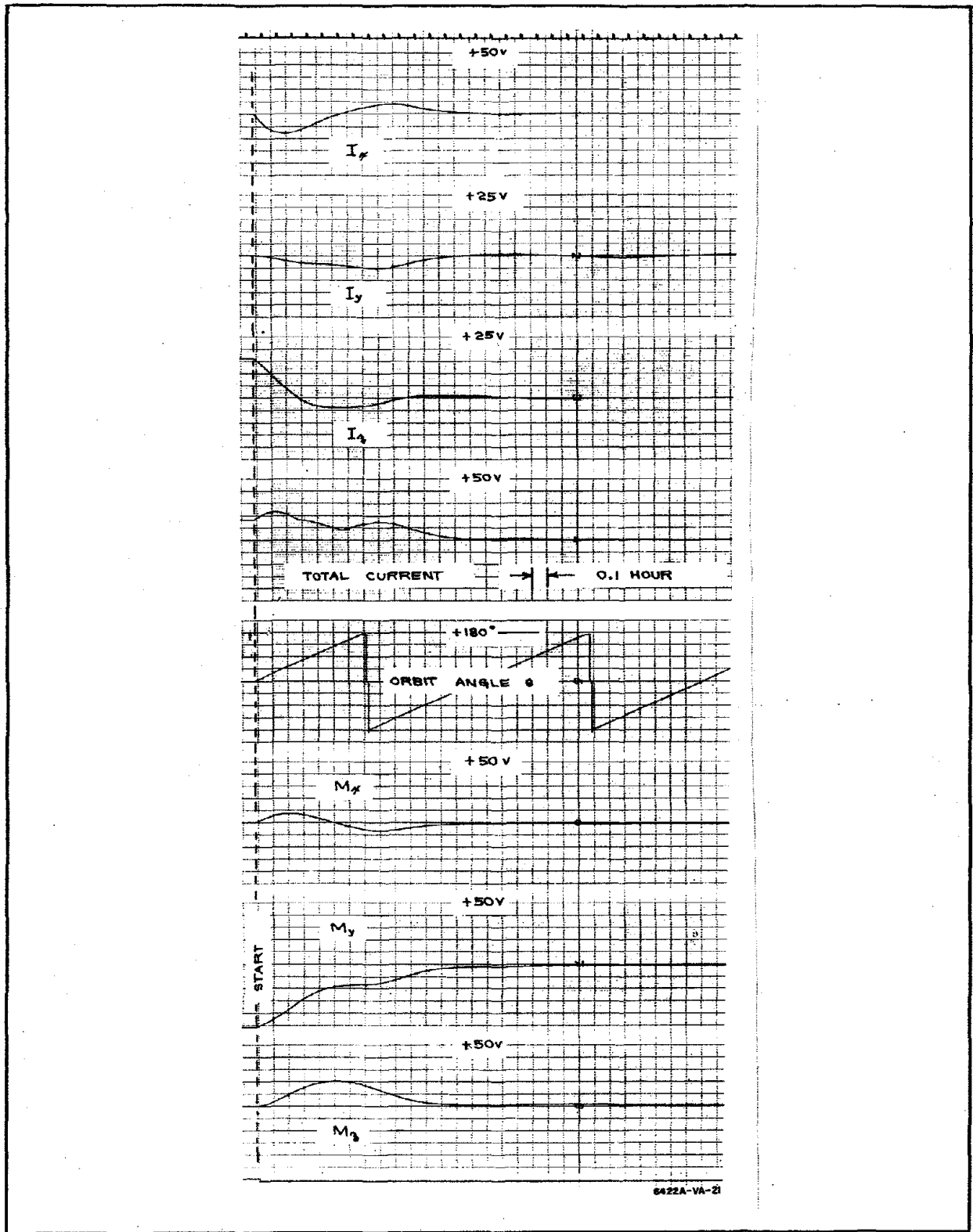


Figure 24. Unloading Response at  $\alpha = 0.60$  and  $\xi = 0$ ,  $\phi = 30^\circ$

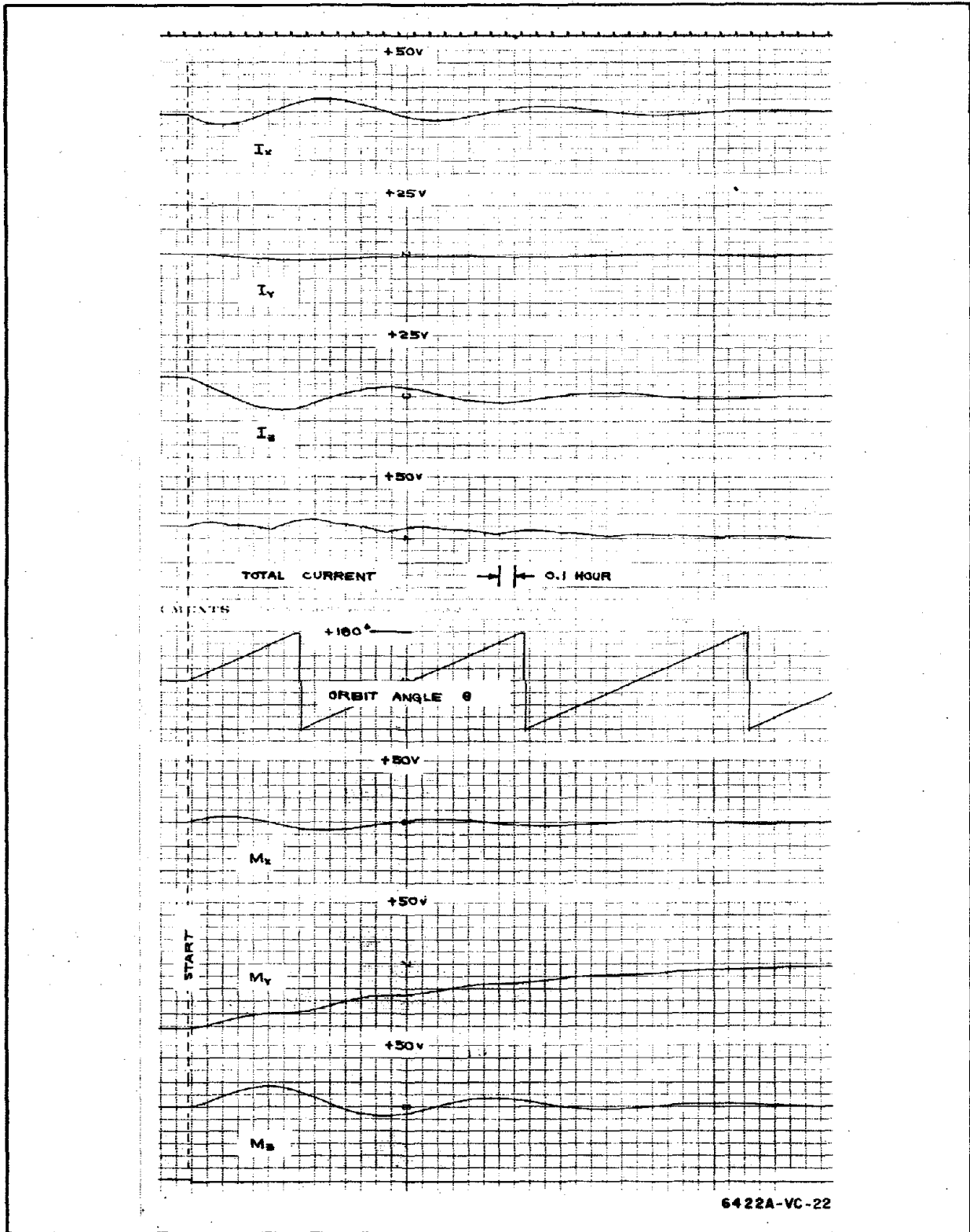


Figure 25. Unloading Response at  $\alpha = 0.60$  and  $\xi = 170$ ,  $\phi = 30^\circ$

When a lower-than-optimum unloading rate is acceptable, the use of a lower-than-optimum gain results in lower peak and average currents. This results in a lower system weight.

### 5.3 HAND SOLUTION

An analytical approach was used to verify the analog computer results and to find mathematical expressions for normalized torque. From the analog program the momentum equations for the three vehicle axes were found, at  $\xi = 180$  degrees, to be:

$$\begin{aligned} M_x &= -M_{x1} \sin(\theta + \mu) \\ M_y &= M_{y0} + M_{y2} \sin[2(\theta + \zeta)] \\ M_z &= M_{z1} \cos(\theta + \psi) \end{aligned}$$

In these equations  $\theta$  is the orbit angle and the magnitudes of the momentum components and their relative phase angles are functions of the system gain and of orbit inclination. The orbit angle is the angle between the right ascending node and the satellite position vector. It is possible to solve for the magnitudes and relative phase angles of the above equations by expressing the magnetic field as a function of the orbit angle and the orbit inclination, inserting these values into the torque expressions, and solving the vehicle equations of motion about the x and z axis.

The magnetic field can be represented by the equations

$$\begin{aligned} B_x &= K_0 \sin \beta \cos \theta \\ B_y &= -K_0 \cos \beta \\ B_z &= 2K_0 \sin \beta \sin \theta \end{aligned}$$

where  $\beta$  is the orbit inclination to the magnetic equator. (This, of course, presumes an orbit angular rate much greater than the earth's rotation rate).

The magnetic control system torques can be found from  $\bar{T} = k_0 (\bar{I} \times \bar{B})$ , where  $\bar{I} = k_1 (\bar{M} \times \bar{B})$ . When these torques are combined with the cross coupling torques about the vehicle axis, the torque expression about the x and z axis are found to be those given below, where  $\alpha = k_0 k_1 K_0^2 / \omega_0$ :

$$\begin{aligned}
\alpha M_{y0} \sin \beta \cos \beta \cos \theta = & M_{x1} \left[ \cos \theta \cos \mu - \sin \theta \sin \mu \right. \\
& + \alpha (\cos^2 \beta \cos \mu \sin \theta + \cos^2 \beta \sin \mu \\
& \cos \theta + 4 \sin^2 \beta \cos \mu \sin^3 \theta \\
& \left. + 4 \sin^2 \beta \sin \mu \cos \theta \sin^2 \theta) \right] \\
- \alpha M_{y2} & \left[ 2 \sin \beta \cos \beta \cos 2 \xi \cos^2 \theta \sin \theta \right. \\
& + \sin \beta \cos \beta \sin 2 \xi (\cos^3 \theta \\
& \left. - \cos \theta \sin^2 \theta) \right] \\
+ M_{z1} & \left[ \cos \psi \cos \theta - \sin \psi \sin \theta \right. \\
& + 2 \alpha \sin^2 \beta (\cos \psi \cos^2 \theta \sin \theta \\
& \left. - \sin \psi \cos \theta \sin^2 \theta) \right].
\end{aligned}$$

$$\begin{aligned}
2 \alpha M_{y0} \sin \beta \cos \beta \sin \theta = & M_{x1} \left[ \cos \mu \sin \theta + \sin \mu \cos \theta \right. \\
& - 2 \alpha \sin^2 \beta (\cos \mu \cos \theta \sin^2 \theta \\
& \left. + \sin \mu \cos^2 \theta \sin \theta) \right] \\
- 2 \alpha M_{y2} \sin \beta \cos \beta & \left[ \cos 2 \xi \cos \theta \sin^2 \theta \right. \\
& \left. + \sin 2 \xi (\cos^2 \theta \sin \theta - \sin^3 \theta) \right] \\
+ M_{z1} & \left[ \cos \psi \sin \theta + \sin \psi \cos \theta \right. \\
& - \alpha (\cos^2 \beta \cos \psi \cos \theta \\
& - \cos^2 \beta \sin \psi \sin \theta \\
& + \sin^2 \beta \cos \psi \cos^3 \theta \\
& \left. - \sin^2 \beta \sin \psi \cos^2 \theta \sin \theta) \right]
\end{aligned}$$

The above expressions are valid for all values of  $\theta$ , therefore substituting  $\theta$  equal to 0, 45, and 90 degrees gives us six equations which can be used to solve for the six unknowns. The six simultaneous equations are given below.

$$\begin{pmatrix} Z_1 \\ Z_2 \\ Z_3 \\ Z_4 \\ Z_5 \\ Z_6 \end{pmatrix} = \begin{pmatrix} N_{11} & N_{12} & N_{13} & N_{14} & N_{15} & N_{16} \\ N_{21} & N_{22} & N_{23} & N_{24} & N_{25} & N_{26} \\ N_{31} & N_{32} & N_{33} & N_{34} & N_{35} & N_{36} \\ N_{41} & N_{42} & N_{43} & N_{44} & N_{45} & N_{46} \\ N_{51} & N_{52} & N_{53} & N_{54} & N_{55} & N_{56} \\ N_{61} & N_{62} & N_{63} & N_{64} & N_{65} & N_{66} \end{pmatrix} \begin{pmatrix} X_1 \\ X_2 \\ X_3 \\ X_4 \\ X_5 \\ X_6 \end{pmatrix}$$

Where the unknowns are,

$$X_1 = M_{z1} \sin \psi / Y_1$$

$$X_2 = M_{z1} \cos \psi / Y_1$$

$$X_3 = M_{x1} \sin \mu / Y_1$$

$$X_4 = M_{x1} \cos \mu / Y_1$$

$$X_5 = M_{y2} \sin 2\zeta / Y_1$$

$$X_6 = M_{y2} \cos 2\zeta / Y_1$$

$$\text{and } Y_1 = M_{y0} \sin \beta \cos \beta$$

and the knowns are,

$$N_{11} = 0$$

$$N_{12} = 1$$

$$N_{13} = \alpha \cos^2 \beta$$

$$N_{14} = 1$$

$$N_{15} = -\alpha \sin \beta \cos \beta$$

$$N_{16} = 0$$

$$N_{21} = -1$$

$$N_{22} = 0$$

$$N_{23} = -1$$

$$N_{24} = \alpha (\cos^2 \beta + 4 \sin^2 \beta)$$

$$N_{25} = 0$$

$$N_{26} = 0$$

$$N_{31} = 1$$

$$N_{32} = -\alpha$$

$$\begin{aligned}
N_{33} &= 1 \\
N_{34} &= 0 \\
N_{35} &= 0 \\
N_{36} &= 0 \\
N_{41} &= N_{13} \\
N_{42} &= 1 \\
N_{43} &= 0 \\
N_{44} &= 1 \\
N_{45} &= -2 N_{15} \\
N_{46} &= 0 \\
N_{51} &= -(1 + \alpha \sin^2 \beta) \\
N_{52} &= -N_{51} \\
N_{53} &= -1 + 2 \alpha \sin^2 \beta + \alpha \cos^2 \beta \\
N_{54} &= N_{53} + 2 \\
N_{55} &= 0 \\
N_{56} &= N_{15} \\
N_{61} &= 1 + \alpha \cos^2 \beta + 0.5 \alpha \sin^2 \beta \\
N_{62} &= 2 - N_{61} \\
N_{63} &= 2 + N_{51} \\
N_{64} &= N_{63} \\
N_{65} &= 0 \\
N_{66} &= 2N_{15}
\end{aligned}$$

$$\begin{aligned}
Z_1 &= \alpha \\
Z_2 &= 0 \\
Z_3 &= 0 \\
Z_4 &= 2\alpha \\
Z_5 &= \alpha \\
Z_6 &= 2\alpha
\end{aligned}$$

When these equations have been solved for the X's, then it is possible to find the phase angles from

$$\begin{aligned}
\psi &= \tan^{-1} \left( \frac{X_1}{X_2} \right) \\
\mu &= \tan^{-1} \left( \frac{X_3}{X_4} \right) \\
2\xi &= \tan^{-1} \left( \frac{X_5}{X_6} \right)
\end{aligned}$$

Using the momentum and the magnetic field expressions, it is possible to obtain the y-axis torque due to the magnetic control system.

$$T_y = \omega_o \alpha \left\{ \begin{aligned}
&M_{x1} \sin \beta \cos \beta [\cos \mu \cos \theta \sin \theta + \sin \mu \cos^2 \theta] \\
&-M_{y0} \sin^2 \beta [\cos^2 \theta + 4 \sin^2 \theta] \\
&-M_{y2} \sin^2 \beta [\sin 2\xi (\cos^4 \theta + 3 \cos^2 \theta \sin^2 \theta - 4 \sin^4 \theta) \\
&\quad + \cos 2\xi (2 \cos^3 \theta \sin \theta + 8 \cos \theta \sin^3 \theta)] \\
&-2M_{z1} \sin \beta \cos \beta [\cos \psi \cos \theta \sin \theta - \sin \psi \sin^2 \theta]
\end{aligned} \right\}$$

The average torque is of interest and is found to be,

$$T_{av} = \omega_o \alpha \left\{ \begin{aligned} &\frac{1}{2} M_{x1} \sin \mu \sin \beta \cos \beta \\ &-\frac{5}{2} M_{y0} \sin^2 \beta \\ &+\frac{3}{4} M_{y2} \sin 2 \zeta \sin^2 \beta \\ &+M_{z1} \sin \psi \sin \beta \cos \beta \end{aligned} \right\}$$

Using the X's found in the solution of the six simultaneous equations, it is possible to get the normalized torque about the y-axis for a disturbance torque having an average value about the y-axis.

$$\text{Normalized Torque} = \frac{-T_{av}}{\omega_o M_{y0} \sin^2 \beta} = \alpha \left[ \begin{aligned} &2.5 - X_1 \cos^2 \beta \\ &- 0.5 X_3 \cos^2 \beta \\ &- 0.75 X_5 \sin \beta \cos \beta \end{aligned} \right]$$

The variation of y-axis unloading torque as a function of the normalized loop gain  $\alpha$  and the orbit-to-magnetic equator angle  $\beta$  is shown in figure 3.

The results of this hand solution check favorably with the analog data, giving added justification to the results.

When a vehicle is vertically aligned, the principal zero frequency torque sources (particularly at lower altitudes) will be due to aerodynamic pressure and gravity gradient effects due to inexact vertical alignment.\* Since these torques will produce a momentum vector buildup along the Y (normal to the orbit plane) axis, the capability of the CMG system to maneuver the vehicle will be compromised unless the magnetic desaturating system continuously transfers this momentum to the earth's field. A design goal of an average of 10 percent of CMG capacity as the steady state y-axis momentum was chosen.\*\* This steady state momentum is necessary to generate the coil

---

\* See Section III for assumed disturbances.

\*\* See table 1.



currents used to produce the desaturating torques.\*\*\* This would leave the vehicle with an average of 90 percent of its maneuvering capability while permitting operation under circumstances which would quickly saturate the CMG system if the magnetic desaturating system was not operating. The minimum inclination is based on the peak normalized y-axis torque as a function of loop gain as defined by the family of curves given on figure 3.

Table 1

STORED y-AXIS MOMENTUM =  $M_{Y0}$

Vehicle	A1	A2	A3	A4	A5	A6
$M_{Y0}$	6.14	141.4	403.	716.	1131.	872.

The required value of  $T_{av}/(\omega_o M_{Y0})$  is computed for each altitude from the equation:

$$\frac{T_{av}}{\omega_o M_{Y0}} = \frac{1}{\omega_o M_{Y0}} \left[ K_A h^n + \frac{3 J_{\Delta} \omega_o^2}{2} \sin 2 (\Delta \theta) \right]$$

where

$\omega_o$  = orbit rate

$M_{Y0}$  = average Y axis momentum

$K_A$  = aerodynamic torque constant proportional to surface area and c.m. - c.p. offset

$h$  = altitude in nautical miles

$n$  = constant = -7.02

$J_{\Delta}$  = difference between polar moments of inertia taken about the transverse and longitudinal axes

---

\*\*\* The alternative use of a bias momentum signal to generate the coil currents was rejected because this would require complex computation circuits and an exact knowledge of the vehicle parameters.

$\Delta\theta$  = average vertical offset about the pitch axis.

Letting  $\Delta\theta = 1^\circ$  as a maximum figure, the required value of  $T_{av}/(\omega_o M_{Y0})$  was computed as a function of altitude for each vehicle configuration and is given in table 2. Since the peak achievable value of  $T_{av}/(\omega_o M_{Y0})$  rises with increasing inclination, a minimum feasible altitude will exist for some vehicle-altitude combinations. This is demonstrated in figure 4.

Table 2  
REQUIRED VALUES OF  $T_{av}/(\omega_o M_{Y0})$

Altitude	Vehicle					
	A1	A2	A3	A4	A5	A6
100	11.31	4.62	3.13	2.82	2.29	2.42
200	0.438	0.218	0.164	0.158	0.137	0.140
300	0.0544	0.0615	0.0584	0.0621	0.0598	0.0582
400	0.0244	0.0477	0.0484	0.0587	0.0518	0.0500
500	0.0199	0.0446	0.0457	0.0500	0.0493	0.0474
600	0.0188	0.0430	0.0441	0.0483	0.0477	0.0459
700	0.0179	0.0413	0.0425	0.0465	0.0459	0.0441
800	0.0172	0.0396	0.0408	0.0446	0.0440	0.0423
900	0.0166	0.0384	0.0395	0.0432	0.0427	0.0411
1000	0.0161	0.0371	0.0382	0.0418	0.0412	0.0396

NOTE: The average disturbance torque can be found by multiplying the above values by the appropriate  $\omega_o$  and  $M_{Y0}$  (table 1)

e.g. for A2 at 200 nmi

$$\begin{aligned} \text{average disturbance torque} &= (0.218) (1.14 \times 10^{-3}) (141.4) \\ &= 0.0352 \text{ foot-pounds} \end{aligned}$$

For those cases where the CMG-stored momentum does not exceed the arbitrary 10 percent of rating level, it is possible to find the minimum value of loop gain that will provide an unloading torque sufficient to counteract the

zero frequency disturbance torque. The values of minimum loop gain  $\alpha$  are given in table 3.

Table 3  
VALUES OF MINIMUM  $\alpha$  THAT COUNTERACT MOMENTUM  
BUILDUP OF ASSUMED DISTURBANCES

Vehicle A1

Incl \ Alt	0	10	20	30	40	50	60	70	80	90
100	--	--	--	--	--	--	--	--	--	7.25
200	--	--	--	0.9	0.5	0.34	0.3	0.25	0.25	0.25
300	0.72	0.4	0.2	0.1	0.1	0.1	0.1	0.1	0.1	0.1
400	0.3	0.2	0.1	0.1	0.1	0.1	0.1	0.1	0.1	0.1
500	0.26	0.14	0.1	0.1	0.1	0.1	0.1	0.1	0.1	0.1
600	0.25	0.13	0.1	0.1	0.1	0.1	0.1	0.1	0.1	0.1
700	0.22	0.12	0.1	0.1	0.1	0.1	0.1	0.1	0.1	0.1
800	0.21	0.11	0.1	0.1	0.1	0.1	0.1	0.1	0.1	0.1
900	0.205	0.105	0.1	0.1	0.1	0.1	0.1	0.1	0.1	0.1
1000	0.2	0.1	0.1	0.1	0.1	0.1	0.1	0.1	0.1	0.1

Vehicle A2

Incl \ Alt	0	10	20	30	40	50	60	70	80	90
100	--	--	--	--	--	--	--	4.45	2.43	2.2
200	--	--	0.77	0.43	0.26	0.15	0.13	0.1	0.1	0.1
300	0.9	0.45	0.24	0.1	0.1	0.1	0.1	0.1	0.1	0.1
400	0.6	0.36	0.2	0.1	0.1	0.1	0.1	0.1	0.1	0.1
500	0.54	0.32	0.17	0.1	0.1	0.1	0.1	0.1	0.1	0.1
600	0.52	0.33	0.16	0.1	0.1	0.1	0.1	0.1	0.1	0.1
700	0.50	0.32	0.15	0.1	0.1	0.1	0.1	0.1	0.1	0.1
800	0.47	0.3	0.14	0.1	0.1	0.1	0.1	0.1	0.1	0.1
900	0.45	0.3	0.14	0.1	0.1	0.1	0.1	0.1	0.1	0.1
1000	0.44	0.27	0.12	0.1	0.1	0.1	0.1	0.1	0.1	0.1

Table 3 (Continued)

## Vehicle A3

Incl Alt	0	10	20	30	40	50	60	70	80	90
100	--	--	--	--	--	--	--	1.9	1.57	1.46
200	--	--	0.57	0.3	0.2	0.1	0.1	0.1	0.1	0.1
300	0.8	0.42	0.23	0.1	0.1	0.1	0.1	0.1	0.1	0.1
400	0.61	0.38	0.2	0.1	0.1	0.1	0.1	0.1	0.1	0.1
500	0.57	0.34	0.17	0.1	0.1	0.1	0.1	0.1	0.1	0.1
600	0.53	0.33	0.16	0.1	0.1	0.1	0.1	0.1	0.1	0.1
700	0.51	0.31	0.15	0.1	0.1	0.1	0.1	0.1	0.1	0.1
800	0.49	0.30	0.15	0.1	0.1	0.1	0.1	0.1	0.1	0.1
900	0.47	0.3	0.14	0.1	0.1	0.1	0.1	0.1	0.1	0.1
1000	0.35	0.22	0.1	0.1	0.1	0.1	0.1	0.1	0.1	0.1

## Vehicle A4

Incl Alt	0	10	20	30	40	50	60	70	80	90
100	--	--	--	--	--	--	2.9	1.7	1.4	1.3
200	--	--	0.53	0.3	0.2	0.1	0.1	0.1	0.1	0.1
300	0.9	0.45	0.25	0.1	0.1	0.1	0.1	0.1	0.1	0.1
400	0.68	0.4	0.2	0.1	0.1	0.1	0.1	0.1	0.1	0.1
500	0.65	0.38	0.2	0.1	0.1	0.1	0.1	0.1	0.1	0.1
600	0.62	0.37	0.2	0.1	0.1	0.1	0.1	0.1	0.1	0.1
700	0.59	0.37	0.18	0.1	0.1	0.1	0.1	0.1	0.1	0.1
800	0.57	0.34	0.15	0.1	0.1	0.1	0.1	0.1	0.1	0.1
900	0.52	0.33	0.15	0.1	0.1	0.1	0.1	0.1	0.1	0.1
1000	0.5	0.32	0.14	0.1	0.1	0.1	0.1	0.1	0.1	0.1

Table 3 (Continued)

Vehicle A5

Alt \ Incl	0	10	20	30	40	50	60	70	80	90
100	--	--	--	--	--	--	1.7	1.3	1.1	1.08
200	--	1.4	0.47	0.27	0.16	0.1	0.1	0.1	0.1	0.1
300	0.83	0.44	0.23	0.1	0.1	0.1	0.1	0.1	0.1	0.1
400	0.67	0.4	0.2	0.1	0.1	0.1	0.1	0.1	0.1	0.1
500	0.63	0.37	0.2	0.1	0.1	0.1	0.1	0.1	0.1	0.1
600	0.6	0.35	0.19	0.1	0.1	0.1	0.1	0.1	0.1	0.1
700	0.57	0.34	0.18	0.1	0.1	0.1	0.1	0.1	0.1	0.1
800	0.55	0.33	0.17	0.1	0.1	0.1	0.1	0.1	0.1	0.1
900	0.52	0.32	0.16	0.1	0.1	0.1	0.1	0.1	0.1	0.1
1000	0.5	0.3	0.15	0.1	0.1	0.1	0.1	0.1	0.1	0.1

Vehicle A6

Alt \ Incl	0	10	20	30	40	50	60	70	80	90
100	--	--	--	--	--	--	1.87	1.43	1.2	1.15
200	--	1.5	0.5	0.27	0.15	0.1	0.1	0.1	0.1	0.1
300	0.8	0.43	0.23	0.1	0.1	0.1	0.1	0.1	0.1	0.1
400	0.65	0.38	0.2	0.1	0.1	0.1	0.1	0.1	0.1	0.1
500	0.6	0.35	0.19	0.1	0.1	0.1	0.1	0.1	0.1	0.1
600	0.58	0.33	0.18	0.1	0.1	0.1	0.1	0.1	0.1	0.1
700	0.53	0.33	0.16	0.1	0.1	0.1	0.1	0.1	0.1	0.1
800	0.52	0.32	0.15	0.1	0.1	0.1	0.1	0.1	0.1	0.1
900	0.5	0.3	0.15	0.1	0.1	0.1	0.1	0.1	0.1	0.1
1000	0.47	0.3	0.14	0.1	0.1	0.1	0.1	0.1	0.1	0.1

In addition to the continuous removal of momentum caused by aerodynamic and gravity gradient disturbances, the dumping of an initial momentum vector is of importance. The time required to dump 90 percent of the momentum is called the decay time.

It can be shown that for an initial momentum vector  $M_o$ , having two components,  $M_{Y_o}$  along the vehicle y (pitch) axis and  $M_{P_o}$  perpendicular to the y-axis, the equations for desaturating the momentum vector in the absence of disturbance torques are:

$$\dot{M}_p + A_1 M_p - A_2 M_y = 0$$

$$-A_3 M_p + \dot{M}_y + A_4 M_y = 0$$

where  $A_1 = (1 + 0.125 \sin^2 \beta) \alpha \omega_o$

$$A_2 = A_3 = 0.5 \alpha \omega_o \sin \beta \cos \beta$$

$$A_4 = 2.5 \alpha \omega_o \sin^2 \beta$$

$M_p$  = momentum vector lying in the orbit plane

$M_y$  = momentum vector lying normal to the orbit plane

$\dot{M}_p, \dot{M}_y$  = time derivatives of  $M_p$  and  $M_y$

$\alpha$  = dimensionless loop gain

$\omega_o$  = orbit angular rate

$\beta$  = orbit magnetic inclination

The solution to this pair of equations in terms of initial values of momentum yields these approximate solutions:

$$M_p(t) = M_{P_o} e^{-\alpha \omega_o t} \frac{0.5 M_{Y_o} \sin \beta \cos \beta}{[2.5 \sin^2 \beta - 1]} (e^{-\alpha \omega_o t} - e^{-2.5 \alpha \omega_o t \sin^2 \beta})$$

$$M_Y(t) = M_{Y_0} e^{-2.5 \alpha \omega_0 t} \frac{0.5 M_{P_0} \sin \beta \cos \beta}{[2.5 \sin^2 \beta - 1]} (e^{-\alpha \omega_0 t} - e^{-2.5 \alpha \omega_0 t \sin^2 \beta})$$

where  $M_P(t)$ ,  $M_Y(t)$  = instantaneous value of momentum vector components at time  $t$

The effect of the cross coupling is to lengthen the time for the desaturation process since momentum buildup occurs out of plane/axis and this momentum must in turn be decreased. The dimensionless time ( $\alpha \omega_0 t$ ) required to reduce the total momentum vector\* to 10 percent of its original value is shown on figure 4 for the cases where  $M_{Y_0} = 0$  and  $M_{P_0} = 0$ . Table 4 gives the values of ( $\alpha \omega_0 t$ ) for various combinations of  $M_{Y_0}$  and  $M_{P_0}$ .

Table 4  
TABLE OF DIMENSIONLESS DECAY TIME ( $\alpha \omega_0 t = T_D$ )

Orbit Inclination Degrees	$M_{Y_0} = M_0$	$M_{Y_0} = 0.972 M_0$	$M_{Y_0} = 0.895 M_0$	$M_{Y_0} = 0.80 M_0$	$M_{Y_0} = 0.707 M_0$	$M_{Y_0} = 0$
	$M_{P_0} = 0$	$M_{P_0} = 0.243 M_0$	$M_{P_0} = 0.447 M_0$	$M_{P_0} = 0.60 M_0$	$M_{P_0} = 0.707 M_0$	$M_{P_0} = M_0$
0	24.5	24.5	23.9	22.9	21.9	2.72
10	14.93	14.97	14.6	14.13	13.54	2.90
20	6.33	6.42	6.37	6.22	6.03	2.93
30	3.52	3.66	3.70	3.67	3.63	2.60
40	2.31	2.53	2.65	2.71	2.73	2.42
50	1.67	1.96	2.17	2.295	2.36	2.35
60	1.305	1.64	1.92	2.09	2.195	2.32
70	1.08	1.42	1.76	1.97	2.09	2.30
80	.99	1.27	1.66	1.89	2.04	2.30
90	.95	1.21	1.61	1.86	2.01	2.30

\*Total momentum is  $\sqrt{M_P^2(t) + M_Y^2(t)}$

The dimensionless decay time can be used to find the actual decay time in orbits when the minimum  $\alpha$  (table 3), the maximum  $\alpha$  (figure 3) or some intermediate  $\alpha$  is used. It is also possible to solve for  $\alpha$  when the decay time is predetermined.

$$N = T_D / (2\pi \alpha)$$

or

$$\alpha = T_D / (2\pi N)$$

where

$$N = \text{Decay time in orbits}$$

$$T_D = (\alpha \omega_o t) \text{ from table 4}$$

$$\alpha = \text{dimensionless loop gain}$$

The determining factor in choosing the magnetic momentum unloading system gain is often the weight. To determine the weight of the system it is necessary to size the coil in peak torque per unit magnetic field (ft-lb/gauss). The current (I) used to find the magnetic system torque has the correct units, and the coils can be sized by finding the peak values of the axial current components.

For that case where the magnetic system counters the momentum buildup caused by zero frequency disturbances the axial currents are found by

$$\bar{I} = K_1 (\bar{M} \times \bar{B}).$$

$$I_x = K_1 K_o [ 2M_{yo} \sin \beta \sin \theta + 2M_{y2} \sin \beta \sin \theta \sin \{2(\theta + \xi)\} \\ + M_{z1} \cos \beta \cos (\theta + \psi) ]$$

$$I_y = K_1 K_o [ 2M_{x1} \sin \beta \sin \theta \sin (\theta + \mu) + M_{z1} \sin \beta \cos \theta \cos (\theta + \psi) ]$$

$$I_z = K_1 K_o [ M_{x1} \cos \beta \sin (\theta + \mu) - M_{yo} \sin \beta \cos \theta \\ - M_{y2} \sin \beta \cos \theta \sin \{2(\theta + \xi)\} ]$$



The above equations are derived from the  $\bar{M}$  and  $\bar{B}$  components given earlier, where  $\theta$  is orbit angle and  $\beta$  is orbit inclination to the magnetic equator. When the high frequency components are dropped from the above equations and they are expressed in terms of the unknowns solved earlier, we find the following to be true:

$$\frac{I_x}{k_1 K_o M_{yo}} = [ 2 \sin \beta \sin \theta + (X_6 + X_2) \sin^2 \beta \cos \beta \cos \theta \\ - (X_5 \sin \beta + X_1 \cos \beta) \sin \beta \cos \beta \sin \theta ]$$

$$\frac{I_y}{k_1 K_o M_{yo}} = \sin^2 \beta \cos \beta [ (2X_3 - X_1) \sin \theta \cos \theta + 2X_4 \sin^2 \theta \\ + X_2 \cos^2 \theta ]$$

$$\frac{I_z}{k_1 K_o M_{yo}} = [ -\sin \beta \cos \theta + (X_3 \cos \beta - 0.5 X_5 \sin \beta) \sin \beta \cos \beta \cos \theta \\ + (X_4 \cos \beta - 0.5 X_6 \sin \beta) \sin \theta ]$$

When the equations defining the X's have been solved and the values of the X's inserted into the above equations, the peak values of the three component currents can be found, for the minimum  $\alpha$ . Using values of  $M_{yo}$  equal to 10 percent of the y-axis momentum storage capacity, in the expression below, the peak currents of table 5 can be found.

$$I_{\text{any axis}} = \alpha \left( \frac{\omega_o}{K_o} \right) M_{yo} \left[ \frac{I}{k_1 K_o M_{yo}} \right]$$

where  $K_o = \text{Dipole field magnitude} = .312 r_e^3 / (r_e + h)^3$

$r_e = \text{radius of the earth} = 3440 \text{ nmi.}$

$h = \text{orbit altitude in nmi.}$

$\omega_o$  = orbit rate in radians/second

$\alpha, M_{yo}$  are from tables 1 and 3

$\frac{I}{k_1 K_o M_{yo}}$  = values from above equations

For cases where the system's main function is unloading of specific initial momenta, the torquer size may be larger than indicated above. These situations can be examined by using the current expressions associated with the momentum decay equations given earlier.

$$I_x = \alpha \left( \frac{\omega_o}{K_o} \right) \left[ - (M_{po} + K_{cc} M_{yo}) \cos \beta \sin \theta \right. \\ \left. + 2 (M_{yo} + K_{cc} M_{po}) \sin \beta \cos \theta \right]$$

$$I_y = \alpha \left( \frac{\omega_o}{K_o} \right) \left[ -1.5 (M_{po} + K_{cc} M_{yo}) \sin \beta \sin 2\theta \right]$$

$$I_z = \alpha \left( \frac{\omega_o}{K_o} \right) \left[ - (M_{po} + K_{cc} M_{yo}) \cos \beta \cos \theta \right. \\ \left. - (M_{yo} + K_{cc} M_{po}) \sin \beta \cos \theta \right]$$

Table 5

PEAK VALUES OF FT-LB/GAUSS, USING MINIMUM  $\alpha$   
 VEHICLE A1 (CURRENTS IN  $10^{-2}$  FT-LB/GAUSS)  
 X-AXIS CURRENT

H \ I	0	10	20	30	40	50	60	70	80	90
100	--	--	--	--	--	--	--	--	--	36.3
200	--	--	--	1.66	1.39	1.04	1.13	1.02	1.08	1.12
300	0.501	0.278	0.320	0.231	0.300	0.354	0.395	0.425	0.450	0.470
400	0.250	0.160	0.171	0.240	0.313	0.368	0.411	0.443	0.469	0.489
500	0.219	0.114	0.177	0.249	0.324	0.380	0.426	0.459	0.486	0.507
600	0.217	0.113	0.183	0.257	0.335	0.394	0.440	0.474	0.502	0.524
700	0.200	0.106	0.190	0.267	0.348	0.410	0.457	0.492	0.521	0.544
800	0.198	0.100	0.198	0.278	0.361	0.425	0.475	0.513	0.542	0.565
900	0.197	0.097	0.204	0.287	0.373	0.438	0.491	0.530	0.560	0.585
1000	0.200	0.100	0.212	0.297	0.386	0.452	0.508	0.548	0.580	0.605

Y-AXIS CURRENT

H \ I	0	10	20	30	40	50	60	70	80	90
100	--	--	--	--	--	--	--	--	--	16.3
200	--	--	--	1.03	0.360	0.174	0.110	0.102	0.182	0.254
300	0.306	0.228	0.131	0.064	0.064	0.053	0.028	0.033	0.072	0.111
400	0.087	0.087	0.058	0.067	0.067	0.055	0.029	0.035	0.075	0.116
500	0.090	0.060	0.060	0.069	0.069	0.057	0.030	0.036	0.078	0.120
600	0.062	0.056	0.062	0.071	0.071	0.059	0.030	0.037	0.081	0.124
700	0.064	0.052	0.064	0.074	0.074	0.061	0.032	0.039	0.084	0.129
800	0.067	0.050	0.067	0.077	0.077	0.064	0.035	0.040	0.087	0.134
900	0.069	0.048	0.069	0.080	0.080	0.066	0.035	0.042	0.090	0.138
1000	0.072	0.047	0.072	0.082	0.082	0.068	0.036	0.043	0.093	0.146

Table 5 (Continued)

Z-AXIS CURRENT

I \ H	0	10	20	30	40	50	60	70	80	90
100	--	--	--	--	--	--	--	--	--	16.9
200	--	--	--	1.47	1.09	0.848	0.830	0.735	0.765	0.768
300	0.500	0.373	0.284	0.192	0.231	0.264	0.289	0.308	0.320	0.320
400	0.235	0.200	0.148	0.200	0.240	0.275	0.302	0.322	0.333	0.333
500	0.201	0.142	0.148	0.200	0.240	0.276	0.405	0.322	0.334	0.334
600	0.201	0.135	0.153	0.204	0.249	0.285	0.312	0.333	0.345	0.345
700	0.183	0.130	0.158	0.214	0.258	0.295	0.322	0.344	0.356	0.356
800	0.184	0.125	0.164	0.222	0.267	0.306	0.335	0.357	0.370	0.370
900	0.190	0.128	0.176	0.238	0.287	0.328	0.359	0.384	0.397	0.397
1000	0.193	0.125	0.182	0.247	0.297	0.340	0.372	0.397	0.411	0.411

VEHICLE A2 (CURRENTS IN  $10^{-2}$  FT-LB/GAUSS)

X-AXIS CURRENT

I \ H	0	10	20	30	40	50	60	70	80	90
100	--	--	--	--	--	--	--	349	229	229
200	--	--	24.1	20.9	16.8	52.2	11.3	9.41	9.96	10.4
300	12.7	7.96	8.60	5.32	6.93	8.15	9.11	9.82	10.4	10.8
400	9.20	6.60	7.67	5.53	7.20	8.47	9.47	10.2	10.8	11.3
500	8.65	6.08	6.92	5.74	7.47	8.78	9.82	10.6	11.2	11.7
600	8.58	6.51	6.51	5.93	7.72	9.08	10.2	10.9	11.6	12.1
700	8.52	6.52	5.04	6.15	8.00	9.41	10.5	11.3	12.0	12.5
800	8.50	6.34	4.87	6.41	8.34	9.82	10.9	11.8	12.5	13.1
900	8.46	6.54	4.71	6.62	8.62	10.1	11.3	12.2	12.9	13.5
1000	8.52	6.12	4.88	6.86	8.93	10.5	11.7	12.6	13.4	13.9

Table 5 (Continued)

## Y-AXIS CURRENT

H \ I	0	10	20	30	40	50	60	70	80	90
100	--	--	--	--	--	--	--	100	55.8	45.2
200	--	--	17.8	8.73	3.93	1.78	0.861	0.738	1.59	2.46
300	8.98	6.54	3.85	1.48	1.48	1.22	0.642	0.770	1.67	2.56
400	6.00	4.53	3.13	1.53	1.53	1.27	0.667	0.800	1.73	2.67
500	5.53	3.87	2.70	1.59	1.59	1.31	0.692	0.830	1.80	2.77
600	5.01	3.86	2.57	1.64	1.64	1.35	0.715	0.858	1.86	2.86
700	5.19	4.15	2.37	1.70	1.70	1.41	0.741	0.889	1.93	2.96
800	4.64	3.94	2.32	1.78	1.78	1.47	0.773	0.927	2.01	3.10
900	3.99	4.70	2.39	1.83	1.83	1.51	0.798	0.957	2.07	3.19
1000	4.13	3.72	2.07	1.90	1.90	1.57	0.827	0.992	2.15	3.31

## Z-AXIS CURRENT

H \ I	0	10	20	30	40	50	60	70	80	90
100	--	--	--	--	--	--	--	147	144	143
200	--	--	22.7	17.7	13.1	8.67	8.30	6.83	7.07	7.07
300	13.3	9.69	7.70	4.43	5.32	6.09	6.68	7.12	7.38	7.38
400	9.80	8.14	6.80	4.60	5.54	6.34	6.94	7.40	7.67	7.67
500	9.27	7.54	5.88	4.77	5.74	6.57	7.20	7.68	7.96	7.96
600	9.22	8.01	5.72	4.93	5.93	6.79	7.44	7.94	8.22	8.22
700	9.19	8.08	5.63	5.11	6.15	7.04	7.71	8.23	8.52	8.52
800	9.04	7.88	5.48	5.33	6.42	7.34	8.04	8.58	8.89	8.89
900	8.86	8.14	5.67	5.51	6.62	7.58	8.30	8.86	9.17	9.17
1000	9.01	7.61	5.04	5.70	6.86	7.86	8.60	9.18	9.51	9.51

Table 5 (Continued)  
 VEHICLE A3 (CURRENTS IN  $10^{-1}$  FT-LB/GAUSS)

X-AXIS CURRENT

I \ H	0	10	20	30	40	50	60	70	80	90
100	--	--	--	--	--	--	--	44.6	41.7	39.7
200	--	--	5.28	4.20	3.78	2.22	2.49	2.68	2.84	2.96
300	3.47	2.03	2.45	1.52	1.98	2.32	2.60	2.80	2.96	3.09
400	2.62	1.88	2.19	1.58	2.05	2.41	2.70	2.91	3.08	3.21
500	2.58	1.83	1.97	1.64	2.13	2.50	2.80	3.01	3.19	3.33
600	2.55	1.86	1.86	1.69	2.20	2.59	2.90	3.12	3.30	3.45
700	2.47	1.79	1.43	1.75	2.28	2.68	3.00	3.23	3.42	3.57
800	2.51	1.80	1.50	1.83	2.38	2.79	3.12	3.37	3.56	3.72
900	2.50	1.86	1.43	1.88	2.45	2.88	3.22	3.47	3.68	3.83
1000	2.07	1.43	1.39	1.95	2.54	2.98	3.34	3.60	3.81	3.97

Y-AXIS CURRENT

I \ H	0	10	20	30	40	50	60	70	80	90
100	--	--	--	--	--	--	--	10.6	7.61	6.46
200	--	--	3.78	1.49	0.840	0.333	0.175	0.210	0.455	0.700
300	2.29	1.68	1.10	0.421	0.421	0.348	0.183	0.220	0.476	0.732
400	1.71	1.43	0.893	0.437	0.437	0.361	0.190	0.228	0.494	0.760
500	1.67	1.22	0.768	0.453	0.453	0.374	0.197	0.236	0.512	0.788
600	1.63	1.10	0.734	0.469	0.469	0.388	0.204	0.245	0.530	0.816
700	1.48	1.12	0.675	0.485	0.485	0.401	0.211	0.253	0.549	0.844
800	1.47	1.12	0.660	0.506	0.506	0.418	0.220	0.264	0.572	0.880
900	1.36	1.16	0.681	0.522	0.522	0.431	0.227	0.272	0.590	0.908
1000	0.940	0.846	0.470	0.541	0.541	0.447	0.235	0.282	0.611	0.940

Table 5 (Continued)

## Z-AXIS CURRENT

H \ I	0	10	20	30	40	50	60	70	80	90
100	--	--	--	--	--	--	--	29.4	28.0	27.4
200	--	--	4.83	3.53	2.87	1.66	1.82	1.94	2.01	2.01
300	3.53	2.60	2.20	1.26	1.52	1.74	1.90	2.03	2.10	2.10
400	2.79	2.43	1.94	1.31	1.58	1.81	1.98	2.11	2.19	2.19
500	2.76	2.27	1.67	1.36	1.64	1.87	2.05	2.19	2.27	2.27
600	2.73	2.28	1.63	1.41	1.69	1.94	2.12	2.26	2.35	2.35
700	2.66	2.24	1.60	1.45	1.75	2.00	2.19	2.34	2.43	2.43
800	2.68	2.24	1.67	1.52	1.83	2.10	2.29	2.44	2.53	2.53
900	2.66	2.32	1.61	1.57	1.88	2.16	2.36	2.52	2.61	2.61
1000	2.09	1.76	1.20	1.62	1.95	2.23	2.44	2.61	2.70	2.70

VEHICLE A4 (CURRENTS IN  $10^{-1}$  FT-LB/GAUSS)

## X-AXIS CURRENT

H \ I	0	10	20	30	40	50	60	70	80	90
100	--	--	--	--	--	--	96.3	72.4	67.3	64.4
200	--	--	8.77	7.49	6.74	3.96	4.43	4.77	5.05	5.27
300	6.41	4.02	4.73	2.69	3.50	4.11	4.60	4.96	5.25	5.48
400	5.27	3.38	3.89	2.81	3.65	4.29	4.80	5.17	5.48	5.71
500	5.25	3.47	4.03	2.91	3.78	4.45	4.97	5.36	5.67	5.92
600	5.18	3.48	4.16	3.00	3.91	4.60	5.14	5.54	5.86	6.12
700	5.10	3.60	3.53	3.11	4.05	4.76	5.33	5.74	6.07	6.34
800	5.12	3.68	2.66	3.25	4.22	4.97	5.55	5.98	6.33	6.61
900	4.86	3.69	2.75	3.36	4.37	5.14	5.75	6.20	6.56	6.84
1000	4.81	3.68	2.63	3.47	4.51	5.31	5.94	6.40	6.77	7.06

Table 5 (Continued)

## Y-AXIS CURRENT

H \ I	0	10	20	30	40	50	60	70	80	90
100	--	--	--	--	--	--	32.7	16.2	11.1	9.48
200	--	--	6.27	2.65	1.49	0.592	0.312	0.374	0.811	1.25
300	4.53	3.30	2.10	0.745	0.745	0.616	0.324	0.389	0.842	1.30
400	3.45	2.77	1.59	0.777	0.777	0.642	0.338	0.406	0.879	1.35
500	3.40	2.63	1.65	0.805	0.805	0.665	0.350	0.420	0.910	1.40
600	3.37	2.64	1.70	0.832	0.832	0.688	0.362	0.434	0.941	1.45
700	3.34	2.74	1.39	0.862	0.862	0.713	0.375	0.450	0.975	1.50
800	3.32	2.15	1.25	0.899	0.899	0.743	0.391	0.469	1.01	1.56
900	2.84	2.19	1.30	0.932	0.932	0.770	0.405	0.486	1.05	1.62
1000	2.93	2.34	1.25	0.961	0.961	0.794	0.418	0.502	1.09	1.67

## Z-AXIS CURRENT

H \ I	0	10	20	30	40	50	60	70	80	90
100	--	--	--	--	--	--	55.1	49.2	46.2	43.9
200	--	--	8.02	6.30	5.12	2.96	3.24	3.46	3.59	3.59
300	6.71	4.89	4.21	2.24	2.69	3.08	3.37	3.60	3.73	3.73
400	5.64	4.53	3.45	2.33	2.81	3.21	3.52	3.75	3.89	3.89
500	5.57	4.48	3.57	2.42	2.91	3.33	3.64	3.89	4.03	4.03
600	5.50	4.53	3.69	2.50	3.00	3.44	3.76	4.02	4.16	4.16
700	5.44	4.69	3.08	2.59	3.11	3.56	3.90	4.16	4.31	4.31
800	5.47	4.50	2.97	2.70	3.25	3.71	4.07	4.34	4.50	4.50
900	5.22	4.54	3.08	2.77	3.36	3.85	4.21	4.50	4.66	4.66
1000	5.18	4.56	2.97	2.88	3.47	3.97	4.35	4.64	4.81	4.81



Table 5 (Continued)

VEHICLE A5 (CURRENTS IN  $10^{-1}$  FT-LB/GAUSS)

## X-AXIS CURRENT

I \ H	0	10	20	30	40	50	60	70	80	90
100	--	--	--	--	--	--	102.0	88.8	82.7	83.7
200	--	16.9	12.3	10.6	8.51	6.25	6.99	7.53	7.97	8.31
300	10.1	6.15	6.87	4.26	5.54	6.52	7.28	7.85	8.31	8.67
400	8.21	5.33	6.13	4.42	5.76	6.77	7.57	8.15	8.63	9.01
500	8.02	5.31	6.36	4.59	5.97	7.02	7.85	8.46	8.96	9.35
600	7.89	5.61	5.95	4.75	6.18	7.26	8.12	8.75	9.27	9.67
700	7.77	5.87	5.57	4.92	6.40	7.53	8.42	9.07	9.61	10.0
800	7.79	5.62	6.18	5.13	6.67	7.85	8.78	9.46	10.0	10.4
900	7.66	5.61	5.81	5.30	6.89	8.10	9.06	9.76	10.3	10.8
1000	7.60	5.42	4.49	5.49	7.14	8.39	9.39	10.1	10.7	11.2

## Y-AXIS CURRENT

I \ H	0	10	20	30	40	50	60	70	80	90
100	--	--	--	--	--	--	26.8	16.2	11.4	10.9
200	--	22.0	7.38	3.74	1.87	0.935	0.492	0.590	1.28	1.97
300	6.67	5.03	3.08	1.18	1.18	0.974	0.513	0.616	1.33	2.05
400	5.33	4.37	2.50	1.23	1.23	1.01	0.533	0.639	1.39	2.13
500	5.20	4.04	2.60	1.27	1.27	1.05	0.553	0.664	1.44	2.21
600	5.15	4.23	2.40	1.32	1.32	1.09	0.572	0.686	1.49	2.29
700	5.04	4.45	2.19	1.36	1.36	1.13	0.593	0.712	1.54	2.37
800	4.76	3.34	2.41	1.42	1.42	1.17	0.618	0.742	1.61	2.47
900	4.66	3.57	2.30	1.47	1.47	1.21	0.638	0.766	1.66	2.55
1000	4.63	3.37	2.12	1.52	1.52	1.26	0.661	0.793	1.72	2.64

Table 5 (Continued)

## Z-AXIS CURRENT

I \ H	0	10	20	30	40	50	60	70	80	90
100	--	--	--	--	--	--	68.2	62.5	57.8	58.3
200	--	18.9	11.3	9.40	6.45	4.67	5.12	5.46	5.66	5.66
300	10.3	7.59	6.16	3.54	4.26	4.87	5.34	5.69	5.90	5.90
400	8.74	7.14	5.44	3.68	4.42	5.06	5.54	5.92	6.13	6.13
500	8.51	6.91	5.64	3.81	4.59	5.25	5.75	6.14	6.36	6.36
600	8.41	7.26	5.26	3.95	4.75	5.43	5.95	6.35	6.58	6.58
700	8.30	7.59	4.86	4.09	4.92	5.63	6.17	6.58	6.82	6.82
800	8.40	6.92	5.25	4.26	5.13	5.87	6.43	6.86	7.11	7.11
900	8.23	6.95	5.10	4.40	5.30	6.06	6.64	7.08	7.34	7.34
1000	8.20	6.74	5.02	4.56	5.49	6.28	6.87	7.34	7.60	7.60

VEHICLE A6 (CURRENTS IN  $10^{-1}$  FT-LB/GAUSS)

## X-AXIS CURRENT

I \ H	0	10	20	30	40	50	60	70	80	90
100	--	--	--	--	--	--	84.3	75.3	69.5	68.8
200	--	13.3	10.0	8.19	6.14	4.81	5.38	5.80	6.14	6.41
300	7.51	4.58	5.29	3.28	4.27	5.02	5.61	6.04	6.40	6.68
400	6.17	4.07	4.73	3.41	4.44	5.22	5.84	6.29	6.66	6.95
500	5.88	4.17	4.43	3.54	4.60	5.41	6.05	6.52	6.90	7.20
600	5.85	4.00	4.14	3.65	4.75	5.59	6.25	6.73	7.13	7.44
700	5.71	4.16	4.16	3.79	4.94	5.80	6.49	6.99	7.40	7.72
800	5.71	4.19	3.24	3.95	5.14	6.05	6.76	7.28	7.71	8.04
900	5.65	4.03	3.34	4.08	5.30	6.24	6.97	7.51	7.95	8.30
1000	5.60	4.17	3.21	4.22	5.50	6.46	7.23	7.79	8.25	8.60

Table 5 (Continued)

Y-AXIS CURRENT

I \ H	0	10	20	30	40	50	60	70	80	90
100	--	--	--	--	--	--	24.7	14.8	10.2	9.63
200	--	18.8	6.06	2.88	1.36	0.720	0.379	0.455	0.985	1.52
300	4.94	3.75	2.37	0.908	0.908	0.751	0.395	0.474	1.03	1.58
400	3.99	3.08	1.93	0.945	0.945	0.781	0.411	0.493	1.07	1.64
500	3.83	3.15	1.79	0.980	0.980	0.809	0.426	0.511	1.11	1.70
600	3.78	2.38	1.63	1.01	1.01	0.836	0.440	0.528	1.14	1.76
700	3.66	2.47	1.65	1.05	1.05	0.868	0.457	0.548	1.19	1.83
800	3.47	2.67	1.52	1.09	1.09	0.904	0.476	0.571	1.24	1.90
900	3.44	2.50	1.57	1.13	1.13	0.933	0.491	0.589	1.28	1.96
1000	3.05	2.60	1.53	1.17	1.17	0.967	0.509	0.611	1.32	2.04

Z-AXIS CURRENT

I \ H	0	10	20	30	40	50	60	70	80	90
100	--	--	--	--	--	--	55.4	52.1	48.5	47.8
200	--	15.1	9.29	7.24	4.66	3.60	3.94	4.21	4.36	4.36
300	7.62	5.73	4.74	2.73	3.28	3.75	4.11	4.38	4.54	4.54
400	6.53	5.26	4.19	2.84	3.41	3.90	4.27	4.56	4.73	4.73
500	6.26	5.41	3.92	2.94	3.54	4.05	4.43	4.73	4.90	4.90
600	6.25	4.93	3.61	3.04	3.65	4.18	4.58	4.88	5.06	5.06
700	6.12	5.12	3.66	3.15	3.79	4.34	4.75	5.07	5.26	5.26
800	6.14	5.19	3.62	3.28	3.95	4.52	4.95	5.28	5.47	5.47
900	6.09	5.01	3.73	3.39	4.08	4.66	5.11	5.45	5.65	5.65
1000	5.96	5.19	3.61	3.51	4.22	4.84	5.29	5.65	5.85	5.85

NOTE: In the above

I = inclination

H = altitude

The values of peak currents can be found by substituting in  $M_{P_0}$ ,  $M_{Y_0}$ ,  $B$ ,  $\beta$ ,  $\alpha$ ,  $K_0$ , and  $K_{cc}$  and finding the peak values with respect to angle  $\theta$ . The values of  $K_{cc}$  are given in figure 26 as a function of the angle  $\beta$ . This variable represents the peak momentum cross-coupling that can occur during the unloading operation.

#### 5.4 DIGITAL COMPUTER PROGRAM

The results of paragraphs 5.2 and 5.3 were verified with the aid of a digital computer. The simulation of momentum decay was accomplished by programming the current and torque equations, and integrating the torques to find momentum.\* This program used magnetic field values obtained from the Cain 48 Coefficient Field Subroutine.\*\*

A comparison of digital and analytical results is presented in table 6. It is seen here that the digital simulation results verify the analytical decay times, the analytical values being conservative except for long decay times.

Table 6

DIGITAL CHECK OF DECAY TIME

Incl	Alt	Loop Gain $\alpha$	$T_D$ Orbits	
			Actual***	Predicted****
0	400	0.975	4.74	4
30	600	0.561	0.78	1
60	200	0.208	0.84	1
90	800	0.07565	2.14	2

\*\*\* From Digital Computer Run

\*\*\*\* From information of table 4

\* Complete equations given in Appendix 1.

\*\*Detailed explanation in paragraph 5.5.

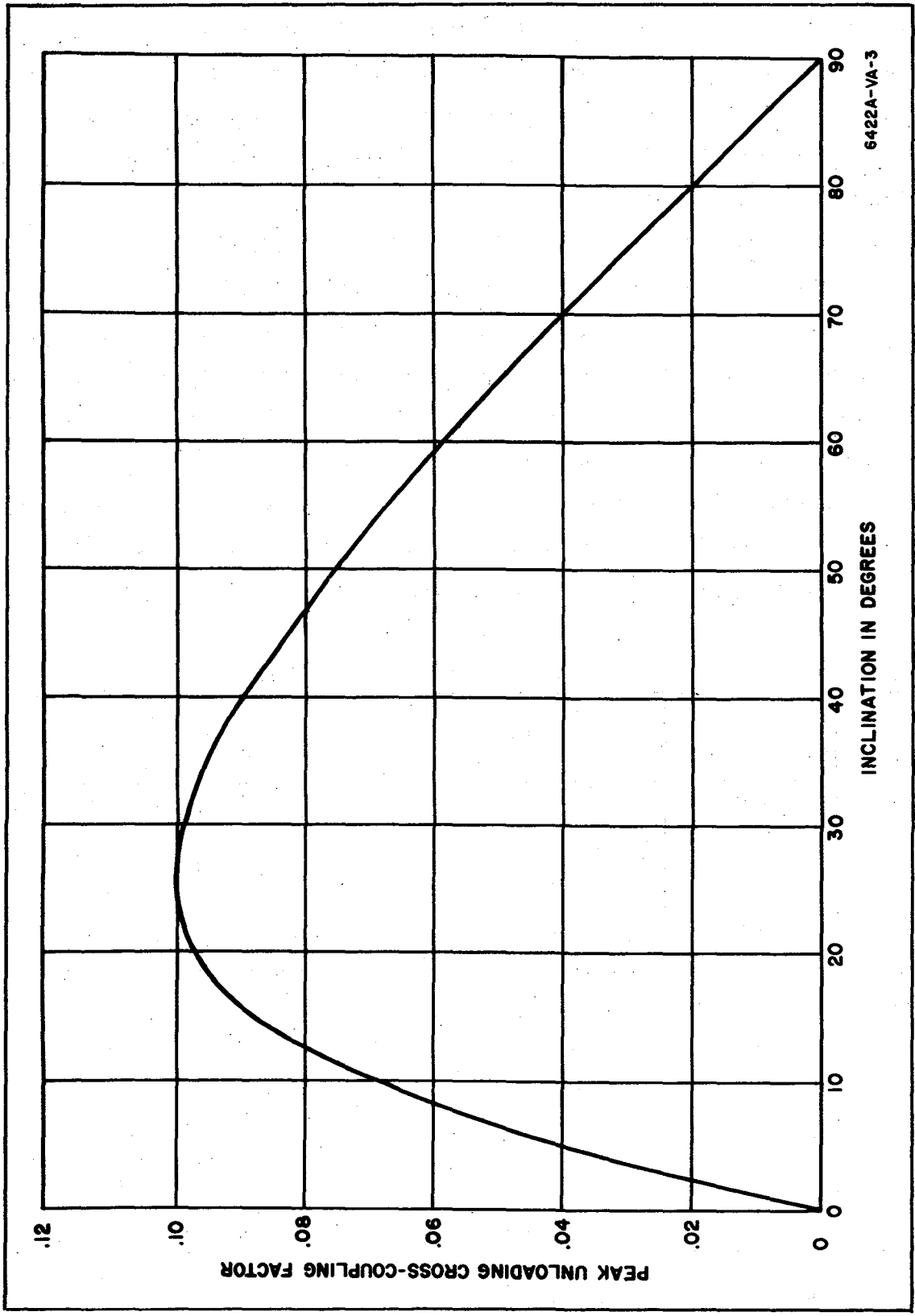


Figure 26. Peak Unloading Cross-Coupling Factor vs. Orbit Inclination  
Relative to Magnetic Equator

By adding disturbance torques to this program\* and setting the initial momenta to zero it was possible to check the minimum  $\alpha$ 's of table 3 for a few selected cases. The results of this simulation appear in table 7. From the average y-axis momentum values in this table it appears that a 10 percent of peak value of y-axis momentum (141 ft-lb-sec) can be maintained with a loop gain of approximately 0.41. This is within 1 percent of the value in table 3.

Table 7  
DIGITAL DATA USED TO CHECK MINIMUM  
LOOP GAIN

Vehicle A2 at 200 nmi and 30° inclination	
Loop Gain $\alpha$	Average y-axis Momentum
.30	181 foot-pound-seconds
.35	158
.40	143
.45	129
.50	112

#### 5.5 CAIN 48-COEFFICIENT FIELD SUBROUTINE

The digital simulation (paragraph 5.4) used the Cain 48-Coefficient spherical harmonic field subroutine<sup>4, 5, 6, 7</sup> to produce the earth's magnetic field components. The output of this program is in gammas ( $10^5$  gauss) and has components that are north, east and down. The inputs to the program are longitude, latitude, and altitude. To use the program the inputs have to be computed and the outputs converted to orbit coordinates.

---

\* See paragraph 5.3 for disturbance equations.

The Cain 48 field subroutine was used in comparison runs to check the effects of using the dipole field equations to generate field components. These runs made with both the dipole and the Cain program representations indicated that the average percent deviation of y-axis momentum for a constant y-axis torque input was approximately 10 percent.

When the magnetic system is used to counter the average disturbance torque the y-axis momentum will have an average value of 10 percent of peak, based on the design goal. A ten percent error in this 10 percent means the average y-axis momentum will be either 9 percent or 11 percent instead of the designed 10 percent.

SECTION VI  
DETAILED STUDY OF A SPECIAL CASE

6.1 SPECIFIC ORBITS

It was desirable to make a detailed study of the particular vehicle in the specific orbit described below:

● Vehicle Configuration

Homogeneous right circular cylinder with a mass of 40,000 pounds, length of 35.4 ft., and diameter of 12 ft. The center of mass was offset from the geometric center by 3.5 ft. along the longitudinal axis of the vehicle. The surface was assumed to be diffuse with a coefficient of reflection of 0.5.

● Orbit Configuration

The orbit inclination was 30 degrees and the altitude 200 nautical miles (circular). The vehicle was assumed to have its longitudinal axis aligned with the local vertical for determining momentum buildup due to disturbances. The nominal orientation is with the z axis down, the x axis along the velocity vector and the y axis normal to the orbit plane.

● Disturbance Inputs

a. Magnetic - zero, since the presence of a magnetic torquing system will permit balancing the magnetic moment generated by on-board equipment.

b. Solar pressure, gravity gradient and aerodynamic torques - per reference 8.

c. Movement of personnel - the accuracy requirement of the paragraph below will apply in the presence of any of the disturbances listed in table 17 of reference 8. The movement of the 160-pound man listed in the report will not apply to the accuracy requirement.



- Accuracy Requirement

The vehicle will maintain a vertical pointing and roll stabilization (rotation about vertical) accuracy of 10 arc seconds when subjected to the disturbance torques of items b and c above.

- Maneuver Requirement

A review of the disturbances detailed above indicated that they were adequate insofar as describing long-period and/or low-amplitude disturbance functions. It was found, however, that the disturbances did not provide an adequate criteria for the design of the control moment gyro system. Therefore the following maneuver requirements were derived:

- a. The system must be capable of slewing 23 degrees and settling down to within the required pointing accuracy with 150 seconds of time.

- b. The required pointing accuracy must be maintained while tracking along a line moving with respect to inertial space at an angular rate defined by  $\omega = \omega_A \sin(2\pi t/T)$  where  $\omega_A = 0.5$  deg/sec and  $T = 800$  seconds. This approximates pointing the longitudinal axis of the vehicle at a ground station offset from the orbit plane during a pass over the ground station.

## 6.2 CMG SYSTEM DESIGN

The system analysis and synthesis was performed to provide a preliminary control system description which would enable the performance of the described tasks. Particular attention was devoted to disturbance and maneuvering momentum requirements to provide a base on which to establish desaturation requirements.

Although system nonlinearities were considered in selecting the system command and control configuration, detailed analyses of nonlinear effects are not included as part of the study.

The vehicle axis nomenclature is shown in figure 27. The inertias about the vehicle pitch and yaw axis are  $I_y = I_z = 141,000$  slug-ft<sup>2</sup>

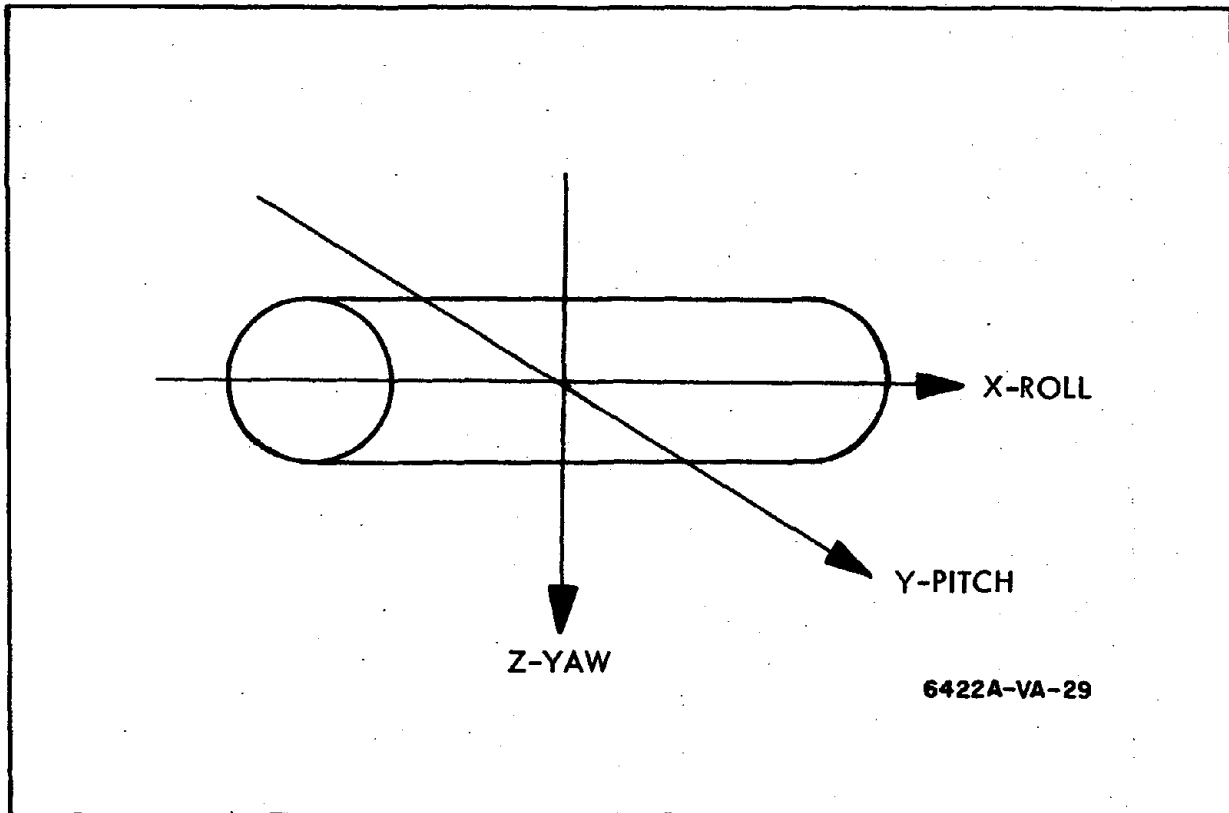


Figure 27. Vehicle Axis Nomenclature

and the inertia about the roll axis is

$$I_x = 22,360 \text{ slug-ft}^2.$$

Using the disturbance and maneuver requirements given earlier, and the gyro configuration of figure 2, the control system was designed. (See Appendix 3) The gyros chosen consist of two 1000 foot-pound-second two-degree-of-freedom gyros and two 500 foot-pound-second one D. O. F. gyros with direct drive gimbal torquers. The two D. O. F. gyros control the vehicle pitch (y) and yaw (z) axis and the one D. O. F. gyros control the roll axis.

The inner gimbal and outer gimbal of each two D. O. F. gyro are slaved to the respective gimbal of the other gyro to minimize cross coupling between axes. The wheel rotation (spin vector) and gimbal torquing direction are controlled to obtain equal torques from each gyro and to null the cross-axis torquers. The one D. O. F. gyros are set up similarly.

For the outer gimbal of the two D. O. F. gyro the open loop gains can be found from the required pointing accuracy and maneuver requirements. Having chosen the open loop gain, the uncompensated transfer function is found to be:

$$A(S) = \frac{180}{S \left(1 + \frac{S}{27.5}\right)}$$

The control is unstable for the above A(S); therefore to obtain a stable system with the desired accuracy capability, the following compensation was added:

$$G_1(S) = \frac{\left(1 + \frac{S}{5.5}\right) \left(1 + \frac{S}{20}\right)}{\left(1 + \frac{S}{.3}\right) \left(1 + \frac{S}{30}\right)}$$

This gave a new open loop transfer function as shown below:

$$A_P(S) = \frac{180 \left(1 + \frac{S}{5.5}\right) \left(1 + \frac{S}{20}\right)}{S \left(1 + \frac{S}{.3}\right) \left(1 + \frac{S}{27.5}\right) \left(1 + \frac{S}{30}\right)}$$

For the inner gimbal (yaw control loop) of the two D. O. F. gyros, the compensated open loop transfer function was found to be as given below:

$$A_y(S) = \frac{180 \left(1 + \frac{S}{5.5}\right) \left(1 + \frac{S}{20}\right)}{S \left(1 + \frac{S}{.3}\right) \left(1 + \frac{S}{27.5 \cos \alpha}\right) \left(1 + \frac{S}{30}\right)}$$

For the single degree of freedom gyro the control loops were also compensated. For these no rate feedback was needed, and the required transfer function between angular pointing error and control torque to the gyro gimbal was found.

$$\frac{T}{\Delta\theta}(S) = \frac{5000 \cos \alpha \left(1 + \frac{S}{6.68}\right)^2}{\left(1 + \frac{S}{30}\right)^2}$$

Using this transfer function to determine gimbal torque, the response of the roll axis to a zero frequency disturbance torque was found using the final value theorem.

$$\frac{\theta}{T_d} = \frac{1.34 (10^{-6})}{\cos^2 \alpha}$$

where  $\alpha$  is the gimbal angle.

When the gimbal is restricted to  $\pm 60^\circ$ , the maximum allowable disturbance torque without exceeding an attitude error of  $\pm 10$  arc seconds is 9 foot-pounds.

For the two D. O. F. gyros the transfer function between angle error and gimbal torque is equal to:

$$\frac{T}{\Delta\theta}(S) = 3.53 (10^8) \frac{\left(1 + \frac{S}{5.5}\right) \left(1 + \frac{S}{20}\right)}{\left(1 + \frac{S}{.3}\right) \left(1 + \frac{S}{30}\right)}$$

The two D. O. F. gyros also have rate feedback (using rate gyros) having a transfer function equivalent to that given below:

$$\frac{T}{\dot{\theta}}(S) = -1.94 (10^6) \frac{\text{foot-pounds}}{\text{radian/second}}$$

The compensations given above for the two D. O. F. gyros were found inadequate for large angular errors. To overcome this difficulty an additional compensating loop was used. This loop caused the angle error signal to go to zero when the gimbal torquer saturated. The transfer function used is shown in figure 28. This technique works to stabilize the system, but reduces the system speed of response for large angular errors.

It was found that the system large angle response could be stabilized without the use of the deadband compensation of figure 28, by reducing the limits on the angular error limiter to  $\pm 0.6$  arc seconds. This low level of saturation caused the maximum rate in response to an angle error to be reduced and also resulted in somewhat slow large angle response.

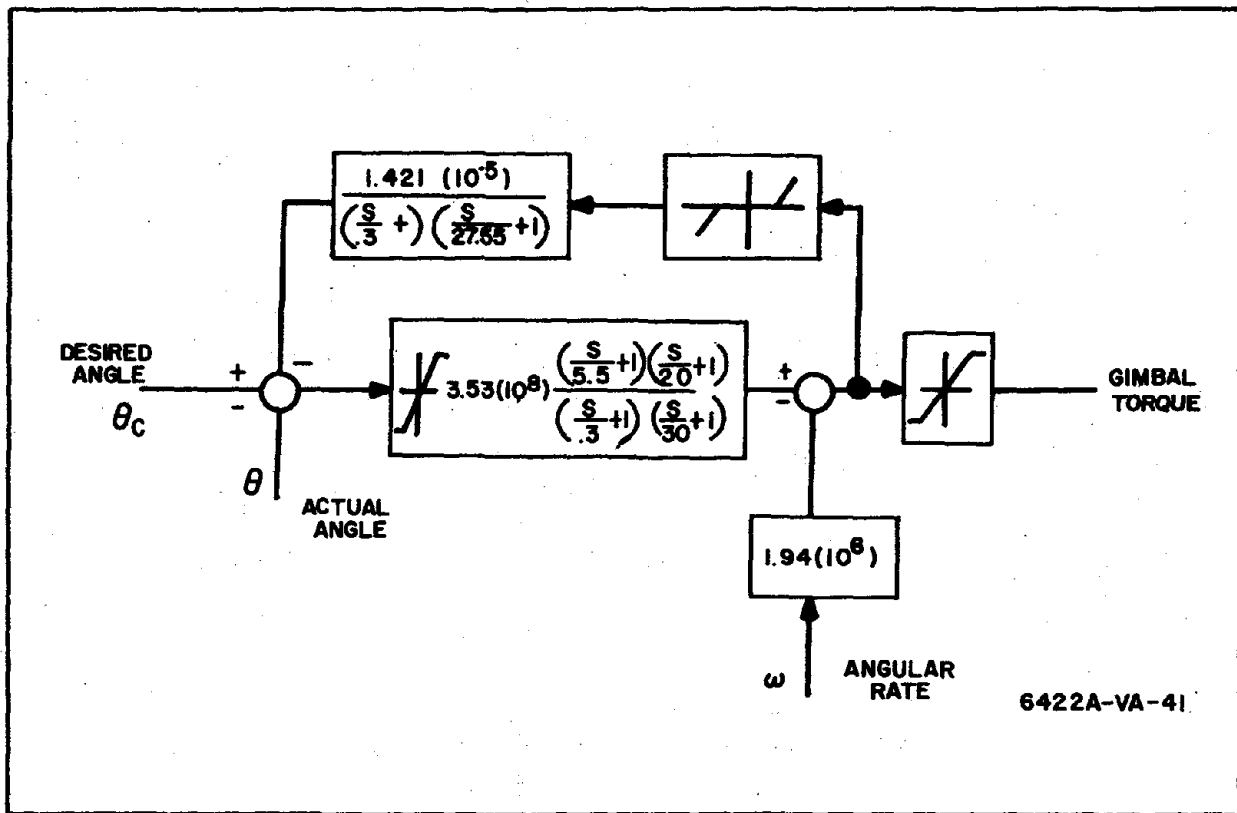


Figure 28. Two-D. O. F. Gyro Gimbal Torquer Control

The following estimates of hardware characteristics are based on a 500-foot-pound-second gyro that is currently undergoing test and a 1000-foot-pound-second gyro which has progressed through preliminary design states. Both of these units are single degree of freedom gyros. An estimate of the weight involved in the second gimbal structure is included in the data reported here. It should be noted that the wheel designs described here are optimized for gyro weight, stress, wheel rigidity and gimbal bending considerations. Table 8 contains the estimated gyro characteristics.

### 6.3 COMPLETE SYSTEM SIMULATION

To check the operation of the control moment gyro system under the influence of disturbance and magnetic desaturation system torques, the complete system equations were programmed on the Univac 1108 digital computer.\*

\*See Appendix 2 for digital computer equations.

TABLE 8  
CONTROL MOMENT GYRO ACTUATOR  
PHYSICAL CHARACTERISTICS

Item	2 - 2DOF	2 - 1DOF	Total
Weight (Lbs.)	342	300	642
Power (Watts)			
Spin	60	52	112
Torquer (Max.)*	500	---	500
(Ave.)	100	---	100
Volume (Ft. <sup>3</sup> )	8.84	6.65	15.4

\*Peak torquer power occurs for an extremely short period at the start of the acquisition and tracking maneuvers combined.

In the simulation there were three degrees of freedom for the vehicle, two D.O.F. for each of the two D.O.F. gyros, and one D.O.F. for each of the single D.O.F. gyros. This gave the simulation a total of nine degrees of freedom.

With the control equations (the transfer functions between angle error and control torque) inserted in the program, a few runs were made to determine system performance and to check the control equations and the simulation equations. For a small initial angle error (approximately 0.7 arc. seconds) the CMG system can reduce the error to zero in less than one second. (See figure 29). When a large initial pitch error is applied to the system, the CMG's behave as shown in figure 30. Initially all the gimbals on the two D.O.F. gyros accelerate while the torque is building up. The lags in the torque controller cause delays in the initial torque buildup. Eventually the torque reaches saturation and the gyro gimbals achieve a steady-state mode of operation. The outer gimbal rate ( $\dot{\alpha}$ ) goes to zero, and the inner gimbal rate ( $\dot{\beta}$ ) maintains a constant value (a constant precession). As long as the error signal indicates that the sign of the torque applied to the vehicle should

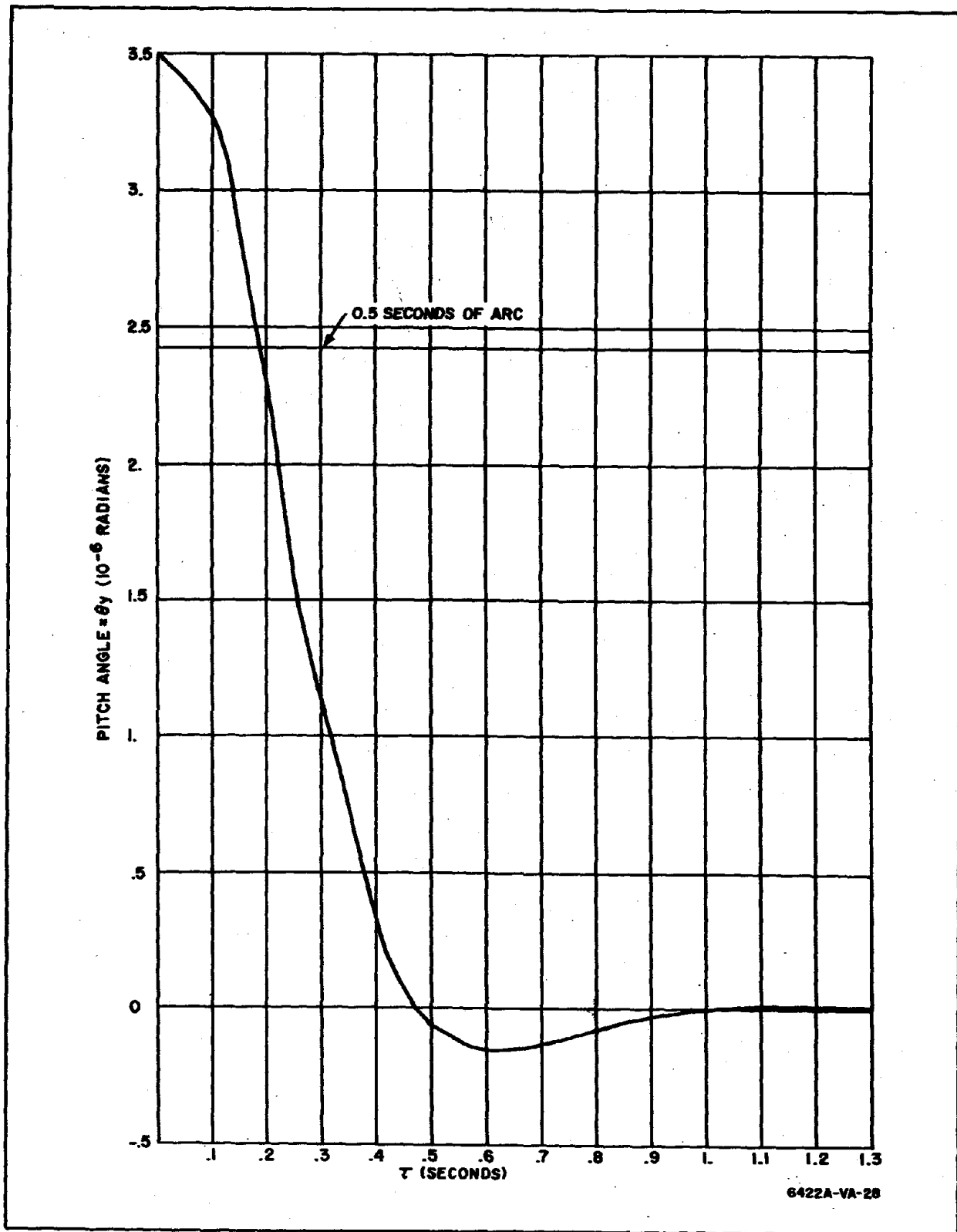
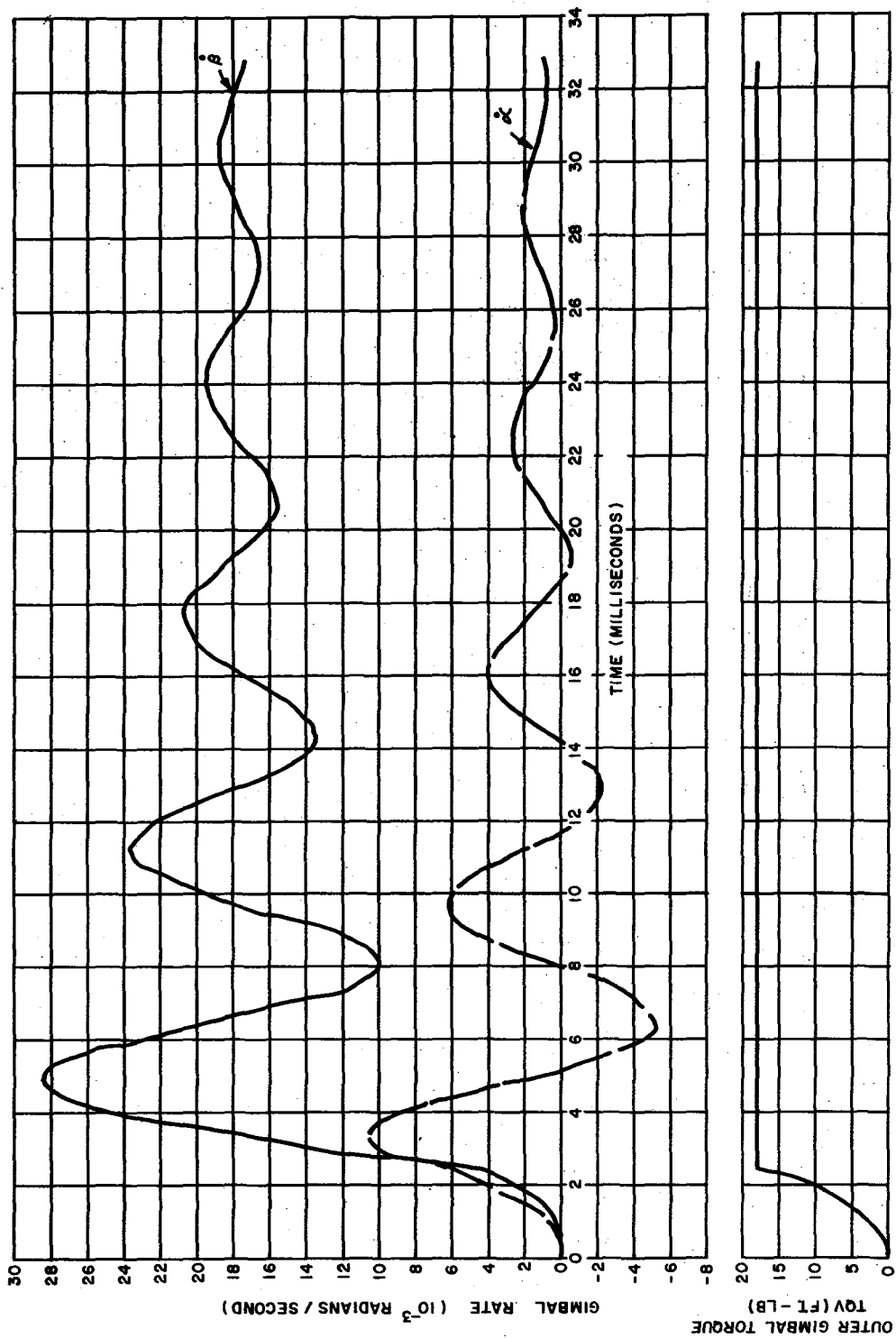


Figure 29. Step Response of CMG Control System for a Small Angle Error



6422A-VC-31

Figure 30. CMG Initial Response to a Large Pitch Error



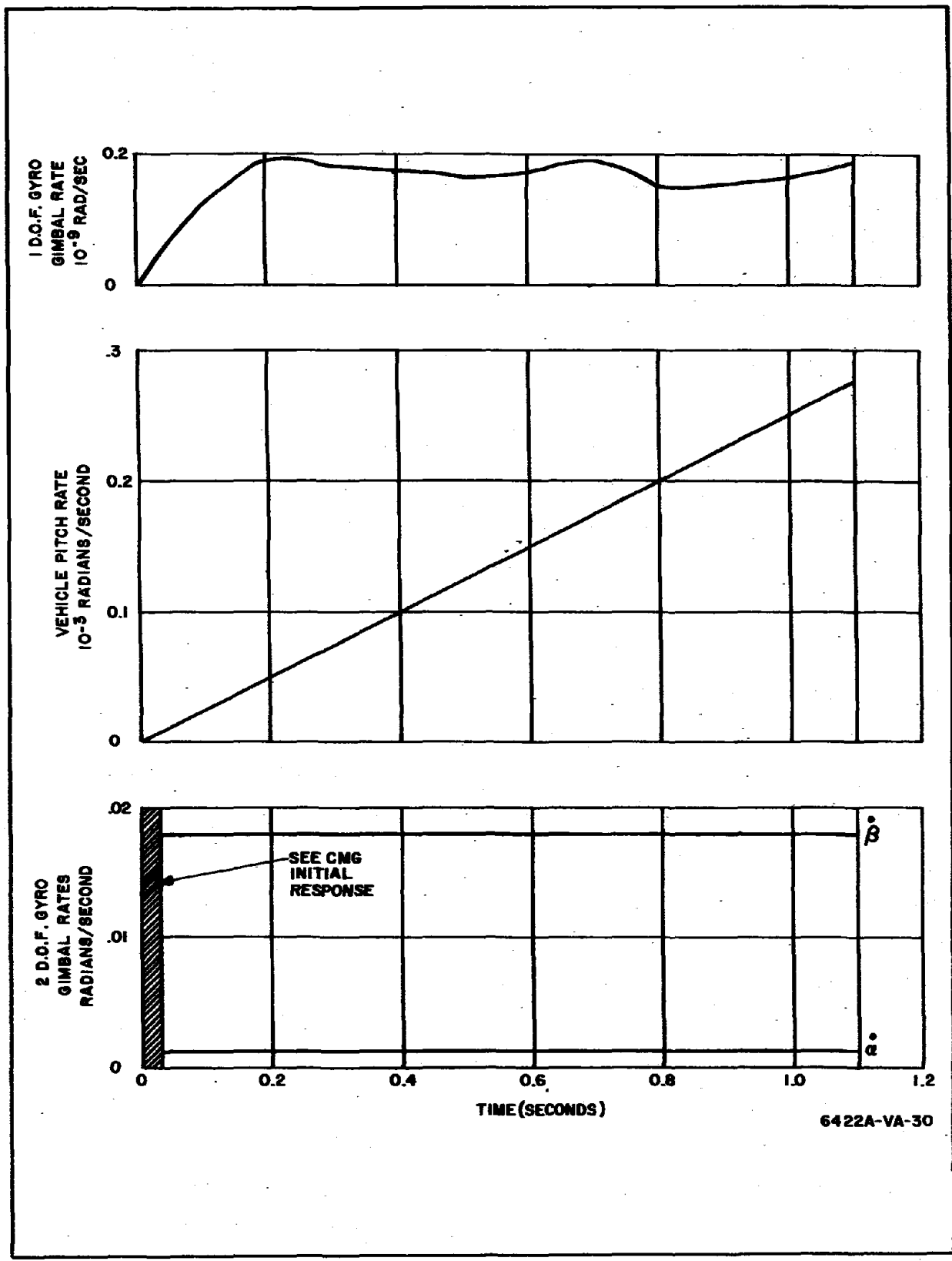
not reverse, the gyro gimbal rates do not change, and the vehicle tends to accelerate as shown in figure 31. Gimbal transients like those of figure 30 will occur when the maximum rate is reached, when the error approaches zero, and when the error finally gets to zero.

After the simulation was completely proven, the program was used to find the pointing errors that the CMG system would have when the vehicle was subjected to the maximum torques that it would encounter. The maximum torques were found by using the momentum unloading simulation with solar, aerodynamic, and gravity gradient disturbances to find the peak vehicle torque, including magnetic system unloading torques, that existed during a 24-hour interval. Runs were made for 100, 200, and 300 nmi. altitudes at inclinations ranging from 0 to 60 degrees on the momentum unloading program. From these runs (table 10 in paragraph 6.4) two cases were isolated: the case having the smallest peak torques and the case having the largest peak torques. These two cases were then simulated on the complete system simulation program to determine pointing errors for each case.

TABLE 9  
POINTING ERRORS FOR THE TWO ISOLATED CASES, VEHICLE A2

Altitude nmi.	Inclination degrees	Peak Torque, Lb-Ft			Maximum Error, arc seconds		
		$T_x$	$T_y$	$T_z$	$\Delta\theta_x$	$\Delta\theta_y$	$\Delta\theta_z$
300	60	0.012	0.012	0.012	0.003	1.26	0.006
200	0	0.10	0.047	0.161	0.060	1.34	0.008

The numbers of table 9 show that the CMG control system is not adversely effected by the magnetic momentum unloading system torques. The above numbers apply to the peak values of torque, which exist for only a short



6422A-VA-30

Figure 31. Large Pitch Error Response Prior to Torque Reversal

period of every orbit, the average torque (and pointing error) being considerably lower. The variation of torques presents no additional problems since the CMG system response is in the order of seconds, while torques change with a frequency less than 0.01 cycles per second.

#### 6.4 VARIATION OF ALTITUDE AND INCLINATION

The particular vehicle was designed to operate at 200 nautical miles and 30 degrees inclination. Variation of the inclination has no effect on the CMG design, since with the sunline assumed in the orbit plane the disturbances are the same at all inclinations and the assumed maneuver requirements could apply at all altitudes and inclinations. Variation of the altitude changes the disturbance torques, but since they are of little importance in the CMG design at 200 nmi. it is assumed that the changed disturbances will also be negligible. The disturbance torques decrease with increasing altitude.

It is evident that the CMG design could apply for all altitudes and inclinations.

It was requested that the performance of the particular vehicle be studied for altitudes of 100, 200 and 300 nmi. at inclinations varying from 0 degree to 60 degrees.

With the aid of the digital momentum unloading program (paragraph 5.4) the peak axial torques were found for the three altitudes at 0 degree, 30 degrees, and 60 degrees of inclination. In these runs the minimum values of  $\alpha$  were used for those cases where stored momentum could be kept to 10 percent of the peak value, and the optimum  $\alpha$  (that producing the greatest desaturation torque) was used in the remaining cases. The results appear in table 10.

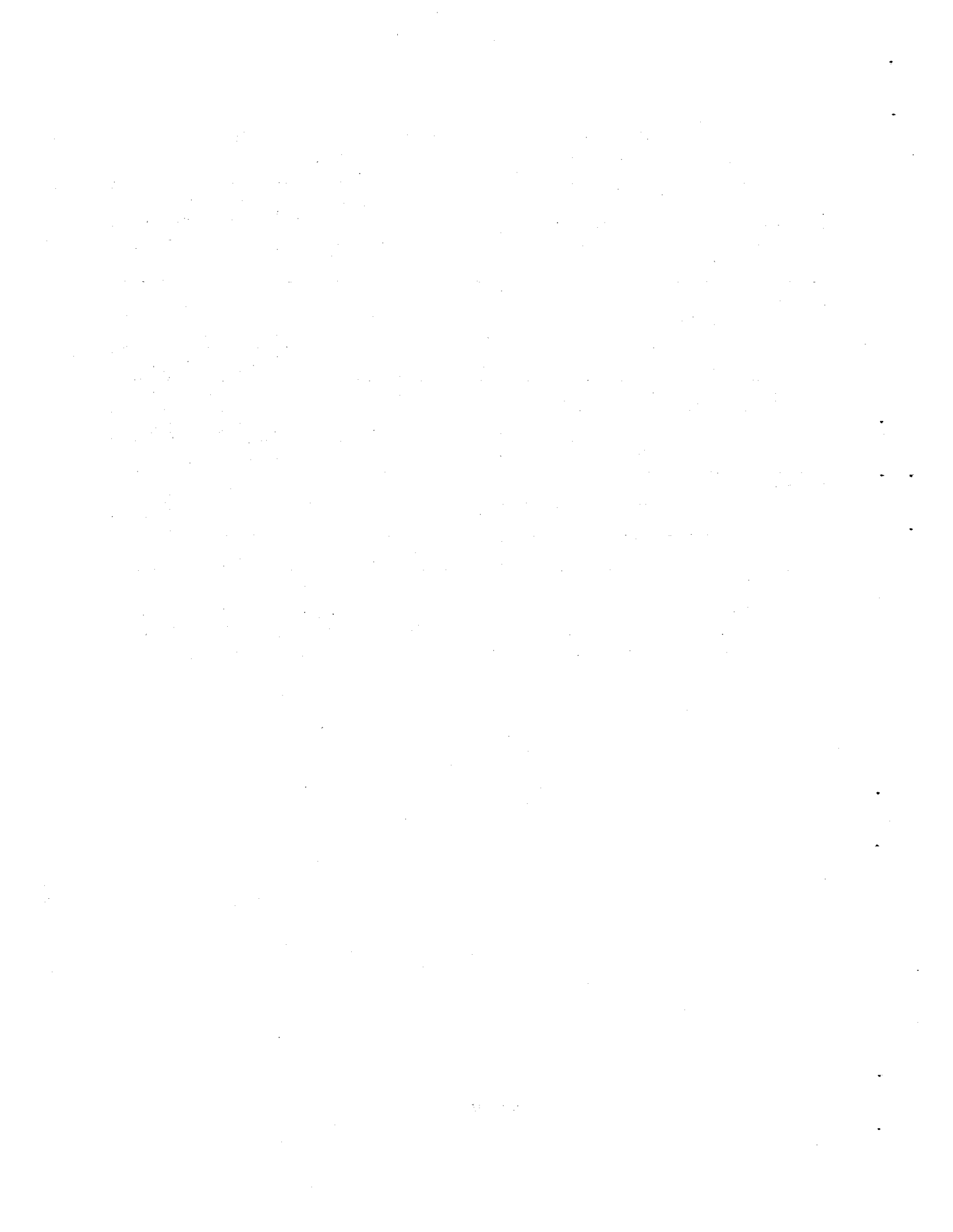
The above peak torques are in all cases less than the maximum CMG control torques, therefore the CMG system is capable of preventing rate buildup. These torques can cause some pointing error as evidenced by the values of  $\Delta\theta$  in table 9. These peak torques are the sum of magnetic momentum unloading torques and the disturbance torques (solar aerodynamic, and gravity gradient).

TABLE 10

EFFECT OF ALTITUDE AND INCLINATION VARIATION FOR  
THE PARTICULAR VEHICLE (VEHICLE A2)

Altitude nmi.	Inclination Degrees	Loop Gain	Average y-axis stored momentum as a percentage of full CMG capability	Peak torques foot-pounds		
				T <sub>X</sub>	T <sub>Y</sub>	T <sub>Z</sub>
300	0	.9	93	.015	.009	.030
	30	.1	112	.037	.018	.038
	60	.1	43	.012	.012	.012
200	0	2.1	260	.10	.047	.161
	30	.43	115	.057	.044	.069
	60	.13	121	.038	.046	.036
100	0	2.1	*	*	*	*
	30	2.2	*	*	*	*
	60	3.4	1146	3.0	3.8	5.8

NOTE: For 100 nmi the stored momentum was over the CMG capacity in the \* cases, and exceeded reasonable limits in all cases. The 100 nmi cases were omitted from the pointing error study for this reason.



SECTION VII  
MAGNETIC SYSTEM MECHANIZATION

7.1 COIL SIZE, WEIGHT, AND POWER REQUIREMENTS

In this section, factors determining coil size, weight, and power requirements are considered. Curves showing coil weight as a function of peak torque requirements are generated, thus allowing coil weight to be determined for each of the cases considered in the parametric analysis (paragraph 5.3). In addition, coil design is carried out for the particular configuration described in Section VI.

Two types of coils are considered, air-core and iron-core. Possible arrangements on the spacecraft for the two types are illustrated in figure 32. However, the weight of the iron-core torquer is not a strong function of length for lengths above those to five feet. The torquer lengths could easily be reduced, in which case the choice of mounting locations would be quite flexible.

The iron-core coil has the advantage of having its field strengthened by the iron, while the air-core coil has the advantage of a larger possible size. However, a comparison of the weight required for each method reveals little advantage for either configuration for the nominal case considered.

In Appendix 4, it is shown that the mass of a circular air-core coil, including power supply, is given by the equation:

$$M = \left( \frac{T}{B_t} \right) \left( \frac{8\sqrt{k\rho g_w}}{D} \right) \quad (7-1)$$

where:

- T = torque
- $B_t$  = effective earth magnetic field
- D = coil diameter

- k = power supply mass/power ratio
- p = coil winding resistivity
- $g_w$  = coil winding density

The mass of a rectangular coil, including power and supply, is given by:

$$M = \left(\frac{r+1}{r}\right) \left(\frac{4}{D}\right) \left(\frac{T}{B_t}\right) \sqrt{k\rho g_w} \quad (7-2)$$

where the rectangle dimensions are D by rD, (r > 1).

The configuration illustrated in figure 32 consists of 2 rectangular coils (about the x and y axes) and a circular coil about the z axis. Equations 7-1 and 7-2 were solved for various configurations of interest and the results are plotted in figures 33 and 34. In figure 33, the z axis torquer weight is plotted as a function of T/B<sub>t</sub> for the 10-, 12-, 14- and 15-ft. vehicle diameters. In figure 34, the weight of a rectangular x or y axis coil is plotted for the 6 vehicles considered in this study.

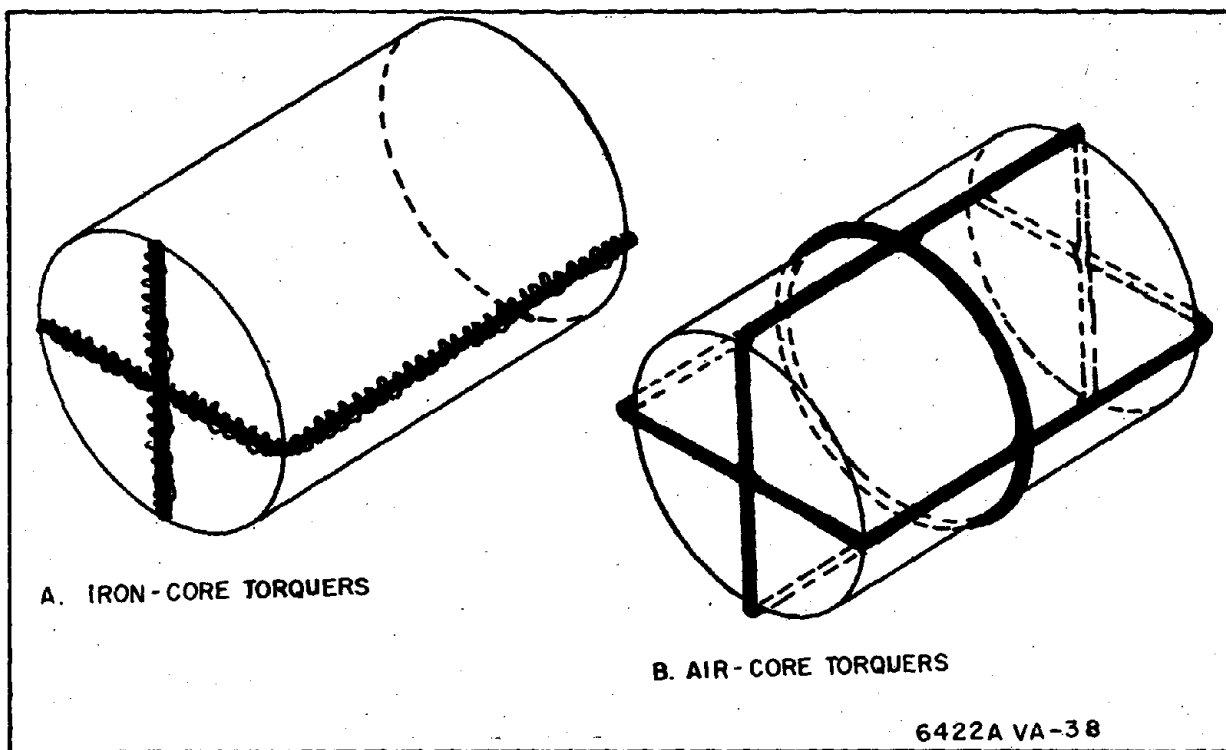


Figure 32. Spacecraft Mounting of Iron-Core and Air-Core Windings

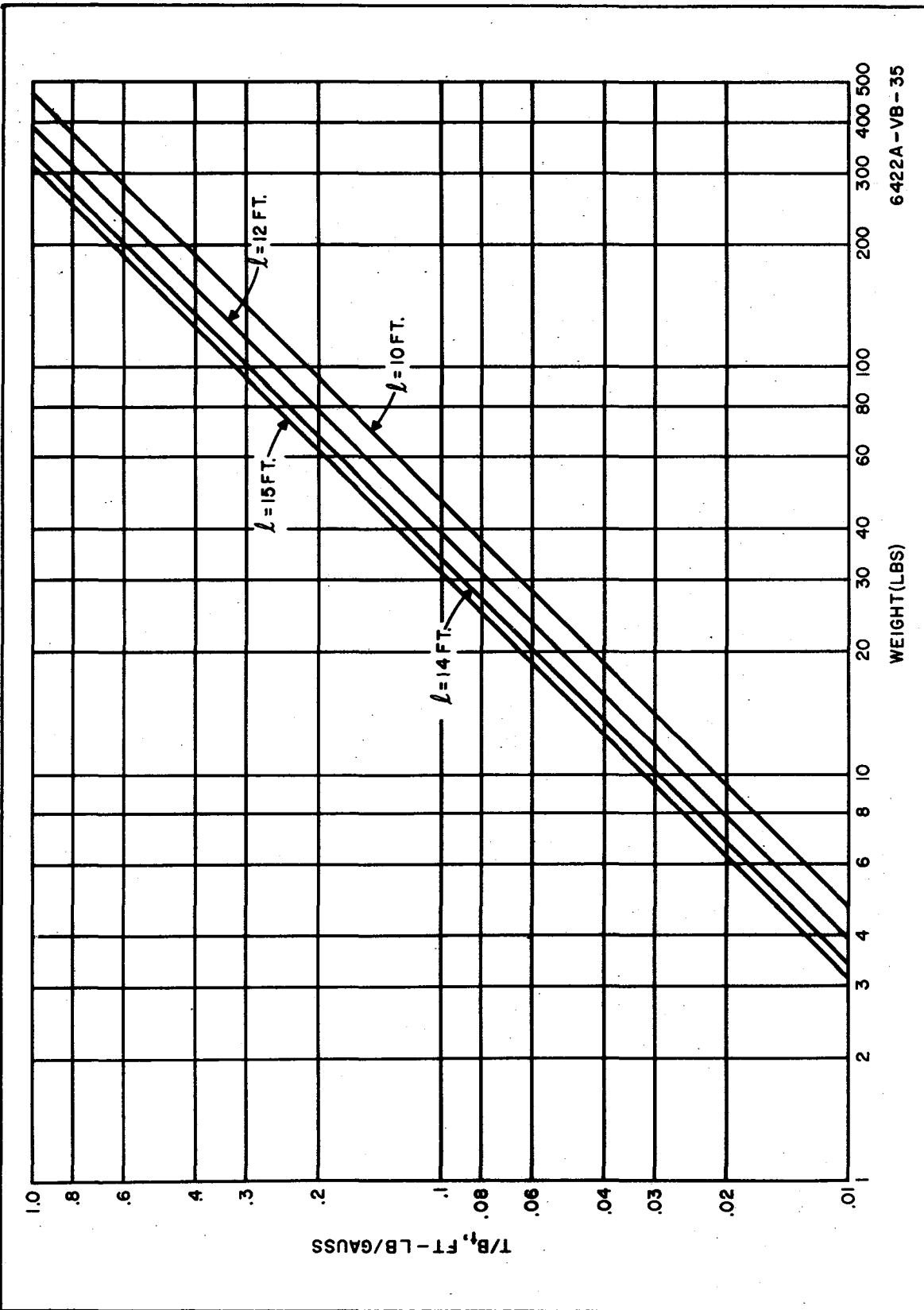


Figure 33. Weight of Air-Core Roll Axis Coil (Including Power Supply)



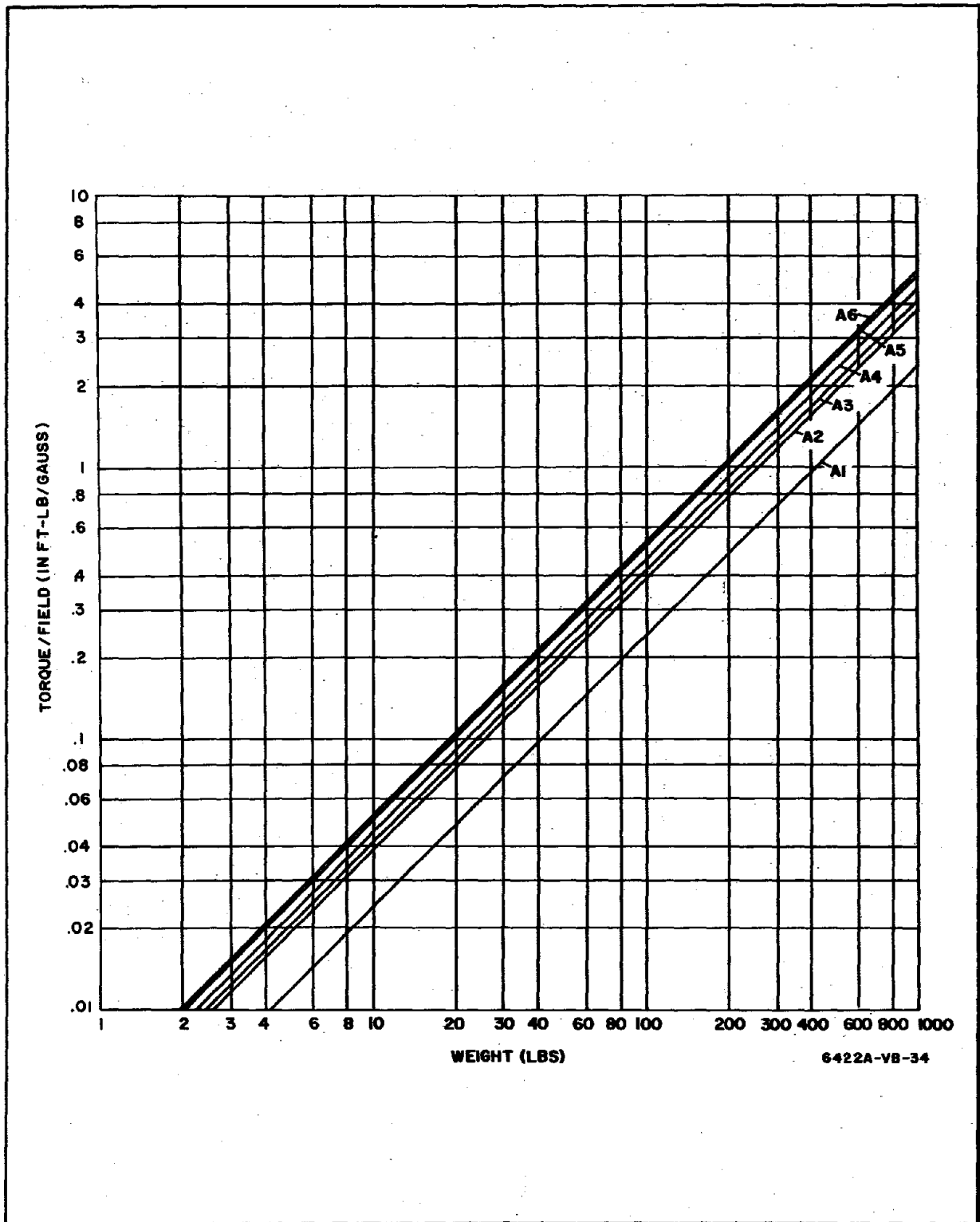


Figure 34. Weight of Air-Core Pitch or Yaw Coils  
(Including Power Supply)

For the nominal case of a 40,000 pound vehicle (12 ft dia and 36 ft long) in a 200 nmi orbit inclined at 30 degrees, the required values of  $T/B_t$  (from Section 5) are given by:

$$\begin{aligned} \left(T/B_t\right)_x &= .209 \text{ ft-lbs./gauss} \\ \left(T/B_t\right)_y &= .0875 \text{ ft-lbs./gauss} \\ \left(T/B_t\right)_z &= .177 \text{ ft-lbs./gauss} \end{aligned} \quad (7-3)$$

The total weight (including coil and power supply) required to produce the above fields is calculated by solving eq. 7-1 for the z axis and eq. 7-2 for the x and y axes. For an aluminum winding of wire size #24 AWG, the density and resistivity are:  $g_w = 2.67 (10^3) \text{ kg/m}^3$ ,  $\rho = 2.83 (10^{-8})$  ohmmeters. For a power supply ratio of 1 pound/watt,  $k = .453 \text{ kg/watt}$ . For the nominal case,  $D = 3.66$  meters (12 feet) and  $r = 2.95$ . Then the coil masses are calculated as

$$\begin{aligned} M_x &= \frac{(13,860) (.209) (8) \sqrt{(2.67) (10^3) (2.83) (10^{-8}) (.454)}}{3.66} = 37.1 \text{ kg} \\ &= 82 \text{ lbs.} \\ M_y &= \frac{(13,860) (.0875) (4) (3.95) \sqrt{(2.67) (10^3) (2.83) (10^{-8}) (.454)}}{(2.95) (3.66)} \\ &= 10.4 \text{ kg} \\ &= 23 \text{ lbs.} \\ M_z &= \frac{(13,860) (.177) (4) (3.95) \sqrt{(2.67) (10^3) (2.83) (10^{-8}) (.454)}}{(2.95) (3.66)} \\ &= 21.2 \text{ kg} \\ &= 46.7 \text{ lbs.} \end{aligned} \quad (7-4)$$

Then, the total mass of the torquing system, using air-core coils and including power supply is given by:

$$M_t = 82 + 23 + 46.7 = 151.7 \text{ lbs.} \quad (7-5)$$

A comparison of this weight with the weight of an equivalent iron-core system (200.6 lbs) reveals a weight saving of 48.9 lbs. However, it is felt that this weight saving is insufficient to justify use of an air-core system, due to the requirement for wrapping the air-core coils around the entire spacecraft. This latter arrangement could conceivably cause problems such as constraints on mounting other external equipment on the spacecraft and interference in the magnetometers due to passing a large magnetic field through the spacecraft. Thus, only iron-core coils are considered in the remainder of this section.

In Appendix 4, it is shown that the mass of an iron core torquer, including the iron, the wire and the power supply is given by:

$$M_t = \left( \frac{T}{B_t} \right) \left( \frac{\mu_o}{\alpha B_m} \right) \left\{ g_i + 0.288 \pi g_w S \left( \frac{d_1}{d} \right)^2 \psi \right\} + \frac{3.464 k \rho \ell B_m^2}{\mu_o^2 S} \left( \frac{d}{d_1} \right)^2 Z^2 \frac{(1 + \sqrt{1 + \psi})^2}{\psi} \quad (7-6)$$

where:

- $T/B_t$  = torque/field required of coil
- $\mu_o$  = permittivity of free space
- $\alpha$  = constant depending on l/m ratio of coil
- $B_m$  = saturation flux of core material
- $g_i$  = density of core material
- $g_w$  = density of wire
- $S$  = space area factor of winding
- $d_1$  = diameter of bare wire
- $d$  = diameter of insulated wire
- $k$  = mass/power ratio of coil power supply
- $\rho$  = resistivity of wire material
- $\ell$  = length of coil

Z = demagnetizing factor depending on l/m ratio of coil

$\psi$  = factor depending on l/m ratio of coil

Equation 7-6 may be solved in terms of coil length and torque/field required by assuming particular types of material for the core and winding. For a core material of 50 percent nickel, 50 percent iron, and aluminum wire material (No. 24 AWG), the following constants are established:

$$\rho = 2.83 (10^{-8}) \text{ ohmmeters}$$

$$d = 5.56 (10^{-4}) \text{ m}$$

$$d_1 = 5.11 (10^{-4}) \text{ m}$$

$$S = 0.845$$

$$g_i = 8.2 (10^3) \text{ kg/m}^3$$

$$B_m = 1 \text{ tesla (10,000 gauss)}$$

$$\mu_r = 10^4$$

$$g_w = 2.67 (10^3) \text{ kg/m}^3$$

Substituting these values and  $k = .454 \text{ kg/watt}$  and  $\alpha = .8$  into equation 7-6 there results:

$$M_t = \left( \frac{T}{B_t} \right) (.01288 + .00272 \psi) + 39,400 Z^2 \frac{(1 + \sqrt{1 + \psi})^2}{\psi} \ell \quad (7-7)$$

$\psi$  and  $Z$  are both functions of  $T/B_t$  and  $\ell$  and are solved for by the following procedure derived in Appendix 4. The coil dimensions  $l$ ,  $m$ , and  $n$  are illustrated in Appendix 4;  $m$  is determined by solving the following equation.

$$m = 2 \sqrt{\left( \frac{\mu_o}{\pi \alpha B_m} \right) \left( \frac{T}{B_t} \right) \left( \frac{l}{\ell} \right)} \quad (7-8)$$

$$m = .001412 \sqrt{\left( \frac{T}{B_t} \right) \left( \frac{l}{\ell} \right)} \quad (7-9)$$

Curves of  $1/m$  vs.  $T/B_t$  for various coil lengths were generated from eq. 7-9 and are shown in figure 35. These curves, together with the demagnetization factor curve given in Appendix 4, were used to generate the curves of  $Z^2$  vs  $T/B_t$  given in figure 36.

In order to find  $\psi$ , the function  $f(\psi)$  is determined by evaluating:

$$f(\psi) = \frac{.0832\pi \mu_o^3 g_w S^2}{\alpha k\rho B_m^3 Z^2} \left(\frac{d_l}{d}\right) \left(\frac{T}{B_t}\right) \left(\frac{1}{l}\right) \quad (7-10)$$

$$f(\psi) = .685 (10^{-7}) \left(\frac{T}{B_t}\right) \left(\frac{1}{l}\right) \left(\frac{1}{Z^2}\right) \quad (7-11)$$

$\psi$  is related to  $f(\psi)$  by the following equation:

$$f(\psi) = \frac{(1 + \sqrt{1 + \psi})^2}{\psi^2 \sqrt{1 + \psi}} \quad (7-12)$$

Equation 7-12 cannot be solved explicitly for  $\psi$ , but the curve of  $f(\psi)$  vs  $\psi$  in figure 37 and  $Z^2$  vs  $T/B_t$  in figure 36 can be used in conjunction with equation 7-12 to derive the plot of  $\psi$  vs  $T/B_t$  for various coil lengths shown in figure 38.

The use of figures 38 and 36 to determine  $\psi$  and  $Z^2$ , allows the solution of equation 7-7. Equation 7-7 was evaluated for mass as a function of  $\frac{T}{B_t}$  for coil lengths of 10, 12 and 15 feet. The results are plotted in figure 39. It can be seen in figure 39 that the coil mass is relatively insensitive to length variations in the range of 10-15 feet.

For the nominal case, the required torque/field inputs,

$$\begin{aligned} (T/B_t)_x &= .209 \text{ ft-lbs/gauss} \\ (T/B_t)_y &= .0875 \text{ ft-lbs/gauss} \\ (T/B_t)_z &= .177 \text{ ft-lbs/gauss} \end{aligned} \quad (7-13)$$

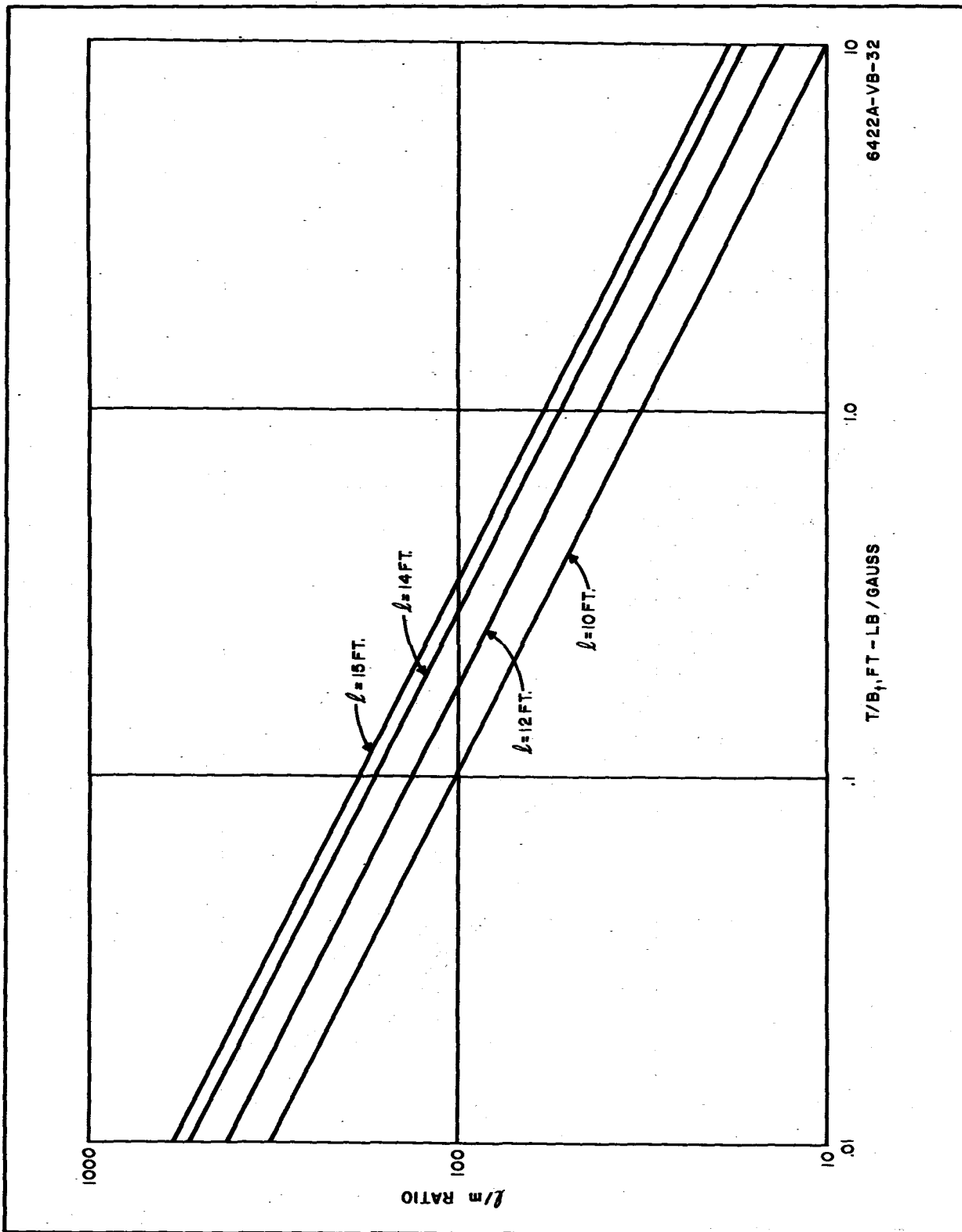


Figure 35.  $l/m$  Ratio vs.  $T/B_t$  for Various Length Coils

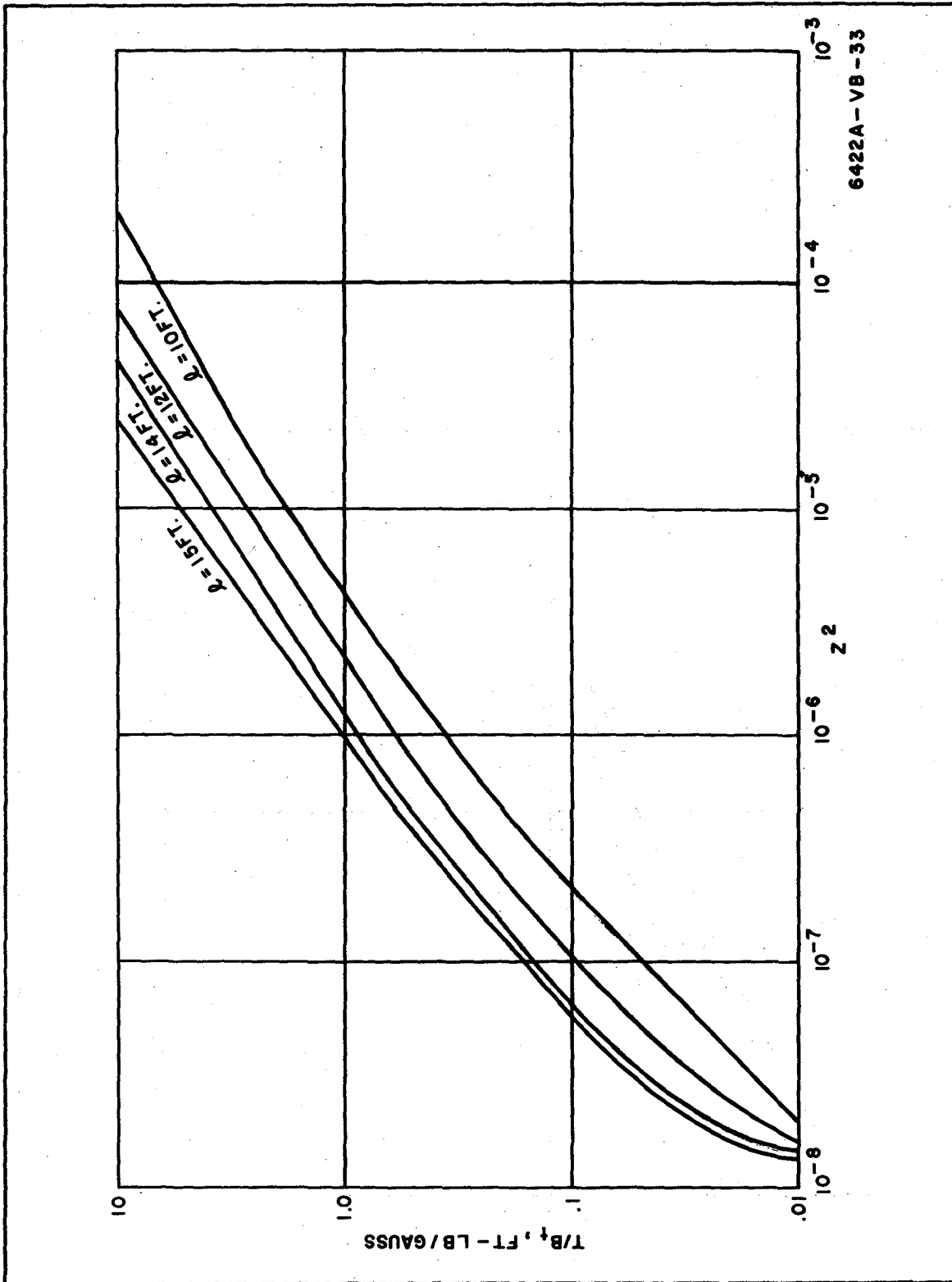


Figure 36.  $Z^2$  vs.  $T/B_t$  for Various Coil Lengths

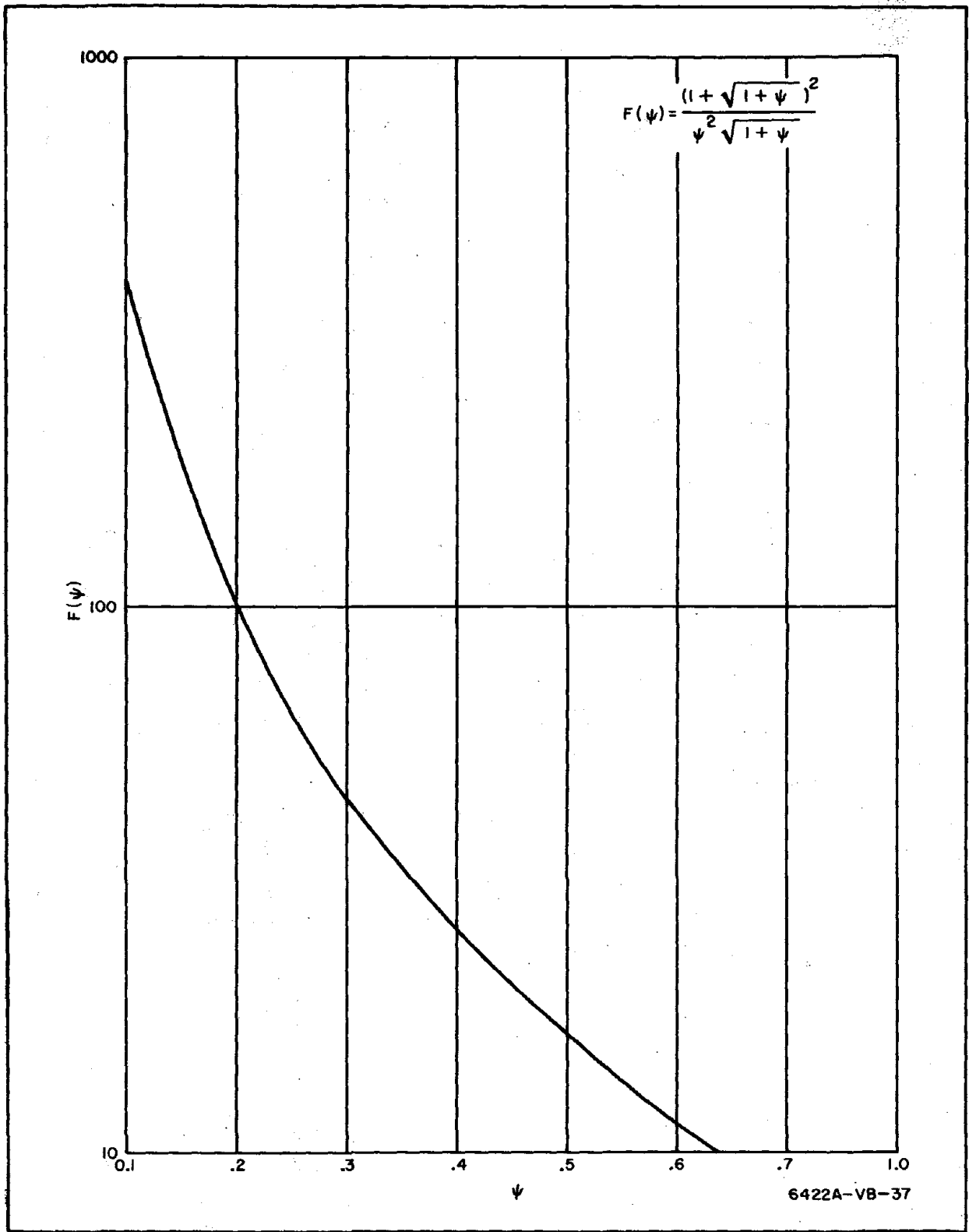
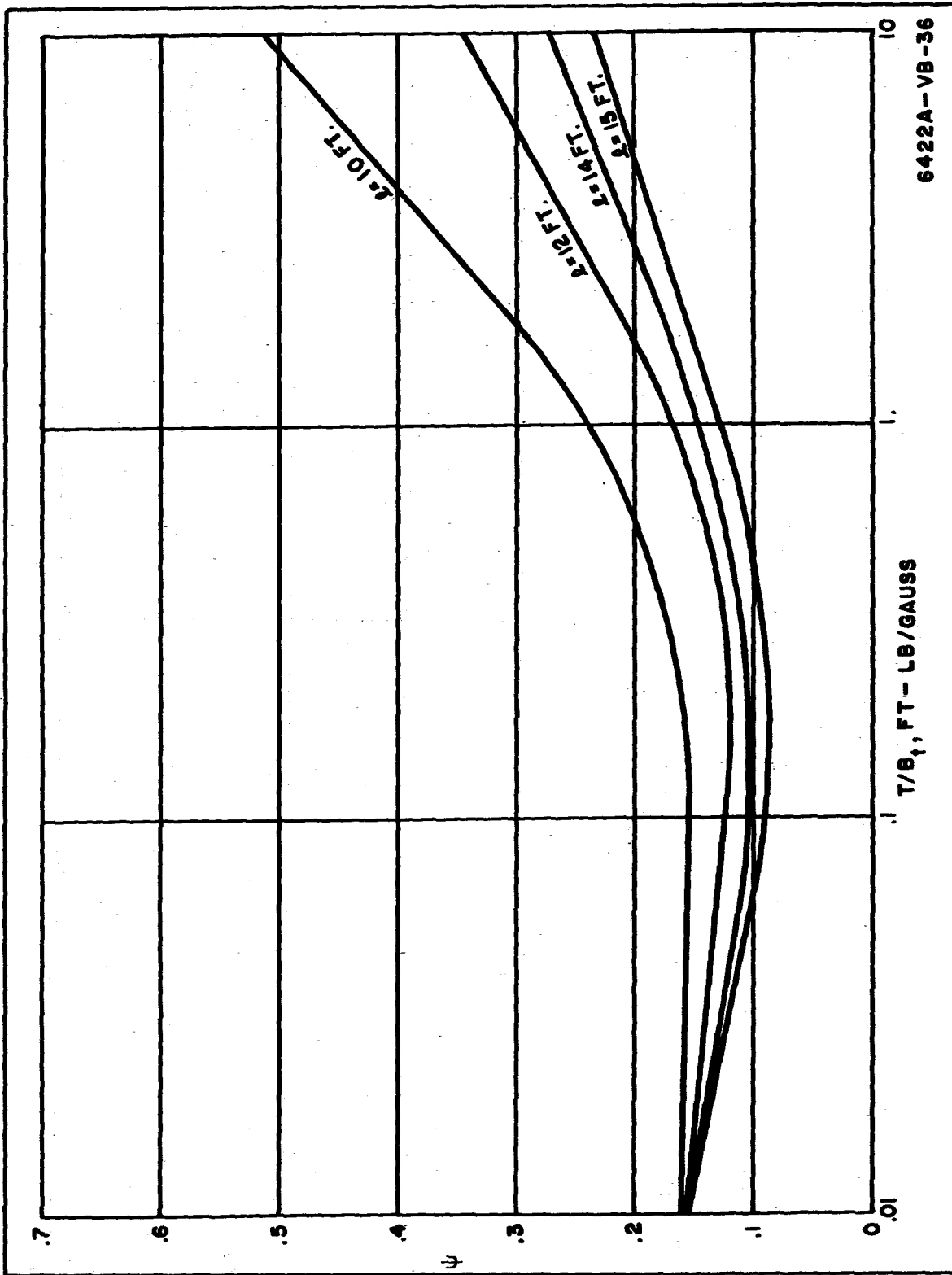


Figure 37.  $\psi$  vs.  $F(\psi)$





6422A-VB-36

Figure 38.  $\psi$  vs.  $T/B_t$  for Various Coil Lengths

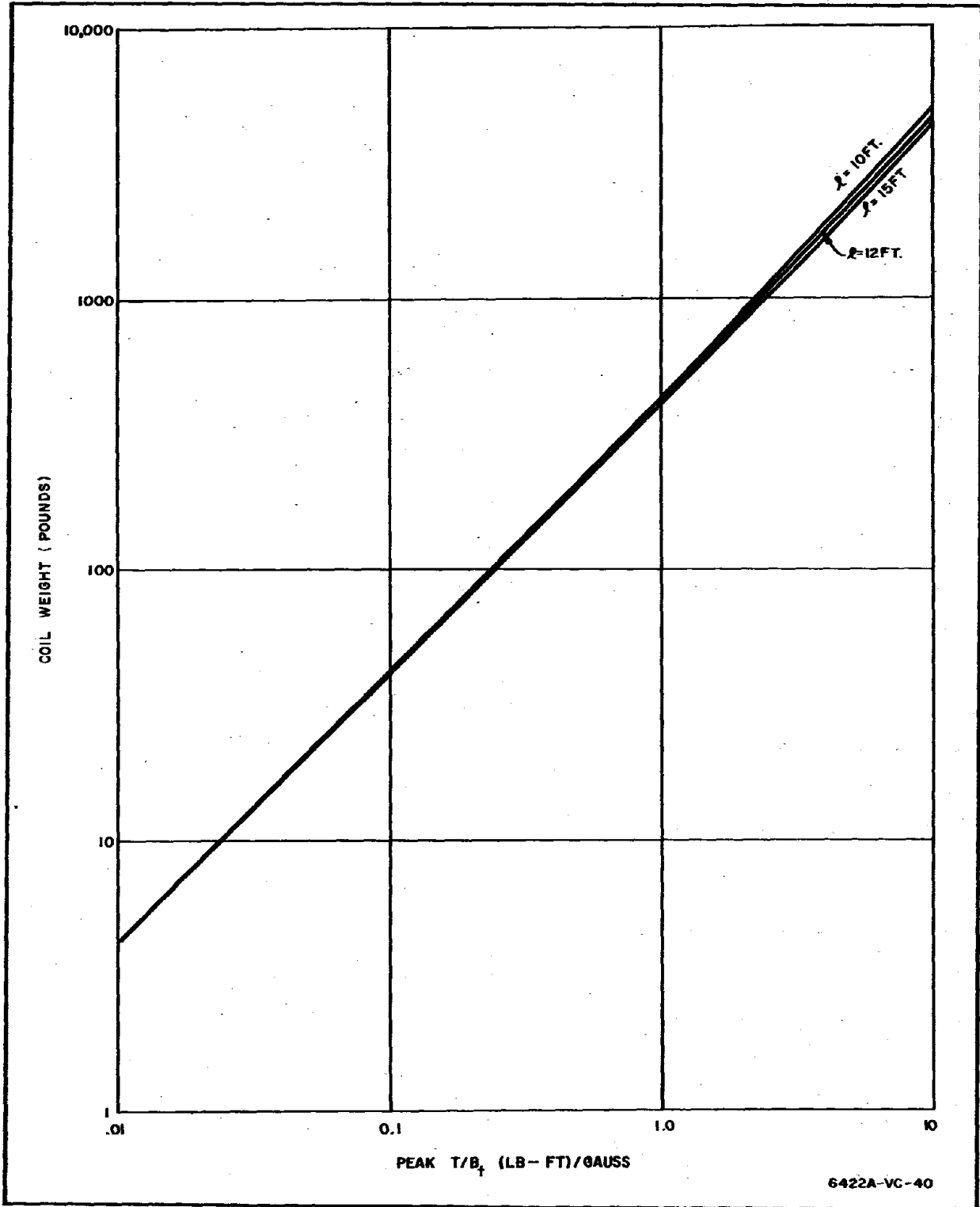


Figure 39. Iron-Core Torquer System Weight as Function of Required Torque/Field Ratio for Coil Lengths of 10 - 15 ft

From figure 7-6, the mass of each coil, including power supply, is given by

$$\begin{aligned} M_x &= 88.3 \\ M_y &= 37.3 \\ M_z &= 75.0 \end{aligned} \tag{7-14}$$

Thus, the total mass required for the iron-core torquer system, including power supply, is given by:

$$M_t = 88.3 + 37.3 + 75.0 = 200.6 \text{ lbs.} \tag{7-15}$$

The coil mass required for other parametric cases from Section 5 can be determined by use of figure 39, i.e., for any given  $\ell$  (which can be no greater than the diameter of the spacecraft considered) the required mass is read directly as a function of the required torque/field ratio.

A summary of the core and coil characteristics is presented below. The equations used to determine winding resistance, peak current and voltage are derived and listed in Appendix 4.

Table 11  
SUMMARY OF CORE AND COIL CHARACTERISTICS

	x Axis	y Axis	z Axis
Required Torque/ Field	0.209 $\frac{\text{ft lbs}}{\text{gauss}}$	0.0875 $\frac{\text{ft lbs}}{\text{gauss}}$	0.177 $\frac{\text{ft lbs}}{\text{gauss}}$
Torquer System Weight, including power supply	88.3 lbs	37.3 lbs	75 lbs
Length	12 ft	12 ft	12 ft
Core Diameter	1.56 inches	1.01 inches	1.44 inches
Winding Resistance	65.7 ohms	28.0 ohms	56.5 ohms
Peak Winding Current	0.105 amps	0.098 amps	0.106 amps
Peak Winding Voltage	6.9 volts	2.74 volts	6.0 volts

## 7.2 WEIGHT COMPARISON OF MAGNETIC TORQUING SYSTEM WITH GAS-JET SYSTEMS

This section, consists of a brief comparison of the magnetic torquing system and gas-jet systems. It was previously shown that the total weight (including power supply) of an iron-core torquer system for the nominal case came to 200.6 pounds while the air-core system weighed 151.7 pounds. By comparison, the following analysis shows that use of a cold gas jet system results in a weight of 1790 pounds for one year of operation.

Inputs to the analysis of weight requirements for a gas jet system on the nominal vehicle are:

- vehicle diameter = 12 feet
- vehicle length = 35.4 feet
- $I_{sp}$  (effective) = 35 secs
- Average disturbance torque = .0352 ft-lbs

The average disturbance torque about the pitch axis (for the nominal case) was obtained from table 2, where

$$T_{avg} = kM_{yo} \omega_o = (.218) (141.4) (1.14) (10^{-3}) = .0352 \text{ ft lbs.} \quad (7-16)$$

It should also be noted that an effective  $I_{sp} = 35$  secs is being used. Although the  $I_{sp}$  of the gas itself is about 65 secs, the lower figure is used to account for the heavy tanks needed to maintain the gas at very high pressure.

For the average torque of .0352 ft-lbs., the total momentum buildup in 1 year is given by:

$$\Sigma \Delta m = .0352 \text{ ft-lb-years} = 11.1 (10^5) \text{ ft-lb-secs.} \quad (7-17)$$

The change in mass,  $\Delta M$ , required to counteract the above momentum is given by:

$$\Delta M = \frac{\Sigma \Delta m}{g_o I_{sp} t} \quad (7-18)$$

where  $g_0$  = sea level gravity and  $l$  = the distance between the gas jet and the vehicle CG. Thus, for the pitch axis jets,  $l = 35.4/2 = 17.7$  ft. and the required mass of fuel is given by:

$$\Delta M = \frac{11.1(10^5)}{32.2(35)(17.7)} = 55.7 \text{ slugs} = 1790 \text{ lbs} \quad (7-19)$$

The number of times the jets must operate for either propellant during a year depends upon the percent of CMG saturation allowed as well as the average torque. Assuming that the allowable pitch axis saturation is 15 percent of its maximum, then the allowable momentum buildup is

$$\Delta m = .15 (1414) = 212 \text{ ft-lb-secs.} \quad (7-20)$$

where 1414 ft-lb-secs is the system capacity about the pitch axis. Then the average number of operations in one year is given by:

$$n = \frac{11.1(10^5)}{212} = 5240 \text{ operations} \quad (7-21)$$

A system employing monopropellant hydrazine instead of cold gas would require less mass, due to its greater  $I_{sp}$ . For an effective  $I_{sp} = 200$  secs, the mass required is:

$$\Delta M = \frac{11.1(10^5)}{32.2(200)(17.7)} = 9.75 \text{ slugs} = 314 \text{ lbs.} \quad (7-22)$$

A summary of system weights and number of operations for the nominal case is given below.

Table 12

SUMMARY OF SYSTEM WEIGHTS AND OPERATIONS

	<u>System Weight</u>	<u>Number of Operations</u>
Iron-Core Magnetic Torquer	200 lbs	continuous
Air Core Magnetic Torquer	150 lbs	continuous
Cold-Gas Jets	1790 lbs	5240/year
Monopropellant Gas Jets	313 lbs	5240/year

### 7.3 INTERFACE OF CMG AND MAGNETIC TORQUERS

This section describes the electronic circuitry required to provide the correct current to the magnetic torquer coils. The function of this circuitry is illustrated in the diagram in figure 8.

According to the magnetic torquer control law the coil current components are determined by solution of the following equations:

$$\begin{aligned} I_x &= K_1 (M_y B_z - M_z B_y) \\ I_y &= K_1 (M_z B_x - M_x B_z) \\ I_z &= K_1 (M_x B_y - M_y B_x) \end{aligned} \quad (7-23)$$

where  $I_x$ ,  $I_y$ ,  $I_z$  are the required currents along the roll, pitch and yaw axes,  $B_x$ ,  $B_y$ ,  $B_z$  are the components of the Earth's magnetic field along these axes,  $K_1$  is a gain constant and  $M_x$ ,  $M_y$ ,  $M_z$  are the components of angular momentum.  $B_x$ ,  $B_y$ ,  $B_z$  are determined from the magnetometers,  $K_1$  is a constant and  $M_x$ ,  $M_y$ ,  $M_z$  are determined directly from the CMG resolver outputs as follows:

$$\begin{aligned} M_x &= -H \sin \beta_3 \\ M_y &= 2H \sin \beta_1 \\ M_z &= -2H \sin \alpha_1 \cos \beta_1 \end{aligned} \quad (7-24)$$

where  $H$  is the spin momentum of the single degree-of-freedom gyros,  $\beta_3$  is the angular displacement of the single degree-of-freedom gyros, and  $\alpha_1$  and  $\beta_1$  are the outer and inner gimbal angles on the two degree-of-freedom gyros.

Figure 40 is a block diagram of the circuit to generate the coil currents  $I_x$ ,  $I_y$ ,  $I_z$ , using the relationships in Equations 7-23 and 7-24. The triangular blocks represent summing, power and buffer amplifiers and the letters within the block represent different types. Buffer amplifiers are used on the outputs of both the magnetometer and the tachometer to provide the necessary load impedance and fail-safe isolation.

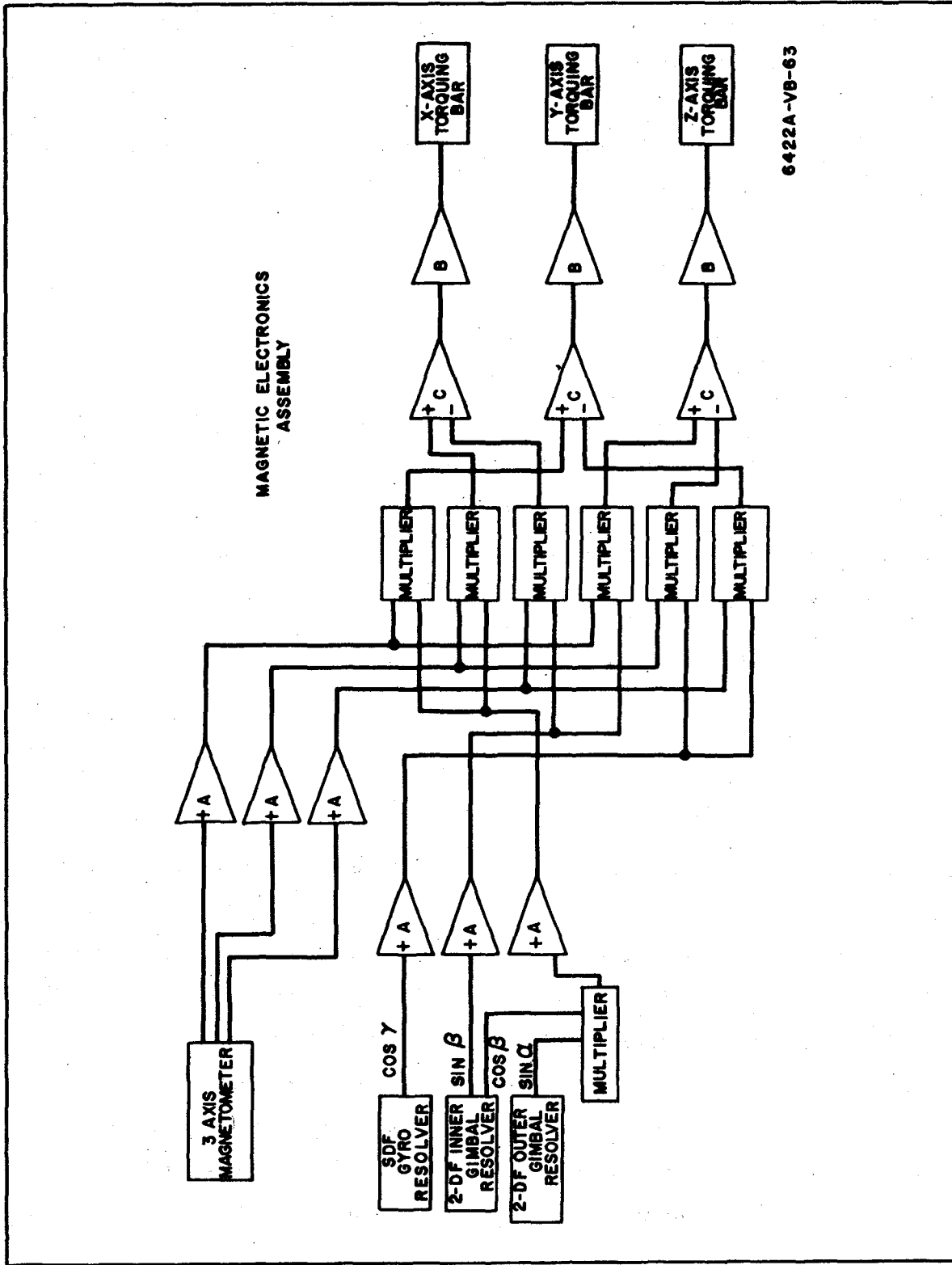


Figure 40. System Block Diagram

### 7.3.1 Circuit Mechanization

The mechanization of the block diagram (figure 40) was designed around the use of MIC's (micro-electronic integrated circuits). This method of mechanization was chosen primarily for two reasons:

a. The use of MIC's permits a substantial weight reduction over that which can be achieved with conventional semi-conductor techniques.

b. The reliability of a circuit is substantially improved by incorporating it in a single "flat pack" since failure-inducing fabrication of separate components is avoided. This makes it possible to meet reliability requirements without weight and power-consuming redundancy.

A typical operational amplifier circuit is shown on figure 41. With the exception of the input resistors, it represents the circuit of the WS 161 operational amplifier, which is in production at the present time. The quiescent power dissipation of each amplifier was reduced to meet the power supply limitations, since a total of forty-five amplifiers are required. In the block diagram of figure 40 and in subsequent paragraphs, letters are used to differentiate between various types of amplifiers. With the exception of the "B" or power amplifier, all of the letters refer to the basic amplifier with variations in the output stages but with common first and intermediary stages.

Type "A" - This amplifier is the same as that shown in figure 41. It is used in the buffer amplifier stages between the sensors and the multipliers, and in the summing amplifier associated with each multiplier. The use of passive input impedance sources permits a high degree of electrical isolation that is fail-safe. The input is normally connected to one of the (+) inputs and the feedback connected to one of the (-) inputs. The good tracking of the differential first stage over the temperature range (approximately 1 nanoamp per °C) insures low drift over the 100°C range of operation for which one must design. Variations in required gains are taken care of by building sub-groups which vary only in their input impedances. When used as a coil-current monitor, the amplifier has both a (+) and (-) input as well as a (-)



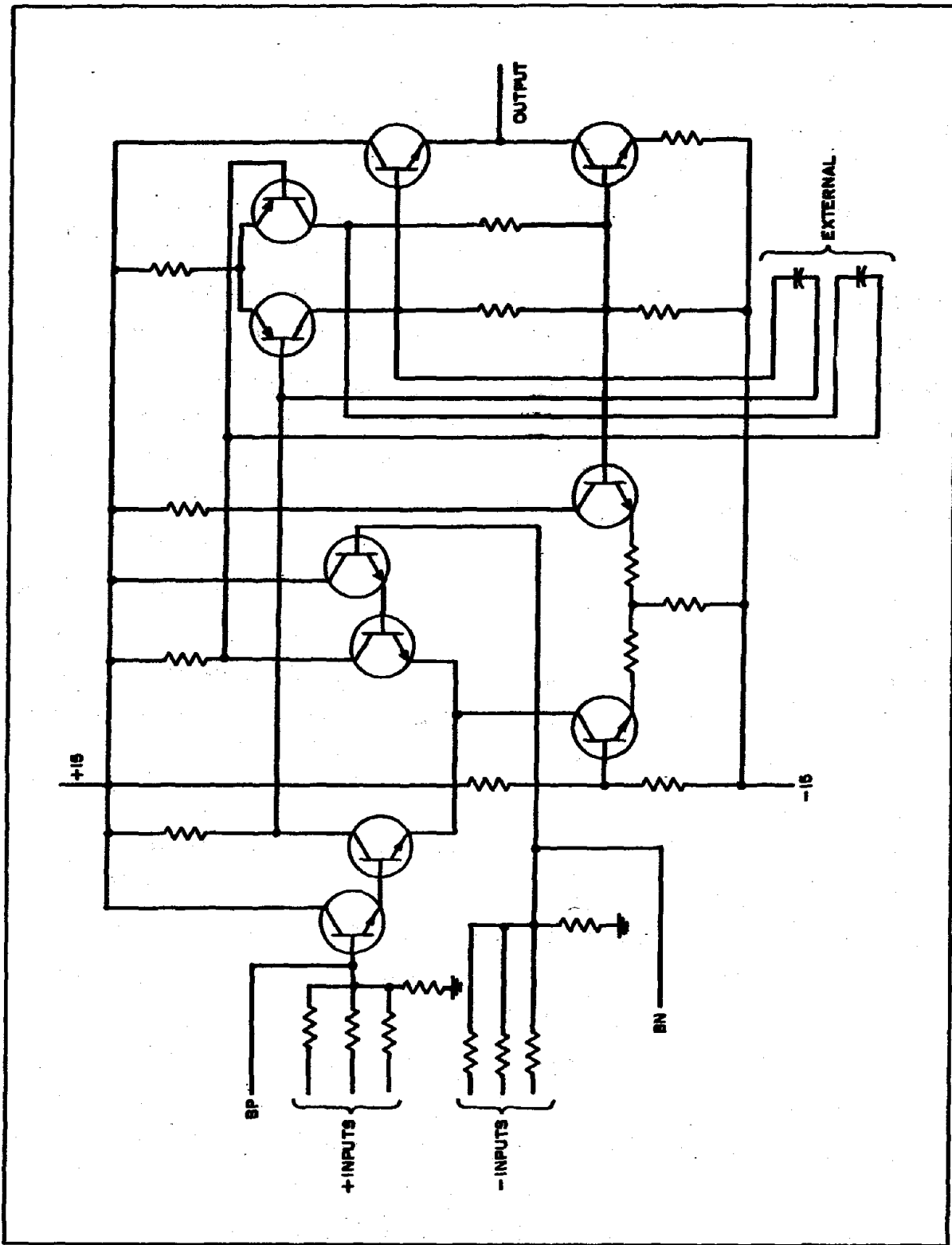


Figure 41. Operational Amplifier

feedback connection. The amplifier then converts the voltage across the current monitoring resistance into a differential voltage.

Type "B" - This is the coil driver stage and is shown schematically on figure 42. The differential outputs of the "C" (summing) amplifiers are used to drive the connected bases of back-to-back NPN-PNP transistors through an emitter follower. Both the NPN and PNP stages on each side are biased to cutoff for a balanced input. When the differential input exceeds the sum of the  $V_{be}$  drops, the current flows through the higher-base-voltage NPN transistor through the coil and then through the opposite PNP transistor to ground. The bases are normally biased at about +13 volts, and permit a coil driving differential swing of  $\pm 16$  volts. Since the deadzone introduced by the base-cutoff characteristic of balanced operation would have a deleterious effect on accuracy, the complete current command loop will be closed around the "C" amplifier by feeding back the output voltage to the differential input stage of the "C" amplifier. The effect on loop stability will be compensated by using larger roll-off capacitors in the "C" amplifier. The circuit elements involved in the coil driver will be made up of separate components to enhance thermal dissipation. To provide fail safe operation, current limiting resistors are put into each current path to limit total power drawn during a single-failure mode. The peak power drawn during normal operation is calculated from the equation:

$$P_m = V_s \sqrt{I_{PM}^2 + I_{YM}^2 + I_{RM}^2} + P_Q \quad (7-25)$$

where

$P_m$  = maximum power drawn from the unregulated supply by combined coil drivers

$V_s$  = unregulated supply voltage

= +28 volts

$I_{PM}, I_{YM}, I_{RM}$  = peak coil currents in the pitch, yaw and roll axis torquing bars

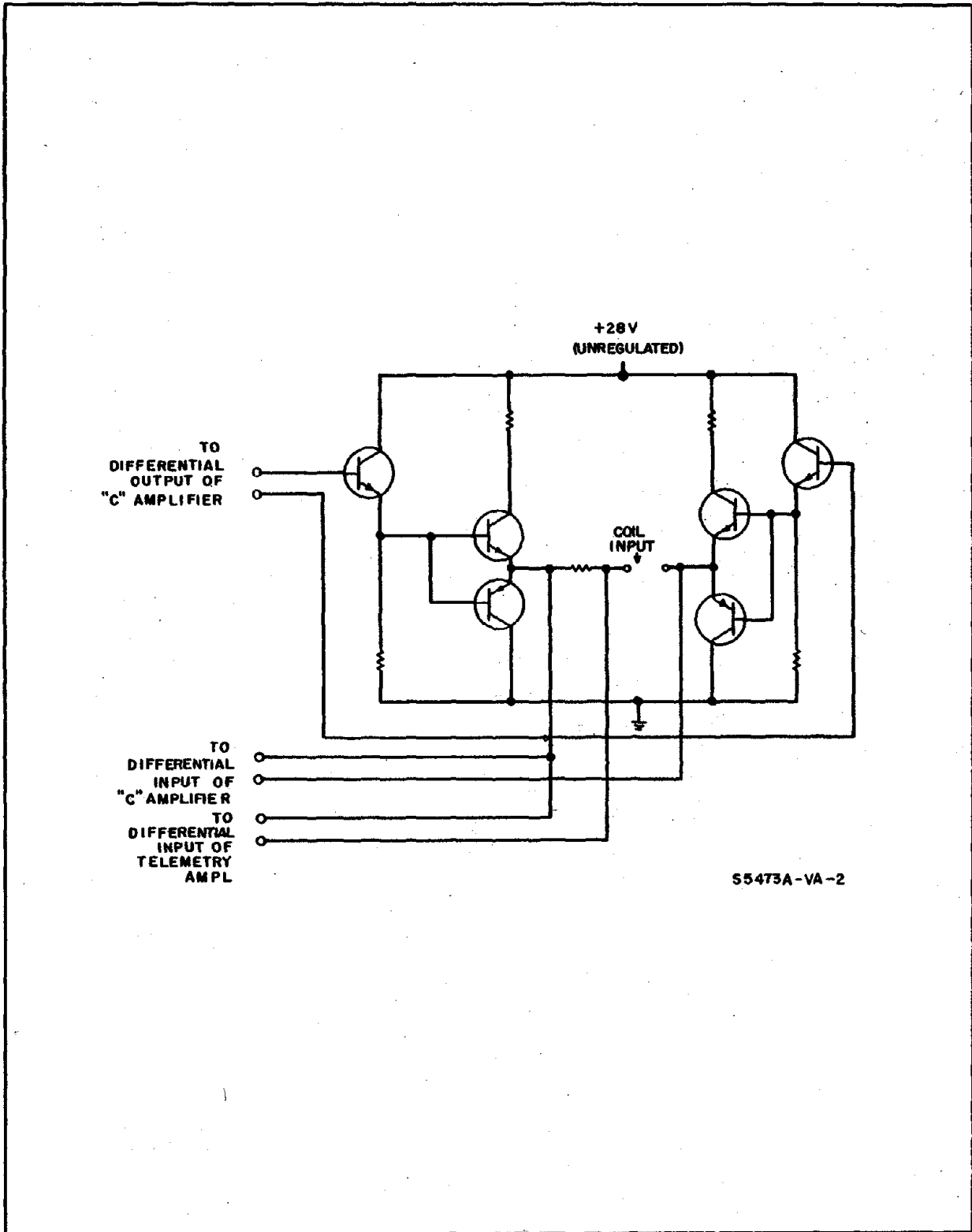


Figure 42. Coil Driver Stage

$$\begin{aligned}
 &= .416 \text{ amps, } .389 \text{ amps and } 0.418 \text{ amps} \\
 P_Q &= \text{quiescent power drawn by the emitter followers} \\
 &= 170 \text{ mw}
 \end{aligned}$$

The peak total power drawn during normal operation is thus computed as 20 watts.

Type "C" - This amplifier differs from the basic amplifier of figure 41 by having an emitter follower on both sides of the differential output. Since the emitter followers are not required to generate negative outputs (the coil driver bases are nominally biased at +13 volts and swing from +5 volts to +21 volts), the constant current source between the emitter and -15 volts may be replaced by a fixed resistor drawing negligible current. To balance the power drain between supplies, the output emitter followers would work with +28 volts supplied from that regulated supply.

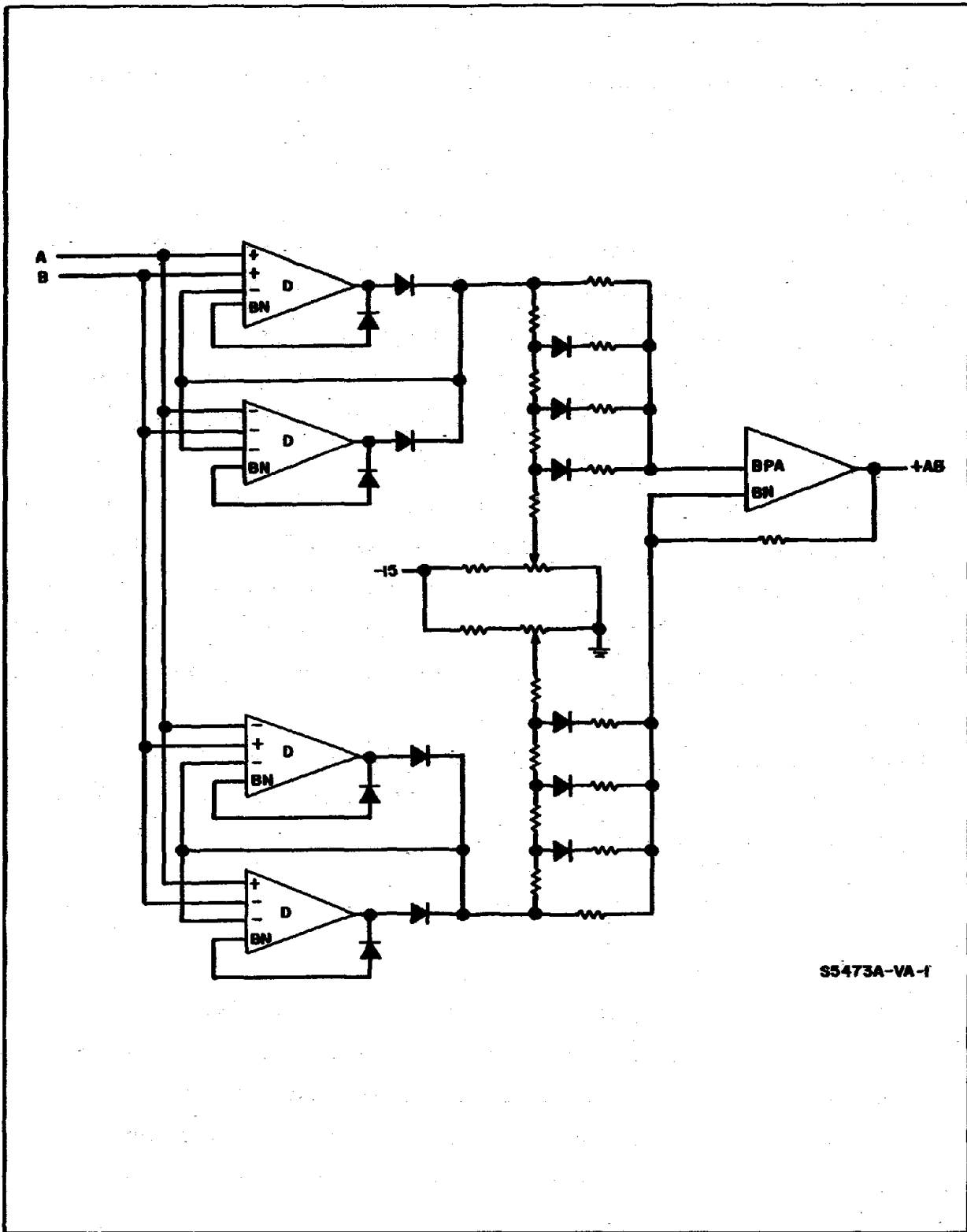
Type "D" - This amplifier is used as the network driver in the multiplier circuit, which will be described in the next paragraph. This amplifier, like the "C" amplifier, only requires positive outputs and uses the +28 volt regulated supply for its output emitter follower stage. Since only a single-ended output is required, however, the output stage will consist of only a single emitter follower.

The block/schematic diagram of the multiplier is shown on figure 43. Using a diode-resistor network to form the nonlinear function, the circuit is a mechanization of the equation:

$$AB = \frac{(A + B)^2 - (A - B)^2}{4} \quad (7-26)$$

where A and B are functions to be multiplied.

In figure 43 the two amplifiers in the upper left of the diagram form the sum  $|A + B|$ , one amplifier functioning for an algebraically positive sum and the other functioning for an algebraically negative sum. The network forms a non-linear input resistor to the positive node of the summing amplifier, and generates a one polarity signal as a measure of  $(A + B)^2$ . In like manner,



S5473A-VA-1

Figure 43. Multiplier Block Diagram

the lower network and two "D" amplifiers generate  $(A - B)^2$ , which is connected to the negative node of the summing amplifier along with the summing amplifier feedback.

The diode-resistor network is the common break-point type in which increased signal causes the diodes to become sequentially forward biased, and thus increases the signal input to the summing amplifier node as a non-linear function of input signal. Since the network is essentially approximating a continuous function ( $y = x^2$ ) by means of a series of straight lines, as shown on figure 44, it becomes necessary to determine the number of break points and their value in terms of full scale input. To demonstrate this, the diagram and symbol shown on figure 45 will be used. The closest fit between the desired function and any straight line segment will be found by defining the parameters of the straight line such that the peak deviation will occur at each breakpoint and at one intermediary point. By using the equation  $U = A_x + B - x^2$  and then defining A and B in terms of the peak error  $U_m$  and the upper break point  $X_1$ , it becomes possible to define the lower break point  $X_0$ :

$$X_0 = X_1 - \sqrt{8 U_m} \quad (7-27)$$

When  $U_m$  is a fixed percentage of the maximum input over the entire range, the break point spacing is equal for all segments. For this system, a multiplication accuracy of 5 percent appears to be sufficient. Since the percentage error in the multiplication is the sum of the errors in each squaring function, it would be desirable to approximate the parabola to within 1 percent of full scale which would leave approximately 3 percent to be taken up by bias and gain variations. For  $U_m = 0.01$  (corresponding to 1 percent error), the maximum spread between break points ( $X_1 - X_0$ ) is found to be 28.3 percent of full scale. This would dictate four segments, or three diode generated break points (the break point near the origin is handled by a resistor).

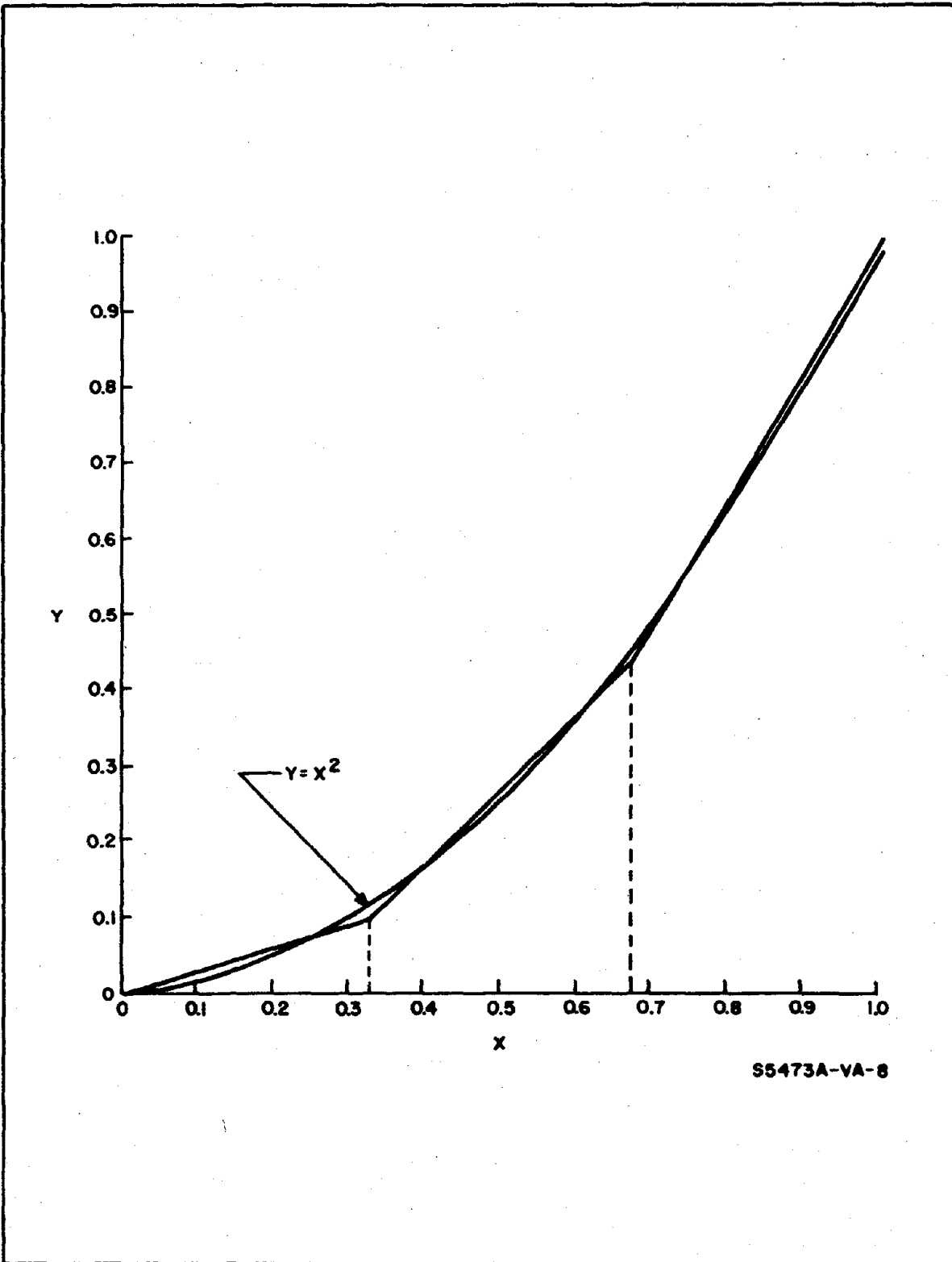
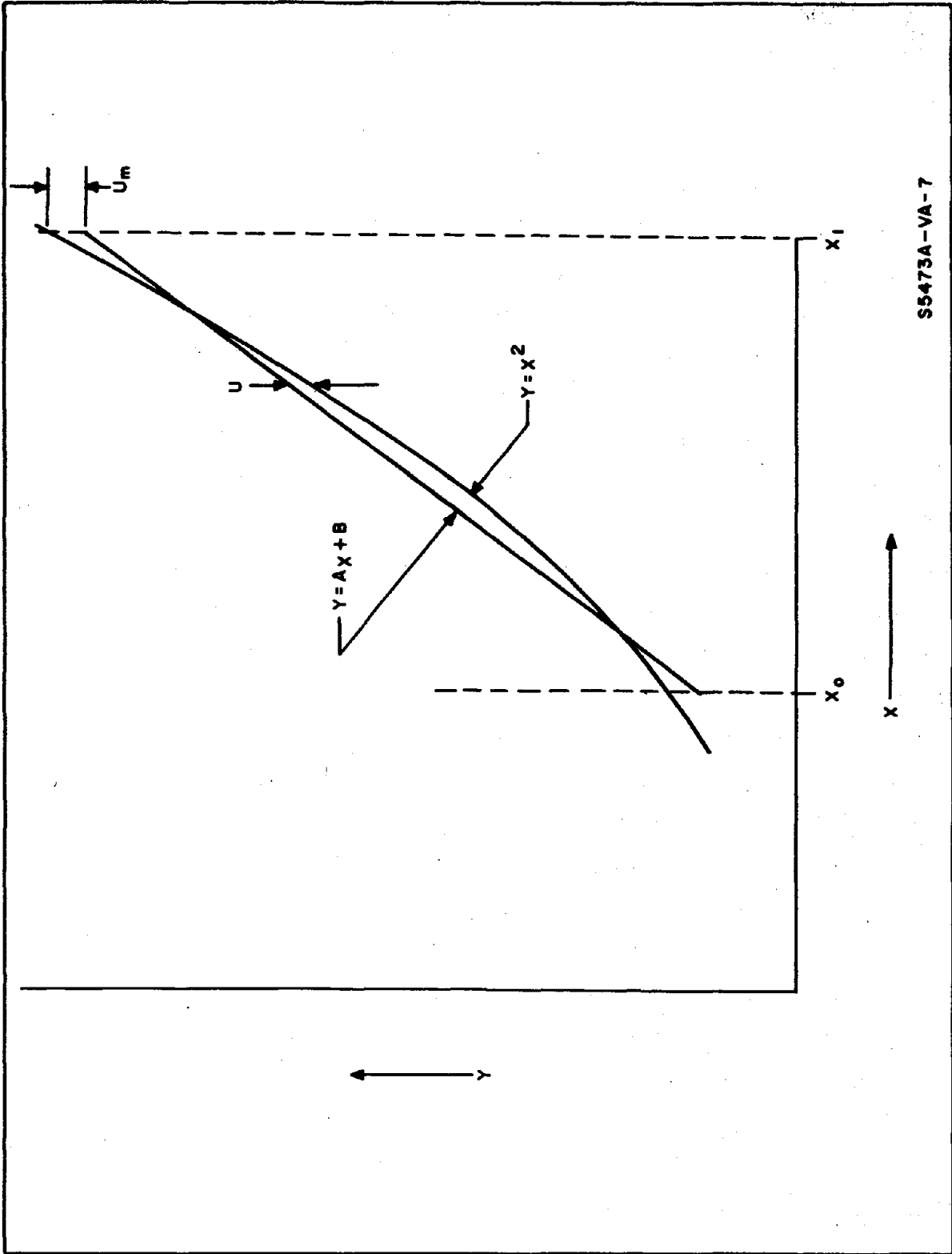


Figure 44. Straight Line Approximations



S5473A-VA-7

Figure 45. Approximation Errors



The gain and multiplying tolerances, it is felt, can be achieved without the use of trimming potentiometers since the gain tolerance of each amplifier will be determined by the ratio of feedback to input resistances. On the normal MIC this ratio can be held to 2 percent. The only exception to this is the trim pots used to adjust for tolerance variations on the forward voltage drop of the diodes in the nonlinear networks of the multiplier.

### 7.3.2 Consideration of Time-Sharing

Using the same computer for both the CMG system and the magnetic unloading system would have no effect on the magnetic system's performance. The magnetic torques have a maximum frequency on the order of one cycle every few hundred seconds and a torque that is low compared to the CMG control torques; therefore, changing the magnetic system torquer a few seconds after the change was desired would have no noticeable effect on performance. This would allow the CMG system to have priority on the computer and to relinquish it only for a few milliseconds every ten or fifteen seconds, which would be allowable for the stated CMG system performance requirements.

Although the use of a time-sharing system is possible, its need is doubtful due to the simplicity of the magnetic system controller circuitry.

### 7.3.3 Mechanical Design of the Magnetic Torquers

Figure 46 shows the physical design typical of all three torquers. The torquer cores end in a short threaded stud at each end. These allow assembly to two end brackets. Several pillow block supports along the 12-foot length prevent excursion and overstressing under shock and vibration.

One end bracket mounts the external connector. The windings terminate on two standoffs and heavier wire connects the standoffs to the external connector. Two wires are used for each lead to improve reliability. The housing for those terminations is encapsulated in RTV silastic rubber as protection from shock and vibration.

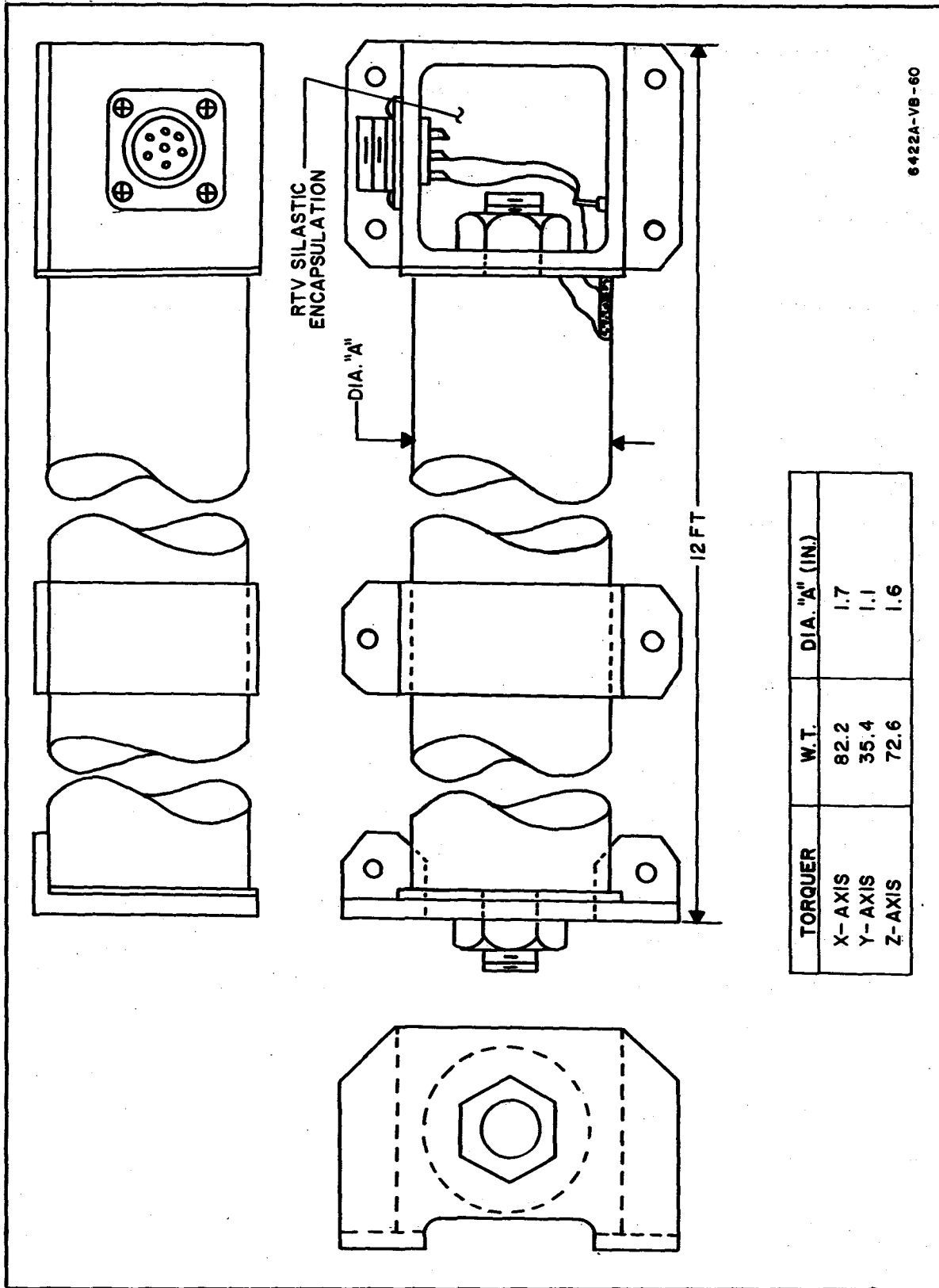


Figure 46. Mechanical Design of Torquer Bars

The coils are machine-wound with end plates in place to retain the windings. A solvent is wiped onto the cement-coated wire during the winding process and the wire sets in place as the solvent evaporates. Subsequent baking outgasses the cement.

The coil is coated with epoxy for handling protection, and this coat is also baked out.

If a reflective coating is required for thermal control, it may now be applied by vapor deposition or by winding the coil with an aluminized Mylar tape.

The coil is now assembled to the end brackets and the leads are connected. The box-like bracket is encapsulated and the assembly is given final baking.

Intermediate supports are assembled at about 1-foot intervals. These pillow block supports have relatively soft facings to prevent damage to the windings.

#### 7.3.4 Electronics Packaging Plan

Figure 47 illustrates a preliminary layout of the electronics assembly. The unit contains a mixture of modules and discrete components, as dictated by component sizes and heat dissipations. Some of the details of the manufacturing techniques required are discussed in succeeding paragraphs.

By referring to the system schematic or block diagram, it can be seen that the components are laid out in a pattern for point-to-point welded intra-connection. The higher power transistors, which do not lend themselves to modular packaging, are laid out with fairly generous spacing to aid in heat distribution on the radiating cold plate. Coupling of the components to the cold plate is accomplished primarily via metal spring finger devices fastened permanently to the cold plate and pressing on the module surfaces or clipping around the transistor bodies. A secondary thermal route is through the printed circuit board and thence to the frame and cold plate.

The two connectors, one for both signal and power connections and the other serving AGE functions, occupy about 1-1/4 inch at one end of the

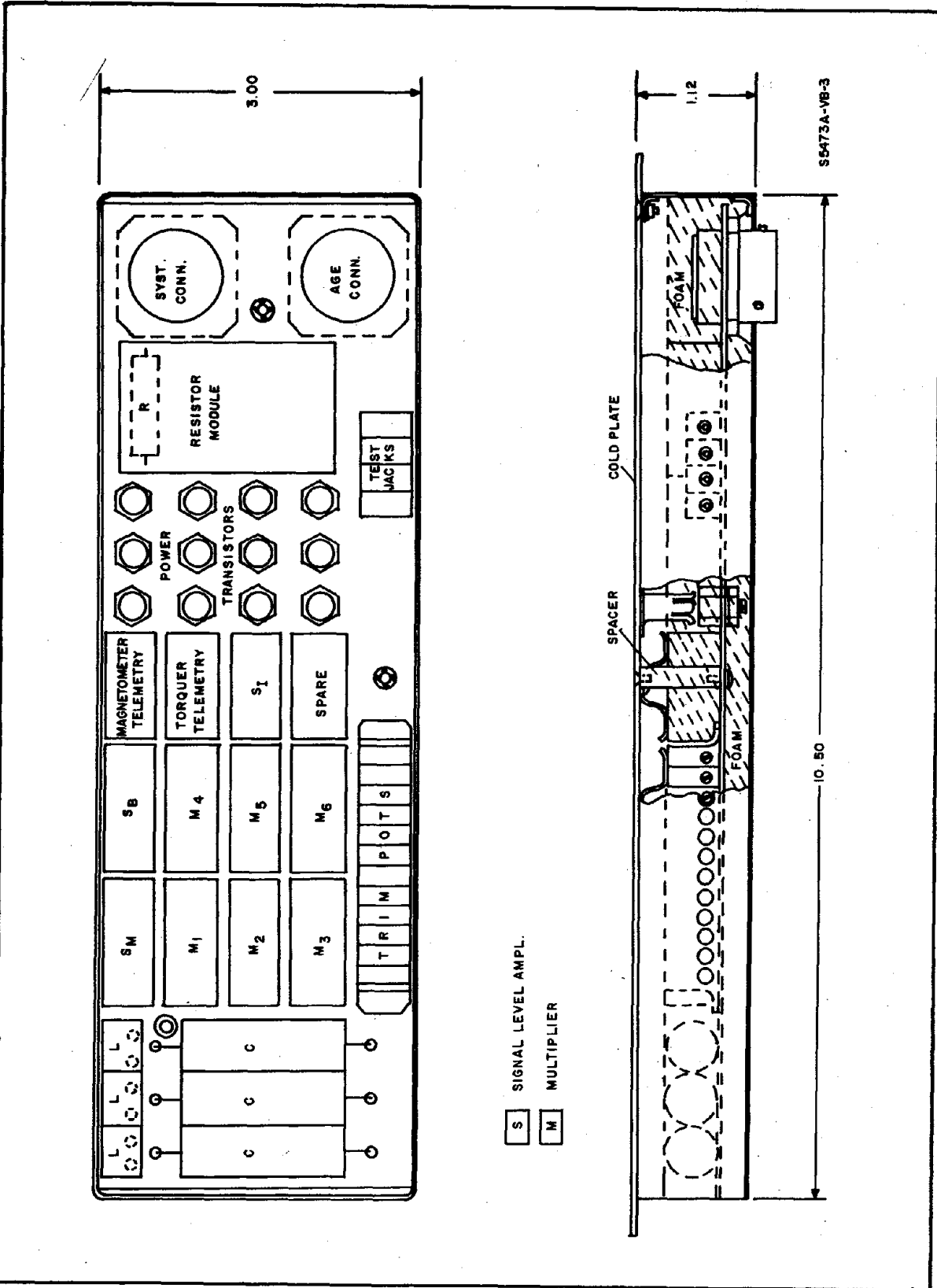


Figure 47. Magnetic Electronics Assembly

package. These are mounted on the side opposite the cold plate for ease of connection.

After assembly and appropriate testing, the entire package is foamed in a mold with a polyurethane foam having a density of 4 pounds per cubic foot. After foaming, the unit is outgassed in an oven and re-tested. The trim pot adjusting screws are kept free of foam for final adjusting as are any test points which may be required.

Overall dimensions of the assembly are 3 inches by 10-1/2 inches by 1-1/8 inches, excluding the flanges necessary to fasten the unit to the spacecraft structure.

Both the cold plate and the opposite cover plate are removable for making repairs. It is possible to cut away the rigid foam, remove a component, and weld in a new one without undue difficulty.

Total weight for the unit is estimated at 1.20 pounds, giving a packaging density of about 60 pounds per cubic foot.

#### 7.3.4.1 Sub-Module Construction

The components which make up the signal level amplifiers, the multipliers (less the trim pots), and the telemetry circuits are packaged into stacked array sub-modules. Basically this sub-module consists of the designated number of integrated circuit flat-packs and filter capacitors stacked on edge within a molded plastic frame. The components are separated from each other by thin spacer blocks which fit into shallow slots in the base plate. The spacers have molded into them three leads going from side to side to act as convenient cross-overs, one lead from each side terminating as an output pin on the bottom, and one other lead that can be used as either a cross-over or an output pin; this is illustrated in figure 48. Holes in the bottom of each slot in the base accept the output pins. Interconnecting welds are made on the side of the assembly, between component leads and spacer block leads, with small rectangular ribbon and using the point-to-point method of wiring.

The inputs and outputs are welded to the pins that exit from the base. After successful completion of all electrical tests, the units are embedded in a filled resin to furnish environmental protection and improve heat transfer. Sub-modules made in this manner are 0.50 inches wide, 0.50 inch high, and approximately 0.100 inch long for each flat-pack or filter capacitor included.

The resistors for the power level amplifiers are formed into a molded sub-module to conserve space and to promote heat transfer to the cold surface. This is similar in concept to a standard cordwood unit, but the resistors are double stacked in a horizontal plane. Interconnections are made by welded ribbon and outputs will terminate in pins exiting from the base of the unit. Filled epoxy is used for encapsulation.

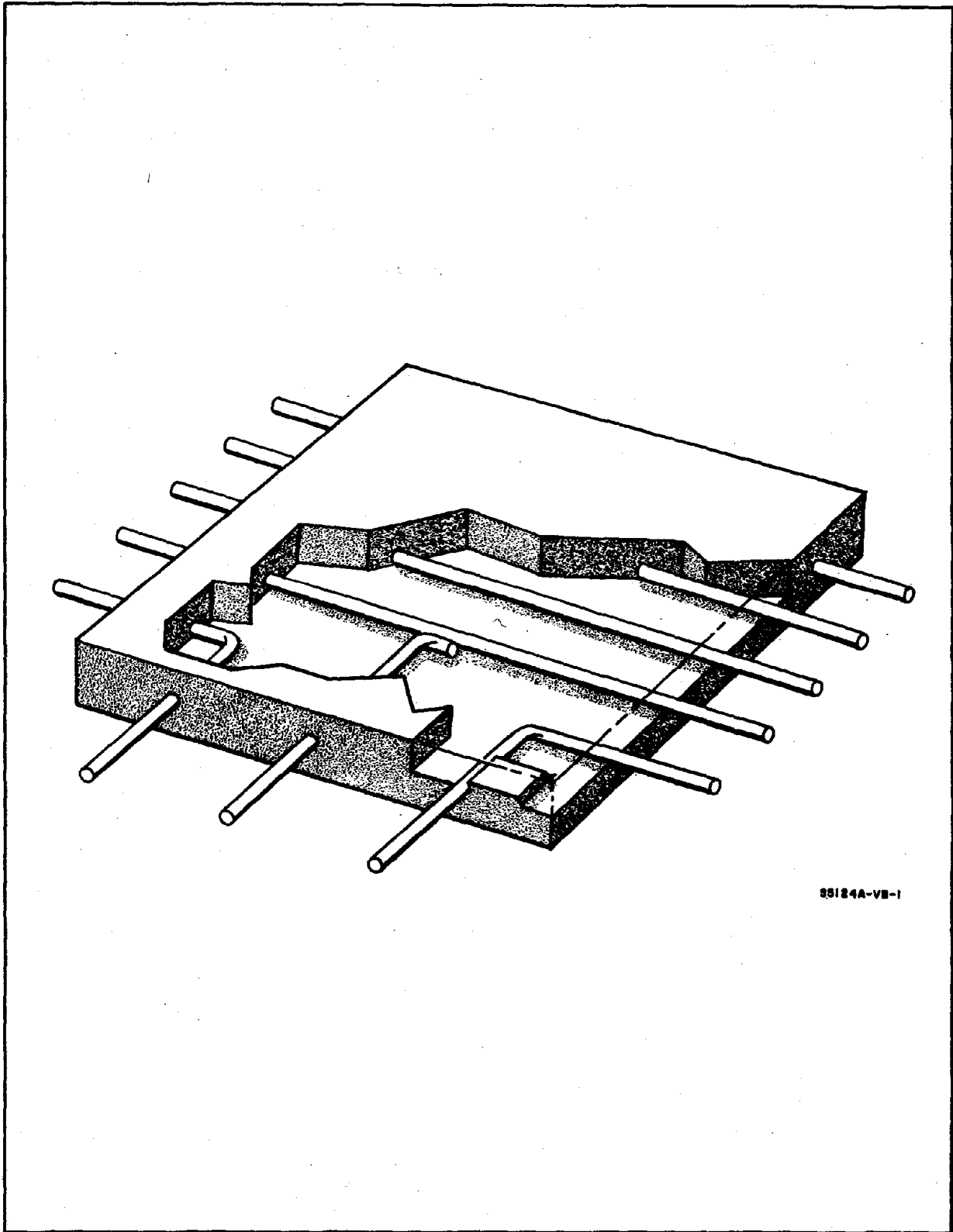
#### 7.3.4.2 Intraconnections

For intraconnections between the various sub-modules output pins and the individual component leads, welded wire connections are used, utilizing rectangular ribbons in the point-to-point method. If the required intraconnections are too numerous to be made in one layer, two layers are used. This is accomplished by inserting any lead which crosses over another lead into a section of thin wall Teflon sleeving before welding it in place. In addition, all leads which terminate at the output connector are sleeved.

Two output connectors are required; these are 44-pin Deutsch STK type. Since these have crimped terminal pins, some experimentation is required to determine the best way to attach the 0.01 inch  $\times$  0.03 inch rectangular ribbons to them. If possible, the terminals will be crimped directly around the ribbons. If this is not reliable, an adaptor will be utilized which will be crimped into the terminal and to which the ribbons will be welded. The objective is the strongest most reliable joint; this is felt to present no serious problem.

#### 7.4 MAGNETOMETER

An example of a magnetometer which is sufficient for the magnetic torquing system is a modification (to incorporate redundancy) of the Dalmo-



88124A-VB-1

Figure 48. Details of Spacer Block

Victor 103-3 design. The electronics package and the probes will be designed as a single assembly which will occupy 36 cubic inches.

The magnetometer operates on the flux-gate principle. A 2400 cycles/sec sine wave is applied to a coil which is wound on a ferromagnetic rod. Under a zero field condition, the flux density variations in the rod will be symmetrical about zero, producing only a fundamental output in a secondary winding. Under conditions where a component of the external field exists along the axis of the rod, the flux density in the rod will no longer operate around zero and the ferromagnetic non-linearities will cause second harmonic voltage components to be developed in the secondary winding. The secondary signal is then passed through a tuned amplifier and then into a phase sensitive demodulator which is switched at 4800 cycles/sec. The demodulator and its associated filter reject all but the zero frequency component of the signal and provides a direct current signal proportional to the amount of flux-density unbalance. The direct current signal is then passed through a buffer amplifier which provides the driving current for the feedback winding on the probe. The current in this feedback winding is phased to cancel the field intensity induced by the external field. Thus the relationship between the feedback coil current and field intensity can be expressed as:

$$\frac{I(S)}{H(S)} \cong \frac{K/(1+K)}{K_f(1+T_f S)}$$

where  $I(S)$  = feedback coil current expressed in Laplace transform

$H(S)$  = field intensity expressed in Laplace transform

$K_f$  = feedback coil gain in equivalent oersted per amp

$K$  = loop gain

$T_f$  = demodulator filter time constant

The coil current is thus relatively independent of loop parameters except for the feedback coil gain, which is a stable parameter. The feasibility of permitting loop gain variation makes it relatively easy to add redundancy,



since the use of parallel amplifier elements connected by resistors (for example) provides a redundancy technique which does not introduce gain and balance problems on an open loop basis. The redundancy to be added will be in portions of the signal amplifier and the demodulator.

To provide the required 2/1 relationship between the probe excitation and the demodulator reference, the 4800-Hz demodulator reference is used to drive a flip-flop to establish the 2400-Hz probe reference.

Some of the parameters of the magnetometer design are:

Electronics weight: 18.5 oz

Probe (3) weight: 11.5 oz

Power drain: Less than 380 mW from +15V

Less than 380 mW from -15V

Less than 100 mW from 4800 Hz

Linearity: Better than 0.5%

Output scale: 40 volts/oersted

Signal ripple: Less than 0.05 volt

Output load impedance: Better than 50K if possible

Output zero offset: Less than 1% of full scale

Reliability (with redundancy):  $P_s = 0.956$  for 1 year

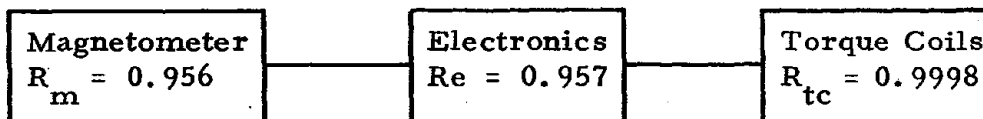
Mounting tolerance: Within 1°

## 7.5 RELIABILITY ESTIMATE

A preliminary reliability estimate based on the preliminary design has been prepared. This estimate is shown in table 13.

The reliability estimate is based on a parts count of the proposed system and the reliability model shown in the sketch below. As is shown in the sketch, the system is essentially a series system composed of 3 components. It has been assumed for the purposes of this estimate that the component parts of the electronics and torque coil assemblies exhibit an exponential failure distribution and therefore have a constant failure rate with time. The magnetometer has some redundant elements and therefore does not

exhibit an exponential failure distribution. The failure data for the magnetometer, which was furnished by the manufacturer, is a reliability (probability) figure. In order to obtain a total system failure rate, all failure rates were converted to a reliability figure and the product rule applied. For reliability calculations for this system, a mission time of 8800 hours is used.



$$R_{\text{system}} = R_m \times R_e \times R_{tc} = 0.915$$

The reliability figure for the electronics and torque coil assemblies was derived as follows:

With the basic assumption of an exponential failure distribution and constant failure rate, the reliability of a part of units whose failure rate is constant may be expressed by:

$$R = e^{-\lambda t} \tag{7-28}$$

where

$R$  = Reliability

$\lambda$  = Failure rate

$t$  = Mission or operating time

A group of  $n$  parts or units in series have a reliability given by the product rule as:

$$R_s = R_1 \cdot R_2 \cdot R_3 \cdot \dots \cdot R_n \tag{7-29}$$

where

$R_s$  = Reliability of the group

$R_1, R_2, R_n$  = Reliability of the elements of the group.

Substituting equation (7-28) into equation (7-29) yields the following expression in terms of the failure rates:

$$R_s = e^{-\lambda_1 t} \cdot e^{-\lambda_2 t} \cdot e^{-\lambda_n t} \quad (7-30)$$

Then:

$$R_s = e^{-(\lambda_1 + \lambda_2 + \lambda_3 \dots + \lambda_n)t} \quad (7-31)$$

and

$$R_s = e^{-\left(\sum_{i=1}^n \lambda_i\right)t} \quad (7-32)$$

where

$\lambda_1, \lambda_2, \lambda_3, \lambda_n$  = failure rates of the elements of the series group.

Consider any unit of the proposed system. The reliability of the unit from equation 7-32 is as follows:

$$R_u = e^{-\lambda_u t} \quad (7-33)$$

where

$R_u$  = Reliability of the unit

$\lambda_u$  = Sum of the failure rates of the component parts in that unit

$t$  = Mission or operating time.

from equations 7-29, 7-31, and 7-32 the reliability of the system is expressed as:

$$R_T = e^{-\lambda_T t} \quad (7-34)$$

where

$R_T$  = The reliability of the system

$\lambda_T$  = Sum of the failure rates of the units composing the system

t = Mission or operating time.

From this discussion, it may be easily seen that the failure rate of each unit is equal to the sum of the failure rates of its parts and it follows from the sketch that the failure rate of the system is equal to the sum of the failure rates of the various units.

Table 13 shows the reliability estimate for the Magnetic System. Surface temperatures in the order of 65° - 70°C have been used in the failure rate calculations. This appears to be the maximum anticipated operating temperature based on preliminary data. The failure rates given are based on manufacturer's data which has been adjusted to reflect reliability improvement through special controls and testing. These controls would include:

- 1) Power and Temperature Burn-In
- 2) Temperature Cycling
- 3) Leak Tests
- 4) Noise Tests
- 5) 100% inspection of all electrical parameters
- 6) Variables data before and after burn-in
- 7) Hermetic Seal Tests
- 8) X-ray inspection

In order to achieve the required reliability, controls of this type will be necessary.

Included in table 13 are the failure rate calculations for the Electronics and Torque Coil sections, the reliability for all 3 sections, and the system reliability. The reliability calculations are based on a mission time of 8800 hours.

Table 13  
RELIABILITY TABULATION

Electronics

Part	No. Used	Based Failure Rate %/1000 Hrs.	Total Failure Rate %/1000 Hrs.	Source Failure Rate
MIC Flat Pack (Amplifier)	36	0.0100	0.3600	Mfg Data
MIC Flat Pack (Resistor-Diode Net- work)	12	0.0050	0.0600	Mfg Data
Capacitors, Mica	66	0.0001	0.0066	Mfg Data
Capacitors, Paper	3	0.0001	0.0003	Mfg Data
Resistor, Wirewound	12	0.0012	0.0144	Mfg Data
Resistor, Trimpots	12	0.0030	0.0360	Mfg Data
Transistor, Power	12	0.0020	0.0240	Mfg Data
Chokes	3	0.0006	0.0018	Mfg Data
Total Electronics			0.5031	
		$R_e = 0.957$		
<u>Torque Coils</u>	3	0.0010	0.0030	Estimate
		$R_{tc} = 0.9998$		
<u>Magnetometer</u>	1	$R_m = 0.956$		Mfg Data

$$R_{\text{system}} = R_e \times R_{tc} \times R_m = 0.957 \times 0.9998 \times 0.956 = 0.915 \text{ (For 8800 hours)}$$

## APPENDIX I

### MOMENTUM UNLOADING SIMULATION DIGITAL PROGRAM

#### A.1.1 VEHICLE MOMENTUM

$$M_x = M_{x0} + \int T_x \, dT$$

$$M_y = M_{y0} + \int T_y \, dT$$

$$M_z = M_{z0} + \int T_z \, dT$$

#### Coil Currents

$$I_x = [M_y B_z - M_z B_y] K_1$$

$$I_y = [M_z B_x - M_x B_z] K_1$$

$$I_z = [M_x B_y - M_y B_x] K_1$$

#### Magnetic Torques

$$T_{xM} = [I_y B_z - I_z B_y]$$

$$T_{yM} = [I_z B_x - I_x B_z]$$

$$T_{zM} = [I_x B_y - I_y B_x]$$

#### Total Torques

$$T_x = T_{xM} + M_z \omega_o$$

$$T_y = T_{yM}$$

$$T_z = T_{zM} - M_x \omega_o$$

where:  $\omega_o$  = orbit rate

$$K_1 = \text{current gain} = \frac{\alpha \omega_o}{K_o^2}$$

- $\alpha$  = Dimensionless loop gain
- $K_o$  = Magnitude of the magnetic field at the equator
- $B$  = Magnetic field from the Cain subroutine

### A.1.2 CAIN SUBROUTINE

This is a subroutine for coupling the orbit coordinate reference frame to the Cain 48 coefficient magnetic field program. The known quantities are orbit angle ( $\theta$ ), orbit inclination ( $\phi$ ), longitude at time zero ( $Q_o$ ), earth rate ( $\omega_e$ ), and time. The longitude and latitude of the vehicle at time  $t$  are needed to get the components of the earth's magnetic field from the Cain program. This output is broken into North, East, and Down components that have to be converted to orbit coordinates.

To get the transformation for orbit coordinates to Longitude and Latitude, perform the following transformations:

where  $\{A\} = \begin{Bmatrix} A_{11} & A_{12} & A_{13} \\ A_{21} & A_{22} & A_{23} \\ A_{31} & A_{32} & A_{33} \end{Bmatrix}$ , etc.

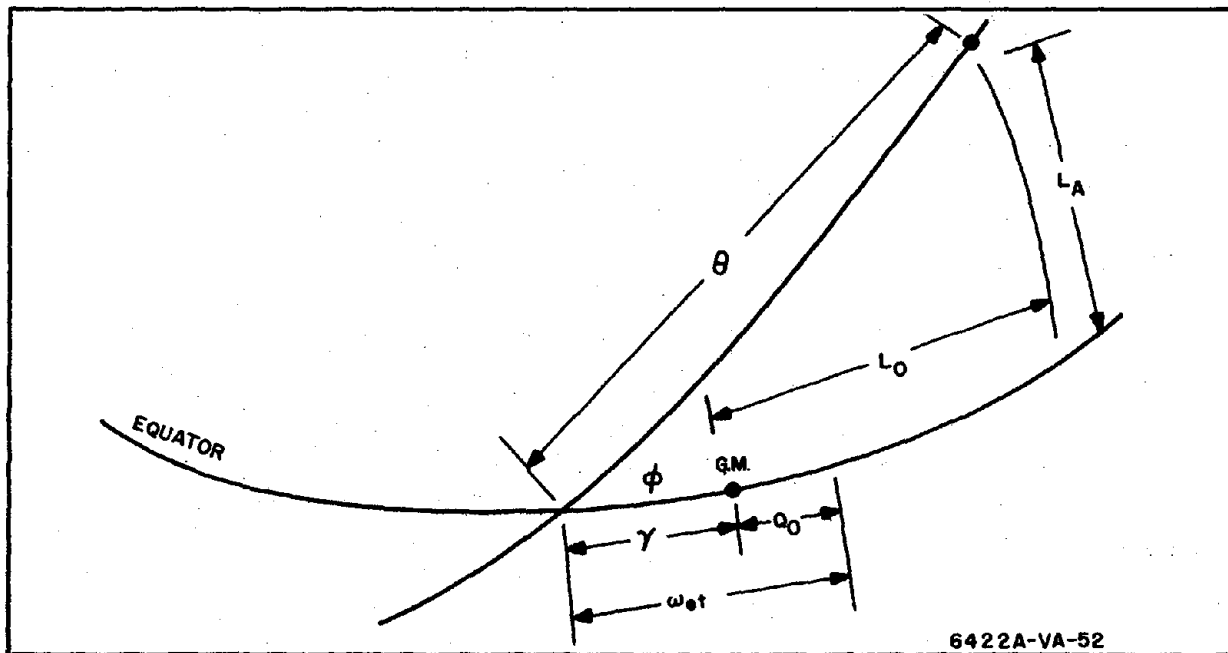


Figure 49. Variable Definitions, First View

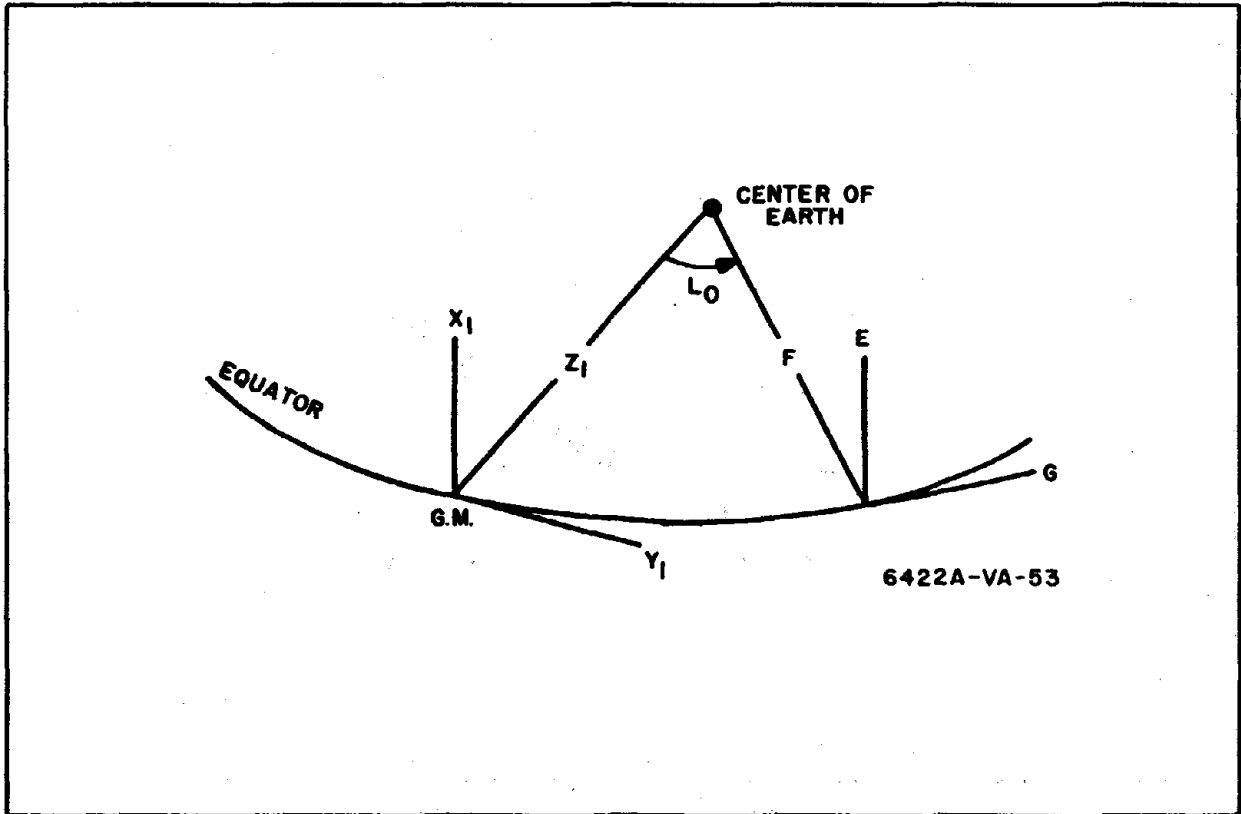


Figure 50. Variable Definitions, Second View

$$\begin{pmatrix} E \\ F \\ G \end{pmatrix} = \begin{bmatrix} 1 & 0 & 0 \\ 0 & \cos L_0 & \sin L_0 \\ 0 & -\sin L_0 & \cos L_0 \end{bmatrix} \begin{pmatrix} X_1 \\ Y_1 \\ Z_1 \end{pmatrix} = \{H\} \begin{pmatrix} X_1 \\ Y_1 \\ Z_1 \end{pmatrix}$$



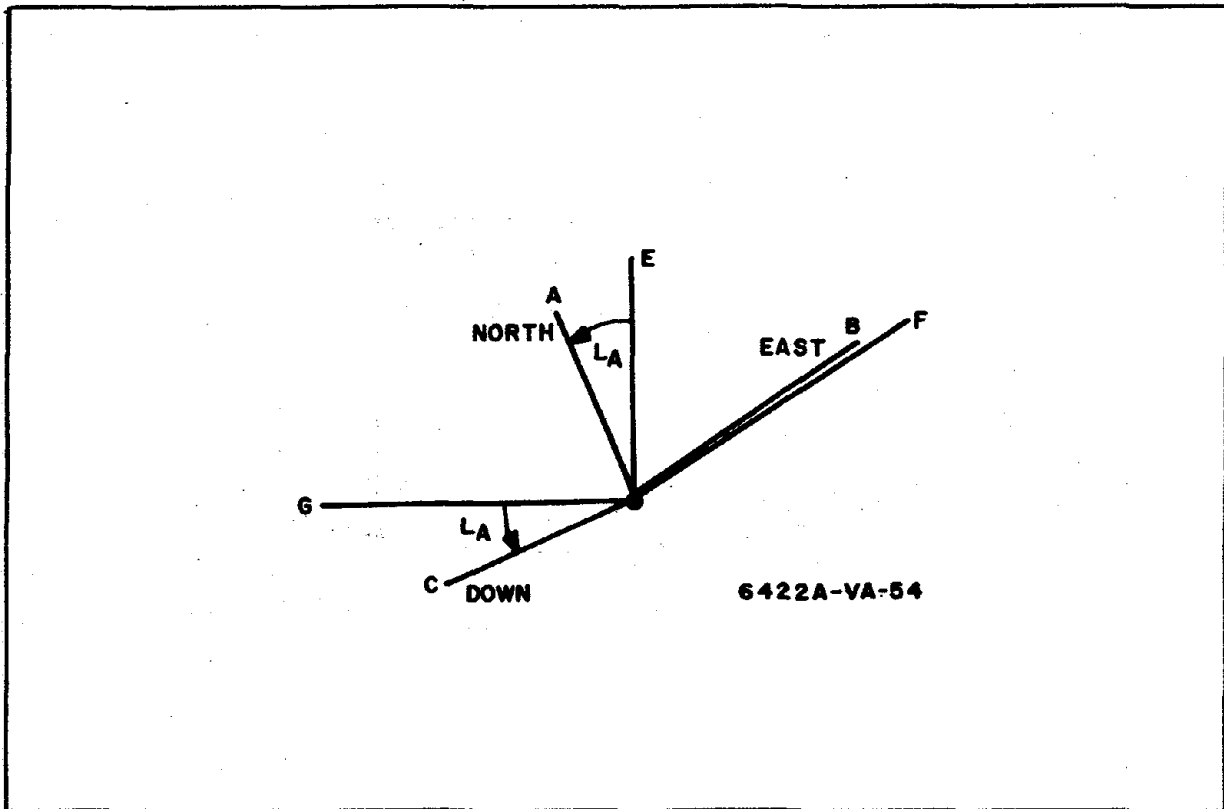


Figure 51. Variable Definitions, Third View

$$\begin{pmatrix} A \\ B \\ C \end{pmatrix} = \begin{bmatrix} \cos L_A & 0 & \sin L_A \\ 0 & 1 & 0 \\ -\sin L_A & 0 & \cos L_A \end{bmatrix} \begin{pmatrix} E \\ F \\ G \end{pmatrix} = \left\{ I \right\} \begin{pmatrix} E \\ F \\ G \end{pmatrix}$$

$$\begin{pmatrix} A \\ B \\ C \end{pmatrix} = \begin{bmatrix} \cos L_A & -\sin L_A \sin L_o & \sin L_A \cos L_o \\ 0 & \cos L_o & \sin L_o \\ -\sin L_A & -\cos L_A \sin L_o & \cos L_A \cos L_o \end{bmatrix} \begin{pmatrix} X_1 \\ Y_1 \\ Z_1 \end{pmatrix}$$

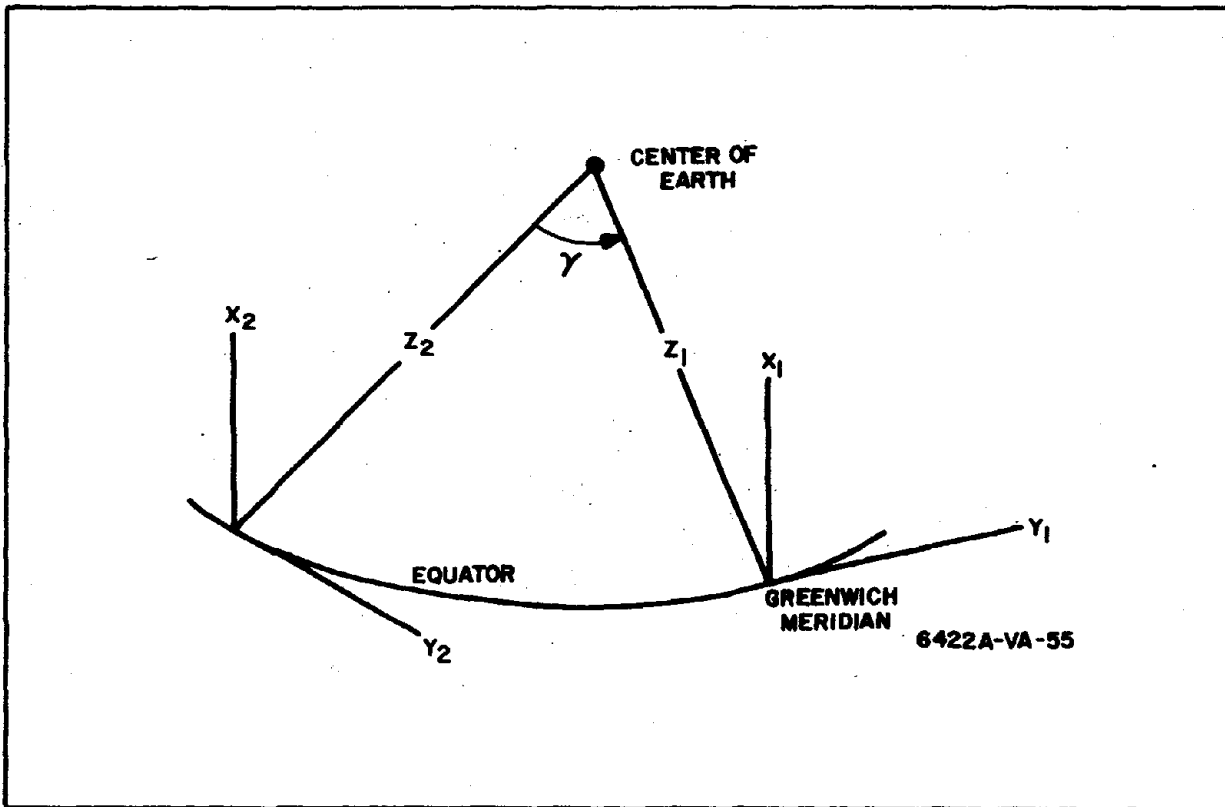


Figure 52. Variable Definitions, Fourth View

$$\begin{pmatrix} X_1 \\ Y_1 \\ Z_1 \end{pmatrix} = \begin{bmatrix} 1 & 0 & 0 \\ 0 & \cos \gamma & \sin \gamma \\ 0 & -\sin \gamma & \cos \gamma \end{bmatrix} \begin{pmatrix} X_2 \\ Y_2 \\ Z_2 \end{pmatrix} = \left\{ G \right\} \begin{pmatrix} X_2 \\ Y_2 \\ Z_2 \end{pmatrix}$$

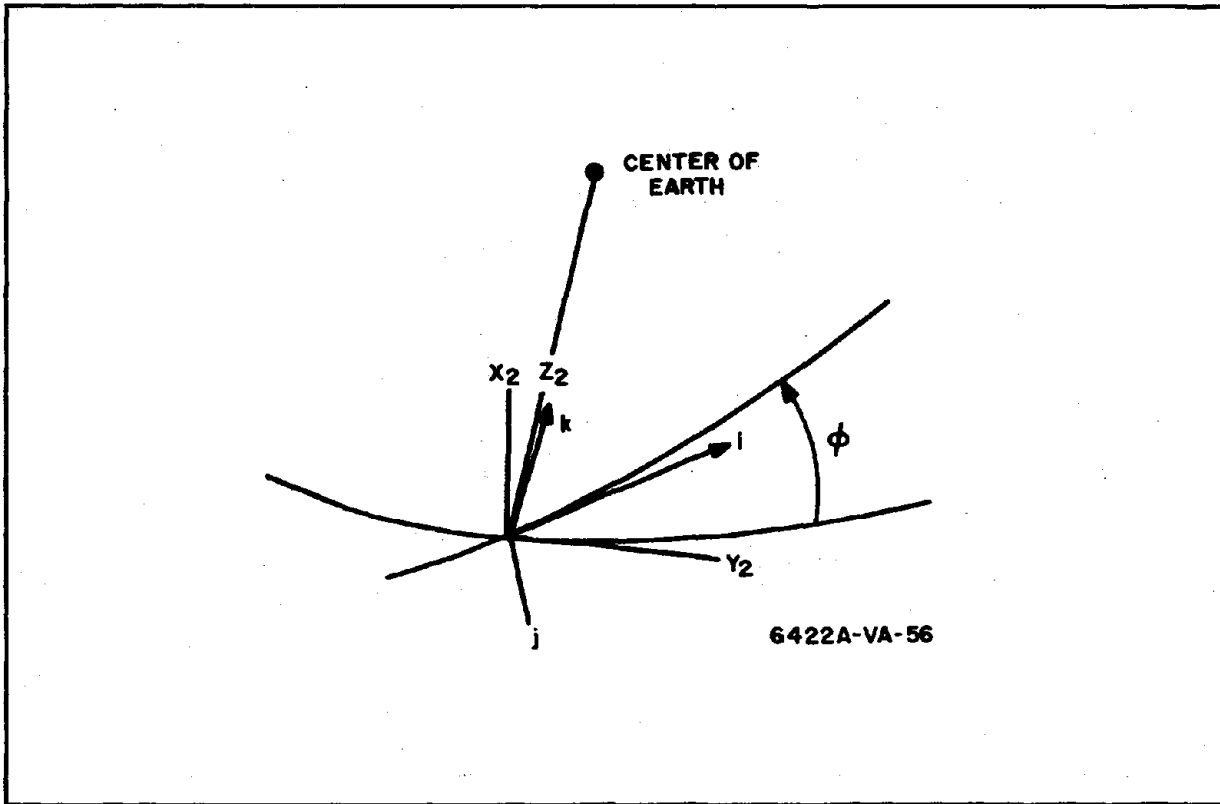


Figure 53. Variable Definitions, Fifth View

$$\begin{pmatrix} X_2 \\ Y_2 \\ Z_2 \end{pmatrix} = \begin{bmatrix} \sin \phi & -\cos \phi & 0 \\ \cos \phi & \sin \phi & 0 \\ 0 & 0 & 1 \end{bmatrix} \begin{pmatrix} i \\ j \\ k \end{pmatrix} = \left\{ F \right\} \begin{pmatrix} i \\ j \\ \delta \end{pmatrix}$$

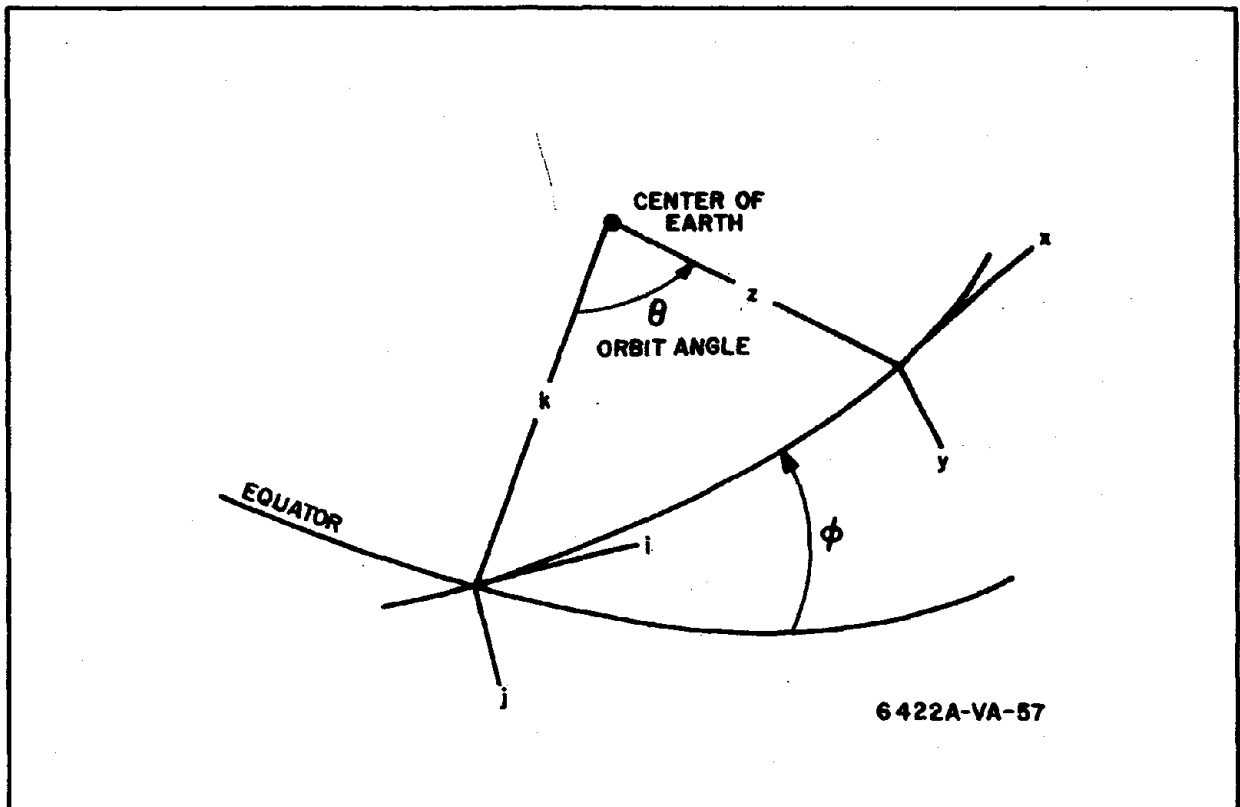


Figure 54. Variable Definitions, Sixth View

$$\begin{pmatrix} i \\ j \\ k \end{pmatrix} = \begin{bmatrix} \cos \theta & 0 & -\sin \theta \\ 0 & 1 & 0 \\ \sin \theta & 0 & \cos \theta \end{bmatrix} \begin{pmatrix} x \\ y \\ z \end{pmatrix} = \left\{ E \right\} \begin{pmatrix} x \\ y \\ z \end{pmatrix}$$

From the above we get

$$\begin{pmatrix} x \\ y \\ z \end{pmatrix} = (E^{-1}) (F^{-1}) (G^{-1}) \begin{pmatrix} X_1 \\ Y_1 \\ Z_1 \end{pmatrix}$$

$\bar{z}$  and  $\bar{c}$  are colinear, therefore the expression defining them in terms of  $X_1$ ,  $Y_1$ ,  $Z_1$  are equal.

$$\bar{z} = \begin{pmatrix} -\sin \theta \sin \phi \\ -\sin \theta \cos \phi \cos \gamma + \cos \theta \sin \gamma \\ \sin \theta \cos \phi \sin \gamma + \cos \theta \cos \gamma \end{pmatrix} \begin{pmatrix} X_1 \\ Y_1 \\ Z_1 \end{pmatrix} = \bar{c} = \begin{pmatrix} -\sin L_A \\ -\cos L_A \sin L_O \\ \cos L_A \cos L_O \end{pmatrix} \begin{pmatrix} X_1 \\ Y_1 \\ Z_1 \end{pmatrix}$$

From the above it is found that

$$L_A = \sin^{-1} \begin{bmatrix} E_{31} & F_{11} \end{bmatrix} \quad \begin{array}{l} \text{is + for } E_{31} \geq 0 \\ \text{is - } E_{31} < 0 \end{array}$$

$$L_O = \tan^{-1} \left[ \frac{E_{31} F_{21} G_{22} + E_{11} G_{32}}{E_{11} G_{22} - E_{31} F_{21} G_{32}} \right]$$

Using these values of  $L_A$  and  $L_O$ , the North, East, and Down components ( $B_N$ ,  $B_E$ ,  $B_D$ ) of field were found. They were then converted to orbit coordinates.

$$B_u = I_{11} B_N + I_{31} B_D$$

$$B_v = B_E$$

$$B_w = -I_{31} B_N + I_{11} B_D$$

$$B_{x1} = B_u$$

$$B_{y1} = H_{22} B_v + H_{32} B_w$$

$$B_{z1} = -H_{32} B_v + H_{22} B_w$$

$$B_{x2} = B_{x1}$$

$$B_{y2} = G_{22} B_{y1} + G_{32} B_{z1}$$

$$B_{z2} = -G_{32} B_{y1} + G_{22} B_{z1}$$

$$B_i = F_{11} B_{x2} + F_{21} B_{y2}$$

$$B_j = -F_{21} B_{x2} + F_{11} B_{y2}$$

$$B_k = B_{z2}$$

$$B_x = E_{11} B_i + E_{31} B_k$$

$$B_y = B_j$$

$$B_z = -E_{31} B_i + E_{11} B_k = B_D$$



## APPENDIX 2

### COMPLETE SYSTEM SIMULATION DIGITAL PROGRAM

This appendix gives the equations used in the digital computer simulation (Flow Chart, figure 55) of the system for the particular vehicle of Section VI. This vehicle had a momentum transfer type of control system consisting of 4 gyros. There were two double gimbal and two single gimbal gyros.

In the equations given below, the angles are those of figure 2.

#### A. 2. 1 VARIABLES USED

$A_{11}$ , etc.		vehicle to orbit matrix elements
$\dot{A}_{11}$ , etc.	$\frac{d}{dt}$	$A_{11}$ , etc.
$B_{11}$ , etc.		2 D. O. F. gyro outer gimbal to vehicle matrix elements
$\dot{B}_{11}$ , etc.	$\frac{d}{dt}$	$B_{11}$ , etc.
$C_{11}$ , etc.	{	2 D. O. F. gyro inner gimbal to vehicle matrix elements
		1 D. O. F. gyro gimbal to vehicle matrix elements
$\dot{C}_{11}$ , etc.	$\frac{d}{dt}$	$C_{11}$ , etc.
$F_{ci}$		2 D. O. F. gyro inner gimbal friction
$F_{co}$		2 D. O. F. gyro outer gimbal friction
$H_o$		gyro momentum in foot-pound-seconds
$J_{\xi}$		inertia about the $\xi$ axis
$K_{CG}$		1 D. O. F. gyro gimbal friction
$K_{FG}$		1 D. O. F. gyro gimbal damping



$K_{Fi}$	2 D. O. F. gyro inner gimbal damping
$K_{Fo}$	2 D. O. F. gyro outer gimbal damping
$P$	orbit period in seconds
$T_{Qt}$	$\left\{ \begin{array}{l} 2 \text{ D. O. F. gyro inner gimbal control torque} \\ 1 \text{ D. O. F. gyro gimbal control torque} \end{array} \right.$
$T_{Qv}$	2 D. O. F. gyro outer gimbal control torque
$V_{\xi}$	components of the vertical on the $\xi$ axis
$X, Y, Z$	orbit coordinate axis
$h$	orbit altitude in n. miles
$r_e$	radius of the earth = 3440 nmi
$r, s, t$	$\left\{ \begin{array}{l} 2 \text{ D. O. F. gyro inner gimbal coordinate axis} \\ 1 \text{ D. O. F. gyro gimbal coordinate axis} \end{array} \right.$
$u, v, w$	2 D. O. F. gyro outer gimbal coordinate axis
$x, y, z$	vehicle coordinate axis
$\pi$	a constant = 3.1415
$\omega_o$	orbit rate in radians/second
$\omega_x, \omega_y, \omega_z$	vehicle angular rates
$\omega_{\xi}$	angular rate about the $\xi$ axis

### A. 2. 2 MATRIX DEFINITIONS

$$\begin{pmatrix} x \\ y \\ z \end{pmatrix} = \left\{ A \right\} \begin{pmatrix} X \\ Y \\ Z \end{pmatrix}$$

$$\left\{ A \right\} = \begin{bmatrix} A_{11} & A_{12} & A_{13} \\ A_{21} & A_{22} & A_{23} \\ A_{31} & A_{32} & A_{33} \end{bmatrix}$$

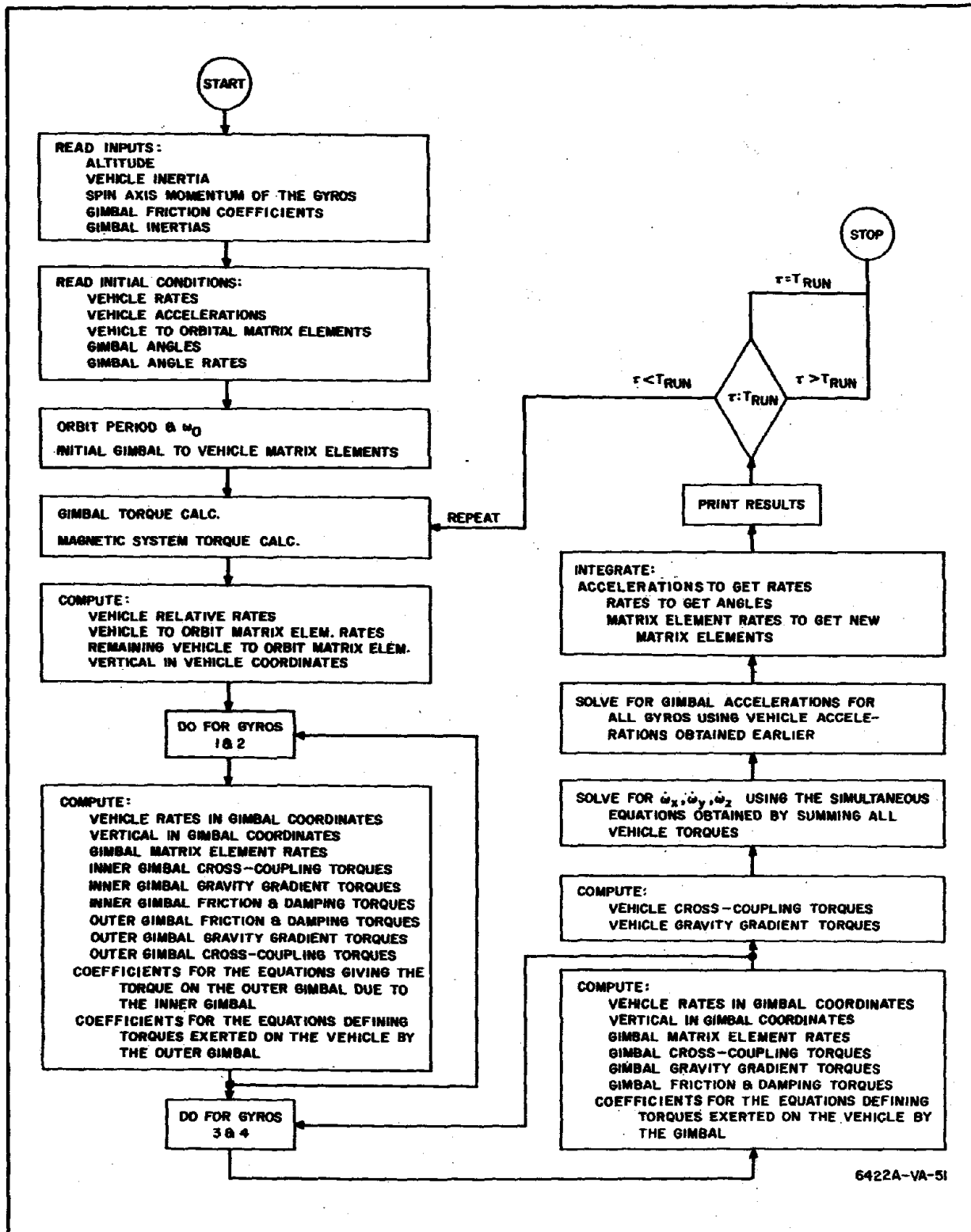
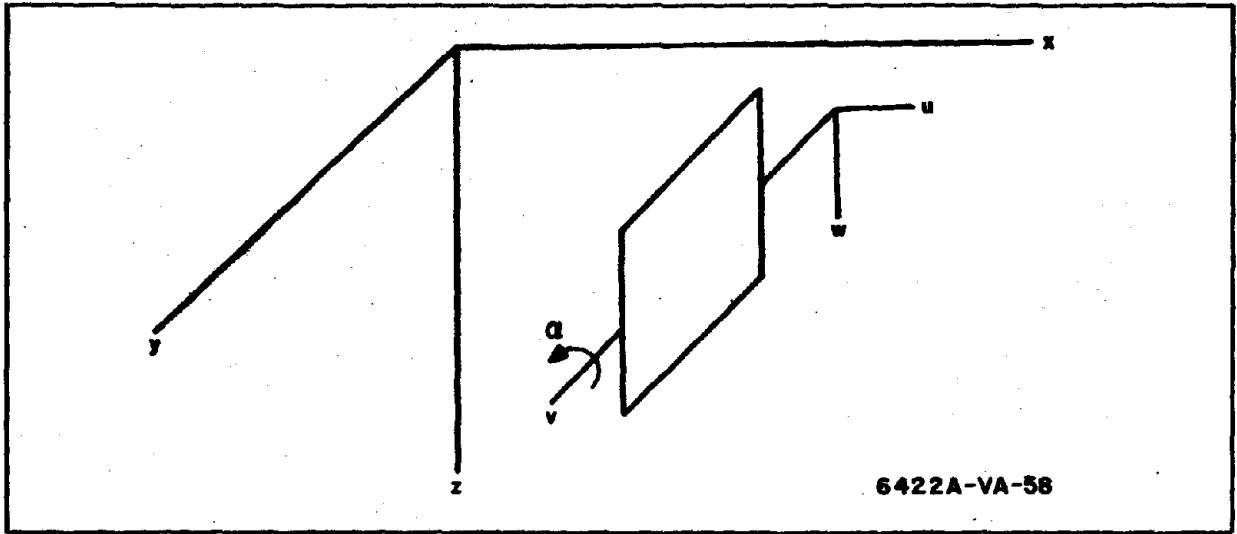


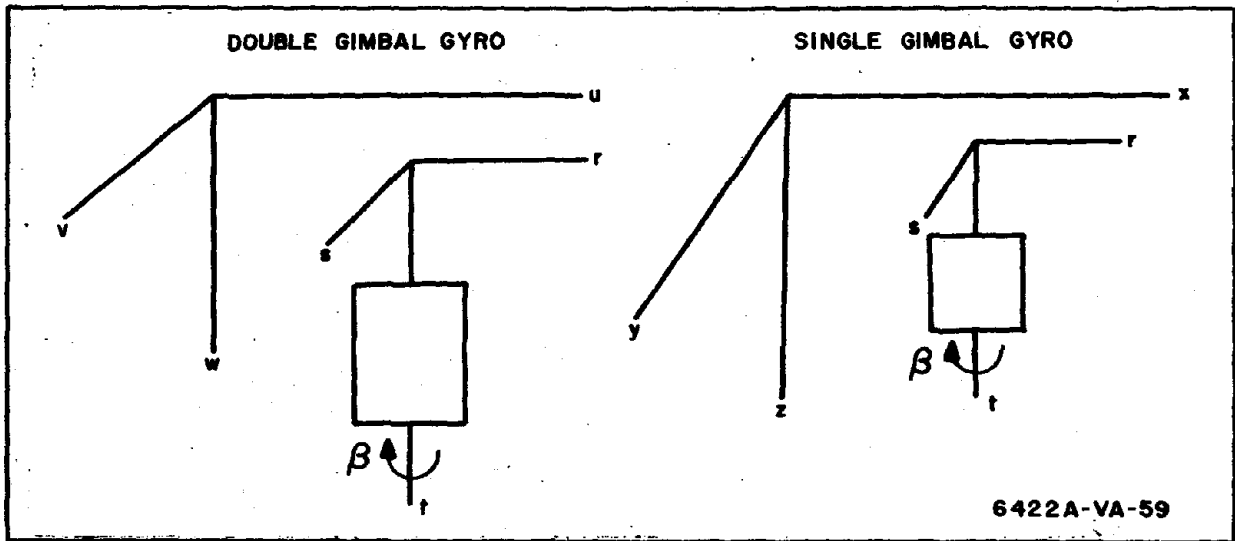
Figure 55. Momentum Unloading of Control Moment Gyros, Digital Flow



6422A-VA-58

Figure 56. Variable Definitions, Seventh View

$$\begin{pmatrix} u \\ v \\ w \end{pmatrix} = \{B\} \begin{pmatrix} x \\ y \\ z \end{pmatrix} = \begin{bmatrix} \cos \alpha & 0 & -\sin \alpha \\ 0 & 1 & 0 \\ \sin \alpha & 0 & \cos \alpha \end{bmatrix} \begin{pmatrix} x \\ y \\ z \end{pmatrix}$$



6422A-VA-59

Figure 57. Variable Definitions, Eighth View

$$\begin{pmatrix} r \\ s \\ t \end{pmatrix} = \{C\} \begin{pmatrix} u \\ v \\ w \end{pmatrix} \quad \begin{pmatrix} r \\ s \\ t \end{pmatrix} = \{C\} \begin{pmatrix} x \\ y \\ z \end{pmatrix} \quad \{C\} = \begin{bmatrix} \cos \beta & \sin \beta & 0 \\ -\sin \beta & \cos \beta & 0 \\ 0 & 0 & 1 \end{bmatrix}$$

### A.2.3 COMPUTATIONS

Initial conditions and constants

$$P = 2\pi \sqrt{\frac{(r_e + h)^3}{6.27464(10^4)}}$$

$$\omega_o = \frac{2\pi}{P}$$

$$\left. \begin{aligned} B_{11o} &= \cos \alpha_o \\ B_{31o} &= \sin \alpha_o \end{aligned} \right\} \text{for both double-gimballed gyros}$$

$$\left. \begin{aligned} C_{11o} &= \cos \beta_o \\ C_{21o} &= -\sin \beta_o \end{aligned} \right\} \text{for all four gyros}$$

Begin the integration loop

#### A.2.3.1 Vehicle Equations

a. Compute: Relative rates of the vehicle

$$\omega_{xR} = \omega_x + A_{12} \omega_o$$

$$\omega_{yR} = \omega_y + A_{22} \omega_o$$

$$\omega_{zR} = \omega_z + A_{32} \omega_o$$

b. Compute: Matrix element rates and matrix elements

$$\dot{A}_{11} = A_{21} \omega_{zR} - A_{31} \omega_{yR}$$

$$\dot{A}_{21} = A_{31} \omega_{xR} - A_{11} \omega_{zR}$$

$$\dot{A}_{31} = A_{11} \omega_{yR} - A_{21} \omega_{xR}$$

$$\dot{A}_{12} = A_{22} \omega_{zR} - A_{32} \omega_{yR}$$

$$\dot{A}_{22} = A_{32} \omega_{xR} - A_{12} \omega_{zR}$$

$$\dot{A}_{32} = A_{12} \omega_{yR} - A_{22} \omega_{xR}$$

$$A_{13} = A_{21} A_{32} - A_{31} A_{22}$$

$$A_{23} = A_{31} A_{12} - A_{11} A_{32}$$

$$A_{33} = A_{11} A_{22} - A_{21} A_{12}$$

c. Transform the vertical into vehicle coordinates

$$V_x = A_{13}$$

$$V_y = A_{23}$$

$$V_z = A_{33}$$

$$\Delta\theta_x = \theta_{cx} - \theta_x$$

$$\Delta\theta_y = \theta_{cy} - \theta_y - e_{sy}$$

$$\Delta\theta_z = \theta_{cz} - \theta_z - e_{sz}$$

$$\Delta\omega_x = \dot{\theta}_{cx} - \omega_x$$

$$\Delta\omega_y = \dot{\theta}_{cy} - \omega_y - \dot{e}_{sy}$$

$$\Delta\omega_z = \dot{\theta}_{cz} - \omega_z - \dot{e}_{sz}$$

limit  $|\Delta\theta_x|$ ,  $|\Delta\theta_y|$ ,  $|\Delta\theta_z|$  to  $4.8472 (10^{-5}) = 10$  arc. seconds

$$E_{x1} = [(5000.) SC_{11} (1)] E_x$$

$$E_{y1} = 1.82 (10^4) E_y$$

$$E_{z1} = 1.82 (10^4) E_z$$

control torques

$$T_{cx} = E_{x1}$$

$$T_{cy} = 1.94 (10^4) [E_{y1} - 100 \omega_y + \omega_{cy}]$$

$$T_{cz} = 1.94 (10^4) [E_{z1} - 100 \omega_z + \omega_{cz}]$$

Gimbal constraint torques

$$T_{D\alpha c} = 1500. [ B_{31} (1) + B_{31} (2) ]$$

$$T_{D\beta c} = 1500. [ -C_{21} (1) - C_{21} (2) ]$$

$$T_{S\beta c} = 1500. [ -SC_{21} (1) - SC_{21} (2) ]$$

for 1 D. O. F. gyros

$$\left. \begin{aligned} T_{Qt} (1) &= T_{cx} \\ T_{Qt} (2) &= -T_{cx} - T_{S\beta c} \end{aligned} \right\} -2.0 \leq \begin{matrix} ST_{Qt} (1) \\ ST_{Qt} (2) \end{matrix} \leq +2.0$$

for 2 D. O. F. gyros

$$\left. \begin{aligned} T_{Qt} (1) &= -T_{cz} \\ T_{Qt} (2) &= -T_{cz} - T_{D\beta c} \\ T_{Qv} (1) &= -T_{cy} \\ T_{Qv} (2) &= -T_{cy} - T_{D\alpha c} \end{aligned} \right\} -18.0 \leq \begin{matrix} T_{Qt} (1) \\ T_{Qt} (2) \\ T_{Qv} (1) \\ T_{Qv} (2) \end{matrix} \leq +18.0$$

$$e_{Ty} = \begin{cases} T_{cy} \pm 18.0 & \text{for } |T_{Qv} (1)| \geq 18.0 \\ 0 & |T_{Qv} (1)| < 18.0 \end{cases}$$

$$e_{Tz} = \begin{cases} T_{cz} \pm 18.0 & \text{for } |T_{Qt} (1)| \geq 18.0 \\ 0 & |T_{Qt} (1)| < 18.0 \end{cases}$$

Note: For  $e_{Ty}$  and  $e_{Tz}$   $\pm$  sign is opposite of sign on  $T_{cy}$  and  $T_{cz}$  respectively.

$$\ddot{e}_{sy} = [ 1.421 (10^{-5}) ] e_{Ty} - (8.27) e_{sy} - (27.85) \dot{e}_{sy}$$

$$\ddot{e}_{sz} = [ 1.421 (10^{-5}) ] e_{Tz} - (8.27) e_{sz} - (27.85) \dot{e}_{sz}$$

$$\Delta \dot{\omega}_x = \ddot{\theta}_{cx} - \dot{\omega}_x$$

$$\begin{aligned} \Delta \dot{\omega}_y &= \ddot{\theta}_{cy} - \dot{\omega}_y - \ddot{e}_{sy} \\ \Delta \dot{\omega}_z &= \ddot{\theta}_{cz} - \dot{\omega}_z - \ddot{e}_{sz} \\ \ddot{E}_x &= \left( \frac{900.}{44.62} \right) [ \Delta \dot{\omega}_x + (13.36) \Delta \omega_x + (44.62) \Delta \theta_x ] \\ &\quad - [ (60.) \dot{E}_x + (900.) E_x ] \\ \ddot{E}_y &= \left( \frac{9}{110} \right) [ \Delta \dot{\omega}_y + (25.5) \Delta \omega_y + (110.) \Delta \theta_y ] \\ &\quad - [ (30.3) \dot{E}_y + (9.) E_y ] \\ \ddot{E}_z &= \left( \frac{9}{110} \right) [ \Delta \dot{\omega}_z + (25.5) \Delta \omega_z + (110.) \Delta \theta_z ] \\ &\quad - [ (30.3) \dot{E}_z + (9.) E_z ] \end{aligned}$$

### A. 2. 3. 2 Two-Gimbal Control Moment Gyro

- a. Transform vehicle angular rates into gimbal coordinates

$$\omega_u = B_{11} \omega_x - B_{31} \omega_z$$

$$\omega_v = \omega_y + \alpha$$

$$\omega_w = B_{31} \omega_x + B_{11} \omega_z$$

$$\omega_r = C_{11} \omega_u - C_{21} \omega_v$$

$$\omega_s = C_{21} \omega_u + C_{11} \omega_v$$

$$\omega_t = \omega_w + \beta$$

- b. Transform the vertical into gimbal coordinates

$$V_u = A_{13} B_{11} - A_{33} B_{31}$$

$$V_v = A_{23}$$

$$V_w = A_{13} B_{31} + A_{33} B_{11}$$

$$V_r = C_{11} V_u - C_{21} A_{23}$$

$$V_s = C_{21} V_u + C_{11} A_{23}$$

$$V_t = V_w$$

c. Compute the gimbal matrix element rates

$$\dot{B}_{11} = -B_{31} \dot{\alpha}$$

$$\dot{B}_{31} = B_{11} \dot{\alpha}$$

$$\dot{C}_{11} = C_{21} \dot{\beta}$$

$$\dot{C}_{21} = -C_{11} \dot{\beta}$$

d. Compute the inner gimbal  $H \times W$  (cross-coupling torques)

$$T_{cpr} = (J_s - J_t) \omega_s \omega_t$$

$$T_{cps} = (J_t - J_r) \omega_r \omega_t - H_o \omega_t$$

$$T_{cpt} = (J_r - J_s) \omega_r \omega_s + H_o \omega_s$$

e. Compute the inner gimbal gravity gradient

$$T_{GGr} = 3 \omega_o^2 (J_t - J_s) V_s V_t$$

$$T_{GGs} = 3 \omega_o^2 (J_r - J_t) V_r V_t$$

$$T_{GGt} = 3 \omega_o^2 (J_s - J_r) V_r V_s$$

f. Compute inner gimbal friction and damping

$$T_{Flt} = K_{Fi} \dot{\beta} + K_{ci} F_{ci}$$

$$\text{where: } K_{ci} = \begin{matrix} +1 & \text{for } \dot{\beta} \geq 0 \\ -1 & \beta < 0 \end{matrix}$$

g. Compute outer gimbal friction and damping

$$T_{Fov} = K_{Fo} \dot{\alpha} + K_{co} F_{co}$$

$$\text{where: } K_{co} = \begin{matrix} +1 & \text{for } \dot{\alpha} \geq 0 \\ -1 & \dot{\alpha} < 0 \end{matrix}$$

h. Compute the outer gimbal gravity gradient

$$T_{GGu} = 3 \omega_o^2 (J_w - J_v) V_v V_w$$

$$T_{GGv} = 3 \omega_o^2 (J_u - J_w) V_u V_w$$

$$T_{GGw} = 3 \omega_o^2 (J_v - J_u) V_u V_v$$



i. Compute the outer gimbal  $\vec{H} \times \vec{W}$  (cross-coupling torques)

$$T_{cpu} = (J_v - J_w) \omega_v \omega_w$$

$$T_{cpv} = (J_w - J_u) \omega_u \omega_w$$

$$T_{cpw} = (J_u - J_v) \omega_v \omega_u$$

j. Compute the K's

$$K_1 = C_{11} (T_{cpr} + T_{GGr}) + C_{21} (T_{cps} + T_{GGs})$$

$$K_2 = -B_{11} (C_{11}^2 J_r + C_{21}^2 J_s)$$

$$K_3 = C_{11} C_{21} (J_r - J_s)$$

$$K_4 = B_{31} (C_{11}^2 J_r + C_{21}^2 J_s)$$

$$K_5 = C_{11} C_{21} (J_r - J_s)$$

$$K_6 = -C_{21} (T_{cpr} + T_{GGr}) + C_{11} (T_{cps} + T_{GGs})$$

$$K_7 = C_{11} C_{21} B_{11} (J_r - J_s)$$

$$K_8 = -(C_{11}^2 J_s + C_{21}^2 J_r)$$

$$K_9 = -C_{11} C_{21} B_{31} (J_r - J_s)$$

$$K_{10} = -(C_{11}^2 J_s + C_{21}^2 J_r)$$

k. Torque on the outer gimbal due to friction between the inner and outer gimbals

$$T_{FIw} = T_{FIv}$$

l. Compute the constants for gimbal torques on the vehicle

$$K_{c1} = B_{11} \left[ T_{cpu} + T_{GGu} + K_1 + \left( \frac{K_5}{J_v - K_{10}} \right) \right.$$

$$\left. (T_{cpv} + T_{GGv} + T_{Qv} + K_6 - T_{Fov}) \right]$$

$$+ B_{31} \left[ T_{cpw} + T_{GGw} + T_{FIw} - T_{Qt} \right]$$

$$K_{c2} = T_{Fov} - T_{Qv}$$

$$K_{c3} = -B_{31} \left[ T_{cpu} + T_{GGu} + K_1 + \left( \frac{K_5}{J_v - K_{10}} \right) \right]$$

$$(T_{cpv} + T_{GGv} + T_{Qv} + K_6 - T_{Fov})]$$

$$+ B_{11} [ T_{cpw} + T_{GGw} + T_{FIw} - T_{Qt} ]$$

$$K_{x1} = + B_{11} [ K_2 - B_{11} J_u + K_7 \left( \frac{K_5}{J_v - K_{10}} \right) ] - B_{31}^2 J_w$$

$$K_{x2} = 0$$

$$K_{x3} = -B_{31} [ K_2 - B_{11} J_u + K_7 \left( \frac{K_5}{J_v - K_{10}} \right) ] - B_{11} B_{31} J_w$$

$$K_{y1} = B_{11} [ K_3 + \left( \frac{K_5}{J_v - K_{10}} \right) (K_8 - J_v) ]$$

$$K_{y2} = 0$$

$$K_{y3} = -B_{31} [ K_3 + \left( \frac{K_5}{J_v - K_{10}} \right) (K_8 - J_v) ]$$

$$K_{z1} = B_{11} [ B_{31} J_u + K_4 + K_9 \left( \frac{K_5}{J_v - K_{10}} \right) ] - B_{11} B_{31} J_w$$

$$K_{z2} = 0$$

$$K_{z3} = -B_{31} [ B_{31} J_u + K_4 + K_9 \left( \frac{K_5}{J_v - K_{10}} \right) ] - B_{11}^2 J_w$$

### A. 2. 3. 3 Single Gimbal Control Moment Gyro

- a. Transform vehicle angular rates into gimbal coordinates

$$\omega_r = C_{11} \omega_x - C_{21} \omega_y$$

$$\omega_s = C_{21} \omega_x + C_{11} \omega_y$$

$$\omega_t = \omega_z + \dot{\beta}$$

- b. Transform the vertical into gimbal coordinates

$$V_r = C_{11} A_{13} - C_{21} A_{23}$$

$$V_s = C_{21} A_{13} + C_{11} A_{23}$$

$$V_t = A_{33}$$

- c. Compute the gimbal matrix element rates

$$\dot{C}_{11} = C_{21} \dot{\beta}$$

$$\dot{C}_{21} = -C_{11} \dot{\beta}$$

- d. Compute the gimbal  $H \times W$  (cross-coupling torques)

$$T_{cpr} = (J_s - J_t) \omega_s \omega_t + H_o \omega_t$$

$$T_{cps} = (J_t - J_r) \omega_r \omega_t$$

$$T_{cpt} = (J_r - J_s) \omega_r \omega_s - H_o \omega_r$$

- e. Compute the gimbal gravity gradient

$$T_{GGr} = 3 \omega_o^2 (J_t - J_s) V_s V_t$$

$$T_{GGs} = 3 \omega_o^2 (J_r - J_t) V_r V_t$$

$$T_{GGt} = 3 \omega_o^2 (J_s - J_r) V_r V_s$$

- f. Compute the gimbal friction and damping

$$T_{FGt} = K_{FG} \dot{\beta} + K_{CG} F_{CG}$$

$$\text{where } K_{CG} = \begin{matrix} +1 & \text{for } \dot{\beta} \geq 0 \\ -1 & \dot{\beta} < 0 \end{matrix}$$

- g. Compute the constants for gimbal torques on the vehicle

$$K_{c1} = C_{11} (T_{cpr} + T_{GGr}) + C_{21} (T_{cps} + T_{GGr})$$

$$K_{c2} = -C_{21} (T_{cpr} + T_{GGr}) + C_{11} (T_{cps} + T_{GGs})$$

$$K_{c3} = T_{FGt} - T_{Qt}$$

$$K_{x1} = -C_{11}^2 J_r - C_{21}^2 J_s$$

$$K_{x2} = C_{11} C_{21} (J_r - J_s)$$

$$K_{x3} = 0$$

$$K_{y1} = C_{11} C_{21} (J_r - J_s)$$

$$K_{y2} = -C_{21}^2 J_r - C_{11}^2 J_s$$

$$K_{y3} = 0$$

$$K_{z1} = 0$$

$$K_{z2} = 0$$

$$K_{z3} = 0$$

### RETURN TO VEHICLE EQUATIONS

- h. Compute the vehicle  $\vec{H} \times \vec{W}$  (cross-coupling torques)

$$T_{cpx} = (J_y - J_z) \omega_y \omega_z$$

$$T_{cpy} = (J_z - J_x) \omega_x \omega_z$$

$$T_{cpz} = (J_x - J_y) \omega_x \omega_y$$

- i. Compute the vehicle gravity gradient

$$T_{GGx} = 3 \omega_o^2 (J_z - J_y) V_y V_z$$

$$T_{GGy} = 3 \omega_o^2 (J_x - J_z) V_x V_z$$

$$T_{GGz} = 3 \omega_o^2 (J_y - J_x) V_x V_y$$

- j. Compute  $\dot{\omega}_x, \dot{\omega}_y, \dot{\omega}_z$

$$-(\Sigma K_{c1}) - T_{cpx} - T_{GGx} - T_{ex} - T_{bx} = (\Sigma K_{x1} - J_x) \dot{\omega}_x$$

$$+ (\Sigma K_{y1}) \dot{\omega}_y + (\Sigma K_{z1}) \dot{\omega}_z$$

$$-(\Sigma K_{c2}) - T_{cpy} - T_{GGy} - T_{ey} - T_{by} = (\Sigma K_{x2}) \dot{\omega}_x + (\Sigma K_{y2} - J_y) \dot{\omega}_y$$

$$+ (\Sigma K_{z2}) \dot{\omega}_z$$

$$\begin{aligned}
 -(\Sigma K_{c3}) - T_{cpz} - T_{GGz} - T_{ez} - T_{bz} &= (\Sigma K_{x3}) \dot{\omega}_x + (\Sigma K_{y3}) \dot{\omega}_y \\
 &+ (\Sigma K_{z3} - J_z) \dot{\omega}_z
 \end{aligned}$$

where  $T_{ex}$ ,  $T_{ey}$ ,  $T_{ez}$  are external torques on the vehicle

$T_{bx}$ ,  $T_{by}$ ,  $T_{bz}$  are magnetic control system torques

k. Compute the gimbal accelerations for the gyros

for the 2 gimbal gyros (1 & 2)

$$\ddot{\beta} = \frac{1}{J_t} [ T_{cpt} + T_{GGt} + T_{Qt} - T_{FIt} ] - B_{31} \dot{\omega}_x - B_{11} \dot{\omega}_z$$

$$\ddot{\alpha} = \frac{T_{cpv} + T_{GGv} + T_{Qv} - T_{Fov} + K_6 + K_7 \dot{\omega}_x + (K_8 - J_v) \dot{\omega}_y + K_9 \dot{\omega}_z}{(J_v - K_{10})}$$

for the single gimbal gyros (3 & 4)

$$\ddot{\beta} = \frac{1}{J_t} [ T_{Qt} - T_{FGt} + T_{cpt} + T_{GGt} ] - \dot{\omega}_z$$

l. Integrate the derivatives

This completes the integration loop.

APPENDIX 3  
CMG SYSTEM DESIGN

The control moment gyro system to control the particular vehicle of Section V was designed for Westinghouse Aerospace by General Electric Company.

Using the assumptions set forth in Section V, the procedure outlined below was used to find the stabilization networks needed. Expected performance was also found mathematically.

A. 3.1 MANEUVER DESCRIPTION AND ANALYSIS

The vehicle enters the period of interest with its long (roll) axis aligned perfectly with the vehicle velocity vector, its yaw axis lies in the orbital plane and pitch axis is normal to the orbital plane.

Assume that all maneuvers take place about the pitch axis, thus maintaining the roll and yaw axis always in the orbital plane. It is desired to slew (about pitch) through 22.5 degrees in 100 seconds or less and acquire a ground target to within 10 arc seconds, then track that target holding attitude error below 10 arc seconds and rate error from a sine profile to less than .5 arc second per second. The maximum rate capability of the gyro system (assuming 45° gimbal angle limit) is

$$\dot{\theta}_{p(\max)} = \frac{2 \times 1000 \times .707}{141,000} \times 57.3 = .575^\circ / \text{sec}$$

One method of performing the maneuver is to accelerate to a rate of .5 degrees per second, holding that rate until the attitude is in the vicinity of the desired 22.5 degrees from the initial condition, then decelerating and settling out at the desired attitude. Thus, the total maneuver time consists of the following time functions:

$$t_m = t_a + t_r + t_d + t_s$$

Assuming the acceleration and deceleration times to be equal, the equation can be rewritten as

$$t_m - t_s = 2t_a + t_r$$

To interpret this equation in terms of attitude changes during each period, the following assumptions are made.

- (1) Attitude changes during settling period are negligible.
- (2) The torque motor time constants are negligible, allowing infinite rate of change of acceleration.

then

$$t_r = \frac{\theta_m - 2\theta_a}{\dot{\theta}}$$

and

$$t_m - t_s = 2t_a + \left( \frac{\theta_m - 2\theta_a}{\dot{\theta}} \right)$$

$$\theta_a = \frac{\dot{\theta}}{2} t_a$$

$$t_m - t_s = 2t_a + \left( \frac{\theta_m}{\dot{\theta}} + t_a \right)$$

$$t_m - t_s - \frac{\theta_m}{\dot{\theta}} = t_a$$

$$t_m = 100 \text{ sec.}$$

$$t_s = 20 \text{ sec. (assumed)}$$

$$\theta_m = 22.7^\circ$$

$$\dot{\theta} = .5^\circ / \text{sec.}$$

$$80 - \frac{22.7}{.5} = t_a$$

$$t_a = 34.6 \text{ sec.}$$

$$\theta_a = \frac{34.6}{2} \times .5 = 8.65^\circ$$

$$\ddot{\theta} = \frac{\dot{\theta}}{t_a} = \frac{.5}{34.6} = .014^\circ/\text{sec}^2$$

The torque required to produce this

$$T = \ddot{\theta} I_v = \frac{.014}{57.3} \times 141,000 = 35.25 \text{ foot pounds}$$

Thus, the minimum size of the torque motor on each gyro is 17.6 foot pounds (considering a 1:1 gimbal torquer interface).

Considering the settling time, the method of command must be derived. The most easily mechanized technique from the control system standpoint would be the insertion of a vehicle rate command at the output of the rate gyro. Thus, a step change in vehicle rate is commanded. A limiter in the torque electronics controls the torquer current so that the capabilities of the torquer are not exceeded.

The maneuver is terminated by commanding zero rate when the vehicle attitude arrives at a predetermined portion of the total commanded attitude.

In the condition calculated above, the rate command would be reduced to zero when the vehicle had attained an attitude of

$$\begin{aligned} \theta_c &= \theta_a + \theta_r \\ &= 8.65 + 5.4 \\ &= 14.05 \text{ degrees.} \end{aligned}$$

Considering that from this point, there is an initial attitude error of 8.65 degrees, and 54.6 seconds remaining in which to settle to  $22.7^\circ \pm 10$  arc seconds, the system apparent time constant can be calculated. In effect, the system sees an apparent step command of 8.65 degrees and must settle to  $\left(1 - \frac{10}{3600 \times 8.65}\right) 100 = 99.968\%$  of its final value in 54.6 seconds. This



is equivalent to approximately eight time constants in a first order system. Thus, the effective time constant of the system should be approximately

$$\frac{54.6}{8} = 6.8 \text{ seconds or less.}$$

This approach although physically realizable, would require a considerably larger torque motor than that required by the initial acceleration during the maneuver. A more compatible approach would be to allow vehicle deceleration by dropping the rate command to zero at the assigned attitude but limiting attitude feedback so that the maximum attitude error apparent at the limiter output is in the order of 1 degree. Thus, for all intents and purposes, the attitude must settle from a 1 degree step command within 20 seconds. The allowable attitude error is now  $\left(1 - \frac{10}{3600}\right) 100 = 99.723\%$  of the initial command. This is representative of six time constants of a first order system. The apparent time constant of the system must be approximately 3.3 seconds.

The tracking portion of the maneuver must also be considered to determine if vehicle accelerations exceed that required in the acquisition maneuver. The tracking maneuver has been defined as a sine wave of rate within amplitude of  $\pm .5$  degrees/second and a period of 800 seconds. The acceleration profile is represented by the equation

$$\ddot{\theta} = \frac{d\dot{\theta}}{dt} = \frac{d}{dt} \left( .5 \sin \frac{2\pi}{800} t \right)$$

$$\ddot{\theta} = .5 \times \frac{2\pi}{800} \cos \frac{2\pi}{800} t$$

$$\ddot{\theta} \text{ max} = \frac{.5\pi}{800} = .004 \text{ deg/sec}^2$$

This is considerably less than that required during the acquisition maneuver and thus, does not represent an additional problem in the system design.

The control system specifications are presented in the following table.

Angular Momentum	1414 foot pound seconds
Vehicle Torque Output	35.25 foot pounds
Effective Time Constant	3.3 seconds
Attitude Accuracy	±10 arc seconds
Rate Accuracy	±.5 arc seconds/second

### A.3.2 DISTURBANCE TORQUE ANALYSIS

The disturbance torques encountered by the vehicle can be divided into two classes:

- (1) Those which occur during normal attitude hold mode.
- (2) Those which occur during acquisition and tracking maneuvers.

In general, the maneuver torque is considerably larger, but of shorter duration than the attitude hold disturbances. The maneuver torques are also cyclic in nature.

During the attitude hold mode, the vehicle roll axis is assumed to be aligned with the vehicle velocity vector and oriented so that its geometric center is aft of the center of mass. Four sources of disturbance torques are considered. These are:

- (1) Gravity gradient

$$T_g = \frac{3K}{2r^3} \Delta I \sin^2 B$$

- (2) Aerodynamic pressure

$$T_a = P_a V_a A_a \sin^2 B$$

- (3) Solar pressure

$$T_s = P_s V_s A_s \cos \alpha$$

- (4) Occupant motion

Considering the vehicle roll axis, the gravity gradient torques are zero, since pitch and yaw axes are assumed to have equal inertias and aerodynamic and solar torques are zero since the geometric and mass centers are both on

the vehicle longitudinal axis. Occupant motion can provide disturbances about the roll axis. The magnitudes of some typical torques are obtained from "Research and Investigation on Satellite Attitude Control," AFFDL-TR-64-168 Part 1, page 108.

The worst single torque is 8 foot pounds and the very unlikely combination of all motions simultaneously produces 14.37 foot pounds. Assuming the motions consist of only acceleration and deceleration (no constant rate), the angular momentum transferred to the vehicle has a maximum value of 3.6 foot pound seconds and is triangular in shape with a base of 1/2 second. The torque level will produce an acceleration of the uncontrolled vehicle of .0368 deg/sec<sup>2</sup>, a maximum rate of 0.0092 deg/sec, and an attitude deviation of 8.28 arc seconds. From these data, the minor movements of body parts are considered negligible during coarse attitude hold mode.

TABLE 14  
PEAK TORQUE GENERATED BY MOVEMENT  
OF VARIOUS BODY APPENDAGES

<u>Motion</u>	<u>Peak Torque (ft lb )</u>
Serving arm through 90° in 1/2 sec.	5.4
Serving leg through 90° in 1/2 sec.	8.0
Twist head through 90° in 1/2 sec.	0.35
Tilt head through 45° in 1/2 sec.	0.62

The motion of the 160 pound man described in the above referenced report may be of importance depending on the attitude hold desired. However, since the motion would be cyclic and would result ideally in no net momentum transfer, further consideration seems unproductive at this time.

Considering the vehicle yaw axis, the gravity gradient torques during attitude hold are a function of the control system error angle in that mode. Putting numerical values into the gravity gradient equation, the following relationship is obtained:

$$T_g = 0.231 \sin^2 B.$$

Similarly, the aerodynamic torque is

$$T_a = 0.575 \sin^2 B.$$

The torque due to solar pressure in the worst case condition (i. e., the roll axis of the vehicle, is normal to the solar radiation) is 0.00020 foot pounds or approximately 0.9 foot pound seconds per orbit. On this basis, solar torques are considered negligible in establishing system desaturation requirements.

The vehicle motion about the yaw axis due to the movements of the occupants discussed as part of the roll disturbance analysis is summarized below

$$\ddot{\theta} = .0059^\circ / \text{sec}^2$$

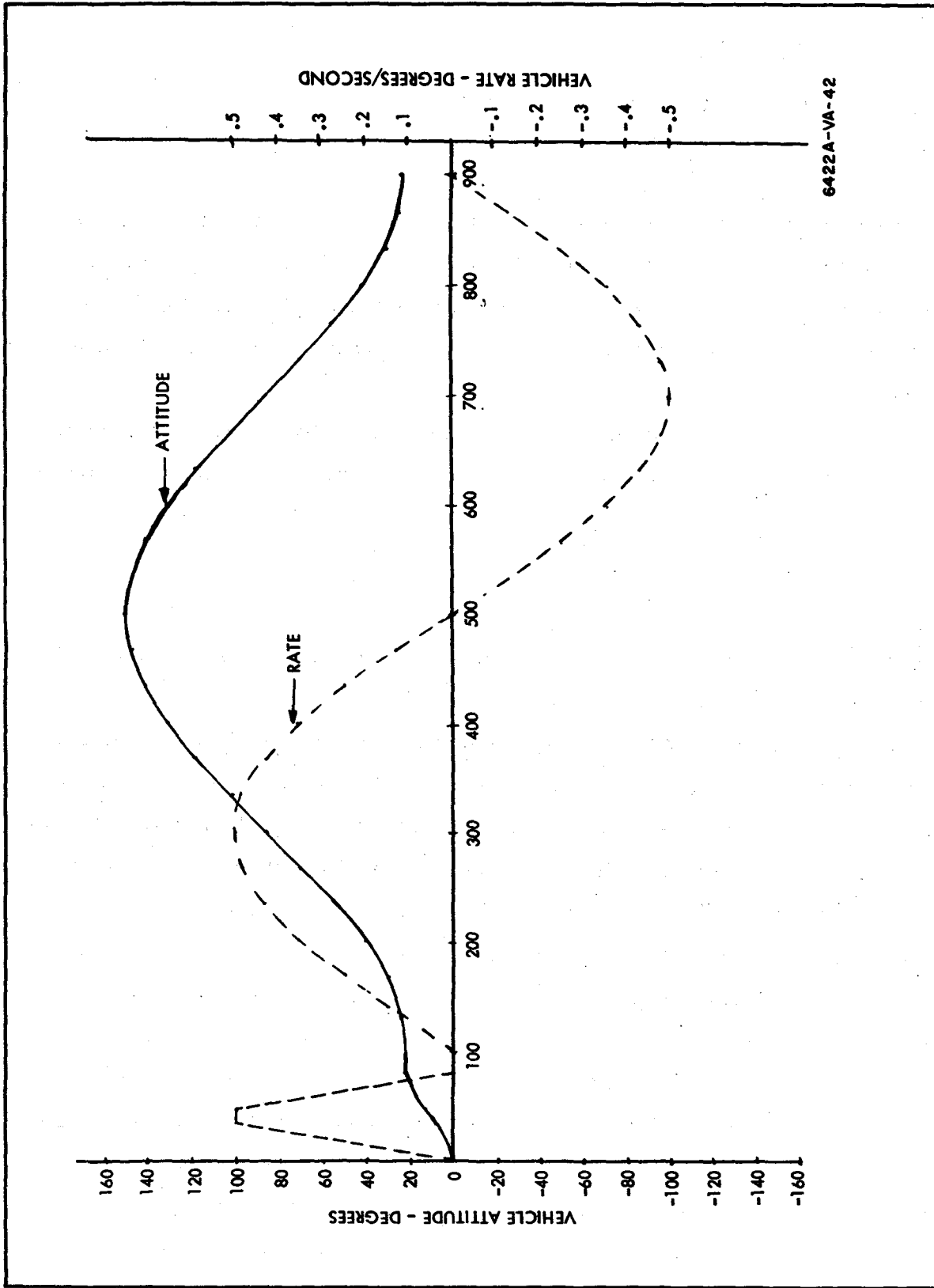
$$\dot{\theta} = .0015^\circ / \text{sec}$$

$$\theta = 1.3 \text{ arc seconds.}$$

Because of the symmetry of the vehicle, all the yaw axis disturbance torque considerations apply equally to the pitch axis.

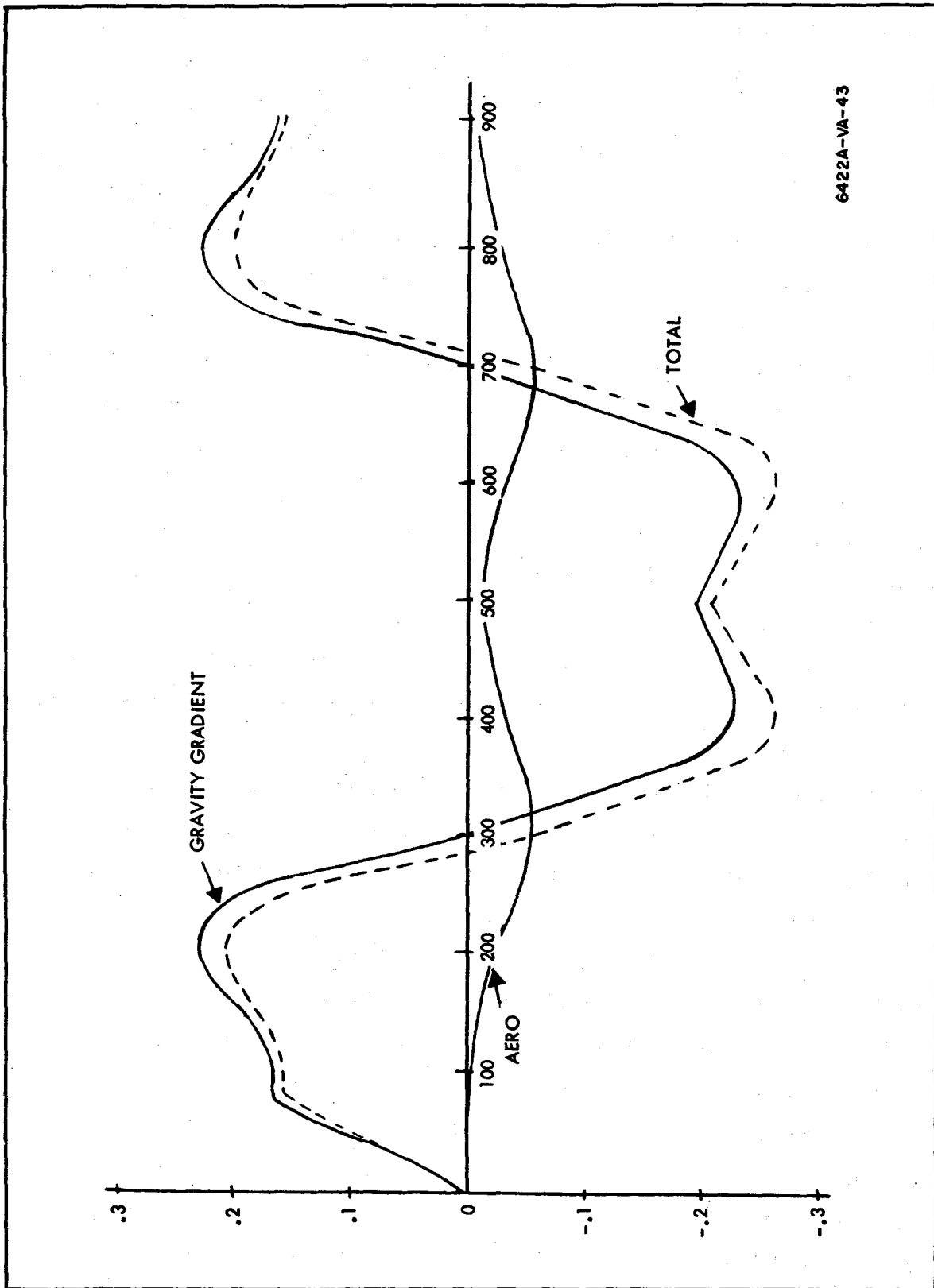
The disturbance torques during the maneuvering modes of operation are constantly varying since the angular relationship of the vehicle with respect to the local vertical and velocity vectors are continuously changing. The plot on figure 58 represents the vehicle angular rate and its attitude relative to the velocity vector. The curves are based on the assumption that the orbit is perfectly circular and that the descriptions of the acquisition and tracking maneuvers include orbital rate. In addition, because of the complexities involved in establishing the location of the target relative to the orbital plane, the maneuvers are assumed to take place entirely about the pitch axis. In reality, both the pitch and yaw axes will be involved, but the selected approach will provide order of magnitude results sufficient for this analysis.

The curves of figure 59 illustrate the aerodynamic and gravity gradient torques on the vehicle during the maneuver. Torques which accelerate the vehicle from the velocity vector toward the local vertical are considered



6422A-VA-42

Figure 58. Vehicle Attitude and Rate Maneuver Profile (Pitch Axis)



6422A-VA-43

Figure 59. Disturbance Torque History During Maneuver (Pitch Axis)

positive. Comparing the torque profile of figure 59 with that of figure 60, the required maneuvering torque profile, the disturbing torques are always in a direction to aid rather than oppose the desired vehicle motion except for a short period of time in the area of zero torque requirements.

The disturbance torques do not present any major pitch axis problems in terms of additional momentum or torque requirements during the maneuver mode specified. Yaw axis disturbance torques, however, will be opposing vehicle motion during part of the maneuver profile. Since the magnitude of the torques are comparatively low, no major problems are anticipated, but any detailed analysis of the system should consider disturbance effects on system accuracy and gain analysis.

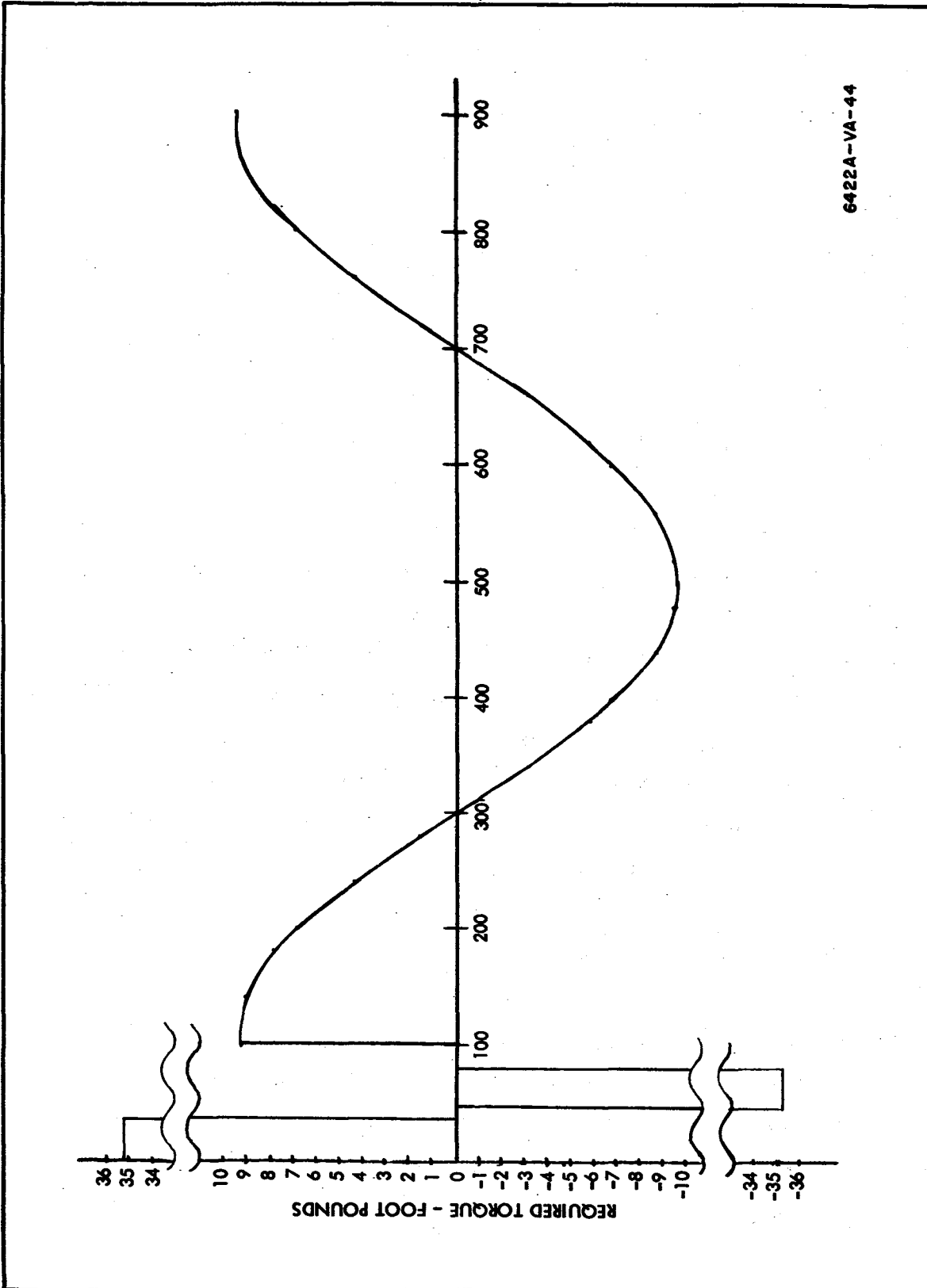
### A. 3. 3 CONTROL SYSTEM DESCRIPTION

The control system designated in the work statement consists of twin two degree of freedom (2 DOF) control moment gyros (CMG) controlling the two large inertia axes and twin single degree of freedom (1 DOF) CMG controlling the low inertia axis. Each of the 2 DOF gyros stores 1000 foot pound seconds angular momentum, and each of the 1 DOF gyros stores 500 foot pound seconds angular momentum.

Each of the gyro configurations has two mechanizations which could be applied to the system design problem. In each case, the gimbals could be driven by a geared or a direct drive torque motor. The control system configuration and dynamics vary according to the method used.

Considering the 2 DOF device, the direct drive motor must be sized so that all required vehicle torques are supplied directly through the torque motor. This approach has fast response since only the motor electrical time constant is included in the control loop. The gyro wheel serves only as a stable element against which the torques can be applied.

The geared torque motor version of the 2 DOF device makes each gimbal react similar to a 1 DOF device, in that the gear train amplifies the non-torqued gimbal friction and inertial, thus resisting the tendency to move as a



6422A-VA-44

Figure 60. Acquisition and Tracking Torque Requirements (Pitch Axis)



result of gyroscopic precession torques. The torque gain inherent in the gyro is now available for control purposes, allowing the use of smaller more efficient torque motors. However, this increase in efficiency is obtained at the expense of increased actuator system complexity since the non-torqued gimbal torque motor must supply a portion of the gimbal restraint. The gyro gimbal dynamics also become part of the control loop, thus producing somewhat slow response characteristics.

The direct drive torque motor gyro has been selected for this analysis. The selection is based partly on the more rapid response available with the selected mechanization, and partly on the comparative simplicity of the system analysis. It is probable that the desired response can be obtained with either mechanization. The results of a paper analysis of the selected configuration will be more representative of the actual response because fewer simplifications are required to make the system amenable to such analysis.

The selection of the 1 DOF actuator configuration presents a somewhat different set of tradeoffs than that described above. Both the direct drive or the geared torquer configuration transmit torque to the vehicle through gyroscopic precession. The direct drive configuration allows the CMG to act as its own rate sensor, and therefore, is an inherently stable system. The geared configuration imposes a large apparent damping on the CMG rate feedback loop thus nullifying the stabilization capabilities of that loop. For this reason, the geared torquer configuration requires external rate information to stabilize the control loop.

The major advantage of the geared torquer configuration lies in the decreased maneuvering power requirements. However, it introduces gear backlash into the loop, a condition which allows vehicle limit cycling during attitude hold modes. Since the mission considered here requires no maneuvering about the axis controlled by the 1 DOF system, the limit cycle tendencies of the geared torquer configuration justifies the elimination of that configuration from further consideration.

Based on the above considerations, the control system which will be analyzed for this application consists of two 1000 foot pound second 2 DOF and two 500 foot pound second 1 DOF gyros with direct drive gimbal torquers.

The orientation of the gyros on the vehicle is shown in figure 61. The 2 DOF gyros control the vehicle pitch (Y) and yaw (Z) axes and the 1 DOF gyros control the roll (X) axis.

The inner gimbal and outer gimbal of each 2 DOF gyro is slaved to the respective gimbal of the other gyro to minimize cross coupling between axes. The wheel rotation (spin vector) and gimbal torquing direction are controlled so that the desired torque components are obtained equally from each gyro while the cross axis torquer are nulled out. The 1 DOF gyros are similarly set up. The equations of motion of the two CMG control systems are contained in Reference 3.

#### A.3.4 SYSTEM ANALYSIS

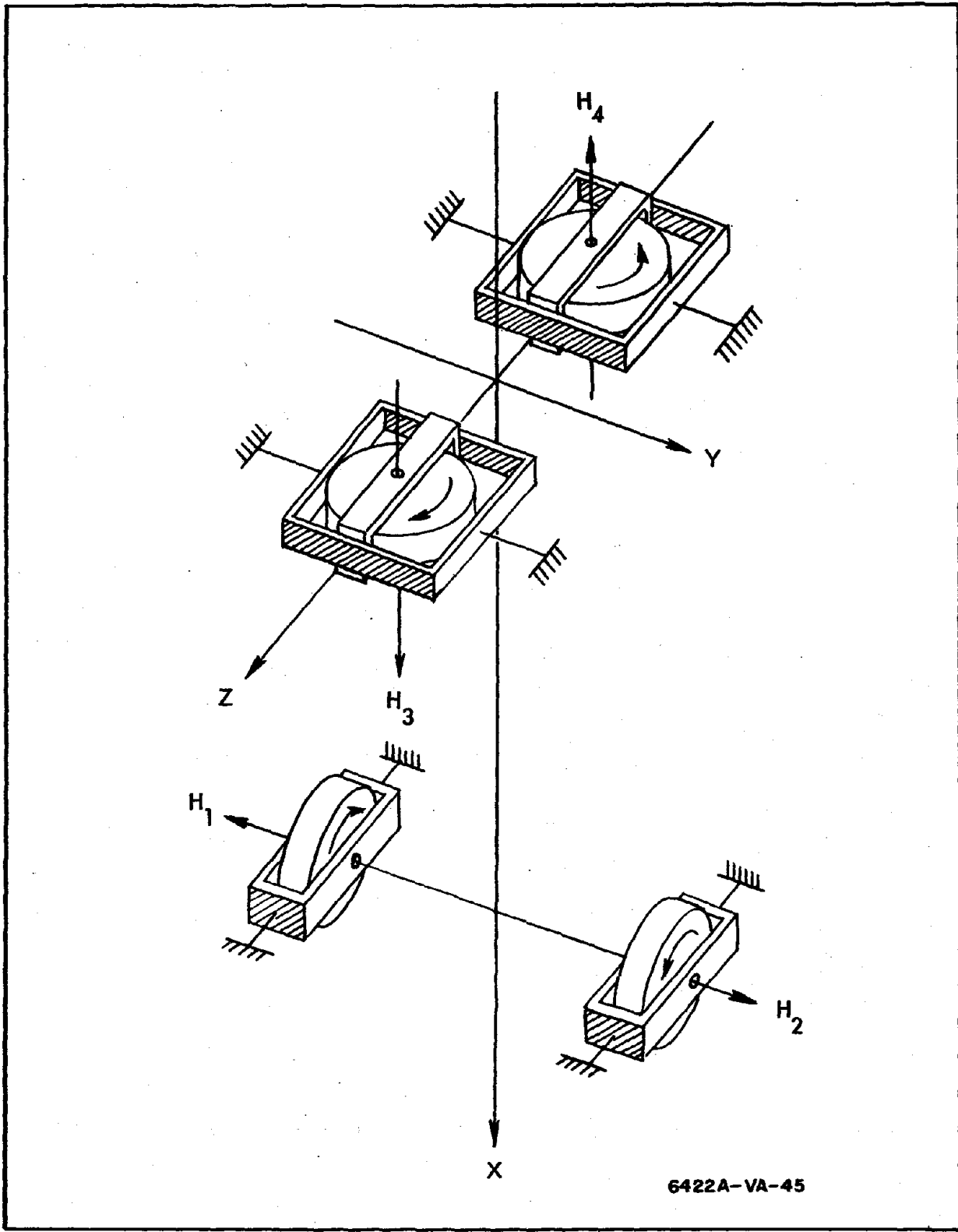
The control system analysis is divided into two separate, but related parts. The analysis of 2 DOF control moment gyro system constitutes the major portion of this section since it is that system which is most closely associated with the control problems. The 1 DOF gyro system is only required to satisfy a fine attitude hold condition, and to be compatible with the 2 DOF system in terms of response characteristics.

##### A.3.4.1 Two Degree of Freedom CMG System

The 2 DOF - CMG system selected as a result of the considerations described in the previous section can be divided into two separate but related functions for purposes of analysis. These functions are:

- (1) The control loop.
- (2) The gyro dynamics.

The block diagram of the vehicle control loop is shown as figure 62. Since the attitude control loop will have a reasonably low bandwidth (see Section III), sensor and torque dynamics have been neglected. A torque motor of the size selected in the maneuver analysis has an electrical time constant of



6422A-VA-45

Figure 61. Gyro Orientation Relative to Vehicle Axes

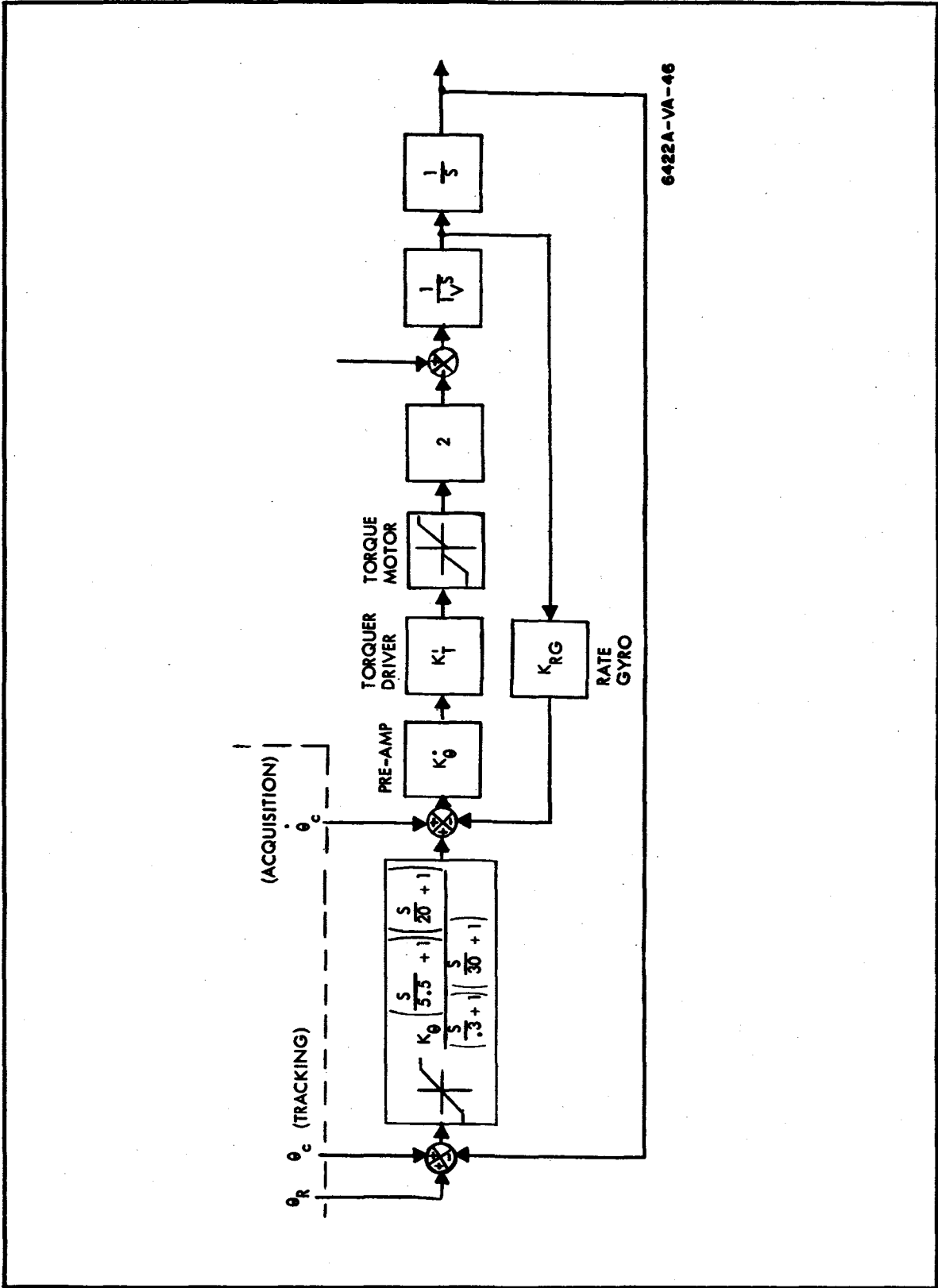


Figure 62. General Control Loop Block Diagram

approximately 0.005 seconds. Considering the rate gyro, a natural frequency of 100 radians per second is a reasonable value. Twenty to thirty radians per second are reasonable frequencies for an attitude sensor loop.

The block diagram of figure 62 is representative of the control loop of both the inner and outer gimbals of the 2 DOF system and also can be converted to represent the 1 DOF system. The block  $K^*$  consists of gyro geometry consideration and the  $K_t$  block includes the torquer dynamics and the torque power amplifier and has the units of foot pounds per volt.

Considering the outer gimbal of the 2 DOF gyro, the  $K^*$  factor has a value of 2 since the vehicle control torque is supplied by the gimbal torquer on each gyro. From the problem statement, the gyro actuators must be able to supply approximately 9.3 foot pounds of torque (based on maximum vehicle acceleration during the tracking maneuvers) at the maximum rate error of 0.5 arc seconds per second ( $2.4 \times 10^{-6}$  rad/sec). This is equivalent to  $2.4 \times 10^{-6} K_{rg}$  volts at the input to the torquer power amplifier.

Then

$$2.4 \times 10^{-6} K_t K_{rg} K^* = 9.3 \text{ foot pounds}$$

$$K_{rg} K_t = 1.94 \times 10^6 \text{ foot pounds/rad/sec}$$

Similarly, a maximum rate command ( $\dot{\theta}_c$ ) must be generated from an attitude error of 10 arc seconds ( $4.88 \times 10^{-5}$  rad)

$$4.88 \times 10^{-5} K_\theta = .00875 K_{rg}$$

$$\frac{K_{rg}}{K_\theta} = .0055 \text{ sec.}$$

Assuming the use of an inertial quality integrating rate gyro with a feedback loop around it, a rate gyro gain of 100 volts per radian per second can be attained.

Then

$$K_t = 1.94 \times 10^4 \text{ foot pound/volt}$$

and

$$K_\theta = 1.82 \times 10^4 \text{ volts/radian.}$$

Now, considering the acquisition maneuvers, the maneuver analysis has shown that an effective time constant of 3.3 seconds is sufficient to provide the desired response. From the block diagram of figure 62, the system closed loop transfer function is

$$\frac{\theta}{\theta_c} = \frac{1}{\frac{I_v}{K_t K^* K_\theta} S^2 + \frac{K_{rg}}{K_\theta} S + 1}$$

Inserting the values from above,

$$\frac{\theta}{\theta_c} = \frac{1}{2 \times 10^{-4} S^2 + .0055 S + 1}$$

The system natural frequency is

$$W_s = 70.8 \text{ radians/second}$$

and the damping factor is:

$$\zeta = \frac{.0055 \times 70.8}{2} = .19$$

This underdamped response is undesirable in terms of settling out after the maneuver.

From figure 62, the open attitude loop transfer function is

$$\frac{\theta}{\theta_c} = \frac{K_\theta / K_{rg}}{S \left( 1 + \frac{I_v}{K_t K^* K_{rg}} S \right)} = \frac{180}{S \left( 1 + \frac{S}{27.5} \right)}$$

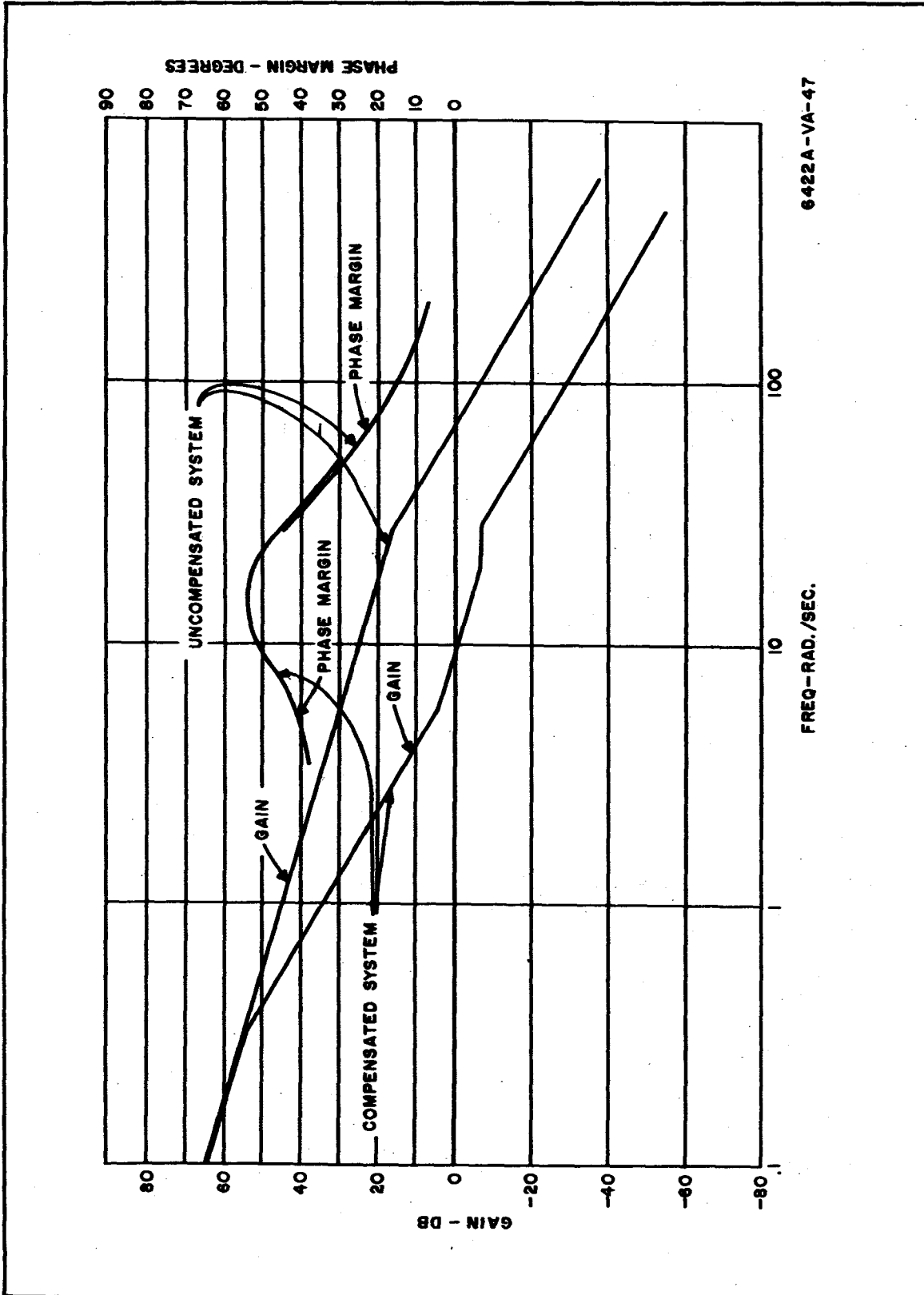
An approximate Bode plot of the crossover region is plotted on figure 63 while a Bode plot of the operating region during the tracking maneuver is shown on figure 64. Also shown on the figures is the Bode plot of the system with one form of compensation. This compensation was selected to reduce the crossover frequency, increase the phase margin and thus, improve the transient response without affecting the frequency response in the region of the tracking maneuver operating point.

This system approach appears to offer the desired response in both acquisition and tracking modes. No attempt was made to optimize the compensation since the presence of nonlinearities in the system, and particularly the hysteresis of the torque motor, could affect the attitude accuracy as vehicle acceleration goes through zero in the tracking mode. Experience with this type of problem indicates that the compensation frequencies are probably well enough separated to provide a minimum disturbance during this period. A rigorous investigation of the nonlinearity problems requires a rather complex simulation program that does not fall within the scope of this effort.

The recommended pitch axis system mechanization is shown in figure 65. As indicated on figure 61, the 2 DOF gyros' gimbal axes are mounted parallel to the pitch ( $\gamma$ ) axis. As discussed previously, an inertial quality rate gyro or an equally sensitive rate measuring device is required to measure vehicle rates about the pitch axis.

Also shown on figure 65, is a method of commanding the acquisition maneuver. It is assumed that both the acquisition and tracking commands are generated by an onboard digital computer.

Because of the high precision required in both the attitude and rate sensors, it is suggested that position signals could be obtained from an inertial platform updated just prior to the maneuvers from star tracker or ground data links. The digital computer could be mechanized to derive the rate signals from the attitude data.



6422A-VA-47

Figure 63. Bode Plot of System Crossover Region



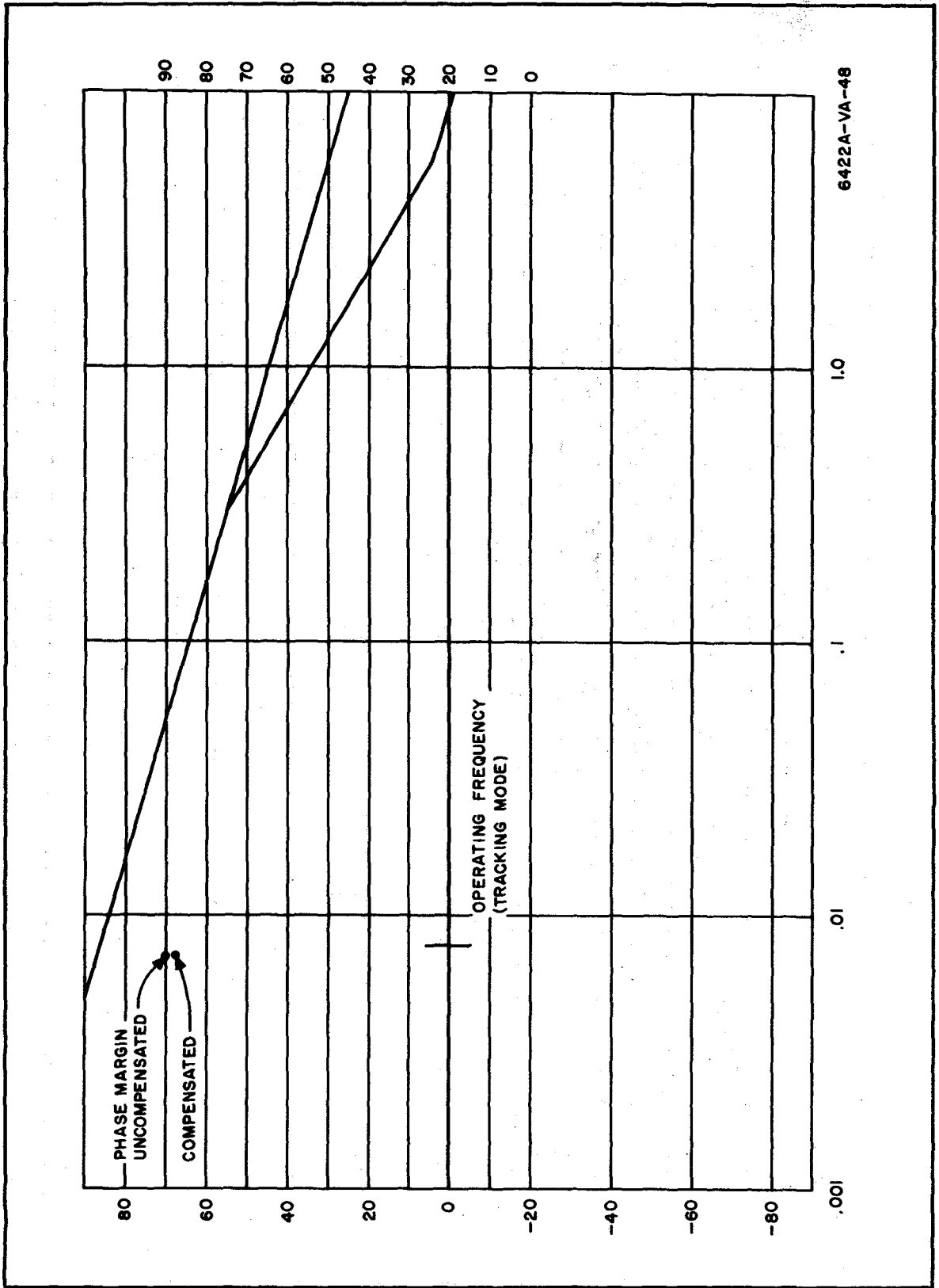
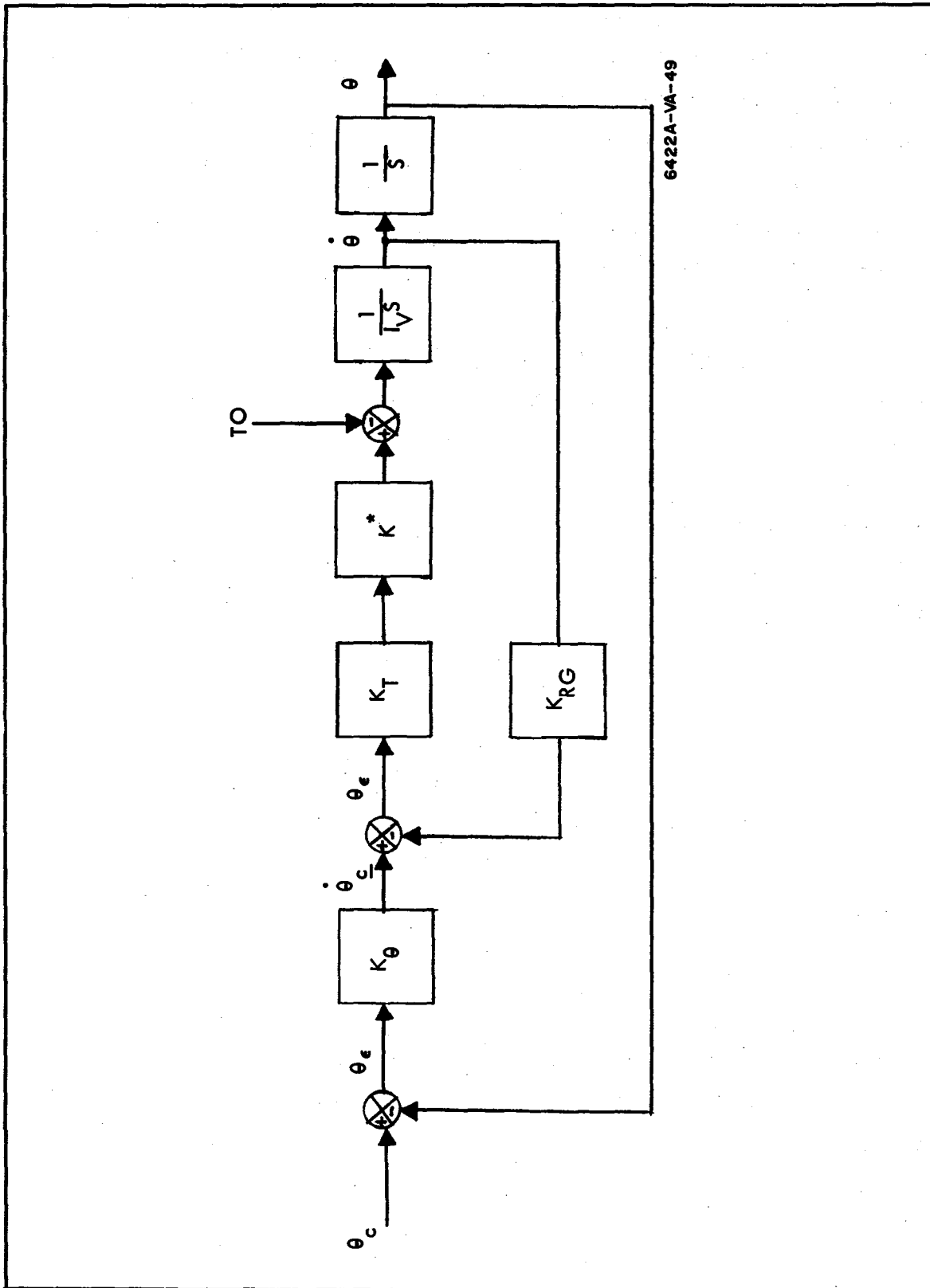


Figure 64. Bode Plot of System Operating Region (Tracking Mode)



6422A-VA-49

Figure 65. Fitch Axis Block Diagram

Considering the inner gimbal or yaw control loop, the mechanization of the control loop will be similar to that of the pitch loop. The major change arises due to the fact that yaw torques and thus, the control loop gain are a function of the cosine of the outer gimbal angle. If gimbal angles become large enough, the gain reduction may require a preamplifier gain which is a function of the cosine of the outer gimbal angle. This possibility could not be analyzed since data on the yaw maneuver requirements were not available during the study.

#### A. 3.4.2 Single Degree of Freedom Gyros

The 1 DOF - CMG system is required to hold roll axis attitude error to less than 10 arc seconds during the tracking maneuvers in the other axis. The only disturbance torques affecting the roll axis are those due to movements of the human occupants, and those due to rates of the inner gimbals of the 2 DOF gyros.

The block diagram of figure 66 shows an uncompensated twin 1 DOF gyro system. The open attitude loop transfer function is

$$\frac{\theta}{E} = \frac{\frac{K_{\theta}}{H \cos \alpha}}{S \left( 1 + \frac{I_v D}{2H^2 \cos^2 \alpha} S + \frac{I_v I_g}{2H^2 \cos^2 \alpha} S^2 \right)}$$

For this loop,

$$W_s = 6.686 \cos \alpha$$

$$\zeta = \frac{.07465}{\cos \alpha} \frac{D}{I_g} \quad \text{where } I_g = 0.50$$

neglecting  $\cos \alpha$  for the moment, the rate loop can be made critically damped by setting

$$\frac{D}{I_g} = \frac{1}{.07465} = 13.5 \text{ sec}^{-1}$$

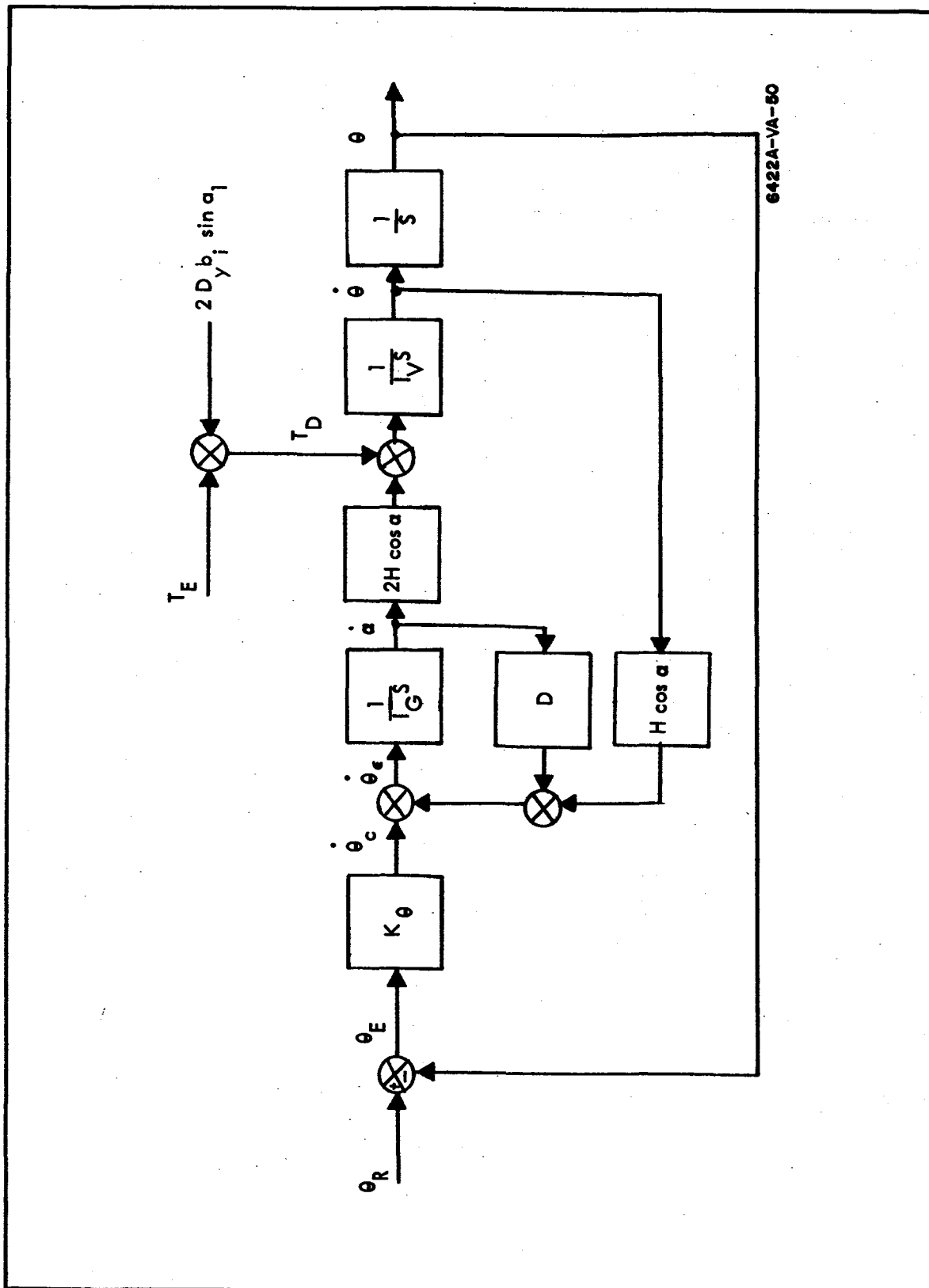


Figure 66. Uncompensated One-D.O.F. Control System Block Diagram

A Bode plot for this system is shown in figure 67. Since it is desired to have a bandpass comparable to that of the pitch and yaw axes, the gain,  $\frac{K_\theta}{H}$ , was set to provide system crossover at approximately 10 radians. This system is unstable and requires a  $K_\theta$  of 110,000 foot pounds per radian. A more desirable mechanization is shown as the compensated system on figure 67. The compensation in this case is

$$\frac{O}{I} = \frac{\left(\frac{S}{6.68} + 1\right)^2}{\left(\frac{S}{30} + 1\right)^2}$$

$$K = 5000 \cos \alpha.$$

Considering the response of this system to a constant (or slowly changing) disturbance torque, the attitude torque response is

$$\frac{\theta}{T_a} = \frac{\frac{D}{2HK_\theta \cos^2 \alpha} \left(\frac{I_g}{D} S + 1\right)}{1 + \frac{H}{K_\theta} S + \frac{I_v D}{2HK_\theta \cos^2 \alpha} S^2 + \frac{\left(\frac{I_v I_g}{2HK_\theta \cos^2 \alpha}\right) S^3}$$

The steady state value of  $\theta$  for a zero frequency disturbance torque is:

$$\theta = \frac{T_d D}{2HK_\theta \cos^2 \alpha}$$

$$\theta = \frac{1.34 \times 10^{-6} T_d \text{ rad}}{\cos^2 \alpha}$$

Thus, for the attitude to exceed 10 arc seconds error from reference

$$T_d = 36 \cos^2 \alpha \text{ foot pounds}$$

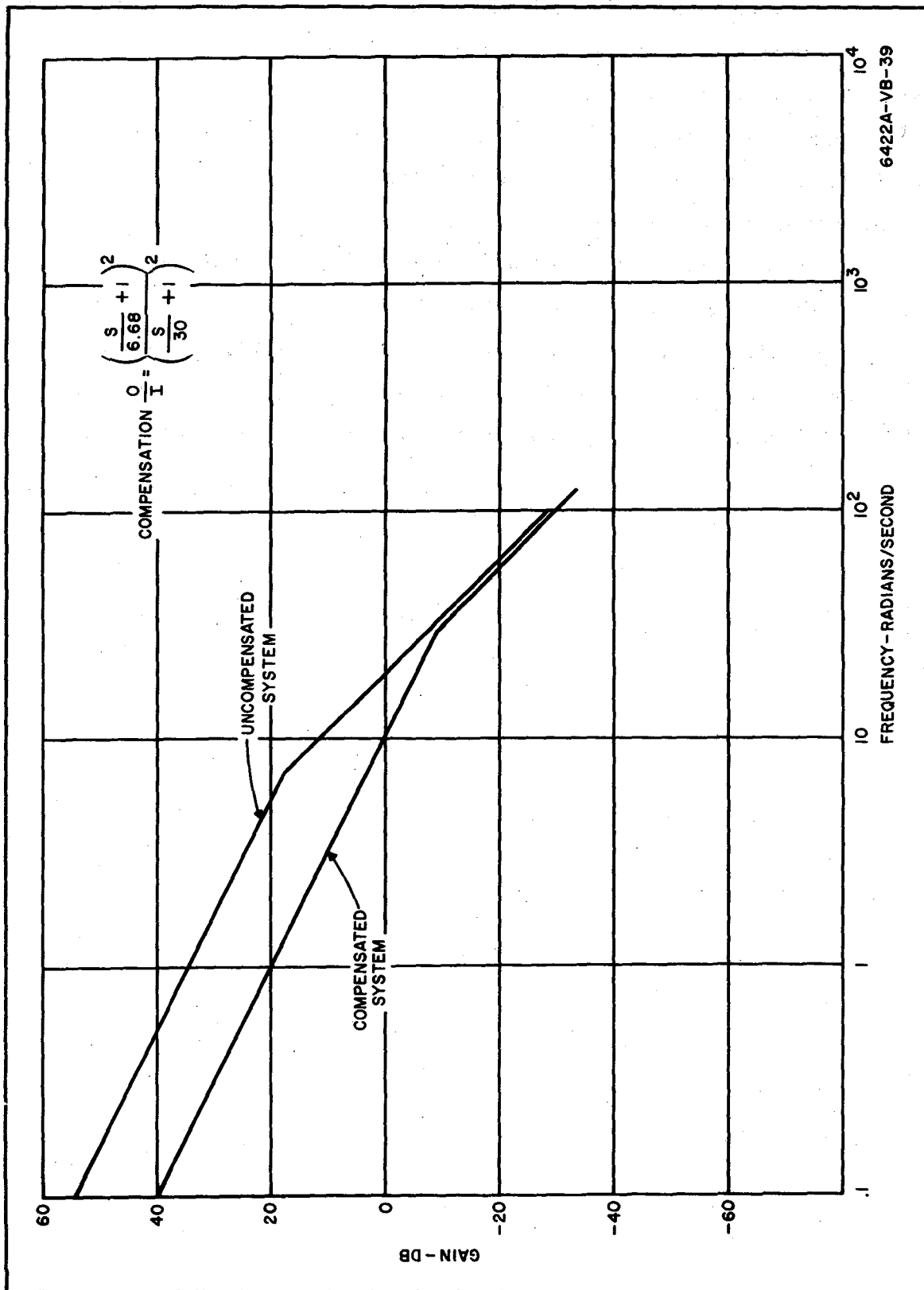


Figure 67. BODE Plots of Roll Axis 1 DOF System

The gyro gimbal angle is normally restricted to  $\pm 60$  degrees travel giving a maximum torque disturbance of 9.0 foot pounds allowable without exceeding the attitude error specifications.

The compensated system meets all the requirements placed on it. No rate sensor is required for the system, and the attitude reference requirements are similar to those of the other two axes.

Considering the desaturation requirements of the two systems, there is not enough data available to this study to fully evaluate the total momentum requirements. However, since an attitude error, and thus, a gravity gradient torque will exist during the attitude hold mode, it is recommended that the 2 DOF gyros be reset just prior to the acquisition and maneuver sequence.

## APPENDIX 4

### ELECTROMAGNETIC ACTUATOR DESIGN

In this appendix, equations for coil weight, power and size are determined for both air-core and iron-core coils. Most of the equations shown were derived in previous studies (see References 9 and 10).

#### A.4.1 INTRODUCTION

In judging efficiencies, some parameter must be chosen for comparative purposes. For a long-lived satellite application the parameter chosen was minimum total mass placed in orbit. Total mass is defined here as the mass of the actuator plus the mass of the solar cell power supply required to provide continuously the maximum power for which the actuator is designed. The design of actuators for this contract assumed an oriented solar cell array capable of delivering 1 watt for every 453 grams of power supply.

#### A.4.2 CRITERIA FOR AIR-CORED COIL OPTIMIZATION

To provide an objective criterion with which the performance of iron-cored solenoids can be compared, the design of air-cored coils was optimized with respect to minimum total mass. In this derivation it is assumed that the shape of the satellite is approximately cylindrical, that the coil can be wound about the outer periphery of the satellite, and that the coil will have a square cross section, the dimensions of which are very small compared to the diameter. The last assumption introduces second order errors which, for diameters greater than 1 meter and torques less than  $5 \times 10^{-4}$  newton-meter, should not exceed 10 percent of the calculated power and mass.

The following symbols are defined for use in this derivation:

T = torque

N = number of turns

A = area included by coil



$B_t$  = terrestrial field  
 $I$  = coil current  
 $D$  = coil diameter  
 $P$  = power to coil  
 $\rho$  = resistivity of wire material  
 $a$  = cross section area of conductor  
 $k$  = mass-to-power ratio of power supply  
 $M_w$  = mass of the wire  
 $M_{ps}$  = mass of power supply  
 $M_t$  = total mass of system  
 $R$  = d-c resistance of coil  
 $g_w$  = density of wire material  
 (mks units are used throughout)

Assuming that the terrestrial field is directed orthogonally to the normal to the plane of the coil, the resulting torque can be expressed as:

$$T = NIAB_t \quad (1)$$

For a cylindrical satellite, with 3 octagonal coils wrapped around the spacecraft as shown in figure 32 the roll-axis coil is circular, with area  $A = \pi D^2/4$ , while the pitch and yaw axis coils are rectangular, with area  $rD^2$  where  $r$  is the length/diameter ratio of the spacecraft.

Considering the circular roll axis coil first, equation 1 may be written:

$$T = \pi NI B_t \frac{D^2}{4} \quad (2)$$

The resistance of the coil may be approximated by:

$$R = \pi ND \frac{\rho}{a}$$

and the power then is:

$$P = \pi ND \rho \frac{I^2}{a}$$

Hence the mass of the power supply is:

$$M_{ps} = k \pi ND \rho \frac{I^2}{a}$$

The mass of the wire in the coil is nearly:

$$M_w = \pi ND a g_w$$

and the total system mass ( $M_{ps} + M_w$ ):

$$M_t = \frac{k \pi ND \rho I^2}{a} + \pi ND a g_w \quad (3)$$

By rearranging equation 2, an expression for N may be obtained:

$$N = \frac{4T}{\pi I B_t D^2} \quad (4)$$

Substituting equation 4 into equation 3:

$$M_t = \frac{4T}{D B_t} \left( \frac{k I \rho}{a} + \frac{a g_w}{I} \right) \quad (5)$$

To minimize the total mass with respect to current, equation 5 can be differentiated with respect to I, the result set equal to zero, the value of I for minimum mass obtained, and this value substituted into equation 5 to obtain minimum total mass. When these operations are performed:

$$M_t = \frac{8 T}{D B_t} (k \rho g_w)^{\frac{1}{2}} \quad (6)$$

Other useful expressions can be derived such as current density in the conductor:

$$\frac{I}{a} = \left( \frac{g_w}{k \rho} \right)^{\frac{1}{2}} \quad (7)$$

power consumption:

$$P = \frac{4T}{B_t D} \left( \frac{g_w \rho}{k} \right)^{\frac{1}{2}} \quad (8)$$

power consumption per unit torque:

$$\frac{P}{T} = \frac{4}{B_t D} \left( \frac{g_w \rho}{k} \right)^{\frac{1}{2}} \quad (9)$$

and total mass per unit torque:

$$\frac{M_t}{T} = \frac{8}{D B_t} (k \rho g_w)^{\frac{1}{2}} \quad (10)$$

By going through the same type of derivation for  $A = rD^2$ , the following equations are derived for the rectangular coils normal to the pitch and yaw axes.

Total mass:

$$M_t = 4 \left( \frac{r+1}{r} \right) \left( \frac{1}{D} \right) (k \rho g_w)^{\frac{1}{2}} \left( \frac{T}{B_t} \right) \quad (10a)$$

Coil current:

$$I = a \sqrt{\frac{g_w}{k \rho}} \quad (10b)$$

Power consumed:

$$P = \frac{2(r+1)}{r} \left( \frac{T}{B_t} \right) \left( \frac{1}{D} \right) \left( \frac{g_w \rho}{k} \right)^{1/2} \quad (10c)$$

Number of turns:

$$N = \frac{T}{I r D^2 B_t} \quad (10d)$$

While the approximations given in equations 2 through 10d will introduce errors, they were derived primarily to serve as a basis of comparison for the iron-cored solenoids. A more rigorous, complicated approach would give answers which would tend to be more favorable to the iron-cored solenoids.

### A.4.3 OPTIMIZED DESIGN OF IRON-CORED ACTUATORS

In addition to symbols defined previously, the following symbols are used:

- M = magnetization per unit volume
- $V_i$  = volume of iron
- B = induction or flux density
- $T_b$  = torque produced by iron
- $T_i$  = maximum torque
- $T_c$  = torque produced by windings
- H = effective magnetic field intensity
- $H_a$  = applied magnetic field intensity
- $\mu_0$  = permeability of freespace
- $\mu_i$  = intrinsic permeability
- $\mu_r$  = relative permeability
- $A_c$  = mean area of coil

### A.4.4 DERIVATION OF SOMEWHAT IDEALIZED EQUATIONS

The torque produced by the iron bar can be expressed vectorially as:

$$\underline{T}_b = V_i (\underline{M} \times \underline{B}_t) \quad (11)$$

As with the air-cored coils of the preceding section, it will be assumed that the terrestrial field is directed orthogonally to the magnetization vector and the maximum torque can then be written.

$$T_i = MV_i B_t \quad (12)$$

Since the magnetization of a core is a difficult parameter with which to deal, a more familiar parameter B will be introduced which is related to M by:

$$M = \frac{B}{\mu_o} - H$$

Substituting this in equation 12:

$$T_i = \left(\frac{B}{\mu_o} - H\right) V_i B_t \quad (13)$$

Recognizing that  $B = \mu_i H$  and  $\mu_i = \mu_o \mu_r$ , equation 13 can be written:

$$T_i = (\mu_r - 1) H V_i B_t \quad (14)$$

Because of the demagnetizing effects associated with the geometry of the cylindrical cores to be used, the field  $H_a$  generated by the solenoidal winding is not equal to the field H which determines the induction state of the material. As a result of the demagnetizing effects, the effective field is related to the applied field by the expression:

$$H = H_a - \frac{L}{4\pi} \left(\frac{B}{\mu_o} - H\right) \quad (15)$$

where  $\frac{L}{4\pi}$  is the demagnetizing factor.

Upon appropriate substitution ( $B = \mu_i H$ ) and after further manipulation, equation 15 can be written:

$$H = \frac{H_a}{1 + (\mu_r - 1) \frac{L}{4\pi}} \quad (16)$$

Since  $B_m = \mu_o \mu_r H$  when H is at some maximum, equation 16 can be written (recognizing that  $\mu_r \gg 1$ ):

$$H_a = \frac{B_m}{\mu_o} \left(\frac{1}{\mu_r} + \frac{L}{4\pi}\right) \quad (17)$$

Combining equations 14, 16, and 17:

$$T_i = \frac{H_a V_i B_t}{\left(\frac{l}{\mu_r} + \frac{L}{4\pi}\right)} \quad (18)$$

or

$$T_i = \frac{B_m B_t V_i}{\mu_o} \quad (18a)$$

For some design calculations equation 18a is written in terms of the bar dimensions

$$m = 2 \left( \frac{\mu \mu_o T_i}{\pi l B_m B_t} \right)^{\frac{1}{2}} \quad (18b)$$

where the dimensions are defined in figure 68.

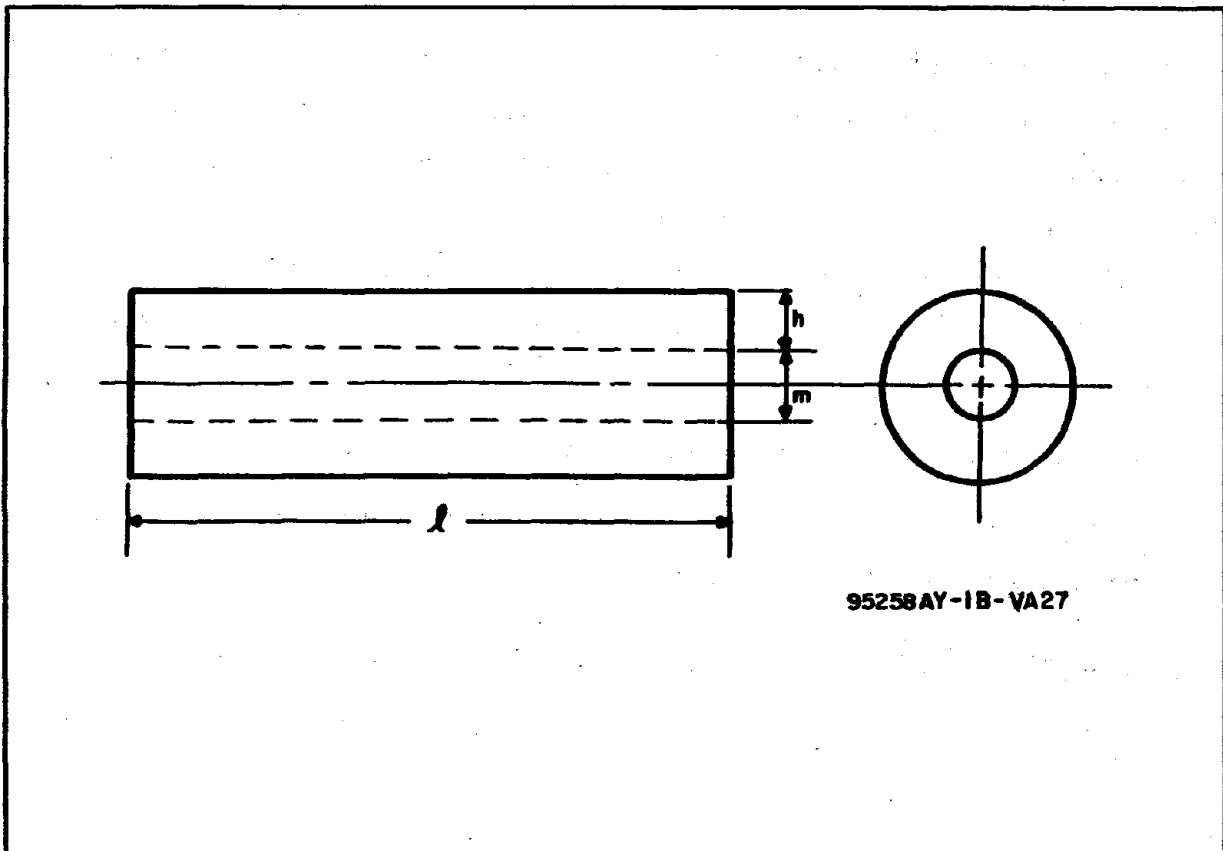


Figure 68. Dimensions of Core-Coil Combination

In addition to the torque produced by the iron, there is a torque produced independently by the current flowing in the solenoidal winding. This torque  $T_c$  can be expressed as

$$T_c = NI A_c B_t \quad (19)$$

Because the magnetic field intensity applied to the iron core is produced by the current in the windings, and is related to it by  $H_a \ell = NI$ , equation 19 can be written in terms of  $H_a$ :

$$T_c = H_a \ell A_c B_t \quad (20)$$

The total torque  $T_t$  produced by the system is the sum of  $T_c$  and  $T_i$  and is written

$$T_t = H_a B_t \left[ \frac{V_i}{Z} + \ell A_c \right] \quad (21)$$

where the notation  $Z = \left( \frac{1}{\mu_r} + \frac{L}{4\pi} \right)$  has been introduced for brevity. It is more convenient, for design calculations, to write equation 21 in terms of physical dimensions of the actuator and magnetic properties of the core used. The meaning of the dimensional symbols is given in figure 68. In rewriting equation 21 it is assumed that:

- a. The length of the winding is equal to the length of the core.
- b. The mean winding area effective in producing the torque due to the coil is expressed as  $A_c = \pi (m^2 + 2mh + 2h^2)/4$
- c. The core volume is expressed as  $V_i = \pi m^2 \ell / 4$

Substituting equation 17 and the dimensional relationships into equation 21 the expression for total torque becomes:

$$T_t = \frac{\pi B_m B_t \ell}{4\mu_o} \left\{ m^2 + [m^2 + 2h(m+h)] \right\} Z \quad (22)$$

As a convenience in further mathematical manipulations, a new variable will be defined as the ratio of the volume of the winding to the volume of the iron:

$$\Psi = \frac{4h(m+h)}{m^2} \quad (23)$$

Equation 23 is needed, for design purposes, in the form:

$$h = \frac{m}{2} \left[ (\Psi + 1) \frac{1}{2} - 1 \right] \quad (23a)$$

Expressing equation 22 in terms of the new variable:

$$T_t = \frac{\pi B_m B_t m^2 l}{4\mu_o} \left[ 1 + \left(1 + \frac{\Psi}{2}\right) Z \right] \quad (24)$$

Expressions for power and mass will now be derived. Additional quantities will be defined as:

P = power

$M_{(x)}$  = mass of x

d = diameter of insulated wire

$d_1$  = diameter of bare wire

s = area space factor of winding

$\rho$  = resistivity of wire material

$g_i$  = density of core material

$g_w$  = density of bare wire

It was originally assumed that the mass of the wire insulation would be negligible with respect to the mass of the conductor material and  $g_w$  was defined accordingly. Subsequently, it was found that the error introduced by this simplifying assumption is a function of wire size and a more accurate expression can be obtained if the value used for  $g_w$  is increased to the density of the insulated wire. Since handbook values of the density of insulated wires are not obtainable, it was decided to accept a nominal error and derive the expressions in terms of values which are available to a designer. An



additional assumption made in these derivations is that no interlayer insulation is used in constructing the windings.

A cross section of turns wound to achieve a maximum space factor for round wire is illustrated in figure 69. It can be shown that the number of turns which can be wound in this manner is:

$$N = \left( s \frac{1}{2} \frac{\ell}{d} \right) \left( s \frac{1}{2} \frac{h}{d \sin \frac{\pi}{3}} \right)$$

$$= 1.15 \ell h s / d^2 \quad (25)$$

The current can be expressed as a function of the magnetic field intensity it produces,  $I = H_a \ell / N$  and by substituting equations 21 and 25 into this expression:

$$I = \frac{0.866 d^2 B_m}{\mu_o h s} Z \quad (26)$$

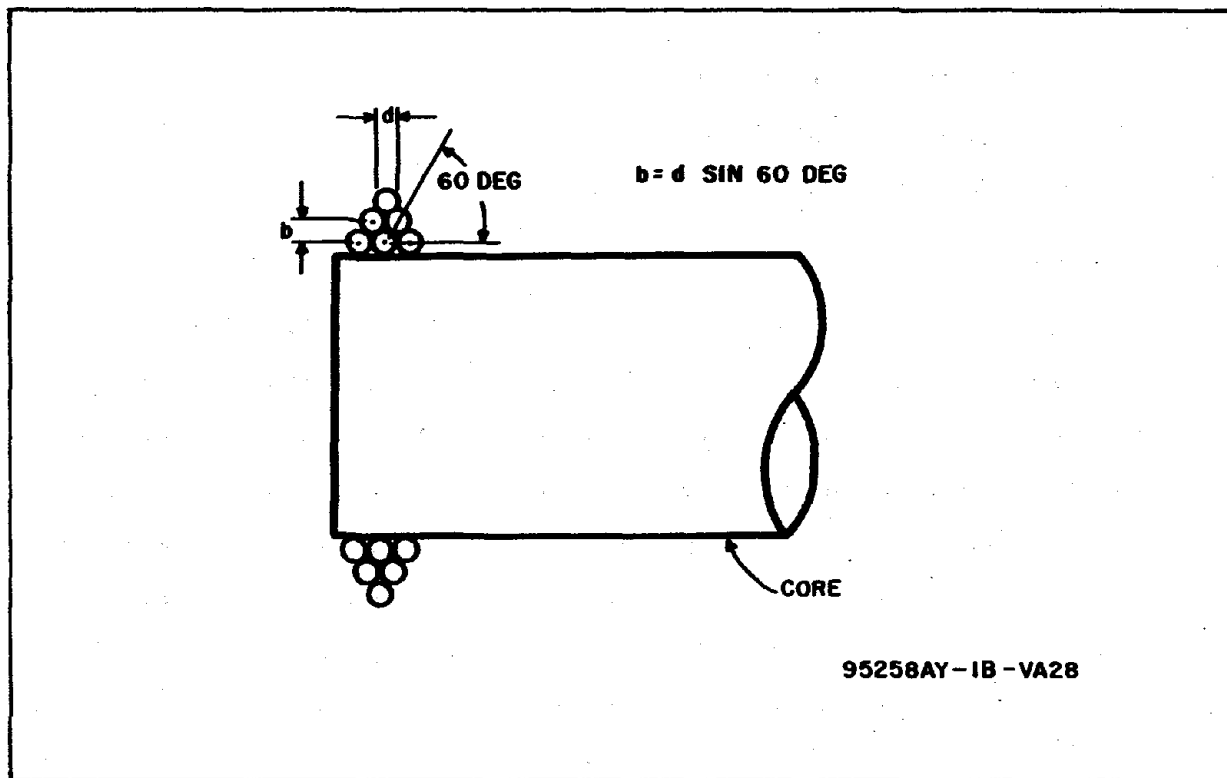


Figure 69. Cross-Section of Winding

The resistance of the coil can be expressed in terms of the wire parameters. The wire length  $\ell_w$  can be found from the mean length of turn,  $\pi (m + h)$ , and the number of turns, equation 25:

$$\ell_w = \frac{1.15 \pi l s h (m + h)}{d^2} \quad (27)$$

The conductor area is given by  $\pi d_1^2/4$  and the resistance can be found from the expression:

$$\begin{aligned} R &= \rho \ell_w / A_w \\ &= 4.60 \rho l s h (m + h) / (d_1 d)^2 \end{aligned} \quad (28)$$

The voltage  $V$  appearing across the actuator terminals when nominal current  $I$  is flowing can be expressed as the product of equations 26 and 28;

$$V = \frac{4 \rho l (m + h) B_m Z}{\mu_o d_1^2} \quad (29)$$

The power dissipated is the product of equations 26 and 29:

$$P = \frac{3.464 \rho l (m + h) B_m^2}{\mu_o^2 h s} \left(\frac{d}{d_1}\right)^2 Z^2 \quad (30)$$

Or, expressing  $P$  in terms of the variable  $\Psi$ , equation 30 becomes:

$$P = \frac{3.464 \rho l B_m^2}{\mu_o^2 s} \left(\frac{d}{d_1}\right)^2 Z^2 \left[ \frac{1 + (1 + \Psi)^{\frac{1}{2}}}{\Psi} \right]^2 \quad (31)$$

The mass of the actuator  $M_a$  can be expressed as the sum of the products of the volume and density of each material used. The wire volume is  $\ell_w A_w$  and the volume of the iron is  $\pi m^2 \ell / 4$ . Multiplying by the densities and summing

$$M_a = 1.15 g_w \pi^2 \ell s h (m + h) \left(\frac{d_1}{d}\right)^2 / 4 + \pi m^2 \ell g_i / 4 \quad (32)$$

Introducing the variable  $\Psi$  again and using a modified form of equation 17, equation 32 can be written:

$$M_a = \frac{T_i \mu_o}{B_m B_t} \left[ g_i + 0.288\pi g_w s \left(\frac{d_1}{d}\right)^2 \Psi \right] \quad (33)$$

It has been stated earlier that the proper criterion to be used in comparing actuators is the total mass of the system which includes the power supply. If it is assumed that the power supply can be characterized by a mass to power ratio expressed as a constant  $k$ , in kilograms per watt, then the total system mass is the sum of the actuator mass and the product of  $k$  and the maximum power required by the actuator:

$$M_t = M_a + k P \quad (34)$$

Making the appropriate substitutions, equation 34 can be written

$$M_t = \frac{T_i \mu_o}{B_m B_t} \left[ g_i + 0.288\pi g_w s \left(\frac{d_1}{d}\right)^2 \Psi \right] + \frac{3.464k\rho l B_m^2}{\mu_o^2 s} \left(\frac{d}{d_1}\right)^2 Z^2$$

$$\frac{\left[ 1 + (1 + \Psi) \frac{l}{Z} \right]^2}{\Psi} \quad (35)$$

It is seen that equation 35 expresses the total mass as a function of the torque due to the iron alone. As will be discussed later, this form of the total mass expression is the easiest to use for design purposes but for completeness, the total mass in terms of total torque will be given.

$$M_t = \frac{T_t \mu_o}{B_m B_t} \left[ \frac{g_i + 0.288 \pi g_w s \left(\frac{d_1}{d}\right)^2 \Psi}{1 + (1 + \Psi/2) \left(\frac{1}{\mu_r} + \frac{L}{4\pi}\right)} \right] + \frac{3.464 k \rho l B_m^2}{\mu_o^2 s} \left(\frac{d}{d_1}\right)^2 Z^2$$

$$\cdot \frac{\left[1 + (1 + \Psi) \frac{1}{2}\right]^2}{\Psi} \quad (36)$$

Since it can be shown that, to a first approximation, the power required to produce a given magnetic field intensity is independent of wire size, it will be recognized that the variable which determines the mass of the power supply as well as the mass of the coil is the coil volume. As coil volume is increased (for a fixed magnetic field intensity), the power supply mass decreases and the coil mass, hence the actuator mass, increases. A coil volume must exist, then, which will optimize the actuator design with respect to minimum total mass of the system. Because, for a given magnetic material, the mass of the core is proportional to core volume and since, in almost all cases, the total torque is almost independent of coil volume and is dependent only on core volume, the ratio  $\Psi$  will, for a given torque, vary directly with coil volume. Therefore, if equation 35 is differentiated with respect to  $\Psi$  to obtain a minimum total mass, only second-order errors are introduced compared to the more rigorous but much more complicated procedure of differentiating equation 36 with respect to coil volume. Differentiating equation 35 with respect to  $\Psi$ , equating the result to zero, and solving for  $\Psi$  yields:

$$\frac{\left[1 + (1 + \Psi) \frac{1}{2}\right]^2}{\Psi^2 (1 + \Psi) \frac{1}{2}} = \frac{0.0832 \pi \mu_o^3 g_w s^2}{k \rho B_t B_m^3 l Z^2} \left(\frac{d_1}{d}\right)^4 T_i \quad (37)$$

The expression on the left-hand side of equation 37 is defined as  $f(\Psi)$  and cannot be solved explicitly for  $\Psi$ . However, it yields readily to numerical analysis and a curve of  $\Psi$  as a function of  $f(\Psi)$  over the range of interest is given in figure 70. The value of  $\Psi$  obtained can be substituted into equation 36 and the minimum total mass capable of producing the desired torque in the desired length is obtained.

#### A. 4. 4. 1 Empirical Corrections to Idealized Conditions

In deriving many of the expressions in paragraph A. 4. 2, it was assumed that the flux density within the iron was uniform along the length of the bar. The actual distribution is indicated in figure 71. In this figure the ratio  $e_o/e_m$  is plotted as a function of distance along the bar for a typical core. The maximum voltage  $e_m$  induced in a single-turn sense coil wrapped close to the windings is equal to  $(\pi m^2/4)dB_m/dt$  and is observed at the midpoint of the bar. As the sense coil is moved toward an end of the bar, the voltage observed decreases as shown in figure 71. Since the other parameters

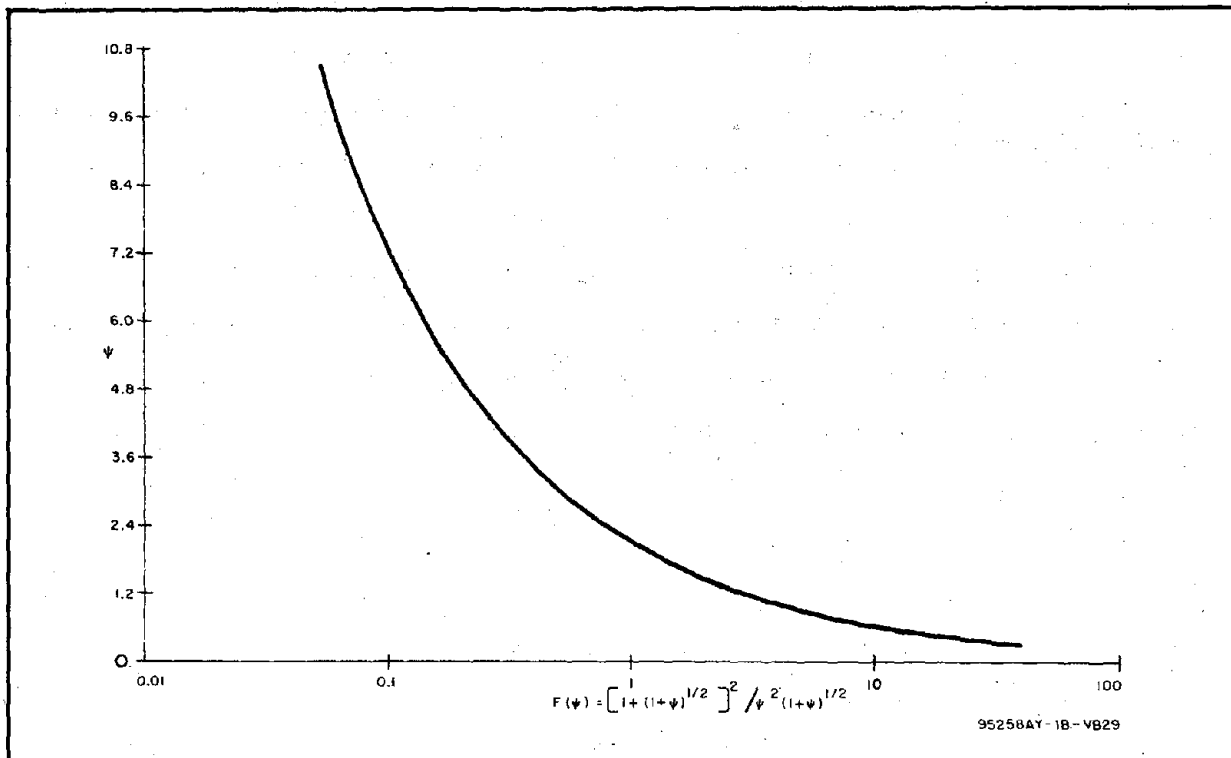


Figure 70.  $\Psi$  Versus  $f(\Psi)$

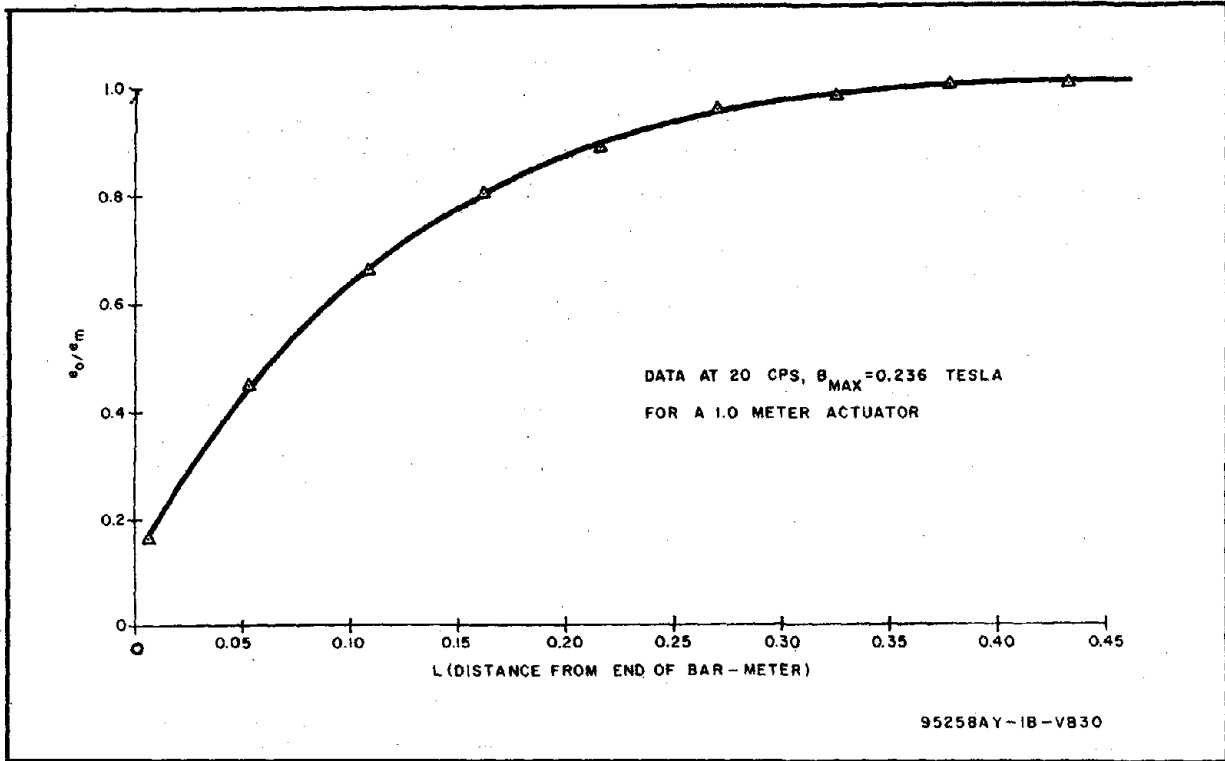


Figure 71. Flux Distribution in Bar as a Function of Distance From End

included in the expression for  $e_o$ ,  $(\pi m^2/4) dB/dt$ , remain relatively constant, the decrease in  $e_o$  must be attributed to a decrease in  $B$  as the sense coil is moved farther from the midpoint of the bar. The voltage is observed by applying a low frequency current to the actuator windings and observing the voltage in a one-turn sense coil.

While the distribution shown in figure 71 is typical of all bars, the exact shape of the curve is a function of  $l/m$  ratio. The change of the average flux density in the bar as  $l/m$  changes is shown in figure 72. Because bars with a small  $l/m$  have a greater buildup than bars with a greater  $l/m$  for the same nominal torque, the results shown in figure 72 are not to be accepted blindly. All of the factors affecting flux distribution along the length of the bar should be investigated more fully before an accurate correction can be made for this phenomenon.

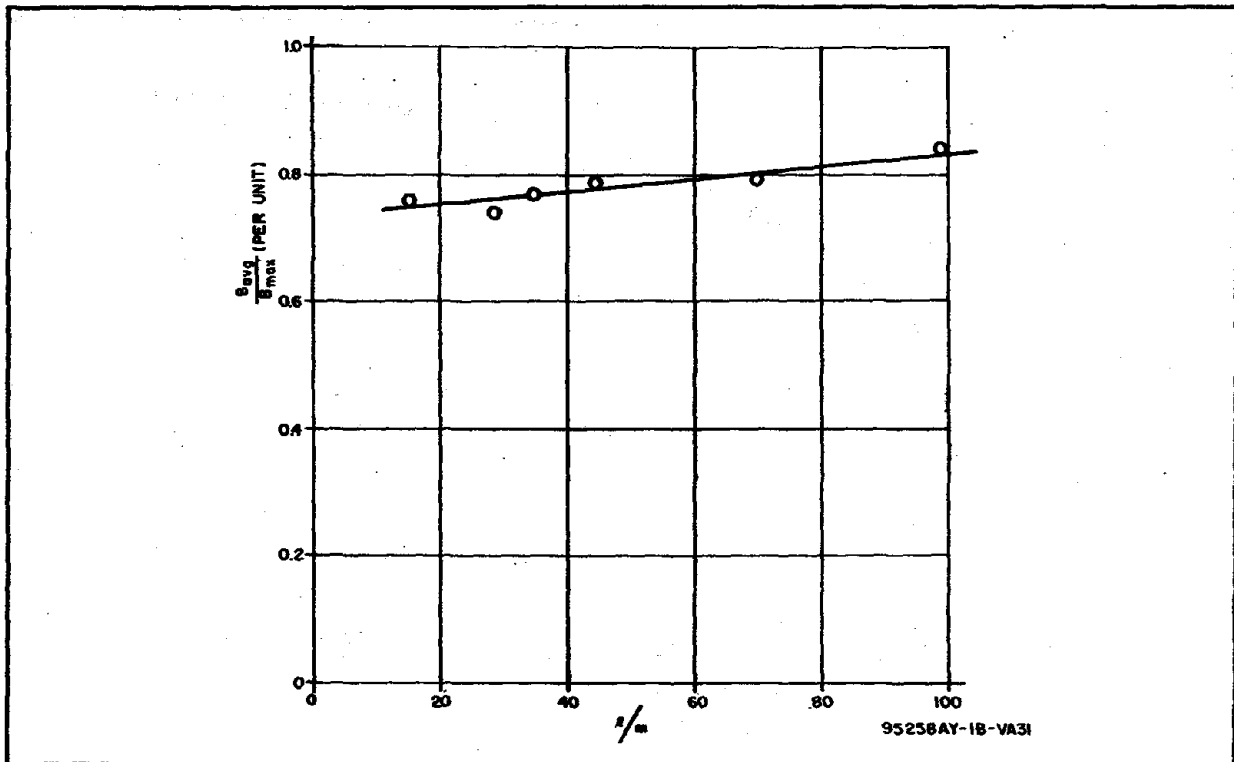


Figure 72. Average Flux Density in Bar Versus Core Length-Diameter Ratio

The correction now applied consists of a numerical integration of the area under the curve (of which figure 72 is a typical example) and then obtaining an average flux density. The ratio of average flux density to idealized flux density is designated as  $\alpha$ . The desired torque is divided by this figure and the actuator optimized with respect to the larger, fictitious torque. Equation 24 becomes:

$$T_t = \frac{\pi B_m B_t m^2 l}{4\mu_o} [\alpha + (1 + \psi/2) Z] \quad (38)$$

and equation 36 becomes:

$$M_t = \frac{\mu_o T_t}{B_m B_t} \left[ \frac{g_i + 0.288 \pi g_w s \left(\frac{d}{d_1}\right)^2 \Psi}{\alpha + (1 + \Psi/2) \left(\frac{1}{\mu_r} + \frac{L}{4\pi}\right)} \right] + \frac{3.464k \ell B_m^2}{\mu_o^2 s} \left(\frac{d}{d_1}\right)^2 Z^2$$

$$\frac{\left[ 1 + (1 + \Psi) \frac{1}{2} \right]^2}{\Psi} \quad (39)$$

Other equations also need correction. Equation 18b should be:

$$m = 2 \left( \frac{\mu_o T_i}{\pi \ell \alpha B_m B_t} \right)^{\frac{1}{2}} \quad (40)$$

Equation 18a should be:

$$T_i = \frac{\alpha B_m B_t V_i}{\mu_o} \quad (41)$$

Equation 21 becomes:

$$T_t = H_a B_t \left[ \frac{\alpha V_i}{Z} \right] + \ell A_c \quad (42)$$

Equation 22 should be:

$$T_t = \frac{\pi B_m B_t \ell}{4\mu_o} \left\{ \alpha m^2 + [m^2 + 2h(m + h)] Z \right\} \quad (43)$$

Equation 33 becomes:

$$M_a = \frac{T_i \mu_o}{\alpha B_m B_t} \left[ g_i + 0.288 \pi g_w s \left(\frac{d}{d_1}\right)^2 \Psi \right] \quad (44)$$



Equation 35 should be:

$$M_t = \frac{T_i \mu_o}{\alpha B_m B_t} \left[ g_i + 0.288 \pi g_w s \left(\frac{d_1}{d}\right)^2 \psi \right] + \frac{3.464 k \rho l B_m^2}{\mu_o^{-2} s} \left(\frac{d}{d_1}\right)^2 Z^2 \left[ \frac{1 + (1 + \psi)^{\frac{1}{2}}}{\psi} \right]^2 \quad (45)$$

$$f(\psi) = \frac{\left[ \frac{1 + (1 + \psi)^{\frac{1}{2}}}{\psi} \right]^2}{\psi^2 (1 + \psi)^{\frac{1}{2}}} = \frac{0.0832 \pi \mu_o^3 g_w s^2}{\alpha k \rho B_t B_m^3 l Z^2} \left(\frac{d_1}{d}\right)^4 T_i \quad (46)$$

#### A. 4. 5 SAMPLE ACTUATOR DESIGN

To clarify the use of the equations derived in the preceding paragraphs, typical design parameters will be assumed and an optimum actuator designed to these parameters. Let it be assumed that a maximum torque of  $7.9 \times 10^{-5}$  newton-meter (790 dyne-cm) is required from an actuator not to exceed one-half meter in length. This torque shall be developed in a terrestrial field of  $1.56 \times 10^{-6}$  tesla (0.0156 gauss). The power source is assumed to produce 1 watt for every 0.388 kilograms of mass.

The preferred core material at this time is annealed 50 percent Ni-50 percent Fe and the preferred wire material is aluminum. A reasonable wire size will be assumed as #24AWG. The following material constants are thus established.

- $\rho = 2.83 \times 10^{-8}$  ohm-m (wire resistivity)
- $d = 5.56 \times 10^{-4}$  m (insulated wire diameter)
- $d_1 = 5.11 \times 10^{-4}$  m (uninsulated wire diameter)
- $s = 0.845$  (winding space factor)
- $g_i = 8.2 \times 10^3$  kg/m<sup>3</sup> (density of core material)
- $B_m = 1$  tesla (core saturation flux density)

$$\mu_r = 10^4 \text{ (relative permeability of core)}$$

$$g_w = 2.67 \times 10^3 \text{ kg/m}^3 \text{ (density of bare wire)}$$

The first step is to assume for the moment that all the torque will be produced by the iron. Making the appropriate numerical substitutions into equation 40

$$m = 2 \left( \frac{4\pi \times 10^{-7} \times 7.9 \times 10^{-5}}{\pi \times 0.5 \times 0.79 \times 1 \times 1.56 \times 10^{-6}} \right)^{1/2} = 0.0143 \text{ meter}$$

Using this value of  $m$ ,

$$l/m = \frac{0.5}{0.0143} = 35$$

From figure 73 the demagnetizing factor  $L/4\pi$  is found for this value of  $l/m$  to be  $2.22 \times 10^{-3}$ . If the proper numerical substitutions are made in equation 46

$$f(\psi) = \frac{0.0832 \pi (4\pi \times 10^{-7})^3 2.67 \times 10^3 (0.845)^2 \left(\frac{5.11}{5.56}\right)^4 7.9 \times 10^{-5}}{0.79 \times 0.388 \times 2.83 \times 10^{-8} \times 1.56 \times 10^{-6} \times 1 \times 0.5 \left(\frac{1}{10^4} + 2.22 \times 10^{-3}\right)^2}$$

$$= 1.524$$

Entering the graph of figure 70 at this value of  $f(\psi)$ ,  $\psi$  is found to be 1.67.

It is now necessary to calculate the total torque from equation 38 to ensure that the original assumption that the torque produced by the coil is negligible. Making the required substitutions

$$T_t = \frac{\pi \times 1 \times 1.56 \times 10^{-6} (0.0143)^2 0.5}{4 \times 4\pi \times 10^{-7}}$$

$$\left[ 0.79 + (1 + 1.67/2) \left( \frac{1}{10^4} + 2.22 \times 10^{-3} \right) \right]$$

$$= 7.9 \times 10^{-5} \text{ newton-meter}$$

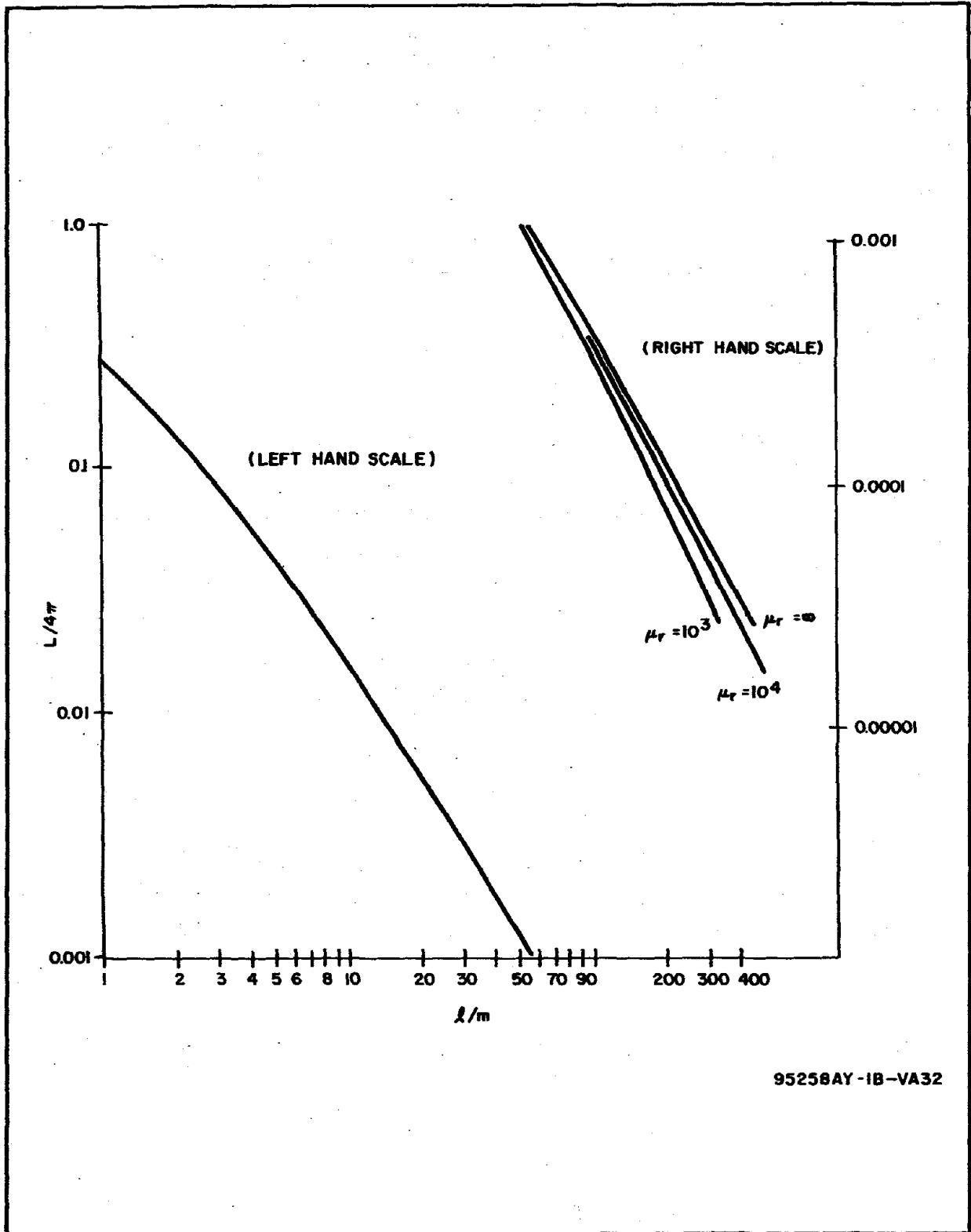


Figure 73. Demagnetizing Factor as a Function of  $l/m$

- Had the value of total torque been higher than the desired value, it would have shown that the torque produced by the coil was appreciable. This usually happens for low  $l/m$  ratios. When this happens, it is necessary to decrease the torque assumed to be produced by the iron by an appropriate amount, solve again for  $m$ ,  $L/4\pi$ , and  $\psi$ , and recheck. This process must be iterated until the total torque calculated agrees with the specified torque. This is a rapidly converging technique, and it has never been necessary to make more than three trials.

With the foregoing constants determined, equation 23a can be solved

$$h = \frac{0.0143}{2} \left[ (1.67 + 1)^{1/2} - 1 \right] = 4.51 \times 10^{-3} \text{ meter}$$

The rest of the calculations are indicated below in proper order and reference made to the appropriate equation without comment.

From equation 25

$$\begin{aligned} N &= 1.15 (0.5) 4.51 \times 10^{-3} \times 0.845 / (5.56 \times 10^{-4})^2 \\ &= 7090 \text{ turns} \end{aligned}$$

From equation 26

$$\begin{aligned} I &= \frac{0.866 (5.56 \times 10^{-4})^2 \times 1}{4\pi \times 10^{-7} \times 4.51 \times 10^{-3} \times 0.845} \left( \frac{1}{10^4} + 2.22 \times 10^{-3} \right) \\ &= 0.130 \text{ ampere} \end{aligned}$$

From equation 28

$$\begin{aligned} R &= \frac{4.60 \times 2.83 \times 10^{-8} \times 0.5 \times 0.845 \times 4.51 \times 10^{-3} (0.0143 + 4.51 \times 10^{-3})}{(5.11 \times 10^{-4} \times 5.56 \times 10^{-4})^2} \\ &= 57.6 \text{ ohms} \end{aligned}$$

From  $P = I^2 R$

$$P = (0.130)^2 57.6 = 0.975 \text{ watt}$$

From equation 45

$$\begin{aligned}
 M_t &= \frac{7.9 \times 10^{-5} \times 4\pi \times 10^{-7}}{0.79 \times 1 \times 1.56 \times 10^{-6}} \\
 &\cdot \left[ 8.2 \times 10^3 + 0.288\pi \times 2.67 \times 10^3 \times 0.845 \left( \frac{5.11}{5.56} \right)^2 1.67 \right] \\
 &+ \frac{3.464 \times 0.388 \times 2.83 \times 10^{-8} \times 0.5 \times 1}{(4\pi \times 10^{-7})^2 0.845} \left( \frac{5.56}{5.11} \right)^2 \\
 &\cdot \left( \frac{1}{10^4} + 2.22 \times 10^{-3} \right) \frac{\left[ 1 + (1 + 1.67)^{1/2} \right]^2}{1.67} \\
 &= 1.267 \text{ kilograms}
 \end{aligned}$$

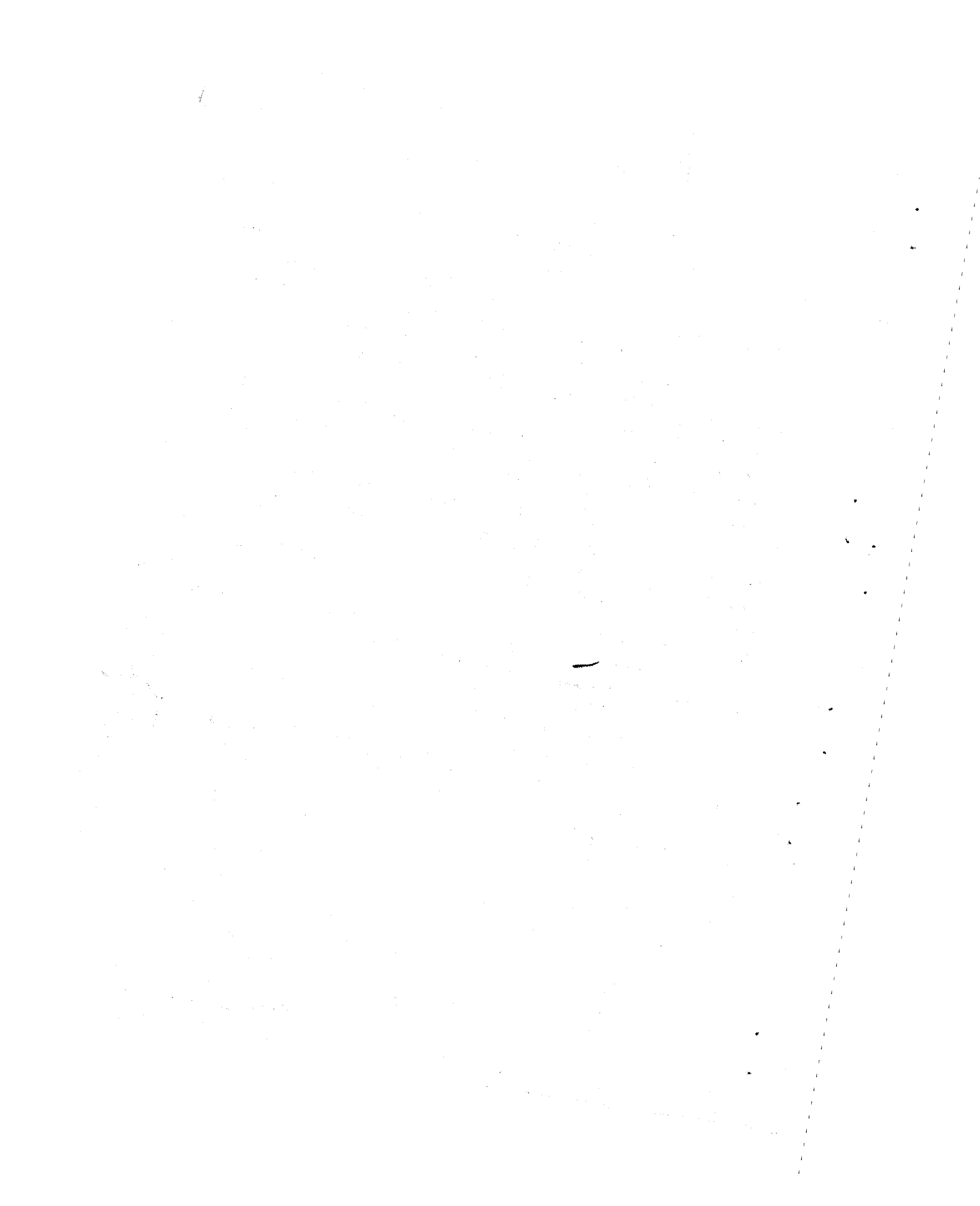
Thus, for the parameters specified, the total actuator system mass is 1.267 kilograms. This figure can be broken down into actuator mass and power supply mass. These figures are

$$M_a = 0.887$$

$$M_{ps} = 0.38$$

APPENDIX 5  
REFERENCES

- 1 J. Braumiller, et al, "Magnetic Torquers for Space Vehicle Control," Air Force Systems Command TDR No. ASD-TDR-63-74, January 1963.
- 2 "Electromagnetic Attitude Control System Study--Final Report," Westinghouse Electric Corporation, Aerospace Division, NASA Contract NAS 5-1728, May 1962.
- 3 "Analysis of Control Moment Gyro System Per Spec PDS 21440--Final Report," General Electric Company, Light Military Electronics Department, August 1966.
- 4 "Computation of the Main Geomagnetic Field from Spherical Harmonic Expansions," J.C. Cain, S. Hendricks, W.E. Daniels, D.C. Jensen, NASA No. X-611-64-316, October 1964.
- 5 "Models of the Earth's Magnetic Field," Joseph C. Cain, NASA No. X-612-65-400.
- 6 "Earth's Magnetic Field: A New Look," Normal F. Nerr, Science--Vol 151, No. 3714, pages 1041 - 1052, March 4, 1966.
- 7 "An Evaluation of the Main Geomagnetic Field, 1940 - 1962," J.C. Cain, W.E. Daniels, S.J. Hendricks, D.C. Jensen, Journal of Geophysical Research, Vol. 70, No. 15, August 1, 1965.
- 8 "Research and Investigation on Satellite Attitude Control," Part 1.A and 1.B, K.C. Nichols, General Electric Company, USAF No. AFFDL-TR-64-168, June 1965.



DOCUMENT CONTROL DATA - R&D

(Security classification of title, body of abstract and indexing annotation must be entered when the overall report is classified)

1. ORIGINATING ACTIVITY (Corporate author) Westinghouse Space & Defense Center Aerospace Division Baltimore, Maryland 21203		2a. REPORT SECURITY CLASSIFICATION Unclassified	
		2b. GROUP N/A	
3. REPORT TITLE 6 APPLICATION OF MAGNETIC TORQUING FOR DESATURATION OF CONTROL MOMENT GYROS IN SPACE VEHICLE CONTROL.			
4. DESCRIPTIVE NOTES (Type of report and inclusive dates) 9 Final Report - 1 Apr - 15 Dec 66			
5. AUTHOR(S) (Last name, first name, initial) 10 Hart, Leonard R. Hart Alatalo, Harold W. Alatalo Braumiller, Jack Braumiller		11 Jun 67 12 203p.	
6. REPORT DATE January 1967		7a. TOTAL NO. OF PAGES	7b. NO. OF REFS
8. CONTRACT OR GRANT NO. 15 AF33(615)-3602 new		9a. ORIGINAL REPORT NUMBER(S) 18 AFFDL-TR-67-8	
16 AF - 8225 Task No. 17 822509		9b. OTHER REPORT NO(S) (Any other numbers that may be assigned this report) 14 6422A	
10. AVAILABILITY/LIMITATION NOTICES This document is subject to special export controls and each transmittal to foreign governments or foreign nationals may be made only with prior approval of AFFDL (FDCL), Wright-Patterson AFB, Ohio.			
11. SUPPLEMENTARY NOTES		12. SPONSORING MILITARY ACTIVITY Air Force Flight Dynamics Laboratory Wright-Patterson AFB, Ohio 45433	
13. ABSTRACT A group of control moment gyros can be used to control the attitude of a space vehicle by exchanging momentum with the rest of the spacecraft. However, externally caused disturbance torques acting on the vehicle would saturate the momentum capability of the gyros if no auxiliary torquing methods were provided to unload the stored momentum. This function can be performed by a set of three current-carrying coils which interact with the earth's magnetic field in a process of continually resetting the control moment gyro gimbal angles to "zero" position.  The performance and weight of a magnetic system to momentum desaturate control moment gyros have been determined as functions of spacecraft size, altitude, and orbit inclination over the ranges of interest for a large, earth orbiting manned space vehicle. In a digital computer simulation of the combined control moment gyro and magnetic systems, the torques exerted by the latter had a negligible effect on the pointing accuracy of the former. Designs have been completed for the elements of the magnetic system and the interface with the control moment gyros has been defined.  This abstract is subject to special export controls and each transmittal to foreign governments or foreign nationals may be made only with prior approval of AFFDL (FDCL), Wright-Patterson AFB, Ohio.			

(375460)

Handwritten signature or initials.



14. KEY WORDS  Magnetic Torquing Control Moment Gyros Attitude Control System Momentum Desaturation	LINK A		LINK B		LINK C	
	ROLE	WT	ROLE	WT	ROLE	WT

**INSTRUCTIONS**

**1. ORIGINATING ACTIVITY:** Enter the name and address of the contractor, subcontractor, grantee, Department of Defense activity or other organization (*corporate author*) issuing the report.

**2a. REPORT SECURITY CLASSIFICATION:** Enter the overall security classification of the report. Indicate whether "Restricted Data" is included. Marking is to be in accordance with appropriate security regulations.

**2b. GROUP:** Automatic downgrading is specified in DoD Directive 5200.10 and Armed Forces Industrial Manual. Enter the group number. Also, when applicable, show that optional markings have been used for Group 3 and Group 4 as authorized.

**3. REPORT TITLE:** Enter the complete report title in all capital letters. Titles in all cases should be unclassified. If a meaningful title cannot be selected without classification, show title classification in all capitals in parenthesis immediately following the title.

**4. DESCRIPTIVE NOTES:** If appropriate, enter the type of report, e.g., interim, progress, summary, annual, or final. Give the inclusive dates when a specific reporting period is covered.

**5. AUTHOR(S):** Enter the name(s) of author(s) as shown on or in the report. Enter last name, first name, middle initial. If military, show rank and branch of service. The name of the principal author is an absolute minimum requirement.

**6. REPORT DATE:** Enter the date of the report as day, month, year; or month, year. If more than one date appears on the report, use date of publication.

**7a. TOTAL NUMBER OF PAGES:** The total page count should follow normal pagination procedures, i.e., enter the number of pages containing information.

**7b. NUMBER OF REFERENCES:** Enter the total number of references cited in the report.

**8a. CONTRACT OR GRANT NUMBER:** If appropriate, enter the applicable number of the contract or grant under which the report was written.

**8b, 8c, & 8d. PROJECT NUMBER:** Enter the appropriate military department identification, such as project number, subproject number, system numbers, task number, etc.

**9a. ORIGINATOR'S REPORT NUMBER(S):** Enter the official report number by which the document will be identified and controlled by the originating activity. This number must be unique to this report.

**9b. OTHER REPORT NUMBER(S):** If the report has been assigned any other report numbers (*either by the originator or by the sponsor*), also enter this number(s).

**10. AVAILABILITY/LIMITATION NOTICES:** Enter any limitations on further dissemination of the report, other than those

imposed by security classification, using standard statements such as:

- (1) "Qualified requesters may obtain copies of this report from DDC."
- (2) "Foreign announcement and dissemination of this report by DDC is not authorized."
- (3) "U. S. Government agencies may obtain copies of this report directly from DDC. Other qualified DDC users shall request through \_\_\_\_\_."
- (4) "U. S. military agencies may obtain copies of this report directly from DDC. Other qualified users shall request through \_\_\_\_\_."
- (5) "All distribution of this report is controlled. Qualified DDC users shall request through \_\_\_\_\_."

If the report has been furnished to the Office of Technical Services, Department of Commerce, for sale to the public, indicate this fact and enter the price, if known.

**11. SUPPLEMENTARY NOTES:** Use for additional explanatory notes.

**12. SPONSORING MILITARY ACTIVITY:** Enter the name of the departmental project office or laboratory sponsoring (*paying for*) the research and development. Include address.

**13. ABSTRACT:** Enter an abstract giving a brief and factual summary of the document indicative of the report, even though it may also appear elsewhere in the body of the technical report. If additional space is required, a continuation sheet shall be attached.

It is highly desirable that the abstract of classified reports be unclassified. Each paragraph of the abstract shall end with an indication of the military security classification of the information in the paragraph, represented as (TS), (S), (C), or (U).

There is no limitation on the length of the abstract. However, the suggested length is from 150 to 225 words.

**14. KEY WORDS:** Key words are technically meaningful terms or short phrases that characterize a report and may be used as index entries for cataloging the report. Key words must be selected so that no security classification is required. Identifiers, such as equipment model designation, trade name, military project code name, geographic location, may be used as key words but will be followed by an indication of technical content. The assignment of links, rules, and weights is optional.